ABSTRACT

Title of Dissertation: SYNTHESIS, DNA BINDING STUDIES AND ANTICANCER PROPERTIES OF ORGANORHENIUM SULFONATO COMPLEXES

Tijesunimi Odebode, Doctor of Philosophy, December 2019

Research Advisor: Santosh Mandal, Ph.D.
Department of Chemistry

Cancer is a worldwide concern. It is the second leading cause of death in the United States after heart disease and the leading cause of death in many states. The most effective treatments currently being used for cancers are associated with significant side effects and tumor resistance after extended use. Previous studies have described organometallic rhenium complexes as highly promising anticancer compounds since low IC_{50} values can be obtained and they exhibit low toxicity on normal cells. Other studies have demonstrated strong anticancer activity of Rhenium(V) Oxo complexes against MCF-7 and MDA-MB-231 breast cancer cell lines. In this study, we are exploring the synthesis and anticancer properties of novel rhenium complexes of the type $XRe(CO)_3Z$ [X = α-diimines and Z = tosylate, 1-naphthalenesulfonate and 2-naphthalenesulfonate] against breast cancer (hormone-dependent MCF-7, triple-negative MDA-MB-231) and lymphoma cells (U-937). Several derivatives were synthesized in two steps. The first step is the synthesis of a pentylcarbonato (PC) complex from dirhenium decacarbonyl. In the last step, the pentylcarbonato (PC) complex was treated with a corresponding sulfonic acid to afford the expected *p*-toluenesulfonato (TOS), 1-naphthalenesulfonato (1NS) or 2-naphthalenesulfonato (2NS) complex. These compounds were characterized using IR,

NMR, and X-ray crystallography. The sulfonato compounds synthesized had yields ranging from 70–99%. Alamar blue and MTT cell viability assays were used to determine the IC_{50} values and demonstrate the potency of the rhenium complexes against breast and lymphoma cells. The complexes were found to be more potent than conventional cancer drug cisplatin. DNA binding studies were performed using UV-Vis titrations, ethidium-bromide displacement assay, cyclic voltammetry, gel electrophoresis, and viscosity. These studies suggested DNA partial intercalation interaction for some of the complexes synthesized.

SYNTHESIS, DNA BINDING STUDIES AND ANTICANCER PROPERTIES OF ORGANORHENIUM SULFONATO COMPLEXES

By

Tijesunimi Odebode

A Dissertation Submitted in Partial Fulfillment
of the Requirements for the Degree
Doctor of Philosophy

MORGAN STATE UNIVERSITY

December 2019

SYNTHESIS, DNA BINDING STUDIES AND ANTICANCER PROPERTIES OF ORGANORHENIUM SULFONATO COMPLEXES

By

Tijesunimi Odebode

has been approved

May 2019

DISSERTATION COMMITTEE APPROVAL:

_____
Santosh Mandal, Ph.D., Committee Chair and Advisor

_____
James Wachira, Ph.D.

_____
Yongchao Zhang, Ph.D.

_____
Fasil Abebe, Ph.D.

_____
Hirendra Banerjee, Ph.D.

DEDICATION

This work is dedicated to God, my lovely and supportive fiancee, Olamipo Adekoya and my beloved family.

ACKNOWLEDGEMENT

I would like to acknowledge my advisor, Dr. Santosh Mandal for his guidance, instruction, support, patience, and encouragement throughout the course of my Ph.D. program. You have been more like a father than a mentor. I really appreciate you Dr. Mandal.

I acknowledge my committee members, Dr. James Wachira, Dr. Yongchao Zhang, Dr. Fasil Abebe and Dr. Hirendra Banerjee for their support and valuable contributions to my dissertation. I extend my gratitude to Dr. James Wachira for guiding me and allowing me to use his lab for the gel electrophoresis and cytotoxicity experiments. I would also like to thank Dr. Yongchao Zhang for giving me the opportunity to use his lab and guiding me through the cyclic voltammetry experiments. Finally, I would extend my gratitude to Dr. Abebe for his guidance throughout the fluorescence experiments.

I would like to thank the Mandal lab members for their support and encouragement, throughout the course of my studies. I also want to thank Dr. Solomon Tadesse for his technical assistance with the NMR, UV-Vis and IR instruments.

I acknowledge the Morgan State University School of Graduate Studies and the School of Computer, Mathematical and Natural Sciences for providing tuition remission and stipend allowance for my doctoral program.

I would like to appreciate my my lovely fiancee Olamipo Adekoya for her immense support and for being a shoulder to lean on during the difficult times of this program. I also appreciate my brothers, Iyanuoluwa Odebode and Israel Odebode for their support, encouragement, and love during my course of study.

Finally, I would like to thank my parents Prof. Timothy Odebode and Prof. Stella Odebode for their financial support, emotional support, love, patience, and encouragement throughout the course of my studies. I want to thank them for being there for me during the tough times and for their constant reassurance that I will make it through.

TABLE OF CONTENTS

LIST OF SCHEMES

LIST OF TABLES

LIST OF FIGURES

ABBREVIATIONS

ER = Estrogen Receptors

PR = Progesteron Receptors

HER2 = Human Epidermal Growth Factor Receptor 2

UV-Vis = Ultraviolet-visible

PC = Pentylcarbonato

1NS = 1-Napthalenesulfonic acid

2NS = 2-Naphthalenesulfonic acid

TOS = *p*-Toluenesulfonic acids

CH_2Cl_2 = Dichloromethane

^{1}H NMR = Proton Nuclear Magnetic Resonance

^{13}C NMR = Carbon 13 Nuclear Magnetic Resonance

DMSO = Dimethyl Sulfoxide

FTIR = Fourier Transform Infrared

IR = Infrared

Rotavap = Rotary Evaporator

IC_{50} = Half-maximal inhibitory concentrations

CHAPTER I: INTRODUCTION

Cancer is a broad group of diseases that occur when abnormal cells in the body divide without stopping and grow uncontrollably. These cells often spread to surrounding tissues in the body. The body's normal process is for normal cells to divide to form new cells when the body needs them and for old and damaged cells to die so that new cells can take their place. However, when cancers develop, this normal process is disrupted, causing new cells to be formed when they are not needed, and old cells survive when they should die.

Cancer is the second leading cause of death in the United States after heart disease, but it is the leading cause of death in many states.[1] In 2015, the most recent year for which incidence data are available, 1,633,390 new cases of cancer were reported, and 595,919 deaths were recorded in the US.[2] In that same year, 438 new cancer cases and 159 cancer deaths were reported for every 100,000 people.[2] In 2018, 1,735,350 new cancer cases and 609,640 cancer deaths are projected to occur in the United States.[1] Table 1 below shows the common cancer types in the United States.[3] The common cancers were determined based on an estimated annual incidence for 2018 of 40,000 cases or more.[3]

Table 1: Common Cancer Types in the United States.[3]

Cancer Type	Estimated New Cases	Estimated Deaths
Breast (Female & Male)	268,670	41,400
Lung (Including Bronchus)	234,030	154,050
Prostate	164,690	29,430
Colon and Rectal (Combined)	140,250	50,630
Melanoma	91,270	9,320
Bladder	81,190	17,240
Non-Hodgkin Lymphoma	74,680	19,910
Kidney	65,340	14,970
Endometrial	63,230	11,350
Leukemia (All types)	60,300	24,370
Pancreatic	55,440	44,330
Thyroid	53,990	2,060
Liver and Intrahepatic Bile Duct	42,220	30,200

It is obvious from the above statistics that cancer is very deadly. Many treatments are currently being used for cancer. The treatment option depends on the type, stage and location of the tumor. Some people are given only one treatment, but most will have a combination of treatments such as surgery with/without chemotherapy or radiation therapy.[4] Other treatment options include hormone therapy, targeted therapy, immunotherapy etc..

Surgery is often used as the first treatment for cancers. It is typically used for solid tumors contained in one area of the body.[4] A drawback for using surgery as a treatment option is that cancers that have spread all over the body cannot be treated. Another drawback is that small amounts of cancer cells often remain after surgery. Surgery is often the only treatment used for early stage cancers. Radiation therapy is also another treatment option used for cancers. It involves using high doses of radiation to kill cancer cells. Radiation therapy works mainly by damaging DNA and preventing it from

replicating.[5] One drawback of radiation therapy is that the radiation could also kill normal cells, especially the ones that are dividing.[6] Also, like surgery, radiation therapy caanot treat cancers that have spread or metastasized. Surgery and radiation treatment are often combined. It is apparent that surgery and radiation therapy are ineffective against systemic cancers. The most common types of systemic cancer treatment include chemotherapy, hormonal therapy, targeted therapy and immunotherapy.

Chemotherapy involves the use of drugs which are either taken intravenously or by mouth to kill cancer cells. Since cancer cells grow and divide quickly, chemotherapy works by slowing or stopping the growth of these cells. As stated earlier, one major advantage of chemotherapy over radiation therapy and surgery is that chemotherapy can be used to treat cancers that have spread throughout the body. However, just like radiation therapy, chemotherapy can slow or stop the growth of normal cells that grow and divide quickly. This drawback often leads to side effects such as hair loss, mouth sores, nausea etc.

Hormonal therapy is another form of systemic therapy for cancer. Some cancer cells require hormones for growth. Homone therapy works by depriving cancer cells of these hormones. This is done by using drugs that either block the activity or the synthesis of the hormone.[5] An example of a type of cancer that is treated using hormone therapy is hormone receptor positive breast cancer. This type of cancer expresses estrogen receptors (proteins) (ER) and progesterone receptors (PR). About 70% of all breast cancers are estrogen receptor positive, and 65% of these cancers are progesteron receptor positive.[7-8] This means that the cancer cells grow in response to estrogen or progesteron hormones. Hormonal therapy is used to prevent the return of the cancer either by blocking estrogen

receptors or stopping estrogen production thereby reducing its levels. Tamoxifen is the leading drug for hormone receptor positive breast cancers. It works by blocking estrogen receptors so that estrogen does not bind to them. Tamoxifen has a few drawbacks. One major drawback is that the tumor develops drug resistance upon extended use.[9] Another major drawback is the possibility for the drug to cause endometrial cancer.[9] Tamoxifen has also been associated with certain side effects such as nausea, hot flushes, anorexia, menstrual irregularities, vaginal bleeding and discharge, etc.

Targeted therapy is a type of systemic cancer therapy that exploits the differences between normal cells and cancer cells. It involves using drugs to either target other cells that help cancer cells grow or target specific parts of cancer cells that differ from other cells. Targeted drugs could work in any of the following ways: triggering the immune system to destroy cancer cells, turning off signals that tell cancer cells to divide, stopping signals that help with the formation of blood vessels, delivering toxins to cancer cells to kill them or interfering with proteins on cancer cells that tell them to divide thereby slowing their uncontrolled growth.[4] An example of targeted therapy is in the treatment of the human epidermal growth factor receptor 2 (HER2) breast cancer. About 25% of breast cancers overexpress the HER2 receptor.[10] This protein normally controls the growth and division of healthy breast cells. However, in breast cancer cells, the HER2 gene works incorrectly and makes too many copies of itself causing it to make too many copies of the HER2 receptor. This leads to overexpression of the HER2 receptor. When this receptor is overexpressed, breast cancer cells grow and divide faster and uncontrollably. The leading medication for HER2 breast cancer is Trastuzumab (Herceptin). Trastuzumab works as an antibody that attaches to HER2 receptors (the

antigen), thereby preventing breast cancer cells from growing and dividing uncontrollably. Trastuzumab has some side effects such as shortness of breath, muscle pains, diarrhea, cutaneous rash, congestive heart failure, headaches etc.[11] In general, targeted therapy could involve other drawbacks such as the possibility of cancer cells being resistant and the difficulty in developing drugs for certain targets.[4, 12]

It is apparent that most of the current systemic therapeutic options for cancer have their individual advantages but also possess significant drawbacks such as severe side effects or development of drug resistance. A cure for cancer would require a kind of therapy that stops cancer cells from growing and multiplying uncontrollably with little or no drawbacks. The discovery of cisplatin (*cis*-$(NH_3)_2PtCl_2$) and its anticancer properties in 1965 paved the way for the development of metal-based anticancer drugs and caused a revolution in cancer therapy.[13-15] Cisplatin structure is shown in Figure 1 below.

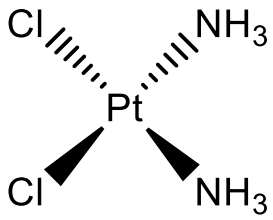

Figure 1: Cisplatin

Cisplatin, a platinum-based drug has been proven to be effective against many cancers.[16] However, it induces toxic side effects such as nephrotoxicity, ototoxicity, neurotoxicity, hair loss etc.[17-19] Also, the development of platinum resistance often occurs which causes tumors to relapse.[17, 20-21] The drawbacks of cisplatin have caused scientists to focus on developing new drugs such as carboplatin and oxaliplatin, analogues of cisplatin.[22] The

structures for these compounds are shown in Figure 2 below. Like cisplatin, these drugs had similar side

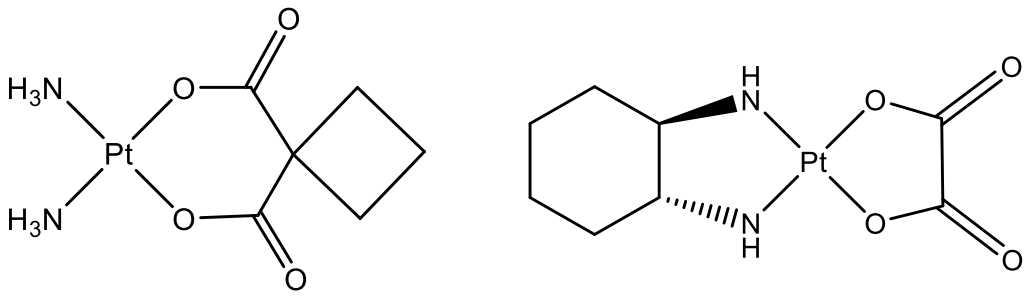

Figure 2: Carboplatin and Oxaliplatin

effects such as nephrotoxicity and neurotoxicity.[23] For many years, research had focused on the development of metal based drugs that are cisplatin analogues. However, none of the platinum drugs screened were able to overcome the drawbacks of cisplatin. As a result, there has been a need to investigate the development of anticancer drugs based on other metals.

In the past, organometallic compounds have been explored and proven to be potential anticancer drugs.[24-28] They have been explored due to to their advantages such as their structural variety which ranges from linear to octahedral and beyond,[25] stereochemical variety, kinetic stability, relative lipophicity, diverse mechanisms of action (such as catalytic activity, ligand exchange, redox activity), possibility for rational ligand design (thereby providing control over key kinetic properties) and their metal atom being in a low oxidation state.[25, 29] Despite the advantages that these compounds posses, many of them have been shown to have adverse effects. For example, Ferrocifens, a class of organometallic compounds have been shown by Gasser et al. to be effective against hormone dependent MCF-7 and triple negative MDA-MB-231 breast cancer cells.[25] As

shown in Figure 3 below, ferrocifens are a derivative of tamoxifen formed by replacing a phenyl group by ferrocene. Their studies showed that the replacement of the phenyl group by ferrocene reduces receptor affinity by about 40%.[25] Also, they confirmed that increasing the dimethylaminoalkyl chain length has an unfavorable effect on receptor binding.[25] An optimum value was seen in ferrocifens with n = 4.[25] Despite the potential of ferrocifens as anticancr agents, their drawback is the possibility of liver damage due to iron overload.

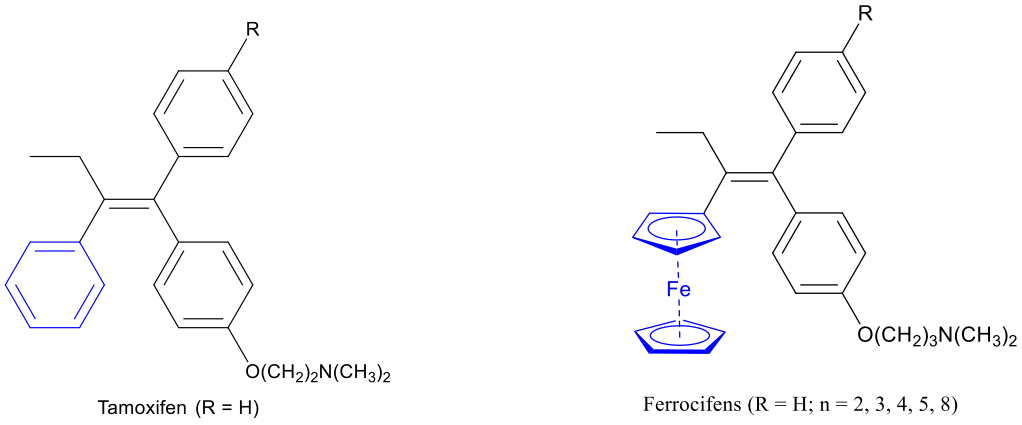

Figure 3: Tamoxifen and Ferrocifens

In addition, studies have shown the immense potential of organometallic rhenium complexes as anticancer agents.[29-38] Rhenium complexes possess certain features that make them excellent anticancer canditates. They serve as excellent luminiscent probes which can be utilized in cellular fluorescence microscopy imaging applications.[17, 29] This property makes it possible to follow them inside cells and see their cellular distribution and mechanism of action.[17, 29] Furthermore, some rhenium complexes have been shown to covalently bind to DNA like platinum-based drugs.[39-41] Studies have shown that cisplatin exhibits its anticancer properties by forming 1,2-intrastrand adducts between N7

atoms of two DNA purine bases.[42-43] Zobi and coworkers have shown that just like cisplatin, the *fac*-$[Re(CO)_3]^+$ core can engage two guanine bases in *cis* binding to yield reasonably stable complexes.[40] They have also demonstrated that the rates of ligand substitution of DNA purine bases can be compared with one of the active forms of cisplatin.[40] As a result, a lot of research has focused on Rhenium complexes with the *fac*-$[Re(CO)_3]^+$ core as potential anticancer drugs.[44-48] For example, studies by Yan and his group have shown the cytotoxicity of rhenium(I) alkoxo carbonyl complexes with the *fac*-$[Re(CO)_3]^+$ core (*fac*-$(CO)_3$(μ-dppfe)Re-OPh) in murine and human tumor cells.[30] Despite the high potency of these rhenium compounds on these cancer cells, they are also toxic to normal cells. Wilson et. al. have shown the anticancer activity of rhenium (I) tricarbonyl aqua complexes of the type *fac*-$[Re(CO)_3(NN)(OH_2)]^+$.[17] Their results also presented adverse effects.

Due to the high toxicity of cisplatin, numerous studies have been carried out to modify its chloro (Cl) and ammine (NH_3) ligands to develop less toxic drugs. For example, the carboplatin and oxaplatin analogues that were mentioned earlier were synthesized by replacing the chloro ligands with carboxylato groups and the ammine ligands with chelated diamines. These drugs were shown to be less toxic than cisplatin. As a result, we hypothesized that if we replaced the diphosphine ligands of the rhenium (I) tricarbonyl complexes of the type *fac*-$(CO)_3$(μ-dppfe)Re-OPh or related rhenium (I) complexes with diimines such as 2,2'-bipyridyl, 1,10-phenanthroline, 5-methyl-1,10-phenanthroline, 2,9-dimethyl-1,10-phenanthroline (neocuproin), 5,6-dimethyl-1,10-phenanthroline, Bathophenanthroline, Bathocuproin, 4,7-dimethyl-1,10-phenanthroline,

3,4,7,8-tetramethyl-1,10-phenanthroline and 4-methyl-1,10-phenanthroline, we could develop less toxic novel rhenium complexes.

In addition, many years ago, we embarked on a study in our lab on the the cytotoxicity of *fac*-$(CO)_3(N\frown N)ReOC(O)OC_5H_{11}$ where the ligands used were the first 7 (2,2'-bipyridyl, 1,10-phenanthroline, 5-methyl-1,10-phenanthroline, 2,9-dimethyl-1,10-phenanthroline, 5,6-dimethyl-1,10-phenanthroline, Bathophenanthroline, Bathocuproin) we are considering in this study. The compounds were studied primarily due to their facile access from Mandal's synthesis.[9, 49] The complexes containing ligands 2,9-dimethyl-1,10-phenanthroline and Bathophenanthroline were observed to be strong anticancer agents (IC_{50} = 4 μM) against BxPC-3 pancreatic cancer cell lines.[9, 49] Considering the success of these previous studies, for this particular study, we decided to replace the pentyl carbonato portion in *fac*-$(CO)_3(N\frown N)ReOC(O)OC_5H_{11}$ with sulfonate groups (p-toluenesulfonate and naphthalenesulfonate) and investigate their anticancer properties to see if we could develop potential anticancer drugs with minimal toxicity.

It is important to also state that studies done by Lippard and his group have demonstrated anticancer activity for some rhenium(V) oxo complexes based on two of the ligands in our study (bathophenanthroline and 3,4,7,8-tetramethyl-1,10-phenanthroline).[50] As shown in Table 2 below, the IC_{50} values of these complexes were much lower than that of tamoxifen and cisplatin when tested against hormone-dependent MCF-7 and triple-negative MDA-MB-231 breast cancer cells.[50]

Table 2: IC_{50} values of 1 and 2

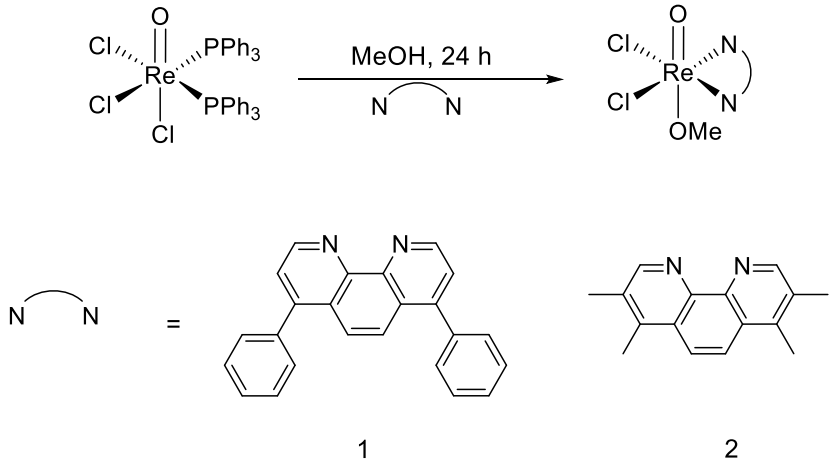

Breast Cancer Cells	**Tamoxifen** (μM)	**Cisplatin** (μM)	**1** (μM)	**2** (μM)
MCF-7	16.200 ± 0.900	9.740 ± 0.537	0.285 ± 0.035	0.805 ± 0.021
MDA-MB-231	13.000 ± 0.200	43.600 ± 7.071	0.475 ± 0.161	1.735 ± 0.275

DNA is the primary intracellular target of most anticancer drugs.[51-52] Many anticancer drugs either interact with DNA directly or prevent the proper relaxation of DNA.[53] When small molecules interact with DNA, they alter it's function. These molecules serve as drugs when alteration of DNA function is required to cure a disease.[52] In cancer cells, such molecules alter DNA function by blocking the division of cancer cells, inhibiting cell proliferation which often results in cell death.[51, 54] Compounds bind to DNA through two modes; covalent and non-covalent. In covalent binding, compounds interact with DNA covalently. Many anticancer drugs have been shown to form covalent adducts with DNA through alkylation, intrastrand crosslinking and interstrand

crosslinking.[51, 55] One major benefit of the covalent mode of binding is the high binding strength. This kind of binding is usually irreversible and can cause complete inhibition of DNA processes and subsequest cell death.[52] Some DNA functions that are inhibited are transcription and DNA replication. An example of a covalent binder is cisplatin.

The non-covalent mode of binding can be classified into three types: intercalation, groove-binding and electrostatic binding. In general, this type of interaction is less cytotoxic than covalent binding. The non-covalent binding mode is reversible and as a result it is preferred over covalent adduct formation.[52] Non-covalent DNA binders can alter DNA conformation and torsional tension, cause DNA strand breaks and interrupt protein-DNA interaction thereby affecting gene expression.[52] Intercalation occurs when planar molecules stack between adjacent DNA base pairs without forming covalent bonds and without breaking hydrogen bonds between the DNA bases.[52] This results in the lengthening of DNA and an unwinding of the DNA double helix.[56] Intercalators also stiffen and stabilize the DNA double helix.[57] Groove-binding occurs when molecules place themselves on the minor groove of DNA. These compounds bind to the minor groove through hydrogen bonding and van der Waals forces.[52] Binding occurs with the edges of base pairs in either of the major (G-C) or minor (A-T) grooves of nucleic acids.[58] Typically, groove binding drugs have several aromatic rings (e.g. benzene, pyrol and furan) that possess rotational freedom.[52] Many groove binding drugs are crescent-shaped that bind similar to the standard lock and key models in ligand-protein interactions. Electrostatic binding occurs when anionic or cationic complexes are attached to DNA's anionic surface. In this binding, the ligand usually self-associates to form higher-order aggregates that stack on the anionic DNA phosphate backbone so as to

reduce charge-charge repulsion between ligand molecules.[52] Charged metal complexes and ions can associate with DNA through electrostatic binding. Figure 4 shows the different modes of binding to DNA.

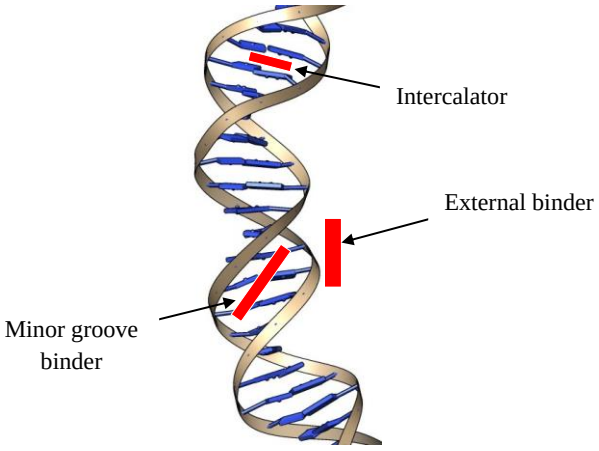

Figure 4: DNA binding modes

In this project, we will be studying the different modes of interaction of our rhenium complexes with DNA. There are several techniques commonly used to study complex-DNA interactions. In this study, we will use the following techniques: UV-Vis absorption spectroscopy, cyclic voltammetry, gel electrophoresis and viscosity. We will first determine the DNA binding strength and binding mode of sulfonato complexes using UV-vis absorption titration experiments. Following this, we will determine the binding abilities of the metal complexes with DNA by observing the changes in relative viscosity of DNA upon addition of DNA to the complexes. We will then investigate the interaction of DNA and sulfonato complexes by observing various changes in the cyclic voltammogram of the complexes upon addition of DNA. Finally, the potential binding of the fluorescent sulfonato complexes will then be investigated via their ability to stain DNA in agarose gels.

The aims of this project are divided into three as follows:

Aim 1: To synthesize a series of organorhenium complexes of the type $XRe(CO)_3Z$ [X = α-diimines and Z = tosylate, 1-naphthalenesulfonate and 2-naphthalenesulfonate] and characterize them using IR, ^1H NMR, ^{13}C NMR and X-ray crystallography.

Hypothesis: *Novel p-toluenesulfonato (TOS), 1-naphthalenesulfonato (1NS) and 2-naphthalenesulfonato (2NS) complexes can be successfully synthesized by treating a pentylcarbonato complex with the corresponding p-toluenesulfonic acid, 1-naphthalenesulfonic acid or 2-naphthalenesulfonic acid.*

(i) Conversion of $Re_2(CO)_{10}$ to the corresponding pentylcarbonato complex in the presence of α-diimine, CO_2 and 1-pentanol under reflux conditions.

(ii) Synthesis of 30 sulfonato complexes by treating the pentylcarbonato complex with the corresponding *p*-toluenesulfonic acid, 1-naphthalenesulfonic acid or 2-naphthalenesulfonic acid in dichloromethane at room temperature.

(iii) Characterization of pentylcarbonato and sulfonato complexes by IR, ^1H NMR, ^{13}C NMR and X-ray crystallography.

Aim 2: To carry out DNA-binding studies of the 30 organorhenium sulfonato complexes synthesized

Hypothesis: *The DNA-binding properties of the TOS, 1NS and 2NS complexes can be investigated to determine their mode of binding and binding strength using the following techniques: UV-vis titrations, cyclic voltammetry, gel electrophoresis and viscosity.*

(i) Determination of DNA binding strength and binding mode with sulfonato complexes using UV-vis absorption titration experiments.

(ii) Investigate the interaction of DNA and sulfonato complexes by observing various changes in the cyclic voltammogram of the complexes upon addition of DNA.

(iii) Investigate the potential binding of the fluorescent sulfonato complexes via their ability to stain DNA in agarose gels.

(iv) Investigate the mode and strength of binding of DNA to the sulfonato complexes by observing the changes in the fluorescence intensity of Ethidium Bromide upon addition of the complexes.

(v) Determination of the binding abilities of the metal complexes with DNA by observing the changes in relative viscosity of DNA upon addition of DNA to the complexes.

Aim 3: To carry out cytotoxicity studies of 30 sulfonato complexes on breast cancer cells (MCF-7 and MDA-MB-231) and lymphoma (U-937) cells.

Hypothesis: *The potency of the TOS, 1NS and 2NS complexes on breast cancer and lymphoma cells can be investigated using MTT cell viability assays.*

(i) Determination of the half maximal inhibitory concentration (IC_{50}) of the sulfonato complexes using MTT and alamar blue cell viability assay.

CHAPTER II: EXPERIMENTAL

2. 1. Materials and Methods

2. 1. 1. Synthesis

^{1}H (Proton), ^{13}C (Carbon), and DEPT NMR spectra were recorded on Bruker AVANCE 400 MHz instruments. Chemical shifts are reported in parts per million (δ) relative to the tetramethylsilane (TMS) resonance (δ = 0 for ^{1}H and ^{13}C). Proton data are recorded as follows: chemical shift, multiplicity (s (singlet), d (doublet), t (triplet), q (quartet), quin (quintet), m (multiplet), dd (doublet of doublets), dt (doublet of triplets)), coupling constant (Hz), and integration. Fourier transform infrared spectroscopy (FT-IR) was performed using a Perkin Elmer FT-IR spectrometer.

All reagents and solvents were purchased from commercial sources and were used without purification unless otherwise stated. Reactions were run in triplicate, and the average yields are recorded.

2. 2. Synthesis of PC series

A series of 10 pentylcarbonato complexes were synthesized according to the Mandal synthesis.[49] Only the synthesis of PC8, PC9 and PC10 are shown below. The synthetic protocol for the PC1–PC7 was published by Mandal et. al.[49]

2. 2. 1. Synthesis of PC8

$Re_2(CO)_{10}$ (1.000 g, 1.532 mmol) and 4,7-dimethyl-1,10-phenanthroline (0.638 g, 3.064 mmol) were refluxed in 1-pentanol (50 mL) for 19 h 50 min. CO_2 gas was bubbled through the solution for the entire reaction time. After the reaction was over, the mixture was allowed to sit (under CO_2) at room temperature overnight to allow crystals to form. The yellow crystals were collected by vacuum filtration and washed with a small amount

of 1-pentanol once and hexanes twice. The dry crystals (1.455 g, 78%) were characterized using IR and NMR. ^{1}H NMR (400 MHz, DMSO-d_6) δ 9.08 (d, J = 5.3 Hz, 2H), 8.17 (s, 2H), 7.74 (d, J = 5.2, 1.0 Hz, 2H), 3.18 (t, J = 4.3 Hz, 2H), 2.72 – 2.70 (m, 6H), 0.91 – 0.82 (m, 2H), 0.77 – 0.61 (m, 4H), 0.51 (t, J = 7.3 Hz, 3H). IR υ 2021.69, 1916.21, 1892.14, 1659.78 cm^{-1}.

2. 2. 2. Synthesis of PC9

$Re_2(CO)_{10}$ (1.000 g, 1.532 mmol) and 3,4,7,8-tetramethyl-1,10-phenanthroline (0.724 g, 3.064 mmol) were refluxed in 1-pentanol (50 mL) for 19 h 50 min. CO_2 gas was bubbled through the solution for the entire reaction time. After the reaction was over, the mixture was allowed to sit (under CO_2) at room temperature overnight to allow crystals to form. The yellow crystals were collected by vacuum filtration and washed with a small amount of 1-pentanol once and hexanes twice. The dry crystals (1.483 g, 76%) were characterized using IR and NMR. ^{1}H NMR (400 MHz, Chloroform-d) δ 9.18 (s, 2H), 8.14 (s, 2H), 3.75 (t, J = 7.1 Hz, 2H), 2.79 (s, 6H), 2.63 (s, 6H), 1.52 – 1.41 (m, 2H), 1.27 – 1.11 (m, 4H), 0.81 (t, J = 6.9 Hz, 3H). IR υ 2020.61, 1914.81, 1890.27, 1660.37 cm^{-1}.

2. 2. 3. Synthesis of PC10

$Re_2(CO)_{10}$ (1.000 g, 1.532 mmol) and 4-methyl-1,10-phenanthroline (0.595 g, 3.064 mmol) were refluxed in 1-pentanol (50 mL) for 19 h 50 min. CO_2 gas was bubbled through the solution for the entire reaction time. After the reaction was over, the mixture was allowed to sit (under CO_2) at room temperature overnight to allow crystals to form. The grey crystals were collected by vacuum filtration and washed with a small amount of 1-pentanol once and hexanes twice. The dry crystals (1.349g, 74%) were characterized using IR and NMR. ^{1}H NMR (400 MHz, Methylene Chloride-d_2) δ 9.31 (dd, J = 5.1, 1.5

Hz, 1H), 9.15 (d, *J* = 5.2 Hz, 1H), 8.48 (dd, *J* = 8.3, 1.5 Hz, 1H), 8.06 (d, *J* = 9.0 Hz, 1H), 7.93 (d, *J* = 9.1 Hz, 1H), 7.75 (dd, *J* = 8.2, 5.1 Hz, 1H), 7.60 (dt, *J* = 5.3, 0.9 Hz, 1H), 3.44 (t, *J* = 6.9 Hz, 2H), 2.79 (d, *J* = 0.9 Hz, 3H), 1.23 – 1.11 (m, 2H), 1.09 – 0.89 (m, 4H), 0.65 (t, *J* = 7.2 Hz, 3H). ^{13}C NMR (101 MHz, CD_2Cl2) δ 158.67, 153.69, 153.02, 147.26, 146.60, 138.46, 130.34, 127.07, 126.50, 125.51, 124.82, 124.11, 65.84, 28.84, 28.05, 22.36, 19.05, 13.72. IR υ 2022.43, 1917.48, 1893.12, 1660.13 cm^{-1}.

2. 3. Synthesis of sulfonato complexes

2. 3. 1. Synthesis of 1NS1

PC1 (0.050 g, 0.090 mmol) was dissolved in dichloromethane (15 mL) after which 1-Naphthalenesulfonic acid (0.019 g, 0.090 mmol) was added. The mixture was stirred at room temperature for 4 hr. After the reaction was over, the mixture was filtered under vacuum over celite. The filtrate was evaporated partially after which drops of hexanes were added to it to crash out the crystals. Some crystals crashed out, but the mixture was left in the refrigerator overnight for further crystallization. The mixture was then vacuum filtered, and the dry crystals were collected and weighed. The yellow crystals (0.053 g, 94%) were characterized using IR and NMR. ^{1}H NMR (400 MHz, Methylene Chloride-d_2) δ 8.64 (dd, *J* = 5.6, 1.5 Hz, 2H), 7.96 – 7.68 (m, 8H), 7.39 – 7.23 (m, 4H), 7.13 – 7.05 (m, 1H). IR υ 2030.58, 1928.27, 1906.26 cm^{-1}.

2. 3. 2. Synthesis of 1NS2

PC2 (0.050 g, 0.086 mmol) was dissolved in dichloromethane (15 mL) after which 1-Naphthalenesulfonic acid (0.018 g, 0.086 mmol) was added. The mixture was stirred at room temperature for 4 hr. After the reaction was over, the mixture was filtered under vacuum over celite. The filtrate was evaporated partially after which drops of

hexanes were added to it to crash out the crystals. Some crystals crashed out, but the mixture was left in the refrigerator overnight for further crystallization. The mixture was then vacuum filtered, and the dry crystals were collected and weighed. The yellow crystals (0.053 g, 95%) were characterized using IR and NMR. ^{1}H NMR (400 MHz, Methylene Chloride-d_2) δ 8.97 (dd, J = 5.1, 1.4 Hz, 2H), 8.26 (dd, J = 8.2, 1.4 Hz, 2H), 7.80 (dd, J = 7.2, 1.3 Hz, 1H), 7.70 (s, 2H), 7.69 – 7.65 (m, 1H), 7.62 – 7.55 (m, 1H), 7.55 (dd, J = 8.2, 5.1 Hz, 2H), 7.39 (dd, J = 8.7, 1.0 Hz, 1H), 7.29 – 7.15 (m, 2H), 6.67 (ddd, J = 8.4, 6.8, 1.3 Hz, 1H). IR υ 2030.89, 1928.12, 1906.18 cm^{-1}.

2. 3. 3. Synthesis of 1NS3

PC3 (0.050 g, 0.084 mmol) was dissolved in dichloromethane (15 mL) after which 1-Naphthalenesulfonic acid (0.017 g, 0.084 mmol) was added. The mixture was stirred at room temperature for 4 hr. After the reaction was over, the mixture was filtered under vacuum over celite. The filtrate was evaporated partially after which drops of hexanes were added to it to crash out the crystals. Some crystals crashed out, but the mixture was left in the refrigerator overnight for further crystallization. The mixture was then vacuum filtered, and the dry crystals were collected and weighed. The yellow crystals (0.042 g, 75%) were characterized using IR and NMR. ^{1}H NMR (400 MHz, Methylene Chloride-d_2) δ 8.96 (dd, J = 5.1, 1.4 Hz, 2H), 8.28 (dd, J = 8.5, 1.4 Hz, 1H), 8.15 (dd, J = 8.2, 1.4 Hz, 1H), 7.74 (dd, J = 7.2, 1.3 Hz, 1H), 7.64 (dd, J = 8.2, 1.2 Hz, 1H), 7.60 – 7.48 (m, 3H), 7.45 (dd, J = 1.2 Hz, 1H), 7.38 (dd, J = 8.7, 0.9 Hz, 1H), 7.25 – 7.14 (m, 2H), 6.70 – 6.61 (m, 1H), 2.63 (d, J = 1.2 Hz, 3H). IR υ 2030.42, 1928.39, 1905.49 cm^{-1}.

2. 3. 4. Synthesis of 1NS4

PC4 (0.050 g, 0.082 mmol) was dissolved in dichloromethane (15 mL) after which 1-Naphthalenesulfonic acid (0.017 g, 0.082 mmol) was added. The mixture was stirred at room temperature for 4 hr. After the reaction was over, the mixture was filtered under vacuum over celite. The filtrate was evaporated partially after which drops of hexanes were added to it to crash out the crystals. Some crystals crashed out, but the mixture was left in the refrigerator overnight for further crystallization. The mixture was then vacuum filtered, and the dry crystals were collected and weighed. The yellow crystals (0.048 g, 86%) were characterized using IR and NMR. ^{1}H NMR (400 MHz, Chloroform-*d*) δ 8.15 (d, *J* = 8.3 Hz, 2H), 7.85 (dd, *J* = 1.7 Hz, 1H), 7.69 (d, 2H), 7.65 (s, 2H), 7.61 – 7.41 (m, 5H), 7.21 – 7.18 (m, 1H), 3.19 (s, 6H). IR υ 2029.90, 1924.54, 1904.46 cm^{-1}.

2. 3. 5. Synthesis of 1NS5

PC5 (0.050 g, 0.082 mmol) was dissolved in dichloromethane (15 mL) after which 1-Naphthalenesulfonic acid (0.017 g, 0.082 mmol) was added. The mixture was stirred at room temperature for 4 hr. After the reaction was over, the mixture was filtered under vacuum over celite. The filtrate was evaporated partially after which drops of hexanes were added to it to crash out the crystals. Some crystals crashed out, but the mixture was left in the refrigerator overnight for further crystallization. The mixture was then vacuum filtered, and the dry crystals were collected and weighed. The yellow crystals (0.045 g, 80%) were characterized using IR and NMR. ^{1}H NMR (400 MHz, Chloroform-*d*) δ 8.96 (dd, *J* = 5.0, 1.3 Hz, 2H), 8.64 (dd, *J* = 8.4, 1.3 Hz, 1H), 8.32 (dd, *J*

= 8.6, 1.3 Hz, 2H), 7.87 – 7.73 (m, 2H), 7.60 – 7.46 (m, 5H), 6.70 (ddd, *J* = 8.4, 6.8, 1.3 Hz, 1H), 2.54 (s, 6H). IR υ 2029.82, 1927.44, 1904.64 cm^{-1}.

2. 3. 6. Synthesis of 1NS6

PC6 (0.050 g, 0.068 mmol) was dissolved in dichloromethane (15 mL) after which 1-Naphthalenesulfonic acid (0.014 g, 0.068 mmol) was added. The mixture was stirred at room temperature for 4 hr. After the reaction was over, the mixture was filtered under vacuum over celite. The filtrate was evaporated partially after which drops of hexanes were added to it to crash out the crystals. Some crystals crashed out, but the mixture was left in the refrigerator overnight for further crystallization. The mixture was then vacuum filtered, and the dry crystals were collected and weighed. The yellow crystals (0.038 g, 70%) were characterized using IR and NMR. ^{1}H NMR (400 MHz, Methylene Chloride-d_2) δ 9.03 (d, *J* = 5.3 Hz, 2H), 7.87 (dd, *J* = 7.2, 1.3 Hz, 1H), 7.76 (s, 2H), 7.69 – 7.43 (m, 15H), 7.25 (dd, *J* = 8.2, 7.2 Hz, 1H), 7.11 (ddd, *J* = 8.1, 6.8, 1.2 Hz, 1H), 6.77 (ddd, *J* = 8.4, 6.8, 1.4 Hz, 1H). ^{13}C NMR (101 MHz, CD_2Cl2) δ 197.08, 192.62, 153.27, 151.82, 147.83, 139.48, 135.78, 133.87, 131.68, 130.31, 130.12, 129.52, 128.67, 128.32, 128.25, 126.71, 126.33, 126.18, 126.08, 125.99, 125.61, 124.70, 104.55, 100.39. IR υ 2029.20, 1927.27, 1904.35 cm^{-1}.

2. 3. 7. Synthesis of 1NS7

PC7 (0.050 g, 0.066 mmol) was dissolved in dichloromethane (15 mL) after which 1-Naphthalenesulfonic acid (0.014 g, 0.066 mmol) was added. The mixture was stirred at room temperature for 4 hr. After the reaction was over, the mixture was filtered under vacuum over celite. The filtrate was evaporated partially after which drops of hexanes were added to it to crash out the crystals. Some crystals crashed out, but the

mixture was left in the refrigerator overnight for further crystallization. The mixture was then vacuum filtered, and the dry crystals were collected and weighed. The yellow crystals (0.041 g, 75%) were characterized using IR and NMR. ^{1}H NMR (400 MHz, Methylene Chloride-d_2) δ 7.86 (dd, *J* = 7.2, 1.3 Hz, 1H), 7.72 – 7.62 (m, 4H), 7.61 – 7.57 (m, 1H), 7.57 – 7.50 (m, 6H), 7.47 (s, 2H), 7.46 – 7.41 (m, 4H), 7.25 (dd, *J* = 8.2, 7.2 Hz, 1H), 7.17 (ddd, *J* = 8.1, 6.8, 1.2 Hz, 1H), 6.88 (ddd, *J* = 8.4, 6.8, 1.4 Hz, 1H), 3.06 (s, 6H). ^{13}C NMR (101 MHz, CD_2Cl2) δ 196.47, 192.24, 163.66, 151.59, 148.94, 138.79, 136.19, 134.04, 131.85, 130.00, 129.81, 129.69, 129.50, 129.34, 128.59, 128.34, 127.32, 126.94, 126.84, 126.58, 126.11, 126.06, 124.67, 124.50, 31.56. IR υ 2028.51, 1922.74, 1903.57 cm^{-1}.

2. 3. 8. Synthesis of 1NS8

PC8 (0.050 g, 0.082 mmol) was dissolved in dichloromethane (15 mL) after which 1-Naphthalenesulfonic acid (0.017 g, 0.082 mmol) was added. The mixture was stirred at room temperature for 4 hr. After the reaction was over, the mixture was filtered under vacuum over celite. The filtrate was evaporated partially after which drops of hexanes were added to it to crash out the crystals. Some crystals crashed out, but the mixture was left in the refrigerator overnight for further crystallization. The mixture was then vacuum filtered, and the dry crystals were collected and weighed. The yellow crystals (0.045 g, 80%) were characterized using IR and NMR. ^{1}H NMR (400 MHz, DMSO-d_6) δ 9.39 (dd, *J* = 5.2 Hz, 1H), 9.00 (d, *J* = 5.3 Hz, 2H), 8.43 (dd, 1H), 8.02 (d, *J* = 5.2, 1.1 Hz, 1H), 7.94 (s, 2H), 7.72 – 7.63 (m, 3H), 7.55 – 7.47 (m, 1H), 7.33 – 7.18 (m, 2H), 2.76 (d, *J* = 0.8 Hz, 6H). IR υ 2028.75, 1925.39, 1903.04 cm^{-1}.

2. 3. 9. Synthesis of 1NS9

PC9 (0.050 g, 0.078 mmol) was dissolved in dichloromethane (15 mL) after which 1-Naphthalenesulfonic acid (0.016 g, 0.078 mmol) was added. The mixture was stirred at room temperature for 4 hr. After the reaction was over, the mixture was filtered under vacuum over celite. The filtrate was evaporated partially after which drops of hexanes were added to it to crash out the crystals. Some crystals crashed out, but the mixture was left in the refrigerator overnight for further crystallization. The mixture was then vacuum filtered, and the dry crystals were collected and weighed. The yellow crystals (0.044 g, 78%) were characterized using IR and NMR. ^{1}H NMR (400 MHz, Chloroform-*d*) δ 8.57 (s, 2H), 7.93 (dd, *J* = 7.2, 1.2 Hz, 1H), 7.77 (s, 2H), 7.59 (d, *J* = 8.1 Hz, 1H), 7.53 – 7.40 (m, 2H), 7.12 (s, 3H), 2.52 (s, 6H), 2.32 (s, 6H). IR υ 2027.91, 1924.01, 1901.52 cm^{-1}.

2. 3. 10. Synthesis of 1NS10

PC10 (0.050 g, 0.084 mmol) was dissolved in dichloromethane (15 mL) after which 1-Naphthalenesulfonic acid (0.017 g, 0.084 mmol) was added. The mixture was stirred at room temperature for 4 hr. After the reaction was over, the mixture was filtered under vacuum over celite. The filtrate was evaporated partially after which drops of hexanes were added to it to crash out the crystals. Some crystals crashed out, but the mixture was left in the refrigerator overnight for further crystallization. The mixture was then vacuum filtered, and the dry crystals were collected and weighed. The yellow crystals (0.040 g, 72%) were characterized using IR and NMR. ^{1}H NMR (400 MHz, Methylene Chloride-d_2) δ 8.98 (dd, *J* = 5.1, 1.4 Hz, 1H), 8.72 (d, *J* = 5.2 Hz, 1H), 8.21 (dd, *J* = 8.2, 1.5 Hz, 1H), 7.77 – 7.67 (m, 2H), 7.67 – 7.57 (m, 2H), 7.54 – 7.52 (m, 1H),

7.50 (d, *J* = 1.3 Hz, 1H), 7.33 (dd, *J* = 8.7, 1.0 Hz, 1H), 7.29 – 7.22 (m, 1H), 7.21 – 7.09 (m, 2H), 6.64 – 6.56 (m, 1H), 2.64 (d, *J* = 0.9 Hz, 3H). ^{13}C NMR (101 MHz, CD_2Cl2) δ 153.35, 152.57, 149.09, 146.88, 146.20, 138.99, 138.51, 133.50, 131.15, 129.83, 127.80, 127.66, 126.69, 126.26, 126.13, 126.03, 125.51, 125.47, 125.32, 125.26, 124.26, 123.70, 19.01. IR υ 2029.61, 1926.80, 1904.69 cm^{-1}.

2. 3. 11. Synthesis of 2NS1

PC1 (0.050 g, 0.090 mmol) was dissolved in dichloromethane (15 mL) after which 2-Naphthalenesulfonic acid (0.019 g, 0.090 mmol) was added. The mixture was stirred at room temperature for 4 hr. After the reaction was over, the mixture was filtered under vacuum over celite. The filtrate was evaporated partially after which drops of hexanes were added to it to crash out the crystals. Some crystals crashed out, but the mixture was left in the refrigerator overnight for further crystallization. The mixture was then vacuum filtered, and the dry crystals were collected and weighed. The yellow crystals (0.056 g, 99%) were characterized using IR and NMR. ^{1}H NMR (400 MHz, Methylene Chloride-d_2) δ 8.97 (dd, 2H), 8.18 – 8.05 (m, 5H), 7.93 – 7.83 (m, 2H), 7.79 – 7.73 (m, 1H), 7.65 – 7.45 (m, 5H). IR υ 2030.59, 1928.32, 1906.63 cm^{-1}.

2. 3. 12. Synthesis of 2NS2

PC2 (0.050 g, 0.086 mmol) was dissolved in dichloromethane (15 mL) after which 2-Naphthalenesulfonic acid (0.018 g, 0.086 mmol) was added. The mixture was stirred at room temperature for 4 hr. After the reaction was over, the mixture was filtered under vacuum over celite. The filtrate was evaporated partially after which drops of hexanes were added to it to crash out the crystals. Some crystals crashed out, but the mixture was left in the refrigerator overnight for further crystallization. The mixture was

then vacuum filtered, and the dry crystals were collected and weighed. The yellow crystals (0.050 g, 90%) were characterized using IR and NMR. ^{1}H NMR (400 MHz, Chloroform-*d*) δ 9.37 (dd, *J* = 5.1, 1.4 Hz, 2H), 8.50 (dd, *J* = 8.2, 1.4 Hz, 2H), 8.10 – 8.04 (m, 1H), 7.91 (s, 2H), 7.87 – 7.74 (m, 4H), 7.63 (d, *J* = 8.5 Hz, 1H), 7.55 (ddd, *J* = 7.8, 5.5, 1.6 Hz, 2H), 7.43 (dd, *J* = 8.5, 1.8 Hz, 1H). IR υ 2031.00, 1927.98, 1906.80 cm^{-1}.

2. 3. 13. Synthesis of 2NS3

PC3 (0.050 g, 0.084 mmol) was dissolved in dichloromethane (15 mL) after which 2-Naphthalenesulfonic acid (0.017 g, 0.084 mmol) was added. The mixture was stirred at room temperature for 4 hr. After the reaction was over, the mixture was filtered under vacuum over celite. The filtrate was evaporated partially after which drops of hexanes were added to it to crash out the crystals. Some crystals crashed out, but the mixture was left in the refrigerator overnight for further crystallization. The mixture was then vacuum filtered, and the dry crystals were collected and weighed. The yellow crystals (0.040 g, 71%) were characterized using IR and NMR. ^{1}H NMR (400 MHz, Chloroform-*d*) δ 9.37 (dd, *J* = 5.0, 1.3 Hz, 1H), 9.27 (dd, *J* = 5.1, 1.4 Hz, 1H), 8.52 (dd, *J* = 8.4, 1.3 Hz, 1H), 8.38 (dd, *J* = 8.3, 1.4 Hz, 1H), 7.94 (d, 1H), 7.88 – 7.68 (m, 4H), 7.64 (d, 1H), 7.59 – 7.48 (m, 3H), 7.28 (s, 1H), 2.69 (s, 3H). IR υ 2030.51, 1927.58, 1905.81 cm^{-1}.

2. 3. 14. Synthesis of 2NS4

PC4 (0.050 g, 0.082 mmol) was dissolved in dichloromethane (15 mL) after which 2-Naphthalenesulfonic acid (0.017 g, 0.082 mmol) was added. The mixture was stirred at room temperature for 4 hr. After the reaction was over, the mixture was filtered under vacuum over celite. The filtrate was evaporated partially after which drops of

hexanes were added to it to crash out the crystals. Some crystals crashed out, but the mixture was left in the refrigerator overnight for further crystallization. The mixture was then vacuum filtered, and the dry crystals were collected and weighed. The yellow crystals (0.046 g, 82%) were characterized using IR and NMR. ^{1}H NMR (400 MHz, Chloroform-*d*) δ 8.08 (d, *J* = 8.3 Hz, 2H), 7.79 – 7.75 (m, 1H), 7.59 – 7.57 (m, 3H), 7.50 (d, *J* = 8.3 Hz, 2H), 7.46 – 7.34 (m, 4H), 7.12 (s, 1H), 3.11 (s, 6H). IR υ 2029.98, 1924.63, 1904.93 cm^{-1}.

2. 3. 15. Synthesis of 2NS5

PC5 (0.050 g, 0.082 mmol) was dissolved in dichloromethane (15 mL) after which 2-Naphthalenesulfonic acid (0.017 g, 0.082 mmol) was added. The mixture was stirred at room temperature for 4 hr. After the reaction was over, the mixture was filtered under vacuum over celite. The filtrate was evaporated partially after which drops of hexanes were added to it to crash out the crystals. Some crystals crashed out, but the mixture was left in the refrigerator overnight for further crystallization. The mixture was then vacuum filtered, and the dry crystals were collected and weighed. The yellow crystals (0.039 g, 70%) were characterized using IR and NMR. ^{1}H NMR (400 MHz, DMSO-d_6) δ 9.48 (dd, *J* = 5.1, 1.2 Hz, 2H), 9.14 (dd, *J* = 8.6, 1.3 Hz, 2H), 8.20 – 8.10 (m, 3H), 7.94 (dd, *J* = 6.2, 3.4 Hz, 1H), 7.90 – 7.80 (m, 2H), 7.70 (dd, *J* = 8.5, 1.7 Hz, 1H), 7.49 (dd, *J* = 6.2, 3.2 Hz, 2H), 2.79 (s, 6H). IR υ 2029.99, 1927.55, 1905.06 cm^{-1}.

2. 3. 16. Synthesis of 2NS6

PC6 (0.050 g, 0.068 mmol) was dissolved in dichloromethane (15 mL) after which 2-Naphthalenesulfonic acid (0.014 g, 0.068 mmol) was added. The mixture was stirred at room temperature for 4 hr. After the reaction was over, the mixture was filtered

under vacuum over celite. The filtrate was evaporated partially after which drops of hexanes were added to it to crash out the crystals. Some crystals crashed out, but the mixture was left in the refrigerator overnight for further crystallization. The mixture was then vacuum filtered, and the dry crystals were collected and weighed. The yellow crystals (0.040 g, 73%) were characterized using IR and NMR. ^{1}H NMR (400 MHz, Methylene Chloride-d_2) δ 9.20 (d, J = 5.3 Hz, 2H), 7.81 (s, 2H), 7.64 – 7.57 (m, 4H), 7.54 – 7.49 (m, 6H), 7.46 – 7.31 (m, 8H), 7.16 (dd, J = 8.6, 1.8 Hz, 1H). ^{13}C NMR (101 MHz, CD_2Cl2) δ 197.19, 192.60, 153.64, 152.22, 148.05, 140.91, 135.79, 134.09, 132.49, 130.34, 130.15, 130.06, 129.74, 129.53, 129.18, 129.03, 128.24, 127.93, 127.90, 127.19, 126.41, 126.29, 125.83, 123.01. IR υ 2029.15, 1926.48, 1905.14 cm^{-1}.

2. 3. 17. Synthesis of 2NS7

PC7 (0.050 g, 0.066 mmol) was dissolved in dichloromethane (15 mL) after which 2-Naphthalenesulfonic acid (0.014 g, 0.066 mmol) was added. The mixture was stirred at room temperature for 4 hr. After the reaction was over, the mixture was filtered under vacuum over celite. The filtrate was evaporated partially after which drops of hexanes were added to it to crash out the crystals. Some crystals crashed out, but the mixture was left in the refrigerator overnight for further crystallization. The mixture was then vacuum filtered, and the dry crystals were collected and weighed. The yellow crystals (0.041 g, 74%) were characterized using IR and NMR. ^{1}H NMR (400 MHz, Chloroform-d) δ 8.15 (dd, J = 1.7 Hz, 1H), 7.84 (s, 2H), 7.67 – 7.45 (m, 17H), 7.40 (dd, J = 8.6, 1.8 Hz, 1H), 3.30 (d, J = 2.0 Hz, 6H). IR υ 2028.44, 1923.00, 1903.75 cm^{-1}.

2. 3. 18. Synthesis of 2NS8

PC8 (0.050 g, 0.082 mmol) was dissolved in dichloromethane (15 mL) after which 2-Naphthalenesulfonic acid (0.017 g, 0.082 mmol) was added. The mixture was stirred at room temperature for 4 hr. After the reaction was over, the mixture was filtered under vacuum over celite. The filtrate was evaporated partially after which drops of hexanes were added to it to crash out the crystals. Some crystals crashed out, but the mixture was left in the refrigerator overnight for further crystallization. The mixture was then vacuum filtered, and the dry crystals were collected and weighed. The yellow crystals (0.043 g, 77%) were characterized using IR and NMR. ^{1}H NMR (400 MHz, DMSO-d_6) δ 9.20 (d, J = 5.2 Hz, 2H), 8.04 (s, 2H), 7.81 (d, J = 5.3, 1.0 Hz, 2H), 7.63 – 7.55 (m, 2H), 7.49 – 7.41 (m, 2H), 6.72 (dd, J = 8.5, 1.8 Hz, 1H), 5.76 (d, 2H), 2.73 (s, 6H). IR υ 2028.17, 1924.36, 1902.05 cm^{-1}.

2. 3. 19. Synthesis of 2NS9

PC9 (0.050 g, 0.078 mmol) was dissolved in dichloromethane (15 mL) after which 2-Naphthalenesulfonic acid (0.016 g, 0.078 mmol) was added. The mixture was stirred at room temperature for 4 hr. After the reaction was over, the mixture was filtered under vacuum over celite. The filtrate was evaporated partially after which drops of hexanes were added to it to crash out the crystals. Some crystals crashed out, but the mixture was left in the refrigerator overnight for further crystallization. The mixture was then vacuum filtered, and the dry crystals were collected and weighed. The yellow crystals (0.042 g, 76%) were characterized using IR and NMR. ^{1}H NMR (400 MHz, Chloroform-d) δ 9.08 (s, 1H), 9.00 (s, 2H), 7.99 (s, 2H), 7.93 – 7.88 (m, 1H), 7.83 – 7.66

(m, 2H), 7.59 – 7.51 (m, 1H), 7.47 – 7.41 (m, 1H), 7.19 (dd, *J* = 8.6, 1.8 Hz, 1H), 2.62 (s, 6H), 2.48 (s, 6H). IR υ 2027.91, 1924.01, 1901.52 cm^{-1}.

2. 3. 20. Synthesis of 2NS10

PC10 (0.050 g, 0.084 mmol) was dissolved in dichloromethane (15 mL) after which 2-Naphthalenesulfonic acid (0.017 g, 0.084 mmol) was added. The mixture was stirred at room temperature for 4 hr. After the reaction was over, the mixture was filtered under vacuum over celite. The filtrate was evaporated partially after which drops of hexanes were added to it to crash out the crystals. Some crystals crashed out, but the mixture was left in the refrigerator overnight for further crystallization. The mixture was then vacuum filtered, and the dry crystals were collected and weighed. The yellow crystals (0.039 g, 70%) were characterized using IR and NMR. ^{1}H NMR (400 MHz, Chloroform-*d*) δ 9.22 (dd, *J* = 5.1, 1.4 Hz, 1H), 9.04 (d, *J* = 5.2 Hz, 1H), 8.37 (dd, *J* = 8.2, 1.4 Hz, 1H), 7.84 (d, *J* = 2.3 Hz, 2H), 7.72 – 7.50 (m, 4H), 7.46 – 7.34 (m, 4H), 7.12 (s, 1H), 2.64 (d, *J* = 0.8 Hz, 3H). IR υ 2030.06, 1926.42, 1905.73 cm^{-1}.

2. 3. 21. Synthesis of TOS1

PC1 (0.050 g, 0.090 mmol) was dissolved in dichloromethane (15 mL) after which *p*-toluenesulfonic acid (0.016 g, 0.090 mmol) was added. The mixture was stirred at room temperature for 1 hr. After the reaction was over, the mixture was filtered under vacuum over celite. The filtrate was evaporated partially after which drops of hexanes were added to it to crash out the crystals. Some crystals crashed out, but the mixture was left in the refrigerator overnight for further crystallization. The mixture was then vacuum filtered, and the dry crystals were collected and weighed. The yellow crystals (0.044 g, 84%) were characterized using IR and NMR. ^{1}H NMR (400 MHz, Methylene Chloride-

d$_2$) δ 9.04 – 8.98 (m, 4H), 8.19 – 8.17 (m, 2H), 7.72 – 7.57 (m, 2H), 7.43 – 7.37 (m, 2H), 7.14 (s, 2H), 2.39 (s, 3H). IR υ 2030.25, 1927.18, 1906.50 cm^{-1}.

2. 3. 22. Synthesis of TOS2

PC2 (0.050 g, 0.086 mmol) was dissolved in dichloromethane (15 mL) after which *p*-toluenesulfonic acid (0.016 g, 0.086 mmol) was added. The mixture was stirred at room temperature for 1 hr. After the reaction was over, the mixture was filtered under vacuum over celite. The filtrate was evaporated partially after which drops of hexanes were added to it to crash out the crystals. Some crystals crashed out, but the mixture was left in the refrigerator overnight for further crystallization. The mixture was then vacuum filtered, and the dry crystals were collected and weighed. The yellow crystals (0.049 g, 90%) were characterized using IR and NMR. ^{1}H NMR (500 MHz, Chloroform-*d*) δ 9.35 (dd, *J* = 4.6 Hz, 2H), 8.57 (dd, 2H), 7.99 (s, 2H), 7.85 (dd, 2H), 7.47 (d, *J* = 8.0, 1.9 Hz, 2H), 7.07 (d, *J* = 7.8 Hz, 2H), 2.34 (d, *J* = 2.3 Hz, 3H). ^{13}C NMR (126 MHz, $CDCl_3$) δ 196.09, 191.88, 153.84, 147.18, 140.73, 139.71, 138.75, 130.55, 128.74, 127.57, 126.35, 125.89, 77.27, 77.22, 77.02, 76.77, 21.38. IR υ 2030.48, 1927.26, 1905.99 cm^{-1}.

2. 3. 23. Synthesis of TOS3

PC3 (0.050 g, 0.084 mmol) was dissolved in dichloromethane (15 mL) after which *p*-toluenesulfonic acid (0.016 g, 0.084 mmol) was added. The mixture was stirred at room temperature for 1 hr. After the reaction was over, the mixture was filtered under vacuum over celite. The filtrate was evaporated partially after which drops of hexanes were added to it to crash out the crystals. Some crystals crashed out, but the mixture was left in the refrigerator overnight for further crystallization. The mixture was then vacuum filtered, and the dry crystals were collected and weighed. The yellow crystals (0.045 g,

85%) were characterized using IR and NMR. ^{1}H NMR (400 MHz, Chloroform-*d*) δ 9.39 (dd, *J* = 5.1, 1.4 Hz, 1H), 9.29 (dd, *J* = 5.1, 1.4 Hz, 1H), 8.69 (dd, *J* = 8.4, 1.4 Hz, 1H), 8.47 (dd, *J* = 8.3, 1.4 Hz, 1H), 7.90 (dd, *J* = 8.4, 5.1 Hz, 1H), 7.85 – 7.80 (m, 2H), 7.47 (d, *J* = 8.2 Hz, 2H), 7.07 (d, *J* = 7.8 Hz, 2H), 2.87 (s, 3H), 2.34 (s, 3H). ^{13}C NMR (101 MHz, $CDCl_3$) δ 196.19, 191.99, 153.55, 153.00, 147.56, 146.64, 140.63, 139.79, 137.80, 135.52, 135.40, 130.95, 130.32, 128.67, 126.38, 126.38, 125.90, 125.63, 77.33, 77.21, 77.01, 76.82, 76.69, 21.38, 18.81. IR υ 2030.03, 1926.69, 1905.28 cm^{-1}.

2. 3. 24. Synthesis of TOS4

PC4 (0.050 g, 0.082 mmol) was dissolved in dichloromethane (15 mL) after which *p*-toluenesulfonic acid (0.015 g, 0.082 mmol) was added. The mixture was stirred at room temperature for 1 hr. After the reaction was over, the mixture was filtered under vacuum over celite. The filtrate was evaporated partially after which drops of hexanes were added to it to crash out the crystals. Some crystals crashed out, but the mixture was left in the refrigerator overnight for further crystallization. The mixture was then vacuum filtered, and the dry crystals were collected and weighed. The yellow crystals (0.046 g, 87%) were characterized using IR and NMR. ^{1}H NMR (400 MHz, Chloroform-*d*) δ 8.21 (d, *J* = 8.3 Hz, 2H), 7.72 (s, 2H), 7.60 (d, *J* = 8.3 Hz, 2H), 7.19 (d, *J* = 8.2 Hz, 2H), 6.90 (dd, *J* = 7.9, 0.7 Hz, 2H), 3.14 (s, 6H), 2.19 (s, 3H). IR υ 2029.64, 1923.28, 1904.34 cm^{-1}.

2. 3. 25. Synthesis of TOS5

PC5 (0.050 g, 0.082 mmol) was dissolved in dichloromethane (15 mL) after which *p*-toluenesulfonic acid (0.015 g, 0.082 mmol) was added. The mixture was stirred at room temperature for 1 hr. After the reaction was over, the mixture was filtered under vacuum over celite. The filtrate was evaporated partially after which drops of hexanes

were added to it to crash out the crystals. Some crystals crashed out, but the mixture was left in the refrigerator overnight for further crystallization. The mixture was then vacuum filtered, and the dry crystals were collected and weighed. The yellow crystals (0.038 g, 72%) were characterized using IR and NMR. ^{1}H NMR (400 MHz, Chloroform-*d*) δ 9.17 (dd, *J* = 5.0, 1.1 Hz, 2H), 8.59 (dd, *J* = 8.6, 1.3 Hz, 2H), 7.73 (dd, *J* = 8.5, 5.0 Hz, 2H), 7.31 (d, *J* = 7.9 Hz, 2H), 6.92 (d, *J* = 7.9 Hz, 2H), 2.67 (s, 6H), 2.20 (s, 3H). IR υ 2029.39, 1925.84, 1904.50 cm^{-1}.

2. 3. 26. Synthesis of TOS6

PC6 (0.050 g, 0.068 mmol) was dissolved in dichloromethane (15 mL) after which *p*-toluenesulfonic acid (0.013 g, 0.068 mmol) was added. The mixture was stirred at room temperature for 1 hr. After the reaction was over, the mixture was filtered under vacuum over celite. The filtrate was evaporated partially after which drops of hexanes were added to it to crash out the crystals. Some crystals crashed out, but the mixture was left in the refrigerator overnight for further crystallization. The mixture was then vacuum filtered, and the dry crystals were collected and weighed. The yellow crystals (0.041 g, 78%) were characterized using IR and NMR. ^{1}H NMR (400 MHz, Chloroform-*d*) δ 9.39 (d, *J* = 5.3 Hz, 2H), 8.04 (s, 2H), 7.78 (d, *J* = 5.3 Hz, 2H), 7.65 – 7.55 (m, 12H), 7.12 (d, 2H), 2.34 (s, 3H). ^{13}C NMR (101 MHz, $CDCl_3$) δ 196.34, 192.24, 153.29, 151.74, 147.87, 140.72, 139.73, 135.45, 129.98, 129.55, 129.41, 129.25, 128.77, 128.76, 128.36, 126.51, 126.00, 125.56, 21.41. IR υ 2028.94, 1926.51, 1904.51 cm^{-1}.

2. 3. 27. Synthesis of TOS7

PC7 (0.050 g, 0.066 mmol) was dissolved in dichloromethane (15 mL) after which *p*-toluenesulfonic acid (0.012 g, 0.066 mmol) was added. The mixture was stirred

at room temperature for 1 hr. After the reaction was over, the mixture was filtered under vacuum over celite. The filtrate was evaporated partially after which drops of hexanes were added to it to crash out the crystals. Some crystals crashed out, but the mixture was left in the refrigerator overnight for further crystallization. The mixture was then vacuum filtered, and the dry crystals were collected and weighed. The yellow crystals (0.042 g, 80%) were characterized using IR and NMR. ^{1}H NMR (400 MHz, Chloroform-*d*) δ 7.86 (s, 2H), 7.67 (s, 2H), 7.61 – 7.56 (m, 6H), 7.54 – 7.50 (m, 4H), 7.43 (d, 2H), 7.06 (d, 2H), 3.31 (s, 6H), 2.30 (s, 3H). ^{13}C NMR (101 MHz, $CDCl_3$) δ 195.78, 192.01, 163.42, 151.38, 148.88, 140.63, 139.55, 135.79, 135.46, 129.67, 129.44, 129.23, 129.05, 128.73, 127.21, 126.49, 126.30, 124.35, 31.19, 21.36. IR υ 2028.36, 1922.94, 1903.18 cm^{-1}.

2. 3. 28. Synthesis of TOS8

PC8 (0.050 g, 0.082 mmol) was dissolved in dichloromethane (15 mL) after which *p*-toluenesulfonic acid (0.015 g, 0.082 mmol) was added. The mixture was stirred at room temperature for 1 hr. After the reaction was over, the mixture was filtered under vacuum over celite. The filtrate was evaporated partially after which drops of hexanes were added to it to crash out the crystals. Some crystals crashed out, but the mixture was left in the refrigerator overnight for further crystallization. The mixture was then vacuum filtered, and the dry crystals were collected and weighed. The yellow crystals (0.040 g, 75%) were characterized using IR and NMR. ^{1}H NMR (400 MHz, Chloroform-*d*) δ 9.07 (d, *J* = 5.2 Hz, 2H), 8.02 (s, 2H), 7.53 (d, *J* = 5.1 Hz, 2H), 7.33 (d, *J* = 8.1 Hz, 2H), 6.93 (d, *J* = 7.9 Hz, 2H), 2.80 (s, 6H), 2.21 (s, 3H). IR υ 2028.55, 1924.51, 1902.79 cm^{-1}.

2. 3. 29. Synthesis of TOS9

PC9 (0.050 g, 0.078 mmol) was dissolved in dichloromethane (15 mL) after which *p*-toluenesulfonic acid (0.015 g, 0.078 mmol) was added. The mixture was stirred at room temperature for 1 hr. After the reaction was over, the mixture was filtered under vacuum over celite. The filtrate was evaporated partially after which drops of hexanes were added to it to crash out the crystals. Some crystals crashed out, but the mixture was left in the refrigerator overnight for further crystallization. The mixture was then vacuum filtered, and the dry crystals were collected and weighed. The yellow crystals (0.042 g, 80%) were characterized using IR and NMR. ^{1}H NMR (400 MHz, Acetone-d_6) δ 9.11 (d, 2H), 8.39 (d, 2H), 6.89 (s, 2H), 6.87 (s, 2H), 5.63 (s, 6H), 2.68 (s, 6H), 2.30 (s, 3H). IR υ 2027.70, 1923.03, 1901.14 cm^{-1}.

2. 3. 30. Synthesis of TOS10

PC10 (0.050 g, 0.084 mmol) was dissolved in dichloromethane (15 mL) after which *p*-toluenesulfonic acid (0.016 g, 0.084 mmol) was added. The mixture was stirred at room temperature for 1 hr. After the reaction was over, the mixture was filtered under vacuum over celite. The filtrate was evaporated partially after which drops of hexanes were added to it to crash out the crystals. Some crystals crashed out, but the mixture was left in the refrigerator overnight for further crystallization. The mixture was then vacuum filtered, and the dry crystals were collected and weighed. The yellow crystals (0.040 g, 75%) were characterized using IR and NMR. ^{1}H NMR (400 MHz, Chloroform-*d*) δ 9.24 (dd, *J* = 5.1, 1.4 Hz, 1H), 9.08 (d, *J* = 5.2 Hz, 1H), 8.50 – 8.41 (m, 1H), 7.93 – 7.81 (m, 1H), 7.74 (d, *J* = 8.2, 5.1 Hz, 1H), 7.55 (d, *J* = 6.7 Hz, 2H), 7.12 (d, 2H), 6.93 (d, *J* = 8.0 Hz, 2H), 2.80 (d, *J* = 0.8 Hz, 3H), 2.21 (s, 3H). IR υ 2029.50, 1925.85, 1904.32 cm^{-1}.

2. 4. X-ray Crystallographic analysis for sulfonato complexes

The following is the x-ray crystallographic analysis performed for the following compounds: 1NS1, 1NS2, 1NS4, 1NS7, 2NS4, 2NS5, 2NS6, 2NS7, TOS3, TOS4, and TOS5.

2. 4. 1. X-ray Crystallographic analysis for 1NS1

The X-ray crystallographic analysis was performed on a yellow needle-like specimen of 1NS1 with approximate dimensions of 0.02 mm × 0.09 mm × 0.23 mm. A Bruker APEX-II CCD system equipped with a graphite monochromator and a MoKα sealed tube (λ = 0.71073 Å) was used to measure the X-ray intensity data. The data collection temperature was 150 K. Also, the total exposure time was 25.25 hours.

Using a narrow-frame algorithm, the frames were integrated with the Bruker SAINT package. The data integration using a monoclinic unit cell produced 6812 reflections to a maximum θ angle of 31.00° (0.69 Å resolution) of which 6812 were independent (average redundancy 1.000, completeness = 99.9%) and 5950 (87.35%) were greater than $2\sigma(F^2)$. The final cell constants are a = 6.7140(6) Å, b = 18.9901(16) Å, c = 16.7714(14) Å, β = 95.9900(10)°, V = 2126.7(3) $Å^3$. These are based upon the refinement of the XYZ-centroids of 3250 reflections above 20 σ(I) with 4.884° < 2θ < 64.76°. Using the multi-scan method (SADABS), data were corrected for absorption effects. The Bruker SHELXTL Software Package was used to solve and refine the structure with Z = 4 for the formula unit, $C_{23}H_{15}N_2O_6ReS$. The final anisotropic full-matrix least-squares refinement on F^2 with 299 variables converged at wR_2 = 6.95% for all data and R_1 = 3.17% for the observed data. The goodness of fit was 1.015. The largest peak in the final difference electron density synthesis was 1.052 $e^-/Å^3$. The largest hole was -3.737 $e^-/Å^3$

with an RMS deviation of 0.154 $e^-/Å^3$. The calculated density was 1.979 g/cm^3 and F(000), 1224 e^- based on the final model.

Table 3: Sample and crystal data for 1NS1

Chemical formula	$C_{23}H_{15}N_2O_6ReS$	
Formula weight	633.63	
Temperature	150(2) K	
Wavelength	0.71073 Å	
Crystal size	0.02 × 0.09 × 0.23 mm	
Crystal habit	yellow needle	
Crystal system	monoclinic	
Unit cell dimensions	a = 6.7140(6) Å	α = 90°
	b = 18.9901(16) Å	β = 95.9900(10) °
	c = 16.7714(14) Å	γ = 90°
Volume	2126.7(3) $Å^3$	
Z	4	
Density (calculated)	1.979 Mg/cm^3	
Absorption coefficient	5.857 mm^{-1}	
F(000)	1224	

Table 4: Atomic coordinates and equivalent isotropic atomic displacement parameters (Å2) for 1NS1.

	x/a	y/b	z/c	U(eq)
Re1	0.13421(2)	0.34457(2)	0.93744(2)	0.01664(4)
C1	0.9887(6)	0.4299(2)	0.9227(2)	0.0240(8)
O1	0.8963(5)	0.48147(16)	0.91299(18)	0.0345(7)
C2	0.9591(7)	0.3053(2)	0.8500(2)	0.0252(8)
O2	0.8548(6)	0.28311(17)	0.79790(19)	0.0385(8)
C3	0.3065(7)	0.3757(2)	0.8595(2)	0.0260(8)
O3	0.4103(6)	0.39534(19)	0.8144(2)	0.0430(9)
O11	0.2945(4)	0.24795(14)	0.96875(16)	0.0217(5)
O12	0.1155(5)	0.15269(16)	0.8957(2)	0.0394(8)
O13	0.4130(6)	0.20373(19)	0.8471(2)	0.0468(10)
S1	0.30809(15)	0.18555(5)	0.91460(5)	0.02105(18)
C10	0.4658(6)	0.12775(19)	0.9762(2)	0.0200(7)
C11	0.6449(6)	0.1095(2)	0.9497(3)	0.0274(8)
C12	0.7785(7)	0.0644(2)	0.9954(3)	0.0352(10)
C13	0.7298(7)	0.0396(2)	0.0668(3)	0.0379(11)
C14	0.5488(7)	0.0578(2)	0.0976(3)	0.0279(9)
C15	0.4986(8)	0.0331(3)	0.1731(3)	0.0384(11)
C16	0.3227(9)	0.0519(3)	0.2021(3)	0.0396(12)
C17	0.1895(8)	0.0974(2)	0.1573(3)	0.0328(10)
C18	0.2304(7)	0.1222(2)	0.0837(2)	0.0244(8)
C19	0.4100(6)	0.1034(2)	0.0518(2)	0.0210(7)
N20	0.3231(5)	0.37738(16)	0.04441(18)	0.0185(6)
C21	0.4942(6)	0.4139(2)	0.0443(3)	0.0236(8)
C22	0.6149(7)	0.4310(2)	0.1139(3)	0.0299(9)
C23	0.5565(7)	0.4087(2)	0.1867(3)	0.0342(10)
C24	0.3806(6)	0.3710(2)	0.1879(2)	0.0268(8)
C25	0.2663(6)	0.35545(18)	0.1159(2)	0.0189(7)
C26	0.0751(5)	0.3167(2)	0.1115(2)	0.0183(7)
C27	0.9967(6)	0.2900(2)	0.1786(2)	0.0234(8)
C28	0.8140(7)	0.2560(2)	0.1695(2)	0.0275(8)
C29	0.7131(6)	0.2483(2)	0.0941(2)	0.0248(8)
C30	0.7990(6)	0.2755(2)	0.0288(2)	0.0215(7)
N31	0.9770(5)	0.30857(16)	0.03683(18)	0.0168(6)

Table 5: Bond lengths (Å) for 1NS1

Re1-C1	1.894(4)	Re1-C3	1.927(4)
Re1-C2	1.931(4)	Re1-O11	2.164(3)
Re1-N31	2.174(3)	Re1-N20	2.177(3)
C1-O1	1.162(5)	C2-O2	1.142(5)
C3-O3	1.143(5)	O11-S1	1.502(3)
O12-S1	1.441(3)	O13-S1	1.436(3)
S1-C10	1.779(4)	C10-C11	1.369(6)
C10-C19	1.436(5)	C11-C12	1.408(6)
C11-H11	0.95	C12-C13	1.358(7)
C12-H12	0.95	C13-C14	1.412(7)
C13-H13	0.95	C14-C15	1.423(7)
C14-C19	1.436(6)	C15-C16	1.371(8)
C15-H15	0.95	C16-C17	1.404(7)
C16-H16	0.95	C17-C18	1.375(6)
C17-H17	0.95	C18-C19	1.415(6)
C18-H18	0.95	N20-C21	1.342(5)
N20-C25	1.361(5)	C21-C22	1.388(6)
C21-H21	0.95	C22-C23	1.388(7)
C22-H22	0.95	C23-C24	1.383(6)
C23-H23	0.95	C24-C25	1.392(5)
C24-H24	0.95	C25-C26	1.474(5)
C26-N31	1.361(4)	C26-C27	1.387(5)
C27-C28	1.381(6)	C27-H27	0.95
C28-C29	1.379(6)	C28-H28	0.95
C29-C30	1.388(5)	C29-H29	0.95
C30-N31	1.345(5)	C30-H30	0.95

Table 6: Bond angles (°) for 1NS1

C1-Re1-C3	89.26(18)	C1-Re1-C2	88.07(17)
C3-Re1-C2	87.95(18)	C1-Re1-O11	173.35(13)
C3-Re1-O11	96.11(15)	C2-Re1-O11	96.01(14)
C1-Re1-N31	94.80(15)	C3-Re1-N31	172.12(15)
C2-Re1-N31	98.92(14)	O11-Re1-N31	79.41(11)
C1-Re1-N20	96.37(14)	C3-Re1-N20	97.58(15)
C2-Re1-N20	172.93(14)	O11-Re1-N20	79.08(11)
N31-Re1-N20	75.28(12)	O1-C1-Re1	178.7(4)
O2-C2-Re1	178.9(4)	O3-C3-Re1	178.5(4)
S1-O11-Re1	125.63(15)	O13-S1-O12	115.7(2)
O13-S1-O11	110.6(2)	O12-S1-O11	111.40(19)
O13-S1-C10	107.1(2)	O12-S1-C10	109.07(19)
O11-S1-C10	101.89(16)	C11-C10-C19	121.6(4)
C11-C10-S1	117.2(3)	C19-C10-S1	121.1(3)
C10-C11-C12	120.6(4)	C10-C11-H11	119.7
C12-C11-H11	119.7	C13-C12-C11	119.5(4)
C13-C12-H12	120.2	C11-C12-H12	120.2
C12-C13-C14	122.3(4)	C12-C13-H13	118.9
C14-C13-H13	118.9	C13-C14-C15	122.6(4)
C13-C14-C19	119.2(4)	C15-C14-C19	118.3(4)
C16-C15-C14	121.5(4)	C16-C15-H15	119.2
C14-C15-H15	119.2	C15-C16-C17	119.6(4)
C15-C16-H16	120.2	C17-C16-H16	120.2
C18-C17-C16	121.1(5)	C18-C17-H17	119.5
C16-C17-H17	119.5	C17-C18-C19	120.7(4)
C17-C18-H18	119.7	C19-C18-H18	119.7
C18-C19-C14	118.8(4)	C18-C19-C10	124.3(4)
C14-C19-C10	116.8(4)	C21-N20-C25	118.6(3)
C21-N20-Re1	124.9(3)	C25-N20-Re1	116.5(2)
N20-C21-C22	123.0(4)	N20-C21-H21	118.5
C22-C21-H21	118.5	C23-C22-C21	118.3(4)
C23-C22-H22	120.8	C21-C22-H22	120.8
C24-C23-C22	119.4(4)	C24-C23-H23	120.3
C22-C23-H23	120.3	C23-C24-C25	119.5(4)
C23-C24-H24	120.3	C25-C24-H24	120.3
N20-C25-C24	121.2(4)	N20-C25-C26	115.5(3)
C24-C25-C26	123.2(4)	N31-C26-C27	121.1(3)
N31-C26-C25	116.0(3)	C27-C26-C25	122.9(3)
C28-C27-C26	119.3(4)	C28-C27-H27	120.3
C26-C27-H27	120.3	C29-C28-C27	119.7(4)
C29-C28-H28	120.1	C27-C28-H28	120.1
C28-C29-C30	118.6(4)	C28-C29-H29	120.7
C30-C29-H29	120.7	N31-C30-C29	122.2(4)
N31-C30-H30	118.9	C29-C30-H30	118.9
C30-N31-C26	119.0(3)	C30-N31-Re1	124.6(2)
C26-N31-Re1	116.3(2)		

Table 7: Anisotropic atomic displacement parameters (Å2) for 1NS1

Re1	0.02064(6)	0.01571(6)	0.01342(6)	0.00004(6)	0.00109(5)	0.00139(6)
C1	0.031(2)	0.0234(19)	0.0166(16)	-0.0005(14)	-0.0014(15)	-0.0010(16)
O1	0.0454(19)	0.0293(16)	0.0272(15)	-0.0004(12)	-0.0042(14)	0.0145(14)
C2	0.033(2)	0.0223(19)	0.0202(17)	0.0007(15)	0.0027(16)	0.0037(17)
O2	0.048(2)	0.0358(17)	0.0279(16)	-0.0032(14)	-0.0139(15)	-0.0021(16)
C3	0.031(2)	0.0230(19)	0.0246(19)	-0.0033(15)	0.0064(17)	0.0004(17)
O3	0.053(2)	0.046(2)	0.0338(17)	0.0004(15)	0.0235(16)	-0.0064(18)
O11	0.0283(14)	0.0174(12)	0.0186(12)	-0.0014(10)	-0.0016(11)	0.0030(11)
O12	0.0384(18)	0.0286(16)	0.046(2)	-0.0025(15)	-0.0211(15)	-0.0016(15)
O13	0.068(3)	0.050(2)	0.0275(16)	0.0160(15)	0.0271(17)	0.0245(19)
S1	0.0286(5)	0.0202(4)	0.0142(4)	-0.0006(3)	0.0020(3)	0.0046(4)
C10	0.0257(18)	0.0139(16)	0.0200(17)	-0.0017(13)	0.0005(14)	0.0003(14)
C11	0.027(2)	0.0216(18)	0.035(2)	-0.0050(16)	0.0076(18)	0.0002(16)
C12	0.027(2)	0.023(2)	0.054(3)	-0.008(2)	0.000(2)	0.0039(17)
C13	0.024(2)	0.026(2)	0.062(3)	-0.002(2)	-0.008(2)	0.0042(18)
C14	0.030(2)	0.0198(18)	0.032(2)	0.0003(16)	-0.0081(17)	-0.0022(16)
C15	0.051(3)	0.029(2)	0.031(2)	0.0075(19)	-0.016(2)	-0.006(2)
C16	0.063(3)	0.034(2)	0.020(2)	0.0047(18)	-0.001(2)	-0.010(2)
C17	0.045(3)	0.032(2)	0.0222(19)	0.0009(17)	0.0050(19)	-0.006(2)
C18	0.030(2)	0.0231(19)	0.0206(18)	0.0001(15)	0.0026(15)	-0.0055(16)
C19	0.0241(18)	0.0182(17)	0.0204(17)	-0.0007(13)	0.0010(14)	-0.0037(14)
N20	0.0196(15)	0.0169(15)	0.0185(14)	-0.0009(11)	0.0002(11)	0.0006(12)
C21	0.0246(19)	0.0176(17)	0.0288(19)	0.0008(15)	0.0033(16)	-0.0014(15)
C22	0.025(2)	0.0228(19)	0.041(2)	-0.0032(18)	-0.0028(18)	-0.0068(16)
C23	0.033(2)	0.035(2)	0.032(2)	-0.0077(19)	-0.0100(19)	-0.0049(19)
C24	0.028(2)	0.029(2)	0.0211(18)	-0.0032(16)	-0.0056(16)	-0.0028(17)
C25	0.0212(17)	0.0177(17)	0.0172(15)	-0.0001(13)	-0.0003(13)	0.0020(13)
C26	0.0174(16)	0.0206(17)	0.0166(16)	-0.0002(13)	0.0004(13)	0.0030(14)
C27	0.0269(19)	0.028(2)	0.0146(16)	0.0025(14)	0.0016(14)	0.0008(16)
C28	0.031(2)	0.029(2)	0.0237(19)	0.0053(16)	0.0060(16)	-0.0002(17)
C29	0.025(2)	0.0229(19)	0.0273(19)	-0.0011(15)	0.0042(16)	-0.0050(15)
C30	0.0194(17)	0.0204(17)	0.0241(18)	-0.0008(15)	-0.0006(15)	-0.0032(14)
N31	0.0177(14)	0.0167(14)	0.0160(13)	-0.0015(11)	0.0013(11)	0.0006(12)

2. 4. 2. X-ray Crystallographic analysis for 1NS2

The X-ray crystallographic analysis was performed on a yellow prism-like specimen of 1NS2 with approximate dimensions of 0.05 mm × 0.14 mm × 0.17 mm. A Bruker APEX-II CCD system equipped with a graphite monochromator and a MoKα sealed tube (λ = 0.71073 Å) was used to measure the X-ray intensity data. The data collection temperature was 150 K. Also, the total exposure time was 4.21 hours.

Using a narrow-frame algorithm, the frames were integrated with the Bruker SAINT package. The data integration using a triclinic unit cell produced 20149 reflections to a maximum θ angle of 31.00° (0.69 Å resolution) of which 7010 were independent (average redundancy 2.874, completeness = 99.0%, R_{int} = 2.58%) and 6358 (90.70%) were greater than $2\sigma(F^2)$. The final cell constants are *a* = 9.5538(8) Å, *b* = 9.8025(8) Å, *c* = 12.7905(11) Å, α = 73.6439(13)°, β = 89.3485(13)°, γ = 75.6584(14)°, *V* = 1111.35(16) $Å^3$. These are based upon the refinement of the XYZ-centroids of 861 reflections above 20 σ(I) with 3.415° < 2θ < 64.21°. Using the integration method (SADABS), data were corrected for absorption effects. The calculated minimum and maximum transmission coefficients (based on crystal size) are 0.4180 and 0.7550.

Table 8: Sample and crystal data for 1NS2

Chemical formula	$C_{25}H_{15}N_2O_6ReS$	
Formula weight	657.65	
Temperature	150(2) K	
Wavelength	0.71073 Å	
Crystal size	0.05 × 0.14 × 0.17 mm	
Crystal habit	yellow prism	
Crystal system	triclinic	
Space group	P-1	
Unit cell dimensions	a = 9.5538(8) Å	α = 73.6439(13)°
	b = 9.8025(8) Å	β = 89.3485(13)°
	c = 12.7905(11) Å	γ = 75.6584(14)°
Volume	1111.35(16) $Å^3$	
Z	2	
Density (calculated)	1.965 Mg/cm^3	
Absorption coefficient	5.608 mm^{-1}	
F(000)	636	

The Bruker SHELXTL Software Package was used to solve and refine the structure, using the space group P-1, with Z = 2 for the formula unit, $C_{25}H_{15}N_2O_6ReS$. The final anisotropic full-matrix least-squares refinement on F^2 with 316 variables converged at wR_2 = 4.44% for all data and R_1 = 2.22% for the observed data. The goodness-of-fit was 1.000. The largest peak in the final difference electron density synthesis was 1.137 $e^-/Å^3$. The largest hole was -1.046 $e^-/Å^3$ with an RMS deviation of 0.104 $e^-/Å^3$. The calculated density was 1.965 g/cm^3 and F(000), 636 e^- based on the final model.

Table 9: Atomic coordinates and equivalent isotropic atomic displacement parameters (Å2) for 1NS2

Re1	0.24148(2)	0.50736(2)	0.17034(2)	0.02306(3)
C1	0.2238(3)	0.6659(3)	0.04103(19)	0.0282(5)
O1	0.2093(2)	0.7583(2)	0.95925(15)	0.0398(5)
C2	0.0509(4)	0.5034(3)	0.1299(2)	0.0394(7)
O2	0.9337(3)	0.5084(3)	0.10437(17)	0.0639(8)
C3	0.3211(4)	0.3851(3)	0.0791(2)	0.0405(7)
O3	0.3734(3)	0.3190(2)	0.02032(16)	0.0618(8)
O11	0.26482(19)	0.33591(18)	0.32463(13)	0.0259(3)
O12	0.0334(2)	0.2715(2)	0.34012(15)	0.0376(4)
O13	0.2440(2)	0.1195(2)	0.46213(13)	0.0305(4)
S1	0.18865(7)	0.21552(7)	0.35472(4)	0.02531(12)
C10	0.2413(3)	0.1127(3)	0.25984(18)	0.0265(5)
C11	0.1342(3)	0.0912(3)	0.2002(2)	0.0354(6)
C12	0.1706(4)	0.0070(3)	0.1252(2)	0.0443(8)
C13	0.3115(4)	0.9505(3)	0.1108(2)	0.0431(8)
C14	0.4255(3)	0.9730(3)	0.16839(19)	0.0330(6)
C15	0.5723(4)	0.9203(3)	0.1490(2)	0.0418(7)
C16	0.6802(4)	0.9484(3)	0.2009(2)	0.0427(7)
C17	0.6472(3)	0.0277(3)	0.2780(2)	0.0371(6)
C18	0.5066(3)	0.0783(3)	0.30108(19)	0.0295(5)
C19	0.3910(3)	0.0554(3)	0.24573(18)	0.0270(5)
N20	0.4468(2)	0.5140(2)	0.23743(16)	0.0274(4)
C21	0.5791(3)	0.4423(3)	0.2200(3)	0.0442(7)
C22	0.7038(3)	0.4463(4)	0.2739(3)	0.0602(11)
C23	0.6926(4)	0.5292(4)	0.3446(3)	0.0602(11)
C24	0.5566(3)	0.6065(3)	0.3653(2)	0.0428(8)
C25	0.5317(5)	0.6962(4)	0.4396(3)	0.0582(11)
C26	0.3976(5)	0.7608(4)	0.4596(2)	0.0551(10)
C27	0.2728(4)	0.7436(3)	0.40975(19)	0.0367(7)
C28	0.1297(4)	0.7997(3)	0.4336(2)	0.0488(9)
C29	0.0185(4)	0.7742(3)	0.3839(2)	0.0464(8)
C30	0.0466(3)	0.6950(3)	0.3073(2)	0.0328(6)
N31	0.1803(2)	0.6399(2)	0.28179(15)	0.0229(4)
C32	0.2930(3)	0.6618(3)	0.33365(18)	0.0252(5)
C33	0.4355(3)	0.5937(3)	0.31077(19)	0.0268(5)

Table 10: Bond lengths (Å) for 1NS2

Re1-C1	1.899(3)	Re1-C2	1.911(3)
Re1-C3	1.921(3)	Re1-N31	2.1703(18)
Re1-N20	2.173(2)	Re1-O11	2.1737(16)
C1-O1	1.158(3)	C2-O2	1.155(4)
C3-O3	1.158(3)	O11-S1	1.4946(18)
O12-S1	1.442(2)	O13-S1	1.4471(17)
S1-C10	1.779(2)	C10-C11	1.375(4)
C10-C19	1.431(4)	C11-C12	1.420(4)
C11-H11	0.95	C12-C13	1.354(5)
C12-H12	0.95	C13-C14	1.417(4)
C13-H13	0.95	C14-C15	1.415(4)
C14-C19	1.432(3)	C15-C16	1.355(5)
C15-H15	0.95	C16-C17	1.408(4)
C16-H16	0.95	C17-C18	1.371(4)
C17-H17	0.95	C18-C19	1.414(4)
C18-H18	0.95	N20-C21	1.335(3)
N20-C33	1.368(3)	C21-C22	1.397(5)
C21-H21	0.95	C22-C23	1.363(6)
C22-H22	0.95	C23-C24	1.397(5)
C23-H23	0.95	C24-C33	1.407(3)
C24-C25	1.447(5)	C25-C26	1.338(6)
C25-H25	0.95	C26-C27	1.426(5)
C26-H26	0.95	C27-C28	1.407(5)
C27-C32	1.409(3)	C28-C29	1.353(5)
C28-H28	0.95	C29-C30	1.397(4)
C29-H29	0.95	C30-N31	1.334(3)
C30-H30	0.95	N31-C32	1.362(3)
C32-C33	1.427(4)		

Table 11: Bond angles (°) for 1NS2

C1-Re1-C2	86.37(11)	C1-Re1-C3	85.01(11)
C2-Re1-C3	89.92(14)	C1-Re1-N31	96.86(9)
C2-Re1-N31	97.41(10)	C3-Re1-N31	172.52(11)
C1-Re1-N20	98.22(9)	C2-Re1-N20	172.23(9)
C3-Re1-N20	96.70(12)	N31-Re1-N20	75.89(8)
C1-Re1-O11	176.01(8)	C2-Re1-O11	95.86(9)
C3-Re1-O11	98.27(9)	N31-Re1-O11	79.59(7)
N20-Re1-O11	79.20(7)	O1-C1-Re1	176.2(2)
O2-C2-Re1	176.6(3)	O3-C3-Re1	175.3(3)
S1-O11-Re1	127.22(10)	O12-S1-O13	115.62(11)
O12-S1-O11	112.09(11)	O13-S1-O11	108.92(10)
O12-S1-C10	106.98(12)	O13-S1-C10	107.40(11)
O11-S1-C10	105.19(11)	C11-C10-C19	121.2(2)
C11-C10-S1	118.1(2)	C19-C10-S1	120.73(18)
C10-C11-C12	120.2(3)	C10-C11-H11	119.9
C12-C11-H11	119.9	C13-C12-C11	119.8(3)
C13-C12-H12	120.1	C11-C12-H12	120.1
C12-C13-C14	121.9(3)	C12-C13-H13	119
C14-C13-H13	119	C15-C14-C13	121.8(2)
C15-C14-C19	119.1(3)	C13-C14-C19	119.1(3)
C16-C15-C14	121.3(2)	C16-C15-H15	119.4
C14-C15-H15	119.4	C15-C16-C17	119.9(3)
C15-C16-H16	120.1	C17-C16-H16	120.1
C18-C17-C16	120.8(3)	C18-C17-H17	119.6
C16-C17-H17	119.6	C17-C18-C19	120.8(2)
C17-C18-H18	119.6	C19-C18-H18	119.6
C18-C19-C10	124.2(2)	C18-C19-C14	118.1(2)
C10-C19-C14	117.7(2)	C21-N20-C33	117.8(3)
C21-N20-Re1	127.2(2)	C33-N20-Re1	114.84(16)
N20-C21-C22	122.4(3)	N20-C21-H21	118.8
C22-C21-H21	118.8	C23-C22-C21	119.8(3)
C23-C22-H22	120.1	C21-C22-H22	120.1
C22-C23-C24	120.0(3)	C22-C23-H23	120
C24-C23-H23	120	C23-C24-C33	117.1(3)
C23-C24-C25	124.8(3)	C33-C24-C25	118.1(3)
C26-C25-C24	121.3(3)	C26-C25-H25	119.3
C24-C25-H25	119.3	C25-C26-C27	121.7(3)
C25-C26-H26	119.1	C27-C26-H26	119.1
C28-C27-C32	117.2(3)	C28-C27-C26	124.3(3)
C32-C27-C26	118.4(3)	C29-C28-C27	119.8(2)
C29-C28-H28	120.1	C27-C28-H28	120.1
C28-C29-C30	119.7(3)	C28-C29-H29	120.1
C30-C29-H29	120.1	N31-C30-C29	122.6(3)
N31-C30-H30	118.7	C29-C30-H30	118.7
C30-N31-C32	117.9(2)	C30-N31-Re1	126.91(18)
C32-N31-Re1	115.08(15)	N31-C32-C27	122.6(2)
N31-C32-C33	117.1(2)	C27-C32-C33	120.3(2)
N20-C33-C24	122.9(3)	N20-C33-C32	117.0(2)
C24-C33-C32	120.0(3)		

Table 12: Anisotropic atomic displacement parameters (Å2) for 1NS2

Re1	0.03149(5)	0.02369(5)	0.01557(4)	-0.00722(3)	0.00044(3)	-0.00802(4)
C1	0.0364(14)	0.0290(12)	0.0236(11)	-0.0113(10)	0.0003(10)	-0.0124(11)
O1	0.0587(14)	0.0350(10)	0.0253(9)	-0.0019(8)	-0.0045(9)	-0.0189(10)
C2	0.0544(19)	0.0539(18)	0.0170(11)	-0.0061(11)	0.0007(11)	-0.0314(15)
O2	0.0571(15)	0.117(2)	0.0265(10)	-0.0072(12)	-0.0058(10)	-0.0535(16)
C3	0.077(2)	0.0251(13)	0.0183(11)	-0.0050(10)	0.0047(12)	-0.0134(14)
O3	0.122(2)	0.0335(11)	0.0260(10)	-0.0137(9)	0.0171(12)	-0.0073(13)
O11	0.0356(10)	0.0242(8)	0.0188(7)	-0.0078(6)	0.0009(7)	-0.0072(7)
O12	0.0294(10)	0.0475(12)	0.0310(9)	-0.0064(9)	0.0054(8)	-0.0068(9)
O13	0.0409(11)	0.0302(9)	0.0171(7)	-0.0032(7)	0.0025(7)	-0.0075(8)
S1	0.0300(3)	0.0275(3)	0.0178(2)	-0.0054(2)	0.0028(2)	-0.0076(2)
C10	0.0368(14)	0.0250(12)	0.0177(10)	-0.0041(9)	-0.0008(9)	-0.0101(10)
C11	0.0484(17)	0.0312(14)	0.0273(12)	-0.0027(10)	-0.0048(11)	-0.0175(12)
C12	0.075(2)	0.0385(16)	0.0274(13)	-0.0073(12)	-0.0093(14)	-0.0306(16)
C13	0.083(2)	0.0321(14)	0.0224(12)	-0.0099(11)	0.0042(13)	-0.0269(16)
C14	0.0620(19)	0.0193(11)	0.0185(10)	-0.0047(9)	0.0059(11)	-0.0129(12)
C15	0.071(2)	0.0241(13)	0.0256(12)	-0.0077(10)	0.0146(13)	-0.0044(13)
C16	0.0508(19)	0.0330(15)	0.0337(14)	-0.0044(12)	0.0139(13)	0.0016(13)
C17	0.0365(15)	0.0352(15)	0.0329(13)	-0.0050(11)	0.0010(11)	-0.0026(12)
C18	0.0387(15)	0.0255(12)	0.0221(11)	-0.0065(9)	0.0005(10)	-0.0045(11)
C19	0.0448(15)	0.0199(11)	0.0163(9)	-0.0046(8)	0.0024(9)	-0.0089(10)
N20	0.0257(11)	0.0270(10)	0.0237(9)	-0.0004(8)	0.0036(8)	-0.0043(8)
C21	0.0319(16)	0.0422(17)	0.0405(15)	0.0064(13)	0.0115(12)	0.0018(13)
C22	0.0235(16)	0.063(2)	0.061(2)	0.0272(19)	0.0060(15)	-0.0020(15)
C23	0.0335(18)	0.068(2)	0.057(2)	0.0305(19)	-0.0186(15)	-0.0276(17)
C24	0.0442(18)	0.0434(17)	0.0330(13)	0.0168(12)	-0.0177(12)	-0.0282(14)
C25	0.089(3)	0.049(2)	0.0363(16)	0.0154(14)	-0.0349(18)	-0.047(2)
C26	0.110(3)	0.0393(17)	0.0229(13)	0.0002(12)	-0.0187(17)	-0.040(2)
C27	0.070(2)	0.0226(12)	0.0176(10)	-0.0029(9)	-0.0034(12)	-0.0145(13)
C28	0.094(3)	0.0238(13)	0.0236(12)	-0.0079(11)	0.0165(15)	-0.0047(15)
C29	0.063(2)	0.0313(15)	0.0347(15)	-0.0072(12)	0.0202(14)	0.0035(14)
C30	0.0315(14)	0.0293(13)	0.0304(12)	-0.0032(10)	0.0061(10)	-0.0010(11)
N31	0.0264(10)	0.0225(9)	0.0186(8)	-0.0058(7)	0.0018(7)	-0.0040(8)
C32	0.0385(14)	0.0199(11)	0.0168(9)	-0.0027(8)	-0.0016(9)	-0.0096(10)
C33	0.0306(13)	0.0256(12)	0.0207(10)	0.0049(9)	-0.0049(9)	-0.0135(10)

2. 4. 3. X-ray Crystallographic analysis for 1NS4

The X-ray examination and data collection was performed on a suitable yellow crystal of 1NS4 with approximate dimensions of 0.25 mm × 0.22 mm × 0.19 mm. The crystal was mounted in a loop with paratone-N and transferred to the goniostat bathed in a cold stream. A Bruker APEX-II DUO CCD diffractometer using Mo Kα radiation, λ = 0.71073 Å (Bruker TRIUMPH curved-graphite monochromator) was used to measure the X-ray intensity data. The data collection temperature was 150 K. The data collection frames were measured for a duration of 10s at 0.5^{o} intervals of ω with a maximum θ value of ~140^{o}. The SAINT program was used to process the data frames. The data were corrected for decay, Lorentz and polarization effects as well as absorption and beam corrections.

A combination of direct methods SHELXTL v6.14 and the difference Fourier technique was used to solve the structure. The structure was refined by full-matrix least squares on F^2. Non-hydrogen atoms were refined with anisotropic displacement parameters except for C28. A partial occupancy (1/4 occupancy) CH_2Cl_2 crystallizes in the lattice. A riding model was used to calculate and treat all H-atom positions in subsequent refinements. The isotropic displacement parameters for the H-atoms were defined as a*U_{eq} of the adjacent atom, (a=1.5 for methyl and 1.2 for all others). The refinement converged with crystallographic agreement factors of wR2=6.54%, R1=2.36%. This was for 6287 reflections with I>2σ(I) (R1=2.41%, wR2=6.57% for all data) and 347 variable parameters.

Table 13: Crystal data and structure refinement for 1NS4

Formula	$C_{27}H_{19}N_2O_6SRe.1/4CH_2Cl_2$	
Formula weight	706.93	
Temperature	150(2) K	
Wavelength	0.71073 Å	
Crystal system	Tetragonal	
Space group	P43212	
Unit cell dimensions	a = 16.4202(7) Å	α = 90°
	b = 16.4202(7) Å	β = 90°
	c = 18.9294(11) Å	γ = 90°
Volume	5103.8(4) Å3	
Z	8	
Density (calculated)	1.840 Mg/m3	
Absorption coefficient	4.942 mm-1	
F(000)	2756	
Crystal size	0.25 x 0.22 x 0.19 mm3	
θ range for data collection	1.64 to 28.36°	
Index ranges	$-21 \leq h \leq 21$, $-21 \leq k \leq 21$, $-24 \leq l \leq 25$	
Reflections collected	135844	
Independent reflections	6374 [Rint = 0.0227]	
Completeness to θ = 28.36°	99.90%	
Absorption correction	Numerical	
Max. and min. transmission	0.4536 and 0.3713	
Refinement method	Full-matrix least-squares on F2	
Data / restraints / parameters	6374 / 0 / 347	
Goodness-of-fit on F2	1.118	
Final R indices [I>2σ(I)]	R1 = 0.0236, wR2 = 0.0654	
R indices (all data)	R1 = 0.0241, wR2 = 0.0657	
Absolute structure parameter	0.014(7)	
Largest diff. peak and hole	2.496 and -0.380 eÅ-3	

Table 14: Atomic coordinates [$x10^4$] and equivalent isotropic displacement parameters [$Å^2 x10^3$] for 1NS4

	x	y	z	U(eq)
Re	6358(1)	3068(1)	5658(1)	25(1)
S(1)	7886(1)	2598(1)	4611(1)	31(1)
O(1)	6173(3)	1219(2)	5821(3)	55(1)
O(2)	7732(3)	2726(2)	6709(2)	50(1)
O(3)	5320(2)	3356(2)	6971(2)	46(1)
O(4)	7038(2)	2917(2)	4692(2)	31(1)
O(5)	8079(2)	1988(2)	5121(2)	50(1)
O(6)	8024(2)	2373(2)	3885(2)	47(1)
N(1)	6614(2)	4344(2)	5378(2)	23(1)
N(2)	5418(2)	3353(2)	4862(2)	25(1)
C(1)	6208(3)	1923(3)	5752(3)	40(1)
C(2)	7246(3)	2876(3)	6303(3)	35(1)
C(3)	5707(3)	3254(3)	6461(2)	33(1)
C(4)	7158(2)	4846(2)	5651(2)	28(1)
C(5)	7401(3)	5562(3)	5294(2)	31(1)
C(6)	7050(3)	5779(2)	4684(2)	31(1)
C(7)	6411(3)	5295(2)	4405(2)	27(1)
C(8)	6221(2)	4573(2)	4766(2)	24(1)
C(9)	5977(3)	5516(3)	3780(2)	36(1)
C(10)	5358(3)	5046(3)	3546(2)	36(1)
C(11)	5144(3)	4317(3)	3898(2)	32(1)
C(12)	5579(2)	4066(2)	4499(2)	26(1)
C(13)	4495(3)	3808(3)	3676(3)	44(1)
C(14)	4324(3)	3133(3)	4046(3)	45(1)
C(15)	4783(3)	2901(3)	4644(3)	35(1)
C(16)	7540(3)	4665(3)	6358(2)	40(1)
C(17)	4572(3)	2142(3)	5037(3)	43(1)
C(18)	8530(3)	3451(3)	4773(3)	38(1)
C(19)	9048(3)	3390(4)	5340(3)	52(1)
C(20)	9598(4)	4007(5)	5517(4)	71(2)
C(21)	9619(4)	4659(5)	5139(4)	70(2)
C(22)	9129(4)	4811(4)	4540(3)	51(1)
C(23)	9135(4)	5515(4)	4156(5)	70(2)
C(24)	8626(4)	5620(4)	3591(4)	66(2)
C(25)	8098(4)	5022(4)	3392(3)	59(2)
C(26)	8048(4)	4285(3)	3776(3)	46(1)
C(27)	8547(3)	4162(3)	4354(3)	46(1)
Cl(1)	7153(4)	3831(3)	2036(2)	104(2)
C(28)	7079(7)	2921(7)	2500	46(3)
H(5)	7817	5894	5490	38
H(6)	7227	6252	4440	37
H(9)	6123	5995	3529	43
H(10)	5062	5207	3139	44
H(13)	4185	3945	3270	52
H(14)	3882	2800	3901	54
H(16A)	7127	4443	6677	60
H(16B)	7763	5168	6558	60
H(16C)	7979	4267	6297	60
H(17A)	4659	2229	5544	65
H(17B)	4918	1695	4874	65
H(17C)	3999	2006	4953	65
H(19)	9033	2912	5621	62
H(20)	9952	3947	5910	85
H(21)	9994	5071	5274	84
H(23)	9499	5940	4284	84
H(24)	8640	6117	3333	79
H(25)	7759	5101	2991	70
H(26)	7673	3875	3637	56
H(28)	7537	2872	2825	56

Table 15: Bond lengths [Å] and angles [°] for 1NS4

Re-C(3)	1.883(4)	Re-C(1)	1.905(5)
Re-C(2)	1.927(5)	Re-O(4)	2.156(3)
Re-N(1)	2.201(3)	Re-N(2)	2.207(3)
S(1)-O(5)	1.428(4)	S(1)-O(6)	1.440(4)
S(1)-O(4)	1.497(3)	S(1)-C(18)	1.782(5)
O(1)-C(1)	1.164(6)	O(2)-C(2)	1.136(6)
O(3)-C(3)	1.169(6)	N(1)-C(4)	1.321(5)
N(1)-C(8)	1.379(5)	N(2)-C(15)	1.346(5)
N(2)-C(12)	1.382(5)	C(4)-C(5)	1.413(6)
C(4)-C(16)	1.507(6)	C(5)-C(6)	1.339(6)
C(6)-C(7)	1.418(6)	C(7)-C(8)	1.403(5)
C(7)-C(9)	1.428(6)	C(8)-C(12)	1.435(5)
C(9)-C(10)	1.351(7)	C(10)-C(11)	1.414(7)
C(11)-C(12)	1.404(6)	C(11)-C(13)	1.417(6)
C(13)-C(14)	1.341(8)	C(14)-C(15)	1.412(7)
C(15)-C(17)	1.491(7)	C(18)-C(19)	1.373(8)
C(18)-C(27)	1.412(7)	C(19)-C(20)	1.398(9)
C(20)-C(21)	1.288(11)	C(21)-C(22)	1.412(10)
C(22)-C(23)	1.364(10)	C(22)-C(27)	1.474(8)
C(23)-C(24)	1.370(11)	C(24)-C(25)	1.363(10)
C(25)-C(26)	1.414(8)	C(26)-C(27)	1.382(9)
Cl(1)-C(28)	1.737(10)	C(28)-Cl(1)	1.737(10)
C(3)-Re-C(1)	90.7(2)	C(3)-Re-C(2)	86.8(2)
C(1)-Re-C(2)	82.9(2)	C(3)-Re-O(4)	175.45(16)
C(1)-Re-O(4)	91.85(18)	C(2)-Re-O(4)	97.28(17)
C(3)-Re-N(1)	98.53(16)	C(1)-Re-N(1)	170.61(18)
C(2)-Re-N(1)	99.40(16)	O(4)-Re-N(1)	78.85(12)
C(3)-Re-N(2)	96.91(17)	C(1)-Re-N(2)	100.53(17)
C(2)-Re-N(2)	174.86(17)	O(4)-Re-N(2)	78.90(12)
N(1)-Re-N(2)	76.56(12)	O(5)-S(1)-	115.6(2)
O(5)-S(1)-O(4)	112.5(2)	O(6)-S(1)-	109.5(2)
O(5)-S(1)-C(18)	107.7(3)	O(6)-S(1)-	105.8(2)
O(4)-S(1)-C(18)	105.01(19)	S(1)-O(4)-Re	127.56(18)
C(4)-N(1)-C(8)	118.3(3)	C(4)-N(1)-Re	129.0(3)
C(8)-N(1)-Re	111.9(2)	C(15)-N(2)-	117.6(4)
C(15)-N(2)-Re	129.4(3)	C(12)-N(2)-	112.7(2)
O(1)-C(1)-Re	175.3(4)	O(2)-C(2)-Re	175.0(5)
O(3)-C(3)-Re	177.9(4)	N(1)-C(4)-	121.5(4)
N(1)-C(4)-C(16)	120.4(4)	C(5)-C(4)-	118.1(4)
C(6)-C(5)-C(4)	120.8(4)	C(5)-C(6)-	119.3(4)
C(8)-C(7)-C(6)	117.2(4)	C(8)-C(7)-	120.5(4)
C(6)-C(7)-C(9)	122.3(4)	N(1)-C(8)-	122.4(4)
N(1)-C(8)-C(12)	118.7(3)	C(7)-C(8)-	118.9(4)
C(10)-C(9)-C(7)	120.1(4)	C(9)-C(10)-	121.1(4)
C(12)-C(11)-C(10)	120.3(4)	C(12)-	116.7(4)
C(10)-C(11)-C(13)	123.0(4)	N(2)-C(12)-	123.6(4)
N(2)-C(12)-C(8)	117.2(3)	C(11)-	119.2(4)
C(14)-C(13)-C(11)	119.3(4)	C(13)-	122.0(4)
N(2)-C(15)-C(14)	120.6(4)	N(2)-C(15)-	119.2(4)
C(14)-C(15)-C(17)	120.1(4)	C(19)-	119.1(5)
C(19)-C(18)-S(1)	116.4(4)	C(27)-	124.5(4)
C(18)-C(19)-C(20)	122.3(7)	C(21)-	119.1(7)
C(20)-C(21)-C(22)	125.3(7)	C(23)-	125.0(7)
C(23)-C(22)-C(27)	119.3(6)	C(21)-	115.6(6)
C(22)-C(23)-C(24)	121.2(7)	C(25)-	120.9(6)
C(24)-C(25)-C(26)	120.8(6)	C(27)-	119.8(6)
C(26)-C(27)-C(18)	123.6(5)	C(26)-	117.9(5)
C(18)-C(27)-C(22)	118.5(6)	Cl(1)#1-	112.1(10)

Table 16: Anisotropic displacement parameters [$Å^2 x10^3$] for 1NS4

	U11	U22	U33	U23	U13	U12
Re	22(1)	22(1)	30(1)	1(1)	1(1)	1(1)
S(1)	27(1)	25(1)	41(1)	-5(1)	5(1)	6(1)
O(1)	51(2)	28(2)	86(3)	9(2)	-1(2)	-1(2)
O(2)	51(2)	49(2)	51(2)	2(2)	-18(2)	5(2)
O(3)	53(2)	48(2)	38(2)	10(2)	17(2)	7(2)
O(4)	23(1)	31(2)	37(2)	-6(1)	0(1)	4(1)
O(5)	43(2)	36(2)	71(2)	15(2)	7(2)	15(2)
O(6)	42(2)	47(2)	52(2)	-18(2)	9(2)	7(2)
N(1)	24(1)	22(2)	24(2)	-4(1)	0(1)	1(1)
N(2)	18(1)	23(2)	33(2)	0(1)	4(1)	-2(1)
C(1)	34(2)	31(2)	54(3)	5(2)	-2(2)	2(2)
C(2)	34(2)	31(2)	40(2)	5(2)	-1(2)	6(2)
C(3)	34(2)	33(2)	32(2)	8(2)	3(2)	2(2)
C(4)	28(2)	28(2)	27(2)	-7(2)	0(2)	-1(1)
C(5)	30(2)	27(2)	37(2)	-10(2)	3(2)	-5(2)
C(6)	33(2)	22(2)	38(2)	0(2)	9(2)	-5(2)
C(7)	30(2)	22(2)	30(2)	-1(2)	7(2)	2(2)
C(8)	23(2)	22(2)	25(2)	-4(1)	4(1)	2(1)
C(9)	43(3)	30(2)	35(2)	6(2)	5(2)	5(2)
C(10)	44(3)	34(2)	31(2)	2(2)	-6(2)	8(2)
C(11)	25(2)	33(2)	39(2)	-2(2)	-7(2)	4(2)
C(12)	22(2)	24(2)	31(2)	0(1)	1(1)	3(1)
C(13)	36(2)	44(3)	50(3)	0(2)	-18(2)	0(2)
C(14)	25(2)	45(3)	64(3)	-5(2)	-15(2)	-5(2)
C(15)	23(2)	36(2)	46(2)	-2(2)	2(2)	-4(2)
C(16)	44(3)	46(3)	29(2)	-5(2)	-7(2)	-9(2)
C(17)	30(2)	43(3)	57(3)	2(2)	1(2)	-13(2)
C(18)	28(2)	31(2)	54(3)	-9(2)	12(2)	5(2)
C(19)	33(2)	62(3)	60(3)	-16(3)	-2(2)	3(2)
C(20)	53(4)	88(5)	72(5)	-17(4)	-12(3)	-7(3)
C(21)	43(3)	82(5)	86(5)	-20(4)	6(3)	-11(3)
C(22)	43(3)	44(3)	66(4)	-12(3)	14(3)	-1(2)
C(23)	55(4)	50(3)	104(6)	-15(4)	27(4)	-13(3)
C(24)	56(4)	63(4)	78(4)	12(3)	32(4)	8(3)
C(25)	62(4)	55(3)	60(3)	10(3)	15(3)	14(3)
C(26)	44(3)	46(3)	49(3)	-6(2)	16(2)	3(2)
C(27)	35(2)	37(2)	66(3)	-3(2)	21(3)	7(2)
Cl(1)	168(5)	64(2)	79(3)	-18(2)	-76(3)	22(2)

2. 4. 4. X-ray Crystallographic analysis for 1NS7

The X-ray crystallographic analysis was performed on a yellow prism-like specimen of 1NS7 with approximate dimensions of 0.08 mm × 0.26 mm × 0.36 mm. A Bruker APEX-II CCD system equipped with a graphite monochromator and a MoKα sealed tube (λ = 0.71073 Å) was used to measure the X-ray intensity data. The data collection temperature was 150 K. Also, the total exposure time was 5.64 hours. Using a narrow-frame algorithm, the frames were integrated with the Bruker SAINT package. The data integration using an orthorhombic unit cell produced 95503 reflections to a maximum θ angle of 31.00° (0.69 Å resolution) of which 10318 were independent (average redundancy 9.256, completeness = 100.0%, R_{int} = 3.88%) and 8228 (79.74%) were greater than $2\sigma(F^2)$. The final cell constants are *a* = 10.8269(5) Å, *b* = 22.9999(11) Å, *c* = 26.0091(12) Å, *V* = 6476.7(5) $Å^3$. These are based upon the refinement of the XYZ-centroids of 9738 reflections above 20 σ(I) with 4.443° < 2θ < 64.80°. Using the integration method (SADABS), data were corrected for absorption effects. The calculated minimum and maximum transmission coefficients (based on crystal size) are 0.3540 and 0.7220. The Bruker SHELXTL Software Package was used to solve and refine the structure, using the space group P-1, with Z = 2 for the formula unit, $C_{25}H_{15}N_2O_6ReS$.

The Bruker SHELXTL Software Package was used to solve and refine the structure, using the space group Pbca, with Z = 8 for the formula unit, $C_{39}H_{27}N_2O_6ReS$. The final anisotropic full-matrix least-squares refinement on F^2 with 444 variables converged at wR_2 = 5.98% for all data and R_1 = 2.81% for the observed data. The goodness-of-fit was 1.000. The largest peak in the final difference electron density synthesis was 2.070 $e^-/Å^3$. The largest hole was -1.243 $e^-/Å^3$ with an RMS deviation of

0.108 $e^-/Å^3$. The calculated density was 1.719 g/cm^3 and F(000), 3312 e^- based on the final model.

Table 17: Sample and crystal data for 1NS7

Identification code	2771	
Chemical formula	$C_{39}H_{27}N_2O_6ReS$	
Formula weight	837.88	
Temperature	150(2) K	
Wavelength	0.71073 Å	
Crystal size	0.08 × 0.26 × 0.36 mm	
Crystal habit	yellow prism	
Crystal system	orthorhombic	
Space group	Pbca	
Unit cell dimensions	a = 10.8269(5) Å	α = 90°
	b = 22.9999(11) Å	β = 90°
	c = 26.0091(12) Å	γ = 90°
Volume	6476.7(5) $Å^3$	
Z	8	
Density (calculated)	1.719 Mg/cm^3	
Absorption coefficient	3.870 mm^{-1}	
F(000)	3312	

Table 18: Atomic coordinates and equivalent isotropic atomic displacement parameters (Å2) for 1NS7

Re1	0.09109(2)	0.48993(2)	0.35771(2)	0.02043(3)
C1	0.1707(3)	0.55313(13)	0.32471(12)	0.0280(6)
O1	0.2145(2)	0.59251(10)	0.30373(10)	0.0422(6)
C2	0.9668(3)	0.54343(13)	0.37966(12)	0.0289(6)
O2	0.8898(2)	0.57609(11)	0.39004(10)	0.0430(6)
C3	0.9851(3)	0.48647(13)	0.29867(11)	0.0250(5)
O3	0.9189(2)	0.48888(10)	0.26405(8)	0.0333(5)
O11	0.01079(19)	0.41775(9)	0.39999(7)	0.0253(4)
O12	0.9107(2)	0.36986(10)	0.32768(8)	0.0333(5)
O13	0.8407(2)	0.35309(10)	0.41563(9)	0.0322(5)
S1	0.94193(7)	0.36556(3)	0.38152(3)	0.02474(14)
C10	0.0496(3)	0.30699(13)	0.38668(11)	0.0273(6)
C11	0.0782(3)	0.27693(14)	0.34285(12)	0.0312(6)
C12	0.1605(3)	0.22925(15)	0.34486(13)	0.0366(7)
C13	0.2135(4)	0.21330(15)	0.38985(14)	0.0392(8)
C14	0.1863(3)	0.24299(14)	0.43631(12)	0.0314(6)
C15	0.2395(4)	0.22679(15)	0.48380(14)	0.0405(8)
C16	0.2122(4)	0.25528(16)	0.52787(14)	0.0406(8)
C17	0.1309(3)	0.30261(15)	0.52722(12)	0.0343(7)
C18	0.0780(3)	0.32036(14)	0.48193(11)	0.0319(7)
C19	0.1028(3)	0.29114(13)	0.43514(11)	0.0269(6)
C20	0.1768(3)	0.41516(14)	0.24738(11)	0.0292(6)
N20	0.2317(2)	0.42363(10)	0.33896(8)	0.0214(4)
C21	0.2498(3)	0.39714(12)	0.29378(10)	0.0225(5)
C22	0.3365(3)	0.35206(13)	0.28854(10)	0.0248(6)
C23	0.4063(3)	0.33259(12)	0.32910(10)	0.0232(5)
C24	0.4982(3)	0.28506(13)	0.32083(10)	0.0248(6)
C25	0.4616(3)	0.23460(14)	0.29507(12)	0.0328(7)
C26	0.5448(3)	0.18976(15)	0.28651(13)	0.0376(7)
C27	0.6664(3)	0.19514(15)	0.30214(13)	0.0362(7)
C28	0.7045(3)	0.24566(14)	0.32621(12)	0.0313(6)
C29	0.6211(3)	0.29019(13)	0.33621(11)	0.0278(6)
C30	0.1229(4)	0.57104(15)	0.46965(14)	0.0414(8)
N30	0.2082(2)	0.48445(10)	0.42681(9)	0.0228(4)
C31	0.2003(3)	0.51734(13)	0.46911(11)	0.0280(6)
C32	0.2632(3)	0.50240(13)	0.51444(11)	0.0298(6)
C33	0.3367(3)	0.45399(13)	0.51781(11)	0.0249(6)
C34	0.3956(3)	0.44067(13)	0.56789(10)	0.0259(6)
C35	0.4460(3)	0.48608(15)	0.59665(11)	0.0323(7)
C36	0.4941(3)	0.47630(16)	0.64545(12)	0.0393(8)
C37	0.4915(3)	0.42101(17)	0.66598(12)	0.0391(8)
C38	0.4410(3)	0.37552(16)	0.63831(12)	0.0344(7)
C39	0.3934(3)	0.38508(14)	0.58929(12)	0.0298(6)
C41	0.3008(3)	0.40524(12)	0.38042(10)	0.0207(5)
C42	0.3874(3)	0.35996(12)	0.37771(10)	0.0223(5)
C43	0.4507(3)	0.34290(13)	0.42356(11)	0.0277(6)
C44	0.4344(3)	0.37164(13)	0.46852(11)	0.0279(6)
C45	0.3516(3)	0.41991(12)	0.47229(10)	0.0230(5)
C46	0.2850(3)	0.43693(12)	0.42795(10)	0.0213(5)

Table 19: Bond lengths (Å) for 1NS7

Re1-C1	1.895(3)	Re1-C2	1.910(3)
Re1-C3	1.918(3)	Re1-O11	2.173(2)
Re1-N30	2.203(2)	Re1-N20	2.210(2)
C1-O1	1.159(4)	C2-O2	1.154(4)
C3-O3	1.153(3)	O11-S1	1.493(2)
O12-S1	1.444(2)	O13-S1	1.439(2)
S1-C10	1.787(3)	C10-C11	1.369(4)
C10-C19	1.433(4)	C11-C12	1.414(5)
C11-H11	0.95	C12-C13	1.354(5)
C12-H12	0.95	C13-C14	1.419(5)
C13-H13	0.95	C14-C15	1.413(5)
C14-C19	1.430(4)	C15-C16	1.353(5)
C15-H15	0.95	C16-C17	1.400(5)
C16-H16	0.95	C17-C18	1.372(4)
C17-H17	0.95	C18-C19	1.416(4)
C18-H18	0.95	C20-C21	1.501(4)
C20-H20A	0.98	C20-H20B	0.98
C20-H20C	0.98	N20-C21	1.338(3)
N20-C41	1.379(3)	C21-C22	1.405(4)
C22-C23	1.373(4)	C22-H22	0.95
C23-C42	1.427(4)	C23-C24	1.493(4)
C24-C29	1.394(4)	C24-C25	1.397(4)
C25-C26	1.388(5)	C25-H25	0.95
C26-C27	1.383(5)	C26-H26	0.95
C27-C28	1.383(5)	C27-H27	0.95
C28-C29	1.390(4)	C28-H28	0.95
C29-H29	0.95	C30-C31	1.493(4)
C30-H30A	0.98	C30-H30B	0.98
C30-H30C	0.98	N30-C31	1.338(4)
N30-C46	1.374(3)	C31-C32	1.404(4)
C32-C33	1.372(4)	C32-H32	0.95
C33-C45	1.429(4)	C33-C34	1.483(4)
C34-C39	1.395(4)	C34-C35	1.396(4)
C35-C36	1.390(4)	C35-H35	0.95
C36-C37	1.379(5)	C36-H36	0.95
C37-C38	1.383(5)	C37-H37	0.95
C38-C39	1.392(4)	C38-H38	0.95
C39-H39	0.95	C41-C42	1.403(4)
C41-C46	1.445(4)	C42-C43	1.430(4)
C43-C44	1.355(4)	C43-H43	0.95
C44-C45	1.430(4)	C44-H44	0.95
C45-C46	1.415(4)		

Table 20: Bond angles (°) for 1NS7

C1-Re1-C2	87.80(13)	C1-Re1-C3	86.63(12)
C2-Re1-C3	81.07(13)	C1-Re1-O11	175.63(11)
C2-Re1-O11	93.39(11)	C3-Re1-O11	97.71(10)
C1-Re1-N30	98.72(11)	C2-Re1-N30	101.44(11)
C3-Re1-N30	174.13(11)	O11-Re1-N30	76.92(8)
C1-Re1-N20	96.66(11)	C2-Re1-N20	174.73(11)
C3-Re1-N20	101.93(10)	O11-Re1-N20	81.96(8)
N30-Re1-N20	75.17(8)	O1-C1-Re1	177.1(3)
O2-C2-Re1	176.1(3)	O3-C3-Re1	174.6(3)
S1-O11-Re1	130.66(12)	O13-S1-O12	115.67(14)
O13-S1-O11	110.02(13)	O12-S1-O11	111.96(12)
O13-S1-C10	107.49(14)	O12-S1-C10	106.10(14)
O11-S1-C10	104.85(13)	C11-C10-C19	120.9(3)
C11-C10-S1	117.8(2)	C19-C10-S1	121.3(2)
C10-C11-C12	120.2(3)	C10-C11-H11	119.9
C12-C11-H11	119.9	C13-C12-C11	120.6(3)
C13-C12-H12	119.7	C11-C12-H12	119.7
C12-C13-C14	121.2(3)	C12-C13-H13	119.4
C14-C13-H13	119.4	C15-C14-C13	122.2(3)
C15-C14-C19	118.7(3)	C13-C14-C19	119.1(3)
C16-C15-C14	121.6(3)	C16-C15-H15	119.2
C14-C15-H15	119.2	C15-C16-C17	120.3(3)
C15-C16-H16	119.9	C17-C16-H16	119.9
C18-C17-C16	120.3(3)	C18-C17-H17	119.9
C16-C17-H17	119.9	C17-C18-C19	121.2(3)
C17-C18-H18	119.4	C19-C18-H18	119.4
C18-C19-C14	118.0(3)	C18-C19-C10	124.0(3)
C14-C19-C10	118.0(3)	C21-C20-H20A	109.5
C21-C20-H20B	109.5	H20A-C20-H20B	109.5
C21-C20-H20C	109.5	H20A-C20-H20C	109.5
H20B-C20-H20C	109.5	C21-N20-C41	117.9(2)
C21-N20-Re1	127.49(19)	C41-N20-Re1	114.38(17)
N20-C21-C22	121.2(2)	N20-C21-C20	120.2(3)
C22-C21-C20	118.5(2)	C23-C22-C21	122.3(3)
C23-C22-H22	118.9	C21-C22-H22	118.9
C22-C23-C42	117.2(3)	C22-C23-C24	119.7(2)
C42-C23-C24	123.1(2)	C29-C24-C25	118.6(3)
C29-C24-C23	122.1(3)	C25-C24-C23	119.2(3)
C26-C25-C24	120.7(3)	C26-C25-H25	119.7
C24-C25-H25	119.7	C27-C26-C25	120.3(3)
C27-C26-H26	119.9	C25-C26-H26	119.9
C28-C27-C26	119.5(3)	C28-C27-H27	120.3
C26-C27-H27	120.3	C27-C28-C29	120.7(3)
C27-C28-H28	119.7	C29-C28-H28	119.7
C28-C29-C24	120.3(3)	C28-C29-H29	119.9
C24-C29-H29	119.9	C31-C30-H30A	109.5
C31-C30-H30B	109.5	H30A-C30-H30B	109.5
C31-C30-H30C	109.5	H30A-C30-H30C	109.5
H30B-C30-H30C	109.5	C31-N30-C46	118.1(2)
C31-N30-Re1	127.0(2)	C46-N30-Re1	114.30(17)
N30-C31-C32	121.4(3)	N30-C31-C30	120.7(3)
C32-C31-C30	117.8(3)	C33-C32-C31	122.3(3)
C33-C32-H32	118.9	C31-C32-H32	118.9
C32-C33-C45	117.2(3)	C32-C33-C34	118.3(3)
C45-C33-C34	124.5(3)	C39-C34-C35	118.6(3)
C39-C34-C33	122.2(3)	C35-C34-C33	119.0(3)
C36-C35-C34	121.0(3)	C36-C35-H35	119.5
C34-C35-H35	119.5	C37-C36-C35	119.7(3)
C37-C36-H36	120.2	C35-C36-H36	120.2
C36-C37-C38	120.3(3)	C36-C37-H37	119.9
C38-C37-H37	119.9	C37-C38-C39	120.2(3)
C37-C38-H38	119.9	C39-C38-H38	119.9
C38-C39-C34	120.3(3)	C38-C39-H39	119.9
C34-C39-H39	119.9	N20-C41-C42	123.4(2)
N20-C41-C46	116.8(2)	C42-C41-C46	119.8(2)
C41-C42-C23	117.9(2)	C41-C42-C43	118.8(2)
C23-C42-C43	123.3(3)	C44-C43-C42	121.6(3)
C44-C43-H43	119.2	C42-C43-H43	119.2
C43-C44-C45	121.3(3)	C43-C44-H44	119.4
C45-C44-H44	119.4	C46-C45-C33	117.8(3)
C46-C45-C44	118.6(2)	C33-C45-C44	123.6(3)
N30-C46-C45	123.1(2)	N30-C46-C41	117.0(2)
C45-C46-C41	119.8(2)		

Table 21: Anisotropic atomic displacement parameters (Å2) for 1NS7

Re1	0.02089(5)	0.02013(5)	0.02027(5)	0.00193(4)	-0.00087(4)	0.00087(4)
C1	0.0260(14)	0.0250(15)	0.0330(15)	0.0001(12)	-0.0037(12)	0.0025(12)
O1	0.0418(14)	0.0311(13)	0.0537(15)	0.0139(11)	0.0011(12)	-0.0074(11)
C2	0.0323(16)	0.0270(15)	0.0274(14)	0.0023(11)	-0.0023(12)	0.0002(12)
O2	0.0381(14)	0.0436(14)	0.0473(14)	-0.0034(11)	0.0031(11)	0.0158(11)
C3	0.0241(13)	0.0247(14)	0.0263(13)	0.0042(11)	0.0031(10)	0.0017(11)
O3	0.0299(11)	0.0420(12)	0.0279(10)	0.0074(9)	-0.0052(9)	0.0009(10)
O11	0.0299(11)	0.0243(10)	0.0218(9)	0.0024(8)	-0.0029(8)	-0.0028(8)
O12	0.0416(13)	0.0323(12)	0.0260(10)	0.0017(8)	-0.0078(10)	-0.0032(10)
O13	0.0266(11)	0.0356(12)	0.0343(11)	0.0047(9)	0.0018(9)	-0.0039(9)
S1	0.0267(3)	0.0253(3)	0.0222(3)	0.0026(3)	-0.0034(3)	-0.0020(3)
C10	0.0284(14)	0.0264(14)	0.0270(14)	0.0019(11)	0.0003(11)	-0.0015(12)
C11	0.0346(17)	0.0309(16)	0.0280(14)	-0.0004(11)	0.0002(12)	-0.0046(13)
C12	0.0414(19)	0.0342(18)	0.0344(16)	-0.0075(13)	0.0057(14)	0.0000(15)
C13	0.044(2)	0.0314(17)	0.0426(18)	-0.0028(14)	0.0037(15)	0.0082(15)
C14	0.0319(16)	0.0268(15)	0.0354(16)	0.0036(12)	-0.0001(13)	0.0022(12)
C15	0.043(2)	0.0318(18)	0.0461(19)	0.0058(14)	-0.0052(16)	0.0109(15)
C16	0.050(2)	0.0366(19)	0.0348(17)	0.0088(14)	-0.0087(15)	0.0012(16)
C17	0.0437(19)	0.0333(17)	0.0260(14)	0.0030(12)	-0.0035(13)	0.0019(14)
C18	0.0382(18)	0.0311(16)	0.0266(14)	0.0015(12)	-0.0004(13)	0.0062(13)
C19	0.0292(15)	0.0244(14)	0.0273(13)	0.0024(10)	-0.0008(11)	-0.0014(12)
C20	0.0288(15)	0.0396(17)	0.0193(12)	-0.0023(12)	-0.0037(11)	0.0037(13)
N20	0.0210(11)	0.0234(11)	0.0197(10)	0.0017(8)	-0.0009(8)	-0.0018(9)
C21	0.0206(13)	0.0266(14)	0.0204(11)	0.0018(10)	-0.0004(10)	-0.0027(10)
C22	0.0261(14)	0.0287(15)	0.0197(12)	-0.0032(10)	0.0021(10)	0.0002(11)
C23	0.0238(13)	0.0245(13)	0.0214(12)	-0.0010(10)	0.0033(11)	0.0009(11)
C24	0.0283(14)	0.0249(14)	0.0210(12)	0.0001(10)	0.0032(11)	0.0034(11)
C25	0.0320(16)	0.0350(17)	0.0314(15)	-0.0063(13)	0.0006(13)	0.0002(13)
C26	0.0444(19)	0.0310(17)	0.0373(17)	-0.0094(14)	0.0018(15)	0.0018(15)
C27	0.0390(18)	0.0344(17)	0.0353(17)	-0.0022(13)	0.0044(14)	0.0122(14)
C28	0.0265(15)	0.0359(17)	0.0316(15)	-0.0021(12)	0.0009(12)	0.0064(13)
C29	0.0302(15)	0.0268(15)	0.0266(13)	-0.0021(11)	0.0015(11)	0.0033(12)
C30	0.055(2)	0.0327(18)	0.0363(17)	-0.0079(14)	-0.0094(16)	0.0129(16)
N30	0.0245(11)	0.0208(11)	0.0232(10)	-0.0004(9)	-0.0024(9)	0.0006(9)
C31	0.0333(16)	0.0236(15)	0.0269(13)	-0.0040(11)	-0.0031(11)	0.0032(12)
C32	0.0383(16)	0.0286(16)	0.0225(12)	-0.0050(11)	-0.0027(12)	0.0017(12)
C33	0.0254(14)	0.0276(14)	0.0218(12)	-0.0009(10)	-0.0020(10)	-0.0028(11)
C34	0.0232(14)	0.0341(15)	0.0204(12)	0.0007(11)	-0.0016(10)	-0.0009(12)
C35	0.0357(16)	0.0373(17)	0.0238(13)	0.0045(12)	-0.0030(12)	-0.0095(14)
C36	0.0419(19)	0.050(2)	0.0262(14)	0.0014(14)	-0.0086(14)	-0.0161(16)
C37	0.0378(18)	0.056(2)	0.0238(14)	0.0094(14)	-0.0066(13)	-0.0078(16)
C38	0.0321(16)	0.0415(18)	0.0296(15)	0.0103(13)	0.0001(13)	0.0013(13)
C39	0.0289(15)	0.0323(16)	0.0281(14)	0.0017(12)	-0.0027(12)	0.0002(13)
C41	0.0226(13)	0.0206(13)	0.0190(11)	0.0012(9)	-0.0014(10)	-0.0009(10)
C42	0.0255(14)	0.0218(13)	0.0195(11)	0.0003(9)	0.0011(10)	0.0008(10)
C43	0.0300(15)	0.0292(15)	0.0238(13)	0.0018(11)	-0.0009(11)	0.0084(12)
C44	0.0309(16)	0.0308(15)	0.0219(13)	0.0020(11)	-0.0023(11)	0.0065(12)
C45	0.0245(14)	0.0239(14)	0.0207(12)	0.0015(10)	-0.0013(10)	0.0002(11)
C46	0.0224(13)	0.0205(12)	0.0210(11)	0.0011(10)	0.0000(10)	-0.0006(10)

2. 4. 5. X-ray Crystallographic analysis for 2NS4

The X-ray examination and data collection was performed on a pale-yellow plate-like crystal of 2NS4 with approximate dimensions of 0.04 mm × 0.03 mm × 0.005 mm. The crystal was mounted in a loop with paratone-N and transferred to the goniostat bathed in a cold stream. Using synchrotron radiation tuned to λ=0.77490ΔA, a Bruker APEX2 CCD detector at Beamline 11.3.1 at the Advanced Light Source (Lawrence Berkeley National Laboratory) was used to measure the X-ray intensity data. The data collection temperature was 150 K. The data collection frames were measured for a duration of 3s at 0.3º intervals of ω with a maximum 2θ value of ~60º. The APEX2 program was used to collect the data frames and the SAINT program, routine within APEX2, was used to process the frames. The data were corrected for absorption and beam corrections based on the multi-scan technique as implemented in SADABS.

A combination of direct methods SHELXTL v6.14 and the difference Fourier technique was used to solve the structure. The structure was refined by full-matrix least squares on F^2. Non-hydrogen atoms were refined with anisotropic displacement parameters except for the minor components of the naphthyl groups. Both molecules show disorder, particularly with the naphthyl ring. The minor component naphthyl rings were refined as a rigid group. A two-component disorder model (major conformer = 80% occupancy) is presented for both independent molecules. A riding model was used to calculate and treat all H-atom positions in subsequent refinements. The isotropic displacement parameters for the H-atoms were defined as $a*U_{eq}$ of the adjacent atom, (a=1.5 for methyl and 1.2 for all others). The refinement converged with crystallographic

agreement factors of wR2 = 9.30%, R1 = 4.17%. This was for 6653 reflections with I>2σ(I) (R1 = 7.58%, wR2 = 10.89% for all data) and 691 variable parameters.

Table 22: Crystal data and structure refinement for 2NS4

Formula	$C_{27}H_{19}N_2O_6SRe$	
Formula weight	685.7	
Temperature	150(2) K	
Wavelength	0.77490 Å	
Crystal system	Monoclinic	
Space group	$P2_1/c$	
Unit cell dimensions	a = 18.5564(15) Å	α = 90°
	b = 9.2062(8) Å	β = 102.389 (1)°
	c = 29.132(2) Å	γ = 90°
Volume	4860.8(7) $Å^3$	
Z	8	
Density (calculated)	1.874 Mg/m^3	
Absorption coefficient	6.366 mm^{-1}	
F(000)	2672	
Crystal size	0.04 x 0.03 x 0.01 mm^3	
θ range for data collection	2.18 to 28.97°	
Index ranges	$-23 \leq h \leq 23$, $-11 \leq k \leq 11$, $-36 \leq l \leq 36$	
Reflections collected	69606	
Independent reflections	9908 [R_{int} = 0.0814]	
Completeness to θ = 28.97°	99.50%	
Absorption correction	Multi-scan	
Max. and min. transmission	0.9689 and 0.7848	
Refinement method	Full-matrix least-squares on F^2	
Data / restraints / parameters	9908 / 0 / 691	
Goodness-of-fit on F^2	1.004	
Final R indices [I>2σ(I)]	R1 = 0.0417, wR2 = 0.0930	
R indices (all data)	R1 = 0.0758, wR2 = 0.1089	
Largest diff. peak and hole	2.709 and -1.614 $eÅ^{-3}$	

Table 23: Atomic coordinates [x10^4] and equivalent isotropic displacement parameters [$Å^2$ x10^3] for 2NS4

	x	y	z	U(eq)
Re(1)	9520(1)	7953(1)	8776(1)	49(1)
S(1)	9124(1)	4891(2)	8174(1)	51(1)
O(1A)	10845(3)	7739(6)	8310(3)	86(2)
O(2A)	10455(3)	5789(8)	9449(2)	95(2)
O(3A)	10284(3)	10333(8)	9435(2)	103(2)
O(4A)	8943(2)	6450(4)	8258(2)	44(1)
O(5A)	9878(3)	4563(6)	8352(2)	78(2)
O(6A)	8818(3)	4534(5)	7694(2)	60(1)
N(1A)	8451(3)	7804(6)	8980(2)	49(1)
N(2A)	8822(3)	9489(6)	8300(2)	45(1)
C(1A)	10349(4)	7888(8)	8481(3)	65(2)
C(2A)	10074(4)	6568(10)	9192(3)	74(2)
C(3A)	9979(4)	9426(10)	9183(3)	71(2)
C(4A)	8268(5)	7017(9)	9327(3)	64(2)
C(5A)	7521(5)	6742(10)	9329(3)	74(2)
C(6A)	6974(4)	7348(10)	9010(3)	69(2)
C(7A)	7137(4)	8238(8)	8659(3)	58(2)
C(8A)	7890(3)	8422(7)	8651(2)	45(2)
C(9A)	6593(4)	8975(9)	8321(3)	69(2)
C(10A)	6780(4)	9853(9)	8000(4)	74(3)
C(11A)	7533(4)	10041(7)	7974(3)	55(2)
C(12A)	8091(3)	9330(7)	8299(2)	45(2)
C(13A)	7751(4)	10950(8)	7653(3)	74(2)
C(14A)	8477(4)	11141(8)	7658(3)	67(2)
C(15A)	9005(3)	10420(7)	7991(3)	51(2)
C(16A)	8856(5)	6423(11)	9708(3)	84(3)
C(17A)	9805(4)	10714(8)	7998(3)	65(2)
C(18A)	8551(5)	3895(9)	8491(3)	47(2)
C(19A)	7784(5)	3828(11)	8303(4)	69(3)
C(20A)	7325(5)	3177(11)	8548(4)	70(3)
C(21A)	7605(5)	2539(10)	8984(3)	55(2)
C(22A)	8387(5)	2565(11)	9172(5)	51(3)
C(23A)	8656(5)	1883(12)	9597(4)	72(3)
C(24A)	8215(6)	1273(13)	9844(4)	80(3)
C(25A)	7466(7)	1255(12)	9683(5)	67(3)
C(26A)	7145(6)	1854(11)	9267(4)	67(3)
C(27A)	8850(4)	3254(7)	8906(3)	53(2)
C(18B)	8928(4)	3953(7)	8640(3)	26(6)
C(19B)	9393(4)	3394(7)	9039(3)	44(7)
C(20B)	9103(4)	2592(7)	9361(3)	42(7)
C(21B)	8348(4)	2348(7)	9284(3)	40(16)
C(22B)	7882(4)	2906(7)	8885(3)	44(9)
C(23B)	7126(4)	2662(7)	8807(3)	64(10)
C(24B)	6836(4)	1860(7)	9129(3)	77(18)
C(25B)	7302(4)	1301(7)	9529(3)	60(20)
C(26B)	8058(4)	1545(7)	9606(3)	100(20)
C(27B)	8172(4)	3709(7)	8563(3)	28(6)
Re(2)	4463(1)	4725(1)	8739(1)	51(1)
S(2)	4084(1)	7741(2)	8117(1)	54(1)
O(1B)	5829(3)	4971(7)	8316(2)	80(2)
O(2B)	5340(3)	6950(8)	9424(2)	99(2)
O(3B)	5250(3)	2391(8)	9412(2)	99(2)
O(4B)	3893(2)	6200(4)	8207(2)	50(1)
O(5B)	4839(3)	8053(6)	8290(2)	74(2)
O(6B)	3784(3)	8088(5)	7633(2)	60(1)

Table 24: Atomic coordinates [$x10^4$] and equivalent isotropic displacement parameters [$Å^2 x10^3$] for 2NS4 cont'd

N(1B)	3378(3)	4800(6)	8928(2)	50(1)
N(2B)	3795(3)	3182(5)	8250(2)	45(1)
C(1B)	5310(4)	4827(8)	8466(3)	61(2)
C(2B)	4982(4)	6147(11)	9162(3)	75(2)
C(3B)	4928(4)	3281(11)	9155(3)	73(2)
C(4B)	3177(4)	5481(9)	9283(3)	62(2)
C(5B)	2422(4)	5692(9)	9287(3)	68(2)
C(6B)	1889(4)	5139(9)	8936(3)	67(2)
C(7B)	2081(3)	4352(8)	8576(3)	54(2)
C(8B)	2836(3)	4191(7)	8581(2)	46(2)
C(9B)	1547(4)	3659(9)	8221(3)	69(2)
C(10B)	1754(4)	2843(9)	7894(3)	68(2)
C(11B)	2518(4)	2632(7)	7888(3)	56(2)
C(12B)	3053(3)	3341(7)	8229(2)	46(2)
C(13B)	2749(4)	1737(8)	7565(3)	68(2)
C(14B)	3484(4)	1546(7)	7605(3)	64(2)
C(15B)	4006(4)	2253(7)	7947(3)	54(2)
C(16B)	3746(5)	6051(12)	9683(3)	85(3)
C(17B)	4806(4)	1957(8)	7977(3)	71(2)
C(18C)	3519(4)	8768(9)	8435(3)	47(2)
C(19C)	2749(5)	8852(10)	8249(4)	61(2)
C(20C)	2310(5)	9549(10)	8482(4)	63(3)
C(21C)	2608(5)	10279(10)	8907(3)	53(2)
C(22C)	3375(5)	10200(14)	9093(5)	56(3)
C(23C)	3687(5)	10957(11)	9517(3)	61(2)
C(24C)	3229(7)	11721(12)	9735(4)	73(3)
C(25C)	2483(9)	11771(13)	9551(6)	74(5)
C(26C)	2163(8)	11076(11)	9162(4)	63(3)
C(27C)	3842(4)	9421(8)	8841(3)	53(2)
C(18D)	3878(4)	8761(8)	8540(3)	50(10)
C(19D)	4372(4)	9320(8)	8927(3)	54(8)
C(20D)	4116(4)	10174(8)	9252(3)	92(14)
C(21D)	3366(4)	10470(8)	9189(3)	60(30)
C(22D)	2873(4)	9911(8)	8802(3)	66(13)
C(23D)	2124(4)	10206(8)	8739(3)	91(15)
C(24D)	1868(4)	11061(8)	9064(3)	110(30)
C(25D)	2361(4)	11620(8)	9451(3)	100(40)
C(26D)	3110(4)	11324(8)	9514(3)	110(20)
C(27D)	3129(4)	9056(8)	8477(3)	47(9)
H(5A)	7403	6114	9561	89
H(6A)	6475	7171	9023	83
H(9A)	6086	8841	8323	82
H(10A)	6405	10360	7786	89
H(13A)	7390	11445	7426	89
H(14A)	8624	11766	7436	80
H(16A)	9238	7161	9807	126
H(16B)	9075	5564	9594	126
H(16C)	8642	6151	9976	126
H(17A)	10085	10737	8324	97
H(17B)	9851	11652	7848	97
H(17C)	9999	9944	7826	97
H(19A)	7587	4241	8003	83
H(20A)	6809	3157	8420	84

Table 25: Atomic coordinates [$x10^4$] and equivalent isotropic displacement parameters [$Å^2 x10^3$] for 2NS4 cont'd

H(23A)	9174	1851	9716	86
H(24A)	8423	840	10138	96
H(25A)	7165	810	9869	81
H(26A)	6624	1828	9160	80
H(27A)	9369	3263	9020	63
H(19B)	9910	3561	9092	53
H(20B)	9422	2210	9634	51
H(23B)	6808	3044	8535	76
H(24B)	6320	1693	9077	92
H(25B)	7104	752	9749	77
H(26B)	8376	1163	9879	116
H(27B)	7854	4091	8290	34
H(5B)	2287	6220	9537	82
H(6B)	1384	5294	8938	81
H(9B)	1038	3779	8217	83
H(10B)	1387	2391	7660	82
H(13B)	2402	1271	7323	81
H(14B)	3649	909	7392	77
H(16D)	4168	5388	9748	128
H(16E)	3533	6127	9963	128
H(16F)	3908	7013	9603	128
H(17D)	5069	1969	8307	107
H(17E)	5011	2706	7803	107
H(17F)	4864	1002	7841	107
H(19C)	2544	8407	7956	74
H(20C)	1792	9557	8362	75
H(23C)	4203	10928	9644	73
H(24C)	3427	12226	10019	88
H(25C)	2182	12329	9710	89
H(26C)	1642	11108	9054	76
H(27C)	4360	9371	8956	63
H(19D)	4884	9118	8970	65
H(20D)	4453	10556	9516	110
H(23D)	1786	9824	8475	109
H(24D)	1355	11263	9021	133
H(25D)	2186	12204	9673	125
H(26D)	3447	11707	9778	137
H(27D)	2792	8674	8213	57

Table 26: Bond lengths [Å] and angles [°] for 2NS4

Re(1)-C(3A)	1.881(8)	Re(1)-C(2A)	1.902(9)
Re(1)-C(1A)	1.917(8)	Re(1)-O(4A)	2.155(4)
Re(1)-N(1A)	2.194(5)	Re(1)-N(2A)	2.198(5)
S(1)-O(5A)	1.417(5)	S(1)-O(6A)	1.431(5)
S(1)-O(4A)	1.505(4)	S(1)-C(18B)	1.712(8)
S(1)-C(18A)	1.800(8)	O(1A)-C(1A)	1.144(9)
O(2A)-C(2A)	1.161(9)	O(3A)-C(3A)	1.173(9)
N(1A)-C(4A)	1.345(10)	N(1A)-C(8A)	1.377(8)
N(2A)-C(15A)	1.338(9)	N(2A)-C(12A)	1.363(7)
C(4A)-C(5A)	1.411(11)	C(4A)-C(16A)	1.484(11)
C(5A)-C(6A)	1.343(11)	C(6A)-C(7A)	1.393(11)
C(7A)-C(8A)	1.413(8)	C(7A)-C(9A)	1.422(11)
C(8A)-C(12A)	1.433(10)	C(9A)-C(10A)	1.336(12)
C(10A)-C(11A)	1.427(10)	C(11A)-C(13A)	1.379(11)
C(11A)-C(12A)	1.407(9)	C(13A)-C(14A)	1.355(10)
C(14A)-C(15A)	1.390(10)	C(15A)-C(17A)	1.504(9)
C(18A)-C(27A)	1.352(11)	C(18A)-C(19A)	1.414(12)
C(19A)-C(20A)	1.361(14)	C(20A)-C(21A)	1.396(13)
C(21A)-C(22A)	1.437(12)	C(21A)-C(26A)	1.452(13)
C(22A)-C(23A)	1.382(15)	C(22A)-C(27A)	1.425(16)
C(23A)-C(24A)	1.324(14)	C(24A)-C(25A)	1.368(16)
C(25A)-C(26A)	1.349(18)	C(18B)-C(19B)	1.39
C(18B)-C(27B)	1.39	C(19B)-C(20B)	1.3897
C(20B)-C(21B)	1.3901	C(21B)-C(26B)	1.3899
C(21B)-C(22B)	1.3901	C(22B)-C(23B)	1.3899
C(22B)-C(27B)	1.3901	C(23B)-C(24B)	1.3901
C(24B)-C(25B)	1.3898	C(25B)-C(26B)	1.3901
Re(2)-C(3B)	1.879(9)	Re(2)-C(1B)	1.911(7)
Re(2)-C(2B)	1.911(9)	Re(2)-O(4B)	2.158(4)
Re(2)-N(2B)	2.198(6)	Re(2)-N(1B)	2.200(5)
S(2)-O(5B)	1.413(5)	S(2)-O(6B)	1.437(5)
S(2)-O(4B)	1.499(4)	S(2)-C(18D)	1.656(9)
S(2)-C(18C)	1.808(8)	O(1B)-C(1B)	1.146(8)
O(2B)-C(2B)	1.163(9)	O(3B)-C(3B)	1.181(10)
N(1B)-C(4B)	1.329(9)	N(1B)-C(8B)	1.382(8)
N(2B)-C(15B)	1.345(9)	N(2B)-C(12B)	1.373(7)
C(4B)-C(5B)	1.419(10)	C(4B)-C(16B)	1.491(11)
C(5B)-C(6B)	1.360(11)	C(6B)-C(7B)	1.383(11)
C(7B)-C(8B)	1.407(8)	C(7B)-C(9B)	1.418(11)
C(8B)-C(12B)	1.415(9)	C(9B)-C(10B)	1.334(11)
C(10B)-C(11B)	1.434(9)	C(11B)-C(13B)	1.387(10)
C(11B)-C(12B)	1.405(9)	C(13B)-C(14B)	1.355(10)
C(14B)-C(15B)	1.395(10)	C(15B)-C(17B)	1.494(9)
C(18C)-C(27C)	1.346(12)	C(18C)-C(19C)	1.417(11)
C(19C)-C(20C)	1.331(12)	C(20C)-C(21C)	1.412(13)
C(21C)-C(22C)	1.412(13)	C(21C)-C(26C)	1.427(13)
C(22C)-C(23C)	1.427(17)	C(22C)-C(27C)	1.442(17)
C(23C)-C(24C)	1.362(14)	C(24C)-C(25C)	1.374(18)
C(25C)-C(26C)	1.33(2)	C(18D)-C(19D)	1.39
C(18D)-C(27D)	1.3901	C(19D)-C(20D)	1.3901
C(20D)-C(21D)	1.3901	C(21D)-C(26D)	1.3898
C(21D)-C(22D)	1.39	C(22D)-C(27D)	1.39
C(22D)-C(23D)	1.39	C(23D)-C(24D)	1.3899
C(24D)-C(25D)	1.39	C(25D)-C(26D)	1.3901
C(3A)-Re(1)-C(2A)	88.4(4)	C(3A)-Re(1)-C(1A)	90.5(3)
C(2A)-Re(1)-C(1A)	83.6(3)	C(3A)-Re(1)-O(4A)	173.8(3)
C(2A)-Re(1)-O(4A)	97.8(3)	C(1A)-Re(1)-O(4A)	89.5(3)
C(3A)-Re(1)-N(1A)	100.8(3)	C(2A)-Re(1)-N(1A)	100.5(3)

Table 27: Bond lengths [Å] and angles [°] for 2NS4 cont'd

C(1A)-Re(1)-N(1A)	168.1(3)	O(4A)-Re(1)-N(1A)	78.88(18)
C(3A)-Re(1)-N(2A)	93.5(3)	C(2A)-Re(1)-N(2A)	176.7(3)
C(1A)-Re(1)-N(2A)	99.1(3)	O(4A)-Re(1)-N(2A)	80.44(17)
N(1A)-Re(1)-N(2A)	76.5(2)	O(5A)-S(1)-O(6A)	117.5(3)
O(5A)-S(1)-O(4A)	112.4(3)	O(6A)-S(1)-O(4A)	108.8(3)
O(5A)-S(1)-C(18B)	87.9(4)	O(6A)-S(1)-C(18B)	123.5(3)
O(4A)-S(1)-C(18B)	105.1(3)	O(5A)-S(1)-C(18A)	110.4(4)
O(6A)-S(1)-C(18A)	103.3(4)	O(4A)-S(1)-C(18A)	103.1(3)
C(18B)-S(1)-C(18A)	24.2(3)	S(1)-O(4A)-Re(1)	129.1(3)
C(4A)-N(1A)-C(8A)	118.0(6)	C(4A)-N(1A)-Re(1)	128.7(5)
C(8A)-N(1A)-Re(1)	112.2(4)	C(15A)-N(2A)-C(12A)	117.7(6)
C(15A)-N(2A)-Re(1)	129.5(4)	C(12A)-N(2A)-Re(1)	112.5(4)
O(1A)-C(1A)-Re(1)	174.9(7)	O(2A)-C(2A)-Re(1)	175.1(8)
O(3A)-C(3A)-Re(1)	178.0(7)	N(1A)-C(4A)-C(5A)	120.5(8)
N(1A)-C(4A)-C(16A)	119.9(7)	C(5A)-C(4A)-C(16A)	119.6(8)
C(6A)-C(5A)-C(4A)	121.3(8)	C(5A)-C(6A)-C(7A)	120.2(7)
C(6A)-C(7A)-C(8A)	116.9(7)	C(6A)-C(7A)-C(9A)	123.7(7)
C(8A)-C(7A)-C(9A)	119.3(7)	N(1A)-C(8A)-C(7A)	122.9(7)
N(1A)-C(8A)-C(12A)	117.6(5)	C(7A)-C(8A)-C(12A)	119.5(6)
C(10A)-C(9A)-C(7A)	121.4(7)	C(9A)-C(10A)-C(11A)	121.0(7)
C(13A)-C(11A)-C(12A)	117.3(6)	C(13A)-C(11A)-C(10A)	122.9(7)
C(12A)-C(11A)-C(10A)	119.7(7)	N(2A)-C(12A)-C(11A)	122.6(7)
N(2A)-C(12A)-C(8A)	118.3(6)	C(11A)-C(12A)-C(8A)	119.1(6)
C(14A)-C(13A)-C(11A)	120.3(7)	C(13A)-C(14A)-C(15A)	119.9(7)
N(2A)-C(15A)-C(14A)	122.1(6)	N(2A)-C(15A)-C(17A)	119.9(6)
C(14A)-C(15A)-C(17A)	118.0(7)	C(27A)-C(18A)-C(19A)	120.8(8)
C(27A)-C(18A)-S(1)	120.5(6)	C(19A)-C(18A)-S(1)	118.7(7)
C(20A)-C(19A)-C(18A)	120.5(9)	C(19A)-C(20A)-C(21A)	120.6(9)
C(20A)-C(21A)-C(22A)	119.3(10)	C(20A)-C(21A)-C(26A)	123.4(9)
C(22A)-C(21A)-C(26A)	117.3(10)	C(23A)-C(22A)-C(27A)	123.1(9)
C(23A)-C(22A)-C(21A)	118.4(11)	C(27A)-C(22A)-C(21A)	118.5(11)
C(24A)-C(23A)-C(22A)	122.1(11)	C(23A)-C(24A)-C(25A)	121.4(12)
C(26A)-C(25A)-C(24A)	121.5(10)	C(25A)-C(26A)-C(21A)	119.2(10)
C(18A)-C(27A)-C(22A)	120.2(8)	C(19B)-C(18B)-C(27B)	120
C(19B)-C(18B)-S(1)	130.5(3)	C(27B)-C(18B)-S(1)	109.4(3)
C(20B)-C(19B)-C(18B)	120	C(19B)-C(20B)-C(21B)	120
C(26B)-C(21B)-C(20B)	120	C(26B)-C(21B)-C(22B)	120
C(20B)-C(21B)-C(22B)	120	C(23B)-C(22B)-C(27B)	120
C(23B)-C(22B)-C(21B)	120	C(27B)-C(22B)-C(21B)	120
C(22B)-C(23B)-C(24B)	120	C(25B)-C(24B)-C(23B)	120
C(24B)-C(25B)-C(26B)	120	C(21B)-C(26B)-C(25B)	120
C(18B)-C(27B)-C(22B)	120	C(3B)-Re(2)-C(1B)	89.9(3)
C(3B)-Re(2)-C(2B)	88.3(4)	C(1B)-Re(2)-C(2B)	83.7(3)
C(3B)-Re(2)-O(4B)	173.9(3)	C(1B)-Re(2)-O(4B)	89.5(3)
C(2B)-Re(2)-O(4B)	97.7(3)	C(3B)-Re(2)-N(2B)	94.4(3)
C(1B)-Re(2)-N(2B)	99.3(3)	C(2B)-Re(2)-N(2B)	175.9(3)
O(4B)-Re(2)-N(2B)	79.61(17)	C(3B)-Re(2)-N(1B)	100.3(3)
C(1B)-Re(2)-N(1B)	169.1(3)	C(2B)-Re(2)-N(1B)	100.3(3)
O(4B)-Re(2)-N(1B)	79.95(18)	N(2B)-Re(2)-N(1B)	76.3(2)
O(5B)-S(2)-O(6B)	116.7(3)	O(5B)-S(2)-O(4B)	112.6(3)
O(6B)-S(2)-O(4B)	109.0(3)	O(5B)-S(2)-C(18D)	89.3(4)
O(6B)-S(2)-C(18D)	120.1(3)	O(4B)-S(2)-C(18D)	107.8(3)

Table 28: Bond lengths [Å] and angles [°] for 2NS4 cont'd

O(5B)-S(2)-C(18C)	110.5(4)	O(6B)-S(2)-C(18C)	104.0(4)
O(4B)-S(2)-C(18C)	102.7(3)	C(18D)-S(2)-C(18C)	21.8(4)
S(2)-O(4B)-Re(2)	128.5(3)	C(4B)-N(1B)-C(8B)	118.6(6)
C(4B)-N(1B)-Re(2)	129.3(5)	C(8B)-N(1B)-Re(2)	111.4(4)
C(15B)-N(2B)-C(12B)	118.0(6)	C(15B)-N(2B)-Re(2)	129.2(4)
C(12B)-N(2B)-Re(2)	112.4(4)	O(1B)-C(1B)-Re(2)	175.7(7)
O(2B)-C(2B)-Re(2)	175.3(8)	O(3B)-C(3B)-Re(2)	177.0(6)
N(1B)-C(4B)-C(5B)	121.0(7)	N(1B)-C(4B)-C(16B)	120.4(7)
C(5B)-C(4B)-C(16B)	118.6(7)	C(6B)-C(5B)-C(4B)	120.1(8)
C(5B)-C(6B)-C(7B)	120.3(7)	C(6B)-C(7B)-C(8B)	117.6(7)
C(6B)-C(7B)-C(9B)	122.3(6)	C(8B)-C(7B)-C(9B)	119.9(7)
N(1B)-C(8B)-C(7B)	122.2(6)	N(1B)-C(8B)-C(12B)	118.6(5)
C(7B)-C(8B)-C(12B)	119.1(6)	C(10B)-C(9B)-C(7B)	120.7(6)
C(9B)-C(10B)-C(11B)	121.4(7)	C(13B)-C(11B)-C(12B)	118.7(6)
C(13B)-C(11B)-C(10B)	122.6(7)	C(12B)-C(11B)-C(10B)	118.6(7)
N(2B)-C(12B)-C(11B)	122.1(6)	N(2B)-C(12B)-C(8B)	117.7(6)
C(11B)-C(12B)-C(8B)	120.1(6)	C(14B)-C(13B)-C(11B)	118.2(7)
C(13B)-C(14B)-C(15B)	122.1(7)	N(2B)-C(15B)-C(14B)	120.7(6)
N(2B)-C(15B)-C(17B)	120.3(7)	C(14B)-C(15B)-C(17B)	119.1(7)
C(27C)-C(18C)-C(19C)	122.3(7)	C(27C)-C(18C)-S(2)	119.0(6)
C(19C)-C(18C)-S(2)	118.7(7)	C(20C)-C(19C)-C(18C)	120.5(9)
C(19C)-C(20C)-C(21C)	120.6(9)	C(20C)-C(21C)-C(22C)	119.0(11)
C(20C)-C(21C)-C(26C)	122.6(9)	C(22C)-C(21C)-C(26C)	118.3(11)
C(21C)-C(22C)-C(23C)	119.7(13)	C(21C)-C(22C)-C(27C)	119.7(13)
C(23C)-C(22C)-C(27C)	120.5(9)	C(24C)-C(23C)-C(22C)	118.6(10)
C(23C)-C(24C)-C(25C)	120.9(11)	C(26C)-C(25C)-C(24C)	123.1(11)
C(25C)-C(26C)-C(21C)	119.4(12)	C(18C)-C(27C)-C(22C)	117.8(8)
C(19D)-C(18D)-C(27D)	120	C(19D)-C(18D)-S(2)	126.6(3)
C(27D)-C(18D)-S(2)	113.4(3)	C(18D)-C(19D)-C(20D)	120.0
C(21D)-C(20D)-C(19D)	120	C(26D)-C(21D)-C(22D)	120.0
C(26D)-C(21D)-C(20D)	120	C(22D)-C(21D)-C(20D)	120.0
C(21D)-C(22D)-C(27D)	120	C(21D)-C(22D)-C(23D)	120.0
C(27D)-C(22D)-C(23D)	120	C(24D)-C(23D)-C(22D)	120.0
C(23D)-C(24D)-C(25D)	120	C(24D)-C(25D)-C(26D)	120.0
C(21D)-C(26D)-C(25D)	120	C(22D)-C(27D)-C(18D)	120.0

Table 29: Anisotropic displacement parameters [$Å^2 x10^3$] for 2NS4

	U11	U22	U33	U23	U13	U12
Re(1)	33(1)	60(1)	53(1)	-7(1)	9(1)	8(1)
S(1)	60(1)	41(1)	61(1)	5(1)	34(1)	12(1)
O(1A)	53(3)	85(4)	136(6)	8(4)	52(4)	12(3)
O(2A)	74(4)	138(6)	69(4)	26(4)	9(3)	56(4)
O(3A)	69(4)	126(6)	103(5)	-54(5)	-3(4)	-9(4)
O(4A)	45(2)	38(2)	53(3)	-3(2)	18(2)	8(2)
O(5A)	64(3)	70(4)	107(5)	-3(3)	30(3)	30(3)
O(6A)	88(4)	42(3)	57(3)	-7(2)	29(3)	-1(2)
N(1A)	49(3)	57(4)	46(3)	-11(3)	19(3)	1(3)
N(2A)	32(2)	42(3)	62(4)	-12(3)	11(2)	-3(2)
C(1A)	43(4)	63(5)	92(6)	-3(4)	21(4)	5(3)
C(2A)	64(5)	99(7)	62(5)	4(5)	22(4)	27(5)
C(3A)	44(4)	92(6)	74(6)	-28(5)	3(4)	0(4)
C(4A)	76(5)	77(5)	44(4)	-17(4)	22(4)	4(4)
C(5A)	80(6)	89(6)	66(6)	-11(5)	44(5)	-9(5)
C(6A)	53(4)	91(6)	72(6)	-23(5)	32(4)	-17(4)
C(7A)	42(4)	58(4)	78(5)	-25(4)	23(4)	-3(3)
C(8A)	36(3)	43(4)	56(4)	-15(3)	13(3)	1(3)
C(9A)	29(3)	65(5)	112(7)	-14(5)	16(4)	-1(3)
C(10A)	37(4)	62(5)	116(8)	-5(5)	1(4)	8(3)
C(11A)	43(3)	38(4)	82(5)	-1(4)	8(4)	-2(3)
C(12A)	34(3)	37(3)	64(4)	-12(3)	10(3)	2(3)
C(13A)	57(4)	49(5)	109(7)	19(5)	0(4)	8(4)
C(14A)	62(4)	42(4)	94(6)	12(4)	12(4)	-6(3)
C(15A)	43(3)	36(4)	75(5)	-12(3)	16(3)	-6(3)
C(16A)	98(6)	105(7)	58(5)	9(5)	39(5)	25(6)
C(17A)	51(4)	57(4)	94(6)	-1(4)	33(4)	-7(3)
C(18A)	52(5)	40(5)	54(5)	2(4)	21(4)	0(4)
C(19A)	52(5)	71(7)	81(7)	18(6)	6(5)	-1(5)
C(20A)	44(5)	74(7)	90(8)	15(6)	9(5)	5(5)
C(21A)	57(5)	53(5)	56(6)	7(5)	12(5)	-4(4)
C(22A)	60(7)	42(5)	55(6)	0(5)	24(5)	-6(4)
C(23A)	52(5)	82(7)	81(8)	7(6)	14(5)	-2(5)
C(24A)	79(7)	101(9)	62(8)	5(7)	19(6)	-15(7)
C(25A)	74(7)	85(9)	51(7)	3(5)	30(6)	-12(6)
C(26A)	51(6)	74(7)	84(8)	1(6)	31(6)	-3(5)
C(27A)	50(5)	56(5)	56(6)	-6(4)	21(4)	-7(4)
Re(2)	31(1)	67(1)	57(1)	5(1)	15(1)	-4(1)
S(2)	52(1)	46(1)	70(1)	-8(1)	30(1)	-14(1)
O(1B)	45(3)	93(4)	112(5)	4(4)	42(3)	-8(3)
O(2B)	65(4)	152(7)	82(4)	-38(4)	17(3)	-52(4)
O(3B)	50(3)	141(6)	102(5)	60(5)	5(3)	5(4)
O(4B)	39(2)	40(2)	72(3)	1(2)	16(2)	-9(2)
O(5B)	56(3)	75(4)	101(4)	-7(3)	35(3)	-23(3)
O(6B)	77(3)	42(3)	69(4)	0(2)	33(3)	-2(2)
N(1B)	40(3)	60(4)	55(4)	3(3)	20(3)	1(3)
N(2B)	36(3)	40(3)	62(4)	16(3)	20(3)	7(2)
C(1B)	44(4)	72(5)	72(5)	-1(4)	22(4)	-6(3)
C(2B)	46(4)	110(7)	75(6)	-11(5)	27(4)	-23(4)
C(3B)	38(4)	113(7)	68(5)	20(5)	13(4)	-13(4)
C(4B)	61(4)	73(5)	57(5)	6(4)	22(4)	1(4)
C(5B)	61(5)	76(5)	79(6)	1(5)	39(4)	8(4)
C(6B)	43(4)	69(5)	95(7)	12(5)	27(4)	10(4)
C(7B)	38(3)	50(4)	81(5)	9(4)	27(4)	5(3)
C(8B)	34(3)	42(4)	63(4)	11(3)	16(3)	1(3)
C(9B)	33(3)	70(5)	106(7)	6(5)	19(4)	4(3)

Table 30: Anisotropic displacement parameters [$Å^2 x10^3$] for 2NS4 cont'd

C(10B)	38(4)	67(5)	97(7)	-1(5)	10(4)	-5(3)
C(11B)	49(4)	40(4)	79(5)	-1(4)	12(4)	-1(3)
C(12B)	37(3)	35(3)	65(5)	8(3)	12(3)	0(3)
C(13B)	61(4)	49(4)	89(6)	-18(4)	7(4)	-2(4)
C(14B)	73(5)	35(4)	89(6)	-2(4)	28(4)	2(3)
C(15B)	56(4)	31(4)	82(5)	14(4)	31(4)	6(3)
C(16B)	75(5)	128(8)	58(5)	-15(5)	24(4)	-9(5)
C(17B)	56(4)	61(5)	106(7)	5(4)	39(4)	14(4)
C(18C)	39(5)	46(5)	61(6)	-8(4)	22(4)	-6(4)
C(19C)	44(5)	66(6)	75(7)	-20(5)	15(5)	-5(4)
C(20C)	41(4)	68(6)	81(7)	-9(5)	17(5)	-6(4)
C(21C)	45(5)	57(6)	58(6)	0(5)	13(5)	-8(4)
C(22C)	77(9)	44(5)	52(6)	7(5)	28(5)	-11(4)
C(23C)	47(5)	81(7)	55(6)	-3(5)	12(4)	-16(5)
C(24C)	93(8)	79(7)	55(7)	-16(6)	33(6)	-12(6)
C(25C)	96(10)	63(8)	74(8)	-15(7)	44(6)	-11(7)
C(26C)	64(7)	72(8)	63(7)	-13(5)	35(6)	-8(5)
C(27C)	39(4)	52(5)	73(6)	3(5)	25(4)	-13(4)

2. 4. 6. X-ray Crystallographic analysis for 2NS5

The X-ray examination and data collection was performed on a suitable yellow crystal of 2NS5. The crystal was mounted on a Cryoloop with Paratone-N oil. A Bruker CMOS detector was used to collect the data using Mo K alpha radiation. The data collection temperature was 100 K. Using the integration method (SADABS), data were corrected for absorption effects. The structure was solved by direct methods. Non-hydrogen atoms were refined anisotropically by full matrix least squares on F^2. Carbon atom C16 was disordered and shared location with H8A (similar sharing of location for atom C16A and atom H9A) and was refined with a two part model with fixed C-C distances of 1.50 (0.01) angstroms for C8-C16 and C9-C16A and C-H distances of 0.90 (0.005) angstroms for C8-H8A and C9-H9A and fixed occupancies of 64/36 %. Hydrogen atoms H8A and H9A were allowed to refine isotropically. Distortion with respect to C-H angles for C8-H8 and and C9-H9A were noted but attempts to treat distortion was not successful. All other hydrogen atoms were placed in calculated positions with appropriate riding parameter.

Table 31: Crystal data and structure refinement for 2NS5

Empirical formula	C26 H17 N2 O6 Re S	
Formula weight	671.68	
Temperature	100(2) K	
Wavelength	0.71073 Å	
Crystal system	Monoclinic	
Space group	P2(1)/n	
Unit cell dimensions	a = 10.0071(3) Å	a= 90°.
	b = 18.6658(7) Å	b= 104.6390(10)°.
	c = 12.6077(5) Å	g = 90°.
Volume	2278.55(14) Å3	
Z	4	
Density (calculated)	1.958 Mg/m^3	
Absorption coefficient	5.473 mm^{-1}	
F(000)	1304	
Crystal size	0.15 x 0.15 x 0.15 mm3	
Crystal color / block	yellow / block	
Theta range for data collection	2.33 to 26.40°.	
Index ranges	-12<=h<=12, -23<=k<=21, -15<=l<=13	
Reflections collected	16553	
Independent reflections	4625 [R(int) = 0.0189]	
Completeness to theta = 25.00°	99.60%	
Absorption correction	multi-scan /sadabs	
Max. and min. transmission	0.4940 and 0.4940	
Refinement method	Full-matrix least-squares on F2	
Data / restraints / parameters	4625 / 4 / 341	
Goodness-of-fit on F2	1.063	
Final R indices [I>2sigma(I)]	R1 = 0.0201, wR2 = 0.0423	
R indices (all data)	R1 = 0.0234, wR2 = 0.0434	
Largest diff. peak and hole	0.635 and -0.394 e.Å-3	

Table 32: Atomic coordinates ($x\ 10^4$) and equivalent isotropic displacement parameters ($Å^2 x\ 10^3$) 2NS5

	x	y	z	U(eq)
Re(1)	709(1)	245(1)	2678(1)	16(1)
S(1)	3113(1)	1150(1)	4484(1)	19(1)
O(2)	733(2)	-1268(1)	3631(2)	29(1)
O(3)	-927(2)	-452(1)	561(2)	32(1)
O(4)	1783(2)	743(1)	4215(2)	19(1)
O(5)	3744(2)	1177(1)	3570(2)	30(1)
O(6)	3998(2)	900(1)	5499(2)	31(1)
O(1)	3347(2)	-200(1)	2022(2)	32(1)
N(1)	615(3)	1360(1)	2149(2)	21(1)
N(2)	-1022(2)	690(1)	3207(2)	18(1)
C(1)	2368(3)	-24(2)	2269(3)	22(1)
C(2)	730(3)	-694(2)	3293(3)	19(1)
C(3)	-323(3)	-172(2)	1357(3)	23(1)
C(4)	1435(3)	1679(2)	1615(3)	29(1)
C(5)	1465(4)	2428(2)	1513(3)	37(1)
C(6)	620(4)	2848(2)	1949(3)	38(1)
C(7)	-291(4)	2530(2)	2484(3)	32(1)
C(8)	-1258(4)	2919(2)	2954(3)	41(1)
C(9)	-2122(4)	2569(2)	3418(3)	38(1)
C(10)	-2112(3)	1807(2)	3518(3)	29(1)
C(11)	-3023(3)	1417(2)	3978(3)	31(1)
C(12)	-2920(3)	688(2)	4048(3)	28(1)
C(13)	-1893(3)	342(2)	3672(2)	22(1)
C(14)	-1146(3)	1416(2)	3108(2)	21(1)
C(15)	-251(3)	1774(2)	2566(3)	23(1)
C(16)	-1336(5)	3720(2)	3015(4)	22(1)
C(16A)	-3026(10)	3132(5)	3678(9)	32(2)
C(17)	2632(3)	2038(2)	4707(2)	18(1)
C(18)	3327(3)	2616(2)	4365(3)	24(1)
C(19)	3018(3)	3303(2)	4591(3)	25(1)
C(20)	2009(3)	3443(2)	5175(2)	20(1)
C(21)	1671(3)	4151(2)	5437(3)	27(1)
C(22)	727(3)	4270(2)	6024(3)	28(1)
C(23)	48(3)	3690(2)	6374(3)	27(1)
C(24)	314(3)	2998(2)	6121(3)	24(1)
C(25)	1305(3)	2862(2)	5516(2)	20(1)
C(26)	1635(3)	2156(2)	5270(2)	20(1)

Table 33: Bond lengths [Å] and angles [°] for 2NS5

Re(1)-C(3)	1.891(3)
Re(1)-C(2)	1.915(3)
Re(1)-C(1)	1.926(3)
Re(1)-N(2)	2.172(2)
Re(1)-O(4)	2.173(2)
Re(1)-N(1)	2.179(2)
S(1)-O(6)	1.438(2)
S(1)-O(5)	1.448(2)
S(1)-O(4)	1.495(2)
S(1)-C(17)	1.770(3)
O(2)-C(2)	1.153(4)
O(3)-C(3)	1.158(4)
O(1)-C(1)	1.148(4)
N(1)-C(4)	1.328(4)
N(1)-C(15)	1.363(4)
N(2)-C(13)	1.335(4)
N(2)-C(14)	1.365(4)
C(4)-C(5)	1.403(5)
C(4)-H(4A)	0.95
C(5)-C(6)	1.366(6)
C(5)-H(5A)	0.95
C(6)-C(7)	1.396(6)
C(6)-H(6A)	0.95
C(7)-C(15)	1.414(4)
C(7)-C(8)	1.452(6)
C(8)-C(9)	1.330(6)
C(8)-C(16)	1.500(4)
C(8)-H(8A)	0.899(10)
C(9)-C(10)	1.429(5)
C(9)-C(16A)	1.477(5)
C(9)-H(9A)	0.907(10)
C(10)-C(11)	1.400(5)
C(10)-C(14)	1.409(4)
C(11)-C(12)	1.366(5)
C(11)-H(11A)	0.95
C(12)-C(13)	1.395(4)
C(12)-H(12A)	0.95
C(13)-H(13A)	0.95
C(14)-C(15)	1.424(5)
C(16)-H(16A)	0.98
C(16)-H(16B)	0.98
C(16)-H(16C)	0.98
C(16)-H(8A)	0.87(11)
C(16A)-H(9A)	0.62(3)
C(16A)-H(16D)	0.98
C(16A)-H(16E)	0.98
C(16A)-H(16F)	0.98
C(17)-C(26)	1.381(4)
C(17)-C(18)	1.408(4)
C(18)-C(19)	1.367(5)
C(18)-H(18A)	0.95
C(19)-C(20)	1.416(4)
C(19)-H(19A)	0.95
C(20)-C(25)	1.418(4)
C(20)-C(21)	1.424(5)
C(21)-C(22)	1.356(5)
C(21)-H(21A)	0.95
C(22)-C(23)	1.408(5)

Table 34: Bond lengths [Å] and angles [°] for 2NS5 cont'd

C(22)-H(22A)	0.95
C(23)-C(24)	1.371(5)
C(23)-H(23A)	0.95
C(24)-C(25)	1.419(4)
C(24)-H(24A)	0.95
C(25)-C(26)	1.412(4)
C(26)-H(26A)	0.95
C(3)-Re(1)-C(2)	85.86(13)
C(3)-Re(1)-C(1)	88.42(13)
C(2)-Re(1)-C(1)	87.01(13)
C(3)-Re(1)-N(2)	97.31(11)
C(2)-Re(1)-N(2)	98.82(11)
C(1)-Re(1)-N(2)	172.08(11)
C(3)-Re(1)-O(4)	176.72(11)
C(2)-Re(1)-O(4)	94.47(11)
C(1)-Re(1)-O(4)	94.85(10)
N(2)-Re(1)-O(4)	79.42(8)
C(3)-Re(1)-N(1)	98.71(12)
C(2)-Re(1)-N(1)	173.24(11)
C(1)-Re(1)-N(1)	98.05(12)
N(2)-Re(1)-N(1)	75.74(10)
O(4)-Re(1)-N(1)	80.68(8)
O(6)-S(1)-O(5)	115.19(15)
O(6)-S(1)-O(4)	110.50(14)
O(5)-S(1)-O(4)	112.31(13)
O(6)-S(1)-C(17)	107.07(14)
O(5)-S(1)-C(17)	106.50(15)
O(4)-S(1)-C(17)	104.47(13)
S(1)-O(4)-Re(1)	129.14(12)
C(4)-N(1)-C(15)	118.3(3)
C(4)-N(1)-Re(1)	126.9(2)
C(15)-N(1)-Re(1)	114.0(2)
C(13)-N(2)-C(14)	118.0(3)
C(13)-N(2)-Re(1)	127.5(2)
C(14)-N(2)-Re(1)	114.4(2)
O(1)-C(1)-Re(1)	178.5(3)
O(2)-C(2)-Re(1)	177.8(3)
O(3)-C(3)-Re(1)	177.3(3)
N(1)-C(4)-C(5)	121.6(4)
N(1)-C(4)-H(4A)	119.2
C(5)-C(4)-H(4A)	119.2
C(6)-C(5)-C(4)	120.3(4)
C(6)-C(5)-H(5A)	119.8
C(4)-C(5)-H(5A)	119.8
C(5)-C(6)-C(7)	119.8(3)
C(5)-C(6)-H(6A)	120.1
C(7)-C(6)-H(6A)	120.1
C(6)-C(7)-C(15)	116.7(4)
C(6)-C(7)-C(8)	124.7(3)
C(15)-C(7)-C(8)	118.6(3)
C(9)-C(8)-C(7)	120.5(3)
C(9)-C(8)-C(16)	114.8(4)
C(7)-C(8)-C(16)	124.6(4)
C(9)-C(8)-H(8A)	143(8)
C(7)-C(8)-H(8A)	95(8)

Table 35: Bond lengths [Å] and angles [°] for 2NS5 cont'd

C(16)-C(8)-H(8A)	31(8)
C(8)-C(9)-C(10)	122.5(3)
C(8)-C(9)-C(16A)	104.5(5)
C(10)-C(9)-C(16A)	132.8(6)
C(8)-C(9)-H(9A)	115(4)
C(10)-C(9)-H(9A)	122(4)
C(16A)-C(9)-H(9A)	12(4)
C(11)-C(10)-C(14)	117.5(3)
C(11)-C(10)-C(9)	124.3(3)
C(14)-C(10)-C(9)	118.2(4)
C(12)-C(11)-C(10)	119.8(3)
C(12)-C(11)-H(11A)	120.1
C(10)-C(11)-H(11A)	120.1
C(11)-C(12)-C(13)	119.3(3)
C(11)-C(12)-H(12A)	120.4
C(13)-C(12)-H(12A)	120.4
N(2)-C(13)-C(12)	122.9(3)
N(2)-C(13)-H(13A)	118.6
C(12)-C(13)-H(13A)	118.6
N(2)-C(14)-C(10)	122.3(3)
N(2)-C(14)-C(15)	117.2(3)
C(10)-C(14)-C(15)	120.5(3)
N(1)-C(15)-C(7)	123.2(3)
N(1)-C(15)-C(14)	117.2(3)
C(7)-C(15)-C(14)	119.6(3)
C(8)-C(16)-H(16A)	109.5
C(8)-C(16)-H(16B)	109.5
H(16A)-C(16)-H(16B)	109.5
C(8)-C(16)-H(16C)	109.5
H(16A)-C(16)-H(16C)	109.5
H(16B)-C(16)-H(16C)	109.5
C(8)-C(16)-H(8A)	33(4)
H(16A)-C(16)-H(8A)	138.2
H(16B)-C(16)-H(8A)	82.5
H(16C)-C(16)-H(8A)	103.2
C(9)-C(16A)-H(9A)	18(5)
C(9)-C(16A)-H(16D)	109.5
H(9A)-C(16A)-H(16D)	124.8
C(9)-C(16A)-H(16E)	109.5
H(9A)-C(16A)-H(16E)	94.2
H(16D)-C(16A)-H(16E)	109.5
C(9)-C(16A)-H(16F)	109.5
H(9A)-C(16A)-H(16F)	107.9
H(16D)-C(16A)-H(16F)	109.5
H(16E)-C(16A)-H(16F)	109.5
C(26)-C(17)-C(18)	120.9(3)
C(26)-C(17)-S(1)	119.4(2)
C(18)-C(17)-S(1)	119.6(2)
C(19)-C(18)-C(17)	119.9(3)
C(19)-C(18)-H(18A)	120
C(17)-C(18)-H(18A)	120
C(18)-C(19)-C(20)	120.7(3)
C(18)-C(19)-H(19A)	119.7
C(20)-C(19)-H(19A)	119.7
C(19)-C(20)-C(25)	119.4(3)
C(19)-C(20)-C(21)	122.3(3)

Table 36: Bond lengths [Å] and angles [°] for 2NS5 cont'd

C(25)-C(20)-C(21)	118.3(3)
C(22)-C(21)-C(20)	121.2(3)
C(22)-C(21)-H(21A)	119.4
C(20)-C(21)-H(21A)	119.4
C(21)-C(22)-C(23)	120.2(3)
C(21)-C(22)-H(22A)	119.9
C(23)-C(22)-H(22A)	119.9
C(24)-C(23)-C(22)	120.9(3)
C(24)-C(23)-H(23A)	119.5
C(22)-C(23)-H(23A)	119.5
C(23)-C(24)-C(25)	119.8(3)
C(23)-C(24)-H(24A)	120.1
C(25)-C(24)-H(24A)	120.1
C(26)-C(25)-C(20)	119.1(3)
C(26)-C(25)-C(24)	121.3(3)
C(20)-C(25)-C(24)	119.6(3)
C(17)-C(26)-C(25)	120.0(3)
C(17)-C(26)-H(26A)	120
C(25)-C(26)-H(26A)	120
C(17)-C(26)-C(25)	120.0(3)
C(17)-C(26)-H(26A)	120
C(25)-C(26)-H(26A)	120

Table 37: Anisotropic displacement parameters (Å2x 10^3) for 2NS5

	U11	**U**22	**U**33	**U**23	**U**13	**U**12
Re(1)	18(1)	13(1)	15(1)	-1(1)	2(1)	-1(1)
S(1)	16(1)	18(1)	21(1)	-3(1)	1(1)	1(1)
O(2)	33(1)	18(1)	35(1)	5(1)	6(1)	-3(1)
O(3)	32(1)	34(1)	25(1)	-13(1)	-1(1)	-2(1)
O(4)	21(1)	19(1)	17(1)	-2(1)	3(1)	-3(1)
O(5)	22(1)	35(1)	37(1)	-14(1)	13(1)	-4(1)
O(6)	30(1)	23(1)	32(1)	-2(1)	-11(1)	4(1)
O(1)	30(1)	33(1)	37(1)	-10(1)	17(1)	-4(1)
N(1)	22(1)	19(1)	17(1)	4(1)	-5(1)	-3(1)
N(2)	18(1)	17(1)	17(1)	-2(1)	-3(1)	2(1)
C(1)	27(2)	18(2)	20(2)	-3(1)	6(1)	-5(1)
C(2)	16(1)	17(2)	25(2)	-2(1)	5(1)	-1(1)
C(3)	26(2)	19(2)	24(2)	0(1)	5(1)	3(1)
C(4)	28(2)	30(2)	22(2)	7(1)	-4(1)	-8(2)
C(5)	32(2)	33(2)	35(2)	18(2)	-14(2)	-16(2)
C(6)	35(2)	19(2)	42(2)	12(2)	-23(2)	-5(2)
C(7)	30(2)	17(2)	35(2)	4(1)	-19(2)	-2(1)
C(8)	35(2)	16(2)	51(2)	-6(2)	-28(2)	8(2)
C(9)	25(2)	28(2)	47(2)	-19(2)	-15(2)	12(2)
C(10)	24(2)	29(2)	25(2)	-11(1)	-10(1)	9(1)
C(11)	19(2)	43(2)	26(2)	-10(2)	-2(1)	12(2)
C(12)	19(2)	39(2)	24(2)	-1(2)	2(1)	6(2)
C(13)	19(2)	26(2)	18(2)	-1(1)	0(1)	2(1)
C(14)	18(2)	20(2)	20(2)	-5(1)	-6(1)	3(1)
C(15)	22(2)	17(2)	21(2)	0(1)	-10(1)	1(1)
C(16)	22(2)	14(2)	28(3)	2(2)	4(2)	0(2)
C(16A)	23(5)	37(6)	39(6)	1(5)	15(4)	13(4)
C(17)	16(1)	18(2)	18(2)	-2(1)	-2(1)	0(1)
C(18)	16(2)	29(2)	26(2)	2(1)	4(1)	-1(1)
C(19)	20(2)	25(2)	27(2)	4(1)	2(1)	-2(1)
C(20)	17(1)	21(2)	17(1)	2(1)	-2(1)	-2(1)
C(21)	25(2)	24(2)	27(2)	3(1)	-2(1)	1(1)
C(22)	32(2)	22(2)	26(2)	-3(1)	0(1)	6(1)
C(23)	28(2)	29(2)	22(2)	-1(1)	4(1)	4(1)
C(24)	24(2)	27(2)	20(2)	0(1)	4(1)	-1(1)
C(25)	19(2)	22(2)	16(1)	0(1)	-2(1)	1(1)
C(26)	18(2)	21(2)	19(2)	1(1)	0(1)	-3(1)

2. 4. 7. X-ray Crystallographic analysis for 2NS6

The X-ray examination and data collection was performed on a suitable yellow crystal of 2NS6. The crystal was mounted on a Cryoloop with Paratone-N oil. A Bruker CMOS detector was used to collect the data using Mo K alpha radiation. The data collection temperature was 100 K. Using the integration method (SADABS), data were corrected for absorption effects. The structure was solved by direct methods. Non-hydrogen atoms were refined anisotropically by full matrix least squares on F^2. All hydrogen atoms were placed in calculated positions with appropriate riding parameters.

Methylene chloride was disordered and treated using a two part model (55.2/44.8 %) with C-Cl distances fixed at 1.78 angstroms. The smaller part of the disordered CH_2Cl_2 generated a symmetry related molecule such that the disordered methylene chloride was in the ratio of 55.2%, 22.4%, 22.4%.

Table 38: **Crystal data and structure refinement for 2NS6**

Empirical formula	$C_{38}H_{25}Cl_2N_2O_6ReS$	
Formula weight	894.76	
Temperature	100(2) K	
Wavelength	0.71073 Å	
Crystal system	Triclinic	
Space group	P-1	
Unit cell dimensions	a = 10.6534(4) Å	a= 105.4700(10)°.
	b = 12.7411(5) Å	b= 109.4920(10)°.
	c = 13.7893(5) Å	g = 90.9840(10)°.
Volume	1688.86(11) Å3	
Z	2	
Density (calculated)	1.760 Mg/m3	
Absorption coefficient	3.869 mm-1	
F(000)	880	
Crystal size	0.20 x 0.06 x 0.06 mm3	
Crystal color / habit	yellow / block	
Theta range for data collection	2.65 to 26.42°.	
Index ranges	-13<=h<=13, -15<=k<=15, -16<=l<=17	
Reflections collected	22550	
Independent reflections	6747 [R(int) = 0.0171]	
Completeness to theta = 25.00°	99.80%	
Absorption correction	multi-scan / sadabs	
Max. and min. transmission	0.8010 and 0.5116	
Refinement method	Full-matrix least-squares on F2	
Data / restraints / parameters	6747 / 6 / 479	
Goodness-of-fit on F2	1.078	
Final R indices [I>2sigma(I)]	R1 = 0.0169, wR2 = 0.0385	
R indices (all data)	R1 = 0.0189, wR2 = 0.0392	
Largest diff. peak and hole	0.701 and -0.669 e.Å-3	

Table 39: Atomic coordinates ($x\ 10^4$) and equivalent isotropic displacement parameters ($Å^2 x\ 10^3$) for 2NS6

	x	y	z	U(eq)
Re(1)	2010(1)	554(1)	3895(1)	16(1)
S(1)	2874(1)	-987(1)	1900(1)	19(1)
O(1)	2604(2)	-664(2)	5616(2)	28(1)
O(2)	-656(2)	-934(2)	2632(2)	37(1)
O(3)	443(2)	1945(2)	5144(2)	45(1)
O(4)	3208(2)	-398(1)	3065(1)	17(1)
O(5)	1451(2)	-1130(2)	1309(1)	29(1)
O(6)	3529(2)	-1971(1)	1802(2)	30(1)
N(1)	1800(2)	1494(2)	2759(2)	17(1)
N(2)	3852(2)	1675(2)	4566(2)	15(1)
C(1)	2393(2)	-222(2)	4961(2)	20(1)
C(2)	362(3)	-402(2)	3103(2)	23(1)
C(3)	1049(3)	1440(2)	4670(2)	26(1)
C(4)	740(2)	1427(2)	1882(2)	20(1)
C(5)	676(2)	2077(2)	1204(2)	20(1)
C(6)	1758(2)	2824(2)	1409(2)	18(1)
C(7)	2931(2)	2868(2)	2304(2)	16(1)
C(8)	4175(2)	3511(2)	2546(2)	17(1)
C(9)	5235(2)	3575(2)	3447(2)	17(1)
C(10)	5160(2)	3028(2)	4214(2)	15(1)
C(11)	6195(2)	3145(2)	5221(2)	16(1)
C(12)	6017(2)	2501(2)	5839(2)	18(1)
C(13)	4857(2)	1775(2)	5488(2)	18(1)
C(14)	4000(2)	2302(2)	3940(2)	14(1)
C(15)	2888(2)	2215(2)	2971(2)	16(1)
C(16)	1669(2)	3545(2)	705(2)	18(1)
C(17)	1148(3)	3086(2)	-407(2)	22(1)
C(18)	1009(3)	3751(2)	-1078(2)	28(1)
C(19)	1365(3)	4872(2)	-648(2)	27(1)
C(20)	1872(3)	5339(2)	457(2)	26(1)
C(21)	2029(2)	4675(2)	1133(2)	22(1)
C(22)	7432(2)	3918(2)	5591(2)	16(1)
C(23)	7389(3)	5000(2)	5546(2)	20(1)
C(24)	8563(3)	5690(2)	5858(2)	25(1)
C(25)	9792(3)	5309(2)	6219(2)	26(1)
C(26)	9848(3)	4247(2)	6289(2)	25(1)
C(27)	8679(2)	3557(2)	5984(2)	20(1)
C(28)	3624(2)	-78(2)	1419(2)	18(1)
C(29)	2871(2)	166(2)	468(2)	18(1)
C(30)	3444(3)	875(2)	102(2)	22(1)
C(31)	4782(3)	1359(2)	660(2)	21(1)
C(32)	5408(3)	2096(2)	304(2)	31(1)
C(33)	6707(3)	2547(2)	862(3)	38(1)
C(34)	7449(3)	2289(2)	1803(2)	34(1)
C(35)	6890(3)	1584(2)	2176(2)	27(1)
C(36)	5549(3)	1102(2)	1617(2)	21(1)
C(37)	4924(2)	371(2)	1980(2)	19(1)
C(38)	5904(17)	6641(10)	2008(10)	36(3)
Cl(1)	6888(1)	7862(1)	2536(1)	34(1)
Cl(2)	6426(6)	5980(4)	3006(5)	87(2)
C(38A)	5970(20)	6375(12)	1979(12)	45(4)
Cl(1A)	6406(5)	6000(2)	3167(4)	33(1)
Cl(2A)	5388(2)	5244(2)	854(2)	63(1)

Table 40: Bond lengths [Å] and angles [°] for 2NS6

Re(1)-C(3)	1.895(3)
Re(1)-C(1)	1.921(3)
Re(1)-C(2)	1.922(3)
Re(1)-O(4)	2.1671(16)
Re(1)-N(1)	2.1721(19)
Re(1)-N(2)	2.1757(19)
S(1)-O(6)	1.4421(19)
S(1)-O(5)	1.4433(19)
S(1)-O(4)	1.4956(17)
S(1)-C(28)	1.775(2)
O(1)-C(1)	1.151(3)
O(2)-C(2)	1.152(3)
O(3)-C(3)	1.153(3)
N(1)-C(4)	1.333(3)
N(1)-C(15)	1.366(3)
N(2)-C(13)	1.334(3)
N(2)-C(14)	1.365(3)
C(4)-C(5)	1.392(3)
C(4)-H(4A)	0.95
C(5)-C(6)	1.384(3)
C(5)-H(5B)	0.95
C(6)-C(7)	1.421(3)
C(6)-C(16)	1.486(3)
C(7)-C(15)	1.405(3)
C(7)-C(8)	1.435(3)
C(8)-C(9)	1.353(3)
C(8)-H(8A)	0.95
C(9)-C(10)	1.435(3)
C(9)-H(9A)	0.95
C(10)-C(14)	1.410(3)
C(10)-C(11)	1.424(3)
C(11)-C(12)	1.382(3)
C(11)-C(22)	1.485(3)
C(12)-C(13)	1.392(3)
C(12)-H(12A)	0.95
C(13)-H(13A)	0.95
C(14)-C(15)	1.436(3)
C(16)-C(17)	1.394(3)
C(16)-C(21)	1.395(3)
C(17)-C(18)	1.388(4)
C(17)-H(17A)	0.95
C(18)-C(19)	1.384(4)
C(18)-H(18A)	0.95
C(19)-C(20)	1.387(4)
C(19)-H(19A)	0.95
C(20)-C(21)	1.390(4)
C(20)-H(20A)	0.95
C(21)-H(21A)	0.95
C(22)-C(27)	1.395(3)
C(22)-C(23)	1.398(3)
C(23)-C(24)	1.387(4)
C(23)-H(23A)	0.95
C(24)-C(25)	1.383(4)
C(24)-H(24A)	0.95
C(25)-C(26)	1.382(4)
C(25)-H(25A)	0.95
C(26)-C(27)	1.384(4)
C(26)-H(26A)	0.95

Table 41: Bond lengths [Å] and angles [°] for 2NS6 cont'd

C(27)-H(27A)	0.95
C(28)-C(37)	1.366(3)
C(28)-C(29)	1.409(3)
C(29)-C(30)	1.369(4)
C(29)-H(29A)	0.95
C(30)-C(31)	1.411(4)
C(30)-H(30A)	0.95
C(31)-C(32)	1.417(4)
C(31)-C(36)	1.428(4)
C(32)-C(33)	1.365(4)
C(32)-H(32A)	0.95
C(33)-C(34)	1.403(5)
C(33)-H(33A)	0.95
C(34)-C(35)	1.363(4)
C(34)-H(34A)	0.95
C(35)-C(36)	1.413(4)
C(35)-H(35A)	0.95
C(36)-C(37)	1.418(4)
C(37)-H(37A)	0.95
C(38)-Cl(1)	1.698(12)
C(38)-Cl(2)	1.742(12)
C(38)-H(38A)	0.99
C(38)-H(38B)	0.99
C(38A)-Cl(2A)	1.732(15)
C(38A)-Cl(1A)	1.746(15)
C(38A)-H(38C)	0.99
C(38A)-H(38D)	0.99
C(3)-Re(1)-C(1)	86.77(11)
C(3)-Re(1)-C(2)	86.92(11)
C(1)-Re(1)-C(2)	89.08(10)
C(3)-Re(1)-O(4)	176.81(9)
C(1)-Re(1)-O(4)	93.14(8)
C(2)-Re(1)-O(4)	96.27(9)
C(3)-Re(1)-N(1)	95.45(10)
C(1)-Re(1)-N(1)	173.94(9)
C(2)-Re(1)-N(1)	96.66(9)
O(4)-Re(1)-N(1)	84.33(7)
C(3)-Re(1)-N(2)	96.80(9)
C(1)-Re(1)-N(2)	98.67(9)
C(2)-Re(1)-N(2)	171.56(9)
O(4)-Re(1)-N(2)	80.05(7)
N(1)-Re(1)-N(2)	75.49(7)
O(6)-S(1)-O(5)	115.84(12)
O(6)-S(1)-O(4)	109.09(10)
O(5)-S(1)-O(4)	112.14(11)
O(6)-S(1)-C(28)	108.07(11)
O(5)-S(1)-C(28)	106.94(11)
O(4)-S(1)-C(28)	103.99(10)
S(1)-O(4)-Re(1)	130.47(10)
C(4)-N(1)-C(15)	117.5(2)
C(4)-N(1)-Re(1)	126.88(16)
C(15)-N(1)-Re(1)	115.59(15)
C(13)-N(2)-C(14)	117.5(2)
C(13)-N(2)-Re(1)	127.13(16)
C(14)-N(2)-Re(1)	115.30(15)

Table 42: Bond lengths [Å] and angles [°] for 2NS6 cont'd

O(1)-C(1)-Re(1)	177.9(2)
O(2)-C(2)-Re(1)	176.9(2)
O(3)-C(3)-Re(1)	177.5(2)
N(1)-C(4)-C(5)	123.3(2)
N(1)-C(4)-H(4A)	118.4
C(5)-C(4)-H(4A)	118.4
C(6)-C(5)-C(4)	120.3(2)
C(6)-C(5)-H(5B)	119.8
C(4)-C(5)-H(5B)	119.8
C(5)-C(6)-C(7)	117.6(2)
C(5)-C(6)-C(16)	120.1(2)
C(7)-C(6)-C(16)	122.3(2)
C(15)-C(7)-C(6)	118.2(2)
C(15)-C(7)-C(8)	117.9(2)
C(6)-C(7)-C(8)	123.8(2)
C(9)-C(8)-C(7)	121.2(2)
C(9)-C(8)-H(8A)	119.4
C(7)-C(8)-H(8A)	119.4
C(8)-C(9)-C(10)	121.8(2)
C(8)-C(9)-H(9A)	119.1
C(10)-C(9)-H(9A)	119.1
C(14)-C(10)-C(11)	117.8(2)
C(14)-C(10)-C(9)	117.8(2)
C(11)-C(10)-C(9)	124.3(2)
C(12)-C(11)-C(10)	117.5(2)
C(12)-C(11)-C(22)	121.0(2)
C(10)-C(11)-C(22)	121.5(2)
C(11)-C(12)-C(13)	120.8(2)
C(11)-C(12)-H(12A)	119.6
C(13)-C(12)-H(12A)	119.6
N(2)-C(13)-C(12)	122.9(2)
N(2)-C(13)-H(13A)	118.5
C(12)-C(13)-H(13A)	118.5
N(2)-C(14)-C(10)	123.3(2)
N(2)-C(14)-C(15)	116.8(2)
C(10)-C(14)-C(15)	119.9(2)
N(1)-C(15)-C(7)	122.9(2)
N(1)-C(15)-C(14)	116.5(2)
C(7)-C(15)-C(14)	120.6(2)
C(17)-C(16)-C(21)	119.4(2)
C(17)-C(16)-C(6)	119.1(2)
C(21)-C(16)-C(6)	121.4(2)
C(18)-C(17)-C(16)	120.1(2)
C(18)-C(17)-H(17A)	120
C(16)-C(17)-H(17A)	120
C(19)-C(18)-C(17)	120.3(2)
C(19)-C(18)-H(18A)	119.9
C(17)-C(18)-H(18A)	119.9
C(18)-C(19)-C(20)	120.2(2)
C(18)-C(19)-H(19A)	119.9
C(20)-C(19)-H(19A)	119.9
C(19)-C(20)-C(21)	119.8(2)
C(19)-C(20)-H(20A)	120.1
C(21)-C(20)-H(20A)	120.1
C(20)-C(21)-C(16)	120.3(2)
C(20)-C(21)-H(21A)	119.8
C(16)-C(21)-H(21A)	119.8

Table 43: Bond lengths [Å] and angles [°] for 2NS6 cont'd

C(27)-C(22)-C(23)	118.6(2)
C(27)-C(22)-C(11)	119.5(2)
C(23)-C(22)-C(11)	122.0(2)
C(24)-C(23)-C(22)	120.6(2)
C(24)-C(23)-H(23A)	119.7
C(22)-C(23)-H(23A)	119.7
C(25)-C(24)-C(23)	120.0(2)
C(25)-C(24)-H(24A)	120
C(23)-C(24)-H(24A)	120
C(26)-C(25)-C(24)	120.0(2)
C(26)-C(25)-H(25A)	120
C(24)-C(25)-H(25A)	120
C(25)-C(26)-C(27)	120.3(2)
C(25)-C(26)-H(26A)	119.8
C(27)-C(26)-H(26A)	119.8
C(26)-C(27)-C(22)	120.5(2)
C(26)-C(27)-H(27A)	119.7
C(22)-C(27)-H(27A)	119.7
C(37)-C(28)-C(29)	121.2(2)
C(37)-C(28)-S(1)	119.20(18)
C(29)-C(28)-S(1)	119.55(19)
C(30)-C(29)-C(28)	119.6(2)
C(30)-C(29)-H(29A)	120.2
C(28)-C(29)-H(29A)	120.2
C(29)-C(30)-C(31)	120.9(2)
C(29)-C(30)-H(30A)	119.5
C(31)-C(30)-H(30A)	119.5
C(30)-C(31)-C(32)	122.5(2)
C(30)-C(31)-C(36)	119.4(2)
C(32)-C(31)-C(36)	118.1(2)
C(33)-C(32)-C(31)	120.9(3)
C(33)-C(32)-H(32A)	119.5
C(31)-C(32)-H(32A)	119.5
C(32)-C(33)-C(34)	120.4(3)
C(32)-C(33)-H(33A)	119.8
C(34)-C(33)-H(33A)	119.8
C(35)-C(34)-C(33)	120.8(3)
C(35)-C(34)-H(34A)	119.6
C(33)-C(34)-H(34A)	119.6
C(34)-C(35)-C(36)	120.2(3)
C(34)-C(35)-H(35A)	119.9
C(36)-C(35)-H(35A)	119.9
C(35)-C(36)-C(37)	122.1(2)
C(35)-C(36)-C(31)	119.5(2)
C(37)-C(36)-C(31)	118.3(2)
C(28)-C(37)-C(36)	120.5(2)
C(28)-C(37)-H(37A)	119.8
C(36)-C(37)-H(37A)	119.8
Cl(1)-C(38)-Cl(2)	104.7(6)
Cl(1)-C(38)-H(38A)	110.8
Cl(2)-C(38)-H(38A)	110.8
Cl(1)-C(38)-H(38B)	110.8
Cl(2)-C(38)-H(38B)	110.8
H(38A)-C(38)-H(38B)	108.9
Cl(2A)-C(38A)-Cl(1A)	111.8(8)
Cl(2A)-C(38A)-H(38C)	109.3
Cl(1A)-C(38A)-H(38C)	109.3
Cl(2A)-C(38A)-H(38D)	109.3
Cl(1A)-C(38A)-H(38D)	109.3
H(38C)-C(38A)-H(38D)	107.9

Table 44: Anisotropic displacement parameters ($Å^2 x\ 10^3$) for 2NS6

	U11	U22	U33	U23	U13	U12
Re(1)	16(1)	14(1)	16(1)	4(1)	5(1)	-1(1)
S(1)	26(1)	15(1)	14(1)	3(1)	6(1)	-3(1)
O(1)	35(1)	29(1)	21(1)	11(1)	7(1)	-4(1)
O(2)	27(1)	40(1)	34(1)	3(1)	5(1)	-13(1)
O(3)	40(1)	32(1)	69(2)	1(1)	38(1)	4(1)
O(4)	19(1)	18(1)	13(1)	4(1)	4(1)	1(1)
O(5)	27(1)	35(1)	18(1)	5(1)	1(1)	-15(1)
O(6)	55(1)	15(1)	27(1)	6(1)	22(1)	6(1)
N(1)	17(1)	13(1)	18(1)	4(1)	4(1)	0(1)
N(2)	16(1)	14(1)	15(1)	3(1)	4(1)	1(1)
C(1)	20(1)	17(1)	19(1)	-1(1)	6(1)	-4(1)
C(2)	26(1)	23(1)	20(1)	7(1)	8(1)	0(1)
C(3)	23(1)	19(1)	34(2)	5(1)	10(1)	-4(1)
C(4)	16(1)	16(1)	23(1)	5(1)	2(1)	-1(1)
C(5)	17(1)	18(1)	20(1)	5(1)	0(1)	0(1)
C(6)	20(1)	14(1)	17(1)	3(1)	5(1)	3(1)
C(7)	17(1)	13(1)	15(1)	2(1)	5(1)	2(1)
C(8)	21(1)	15(1)	17(1)	6(1)	7(1)	2(1)
C(9)	18(1)	13(1)	19(1)	3(1)	6(1)	0(1)
C(10)	16(1)	13(1)	15(1)	2(1)	5(1)	3(1)
C(11)	15(1)	13(1)	16(1)	1(1)	5(1)	3(1)
C(12)	17(1)	20(1)	15(1)	4(1)	3(1)	2(1)
C(13)	19(1)	17(1)	17(1)	5(1)	7(1)	3(1)
C(14)	16(1)	13(1)	14(1)	2(1)	6(1)	4(1)
C(15)	15(1)	14(1)	17(1)	2(1)	6(1)	2(1)
C(16)	14(1)	18(1)	20(1)	7(1)	2(1)	1(1)
C(17)	22(1)	20(1)	20(1)	6(1)	2(1)	0(1)
C(18)	27(1)	31(1)	21(1)	10(1)	3(1)	-1(1)
C(19)	26(1)	28(1)	30(2)	18(1)	4(1)	0(1)
C(20)	22(1)	19(1)	34(2)	11(1)	3(1)	-2(1)
C(21)	20(1)	20(1)	21(1)	5(1)	2(1)	0(1)
C(22)	18(1)	18(1)	11(1)	1(1)	5(1)	0(1)
C(23)	22(1)	18(1)	21(1)	2(1)	10(1)	3(1)
C(24)	32(2)	15(1)	27(1)	-2(1)	15(1)	-2(1)
C(25)	24(1)	28(1)	20(1)	-4(1)	8(1)	-11(1)
C(26)	16(1)	34(2)	20(1)	5(1)	4(1)	0(1)
C(27)	18(1)	23(1)	17(1)	5(1)	3(1)	1(1)
C(28)	23(1)	13(1)	17(1)	3(1)	8(1)	1(1)
C(29)	20(1)	19(1)	12(1)	3(1)	3(1)	1(1)
C(30)	33(1)	19(1)	15(1)	6(1)	9(1)	7(1)
C(31)	32(1)	14(1)	20(1)	2(1)	14(1)	2(1)
C(32)	53(2)	20(1)	26(1)	6(1)	21(1)	0(1)
C(33)	58(2)	23(1)	39(2)	1(1)	32(2)	-13(1)
C(34)	36(2)	30(2)	30(2)	-7(1)	19(1)	-12(1)
C(35)	30(1)	25(1)	24(1)	-4(1)	14(1)	-6(1)
C(36)	24(1)	20(1)	16(1)	-2(1)	9(1)	2(1)
C(37)	23(1)	17(1)	15(1)	4(1)	5(1)	1(1)
C(38)	39(4)	11(5)	47(5)	17(3)	-3(4)	3(4)
Cl(1)	32(1)	34(1)	35(1)	9(1)	11(1)	-10(1)
Cl(2)	56(2)	131(3)	117(4)	93(3)	40(2)	37(2)
C(38A)	43(6)	21(8)	86(9)	32(6)	28(6)	9(5)
Cl(1A)	42(2)	25(1)	43(1)	18(1)	22(1)	15(1)
Cl(2A)	48(1)	87(2)	51(1)	7(1)	23(1)	11(1)

2. 4. 8. X-ray Crystallographic analysis for 2NS7

The X-ray examination and data collection was performed on a yellow crystal of 2NS7. The crystal was mounted on a Cryoloop with Paratone-N oil. A Bruker CMOS detector was used to collect the data using Mo K alpha radiation. The data collection temperature was 100 K. Using the integration method (SADABS), data were corrected for absorption effects. The structure was solved by direct methods. Non-hydrogen atoms were refined anisotropically by full matrix least squares on F^2. All hydrogen atoms were placed in calculated positions with appropriate riding parameters.

Table 45: Crystal data and structure refinement for 2NS7

Empirical formula	C41 H31 Cl4 N2 O6 Re S	
Formula weight	1007.74	
Temperature	100(2) K	
Wavelength	0.71073 Å	
Crystal system	Monoclinic	
Space group	P2(1)/c	
Unit cell dimensions	a = 9.0709(3) Å	a= 90°.
	b = 19.0092(6) Å	b= 95.3450(10)°.
	c = 23.0604(7) Å	g = 90°.
Volume	3959.0(2) Å3	
Z	4	
Density (calculated)	1.691 Mg/m3	
Absorption coefficient	3.442 mm-1	
F(000)	1992	
Crystal size	0.18 x 0.06 x 0.06 mm3	
Crystal color / habit	yellow / block	
Theta range for data collection	2.50 to 26.41°.	
Index ranges	-11<=h<=9, -23<=k<=22, -25<=l<=28	
Reflections collected	27889	
Independent reflections	8008 [R(int) = 0.0283]	
Completeness to theta = 25.00°	99.40%	
Absorption correction	multi-scan / sadabs	
Max. and min. transmission	0.8201 and 0.5762	
Refinement method	Full-matrix least-squares on F2	
Data / restraints / parameters	8008 / 0 / 498	
Goodness-of-fit on F2	1.048	
Final R indices [I>2sigma(I)]	R1 = 0.0272, wR2 = 0.0573	
R indices (all data)	R1 = 0.0368, wR2 = 0.0605	
Largest diff. peak and hole	1.099 and -0.730 e.Å-3	

Table 46: Atomic coordinates ($x\ 10^4$) and equivalent isotropic displacement parameters ($Å^2 x\ 10^3$) for 2NS7

	x	y	z	U(eq)
Re(1)	7891(1)	8562(1)	1330(1)	14(1)
S(1)	5107(1)	8171(1)	2125(1)	19(1)
O(1)	5256(3)	9196(1)	571(1)	32(1)
O(2)	9896(3)	9172(1)	465(1)	35(1)
O(3)	7702(3)	9981(1)	1956(1)	26(1)
O(4)	6665(2)	8069(1)	1983(1)	18(1)
O(5)	4556(3)	8856(1)	1956(1)	29(1)
O(6)	5003(3)	7979(1)	2723(1)	26(1)
N(1)	9635(3)	8037(1)	1899(1)	14(1)
N(2)	7809(3)	7462(1)	1043(1)	16(1)
C(1)	6232(4)	8938(2)	854(2)	21(1)
C(2)	9144(4)	8937(2)	792(2)	20(1)
C(3)	7831(4)	9451(2)	1718(1)	18(1)
C(4)	10657(4)	8325(2)	2284(1)	15(1)
C(5)	11354(4)	7926(2)	2742(1)	16(1)
C(6)	11063(4)	7225(2)	2810(1)	15(1)
C(7)	10127(4)	6894(2)	2360(1)	15(1)
C(8)	9919(4)	6148(2)	2320(1)	16(1)
C(9)	9016(4)	5860(2)	1888(1)	18(1)
C(10)	8218(4)	6284(2)	1451(1)	16(1)
C(11)	7250(4)	6001(2)	988(1)	18(1)
C(12)	6722(4)	6455(2)	553(1)	20(1)
C(13)	7016(4)	7178(2)	583(1)	19(1)
C(14)	8452(4)	7013(2)	1463(1)	15(1)
C(15)	9424(3)	7323(2)	1923(1)	13(1)
C(16)	11697(4)	6830(2)	3333(1)	17(1)
C(17)	13196(4)	6900(2)	3523(1)	19(1)
C(18)	13778(4)	6545(2)	4022(2)	24(1)
C(19)	12879(4)	6130(2)	4334(2)	26(1)
C(20)	11385(4)	6062(2)	4150(2)	26(1)
C(21)	10796(4)	6409(2)	3649(1)	21(1)
C(22)	6812(4)	5249(2)	972(2)	19(1)
C(23)	6276(4)	4942(2)	1460(2)	24(1)
C(24)	5854(4)	4243(2)	1454(2)	30(1)
C(25)	5971(4)	3841(2)	963(2)	32(1)
C(26)	6490(4)	4137(2)	474(2)	31(1)
C(27)	6902(4)	4844(2)	478(2)	22(1)
C(28)	11018(4)	9092(2)	2235(2)	19(1)
C(29)	6370(4)	7643(2)	98(2)	26(1)
C(30)	4061(4)	7529(2)	1704(2)	26(1)
C(31)	4149(4)	6815(2)	1906(2)	29(1)
C(32)	3297(5)	6320(2)	1600(2)	34(1)
C(33)	2373(4)	6500(2)	1100(2)	32(1)
C(34)	1436(5)	5985(3)	788(2)	39(1)
C(35)	557(5)	6184(3)	308(2)	41(1)
C(36)	553(5)	6884(3)	110(2)	46(1)
C(37)	1404(5)	7385(3)	399(2)	42(1)
C(38)	2311(4)	7205(2)	891(2)	30(1)
C(39)	3203(4)	7720(2)	1221(2)	30(1)
C(40)	3731(5)	296(2)	1348(2)	33(1)
C(41)	2033(5)	3528(2)	1631(2)	39(1)
Cl(1)	2612(1)	517(1)	710(1)	44(1)
Cl(4)	560(1)	4054(1)	1314(1)	46(1)
Cl(2)	3236(1)	788(1)	1946(1)	48(1)
Cl(3)	2077(2)	2700(1)	1298(1)	56(1)

Table 47: Bond lengths [Å] and angles [°] for 2NS7

Re(1)-C(2)	1.898(4)
Re(1)-C(3)	1.914(3)
Re(1)-C(1)	1.916(4)
Re(1)-O(4)	2.165(2)
Re(1)-N(2)	2.193(3)
Re(1)-N(1)	2.198(3)
S(1)-O(5)	1.435(3)
S(1)-O(6)	1.438(3)
S(1)-O(4)	1.493(2)
S(1)-C(30)	1.777(4)
O(1)-C(1)	1.160(4)
O(2)-C(2)	1.153(4)
O(3)-C(3)	1.159(4)
N(1)-C(4)	1.339(4)
N(1)-C(15)	1.373(4)
N(2)-C(13)	1.339(4)
N(2)-C(14)	1.380(4)
C(4)-C(5)	1.402(4)
C(4)-C(28)	1.500(4)
C(5)-C(6)	1.369(5)
C(5)-H(5A)	0.95
C(6)-C(7)	1.424(4)
C(6)-C(16)	1.490(4)
C(7)-C(15)	1.403(4)
C(7)-C(8)	1.433(5)
C(8)-C(9)	1.346(5)
C(8)-H(8A)	0.95
C(9)-C(10)	1.433(4)
C(9)-H(9A)	0.95
C(10)-C(14)	1.402(4)
C(10)-C(11)	1.423(5)
C(11)-C(12)	1.374(5)
C(11)-C(22)	1.484(5)
C(12)-C(13)	1.400(5)
C(12)-H(12A)	0.95
C(13)-C(29)	1.502(4)
C(14)-C(15)	1.440(4)
C(16)-C(17)	1.396(5)
C(16)-C(21)	1.397(5)
C(17)-C(18)	1.394(5)
C(17)-H(17A)	0.95
C(18)-C(19)	1.384(5)
C(18)-H(18A)	0.95
C(19)-C(20)	1.388(5)
C(19)-H(19A)	0.95
C(20)-C(21)	1.392(5)
C(20)-H(20A)	0.95
C(21)-H(21A)	0.95
C(22)-C(27)	1.383(5)
C(22)-C(23)	1.396(5)
C(23)-C(24)	1.382(5)
C(23)-H(23A)	0.95
C(24)-C(25)	1.380(6)
C(24)-H(24A)	0.95
C(25)-C(26)	1.380(6)
C(25)-H(25A)	0.95
C(26)-C(27)	1.393(5)
C(26)-H(26A)	0.95
C(27)-H(27A)	0.95
C(28)-H(28A)	0.98
C(28)-H(28B)	0.98
C(28)-H(28C)	0.98

Table 48: Bond lengths [Å] and angles [°] for 2NS7 cont'd

C(29)-H(29A)	0.98
C(29)-H(29B)	0.98
C(29)-H(29C)	0.98
C(30)-C(39)	1.349(5)
C(30)-C(31)	1.434(5)
C(31)-C(32)	1.371(6)
C(31)-H(31A)	0.95
C(32)-C(33)	1.403(6)
C(32)-H(32A)	0.95
C(33)-C(38)	1.424(6)
C(33)-C(34)	1.444(6)
C(34)-C(35)	1.356(6)
C(34)-H(34A)	0.95
C(35)-C(36)	1.407(7)
C(35)-H(35A)	0.95
C(36)-C(37)	1.361(6)
C(36)-H(36A)	0.95
C(37)-C(38)	1.381(6)
C(37)-H(37A)	0.95
C(38)-C(39)	1.442(6)
C(39)-H(39A)	0.95
C(40)-Cl(2)	1.759(4)
C(40)-Cl(1)	1.761(4)
C(40)-H(40A)	0.99
C(40)-H(40B)	0.99
C(41)-Cl(3)	1.754(5)
C(41)-Cl(4)	1.771(4)
C(41)-H(41A)	0.99
C(41)-H(41B)	0.99
C(2)-Re(1)-C(3)	91.10(14)
C(2)-Re(1)-C(1)	88.35(15)
C(3)-Re(1)-C(1)	83.31(14)
C(2)-Re(1)-O(4)	173.85(12)
C(3)-Re(1)-O(4)	91.07(12)
C(1)-Re(1)-O(4)	97.62(12)
C(2)-Re(1)-N(2)	99.52(12)
C(3)-Re(1)-N(2)	168.83(12)
C(1)-Re(1)-N(2)	100.33(12)
O(4)-Re(1)-N(2)	78.01(9)
C(2)-Re(1)-N(1)	96.86(13)
C(3)-Re(1)-N(1)	99.91(12)
C(1)-Re(1)-N(1)	173.80(12)
O(4)-Re(1)-N(1)	77.10(9)
N(2)-Re(1)-N(1)	75.53(9)
O(5)-S(1)-O(6)	115.97(16)
O(5)-S(1)-O(4)	111.74(15)
O(6)-S(1)-O(4)	109.02(14)
O(5)-S(1)-C(30)	108.70(17)
O(6)-S(1)-C(30)	105.64(17)
O(4)-S(1)-C(30)	105.04(15)
S(1)-O(4)-Re(1)	130.92(13)
C(4)-N(1)-C(15)	117.9(3)
C(4)-N(1)-Re(1)	128.7(2)
C(15)-N(1)-Re(1)	112.1(2)
C(13)-N(2)-C(14)	117.8(3)
C(13)-N(2)-Re(1)	128.8(2)
C(14)-N(2)-Re(1)	112.2(2)
O(1)-C(1)-Re(1)	176.9(3)
O(2)-C(2)-Re(1)	179.2(3)
O(3)-C(3)-Re(1)	175.7(3)
N(1)-C(4)-C(5)	120.9(3)
N(1)-C(4)-C(28)	119.3(3)

Table 49: Bond lengths [Å] and angles [°] for 2NS7 cont'd

C(5)-C(4)-C(28)	119.8(3)
C(6)-C(5)-C(4)	122.2(3)
C(6)-C(5)-H(5A)	118.9
C(4)-C(5)-H(5A)	118.9
C(5)-C(6)-C(7)	117.1(3)
C(5)-C(6)-C(16)	121.2(3)
C(7)-C(6)-C(16)	121.7(3)
C(15)-C(7)-C(6)	117.8(3)
C(15)-C(7)-C(8)	118.7(3)
C(6)-C(7)-C(8)	123.4(3)
C(9)-C(8)-C(7)	121.2(3)
C(9)-C(8)-H(8A)	119.4
C(7)-C(8)-H(8A)	119.4
C(8)-C(9)-C(10)	121.6(3)
C(8)-C(9)-H(9A)	119.2
C(10)-C(9)-H(9A)	119.2
C(14)-C(10)-C(11)	118.0(3)
C(14)-C(10)-C(9)	118.5(3)
C(11)-C(10)-C(9)	123.4(3)
C(12)-C(11)-C(10)	117.3(3)
C(12)-C(11)-C(22)	120.8(3)
C(10)-C(11)-C(22)	121.9(3)
C(11)-C(12)-C(13)	121.9(3)
C(11)-C(12)-H(12A)	119
C(13)-C(12)-H(12A)	119
N(2)-C(13)-C(12)	121.4(3)
N(2)-C(13)-C(29)	119.7(3)
C(12)-C(13)-C(29)	118.9(3)
N(2)-C(14)-C(10)	123.0(3)
N(2)-C(14)-C(15)	117.0(3)
C(10)-C(14)-C(15)	120.0(3)
N(1)-C(15)-C(7)	123.2(3)
N(1)-C(15)-C(14)	117.0(3)
C(7)-C(15)-C(14)	119.8(3)
C(17)-C(16)-C(21)	119.4(3)
C(17)-C(16)-C(6)	119.9(3)
C(21)-C(16)-C(6)	120.7(3)
C(18)-C(17)-C(16)	119.8(3)
C(18)-C(17)-H(17A)	120.1
C(16)-C(17)-H(17A)	120.1
C(19)-C(18)-C(17)	120.6(3)
C(19)-C(18)-H(18A)	119.7
C(17)-C(18)-H(18A)	119.7
C(18)-C(19)-C(20)	120.0(3)
C(18)-C(19)-H(19A)	120
C(20)-C(19)-H(19A)	120
C(19)-C(20)-C(21)	119.8(4)
C(19)-C(20)-H(20A)	120.1
C(21)-C(20)-H(20A)	120.1
C(20)-C(21)-C(16)	120.5(3)
C(20)-C(21)-H(21A)	119.8
C(16)-C(21)-H(21A)	119.8
C(27)-C(22)-C(23)	118.9(3)
C(27)-C(22)-C(11)	121.4(3)
C(23)-C(22)-C(11)	119.6(3)
C(24)-C(23)-C(22)	120.7(4)
C(24)-C(23)-H(23A)	119.7
C(22)-C(23)-H(23A)	119.7

Table 50: Bond lengths [Å] and angles [°] for 2NS7 cont'd

C(25)-C(24)-C(23)	119.9(4)
C(25)-C(24)-H(24A)	120.1
C(23)-C(24)-H(24A)	120.1
C(24)-C(25)-C(26)	120.2(4)
C(24)-C(25)-H(25A)	119.9
C(26)-C(25)-H(25A)	119.9
C(25)-C(26)-C(27)	120.0(4)
C(25)-C(26)-H(26A)	120
C(27)-C(26)-H(26A)	120
C(22)-C(27)-C(26)	120.3(4)
C(22)-C(27)-H(27A)	119.8
C(26)-C(27)-H(27A)	119.8
C(4)-C(28)-H(28A)	109.5
C(4)-C(28)-H(28B)	109.5
H(28A)-C(28)-H(28B)	109.5
C(4)-C(28)-H(28C)	109.5
H(28A)-C(28)-H(28C)	109.5
H(28B)-C(28)-H(28C)	109.5
C(13)-C(29)-H(29A)	109.5
C(13)-C(29)-H(29B)	109.5
H(29A)-C(29)-H(29B)	109.5
C(13)-C(29)-H(29C)	109.5
H(29A)-C(29)-H(29C)	109.5
H(29B)-C(29)-H(29C)	109.5
C(39)-C(30)-C(31)	122.3(4)
C(39)-C(30)-S(1)	120.2(3)
C(31)-C(30)-S(1)	117.5(3)
C(32)-C(31)-C(30)	118.1(4)
C(32)-C(31)-H(31A)	120.9
C(30)-C(31)-H(31A)	120.9
C(31)-C(32)-C(33)	121.3(4)
C(31)-C(32)-H(32A)	119.3
C(33)-C(32)-H(32A)	119.3
C(32)-C(33)-C(38)	120.7(4)
C(32)-C(33)-C(34)	121.5(4)
C(38)-C(33)-C(34)	117.8(4)
C(35)-C(34)-C(33)	119.5(4)
C(35)-C(34)-H(34A)	120.2
C(33)-C(34)-H(34A)	120.2
C(34)-C(35)-C(36)	120.7(4)
C(34)-C(35)-H(35A)	119.6
C(36)-C(35)-H(35A)	119.6
C(37)-C(36)-C(35)	121.3(4)
C(37)-C(36)-H(36A)	119.4
C(35)-C(36)-H(36A)	119.4
C(36)-C(37)-C(38)	119.8(5)
C(36)-C(37)-H(37A)	120.1
C(38)-C(37)-H(37A)	120.1
C(37)-C(38)-C(33)	120.9(4)
C(37)-C(38)-C(39)	121.9(4)
C(33)-C(38)-C(39)	117.2(4)
C(30)-C(39)-C(38)	120.3(4)
C(30)-C(39)-H(39A)	119.8
C(38)-C(39)-H(39A)	119.8
Cl(2)-C(40)-Cl(1)	111.0(2)
Cl(2)-C(40)-H(40A)	109.4
Cl(1)-C(40)-H(40A)	109.4
Cl(2)-C(40)-H(40B)	109.4
Cl(1)-C(40)-H(40B)	109.4
H(40A)-C(40)-H(40B)	108
Cl(3)-C(41)-Cl(4)	111.9(2)
Cl(3)-C(41)-H(41A)	109.2
Cl(4)-C(41)-H(41A)	109.2
Cl(3)-C(41)-H(41B)	109.2
Cl(4)-C(41)-H(41B)	109.2
H(41A)-C(41)-H(41B)	107.9

Table 51: Anisotropic displacement parameters ($Å^2 x\ 10^3$) for 2NS7

	U11	U22	U33	U23	U13	U12
Re(1)	15(1)	13(1)	13(1)	1(1)	-1(1)	1(1)
S(1)	17(1)	19(1)	21(1)	-3(1)	4(1)	-1(1)
O(1)	33(2)	32(2)	27(1)	-3(1)	-11(1)	13(1)
O(2)	44(2)	33(2)	30(2)	4(1)	17(1)	-5(1)
O(3)	28(2)	18(1)	32(1)	-6(1)	-3(1)	2(1)
O(4)	14(1)	19(1)	20(1)	1(1)	3(1)	1(1)
O(5)	23(1)	24(1)	40(2)	3(1)	9(1)	7(1)
O(6)	27(2)	29(1)	25(1)	-2(1)	9(1)	-4(1)
N(1)	12(1)	13(1)	16(1)	-1(1)	2(1)	1(1)
N(2)	16(2)	15(1)	16(1)	0(1)	-1(1)	1(1)
C(1)	24(2)	17(2)	20(2)	-3(1)	0(2)	-1(2)
C(2)	23(2)	18(2)	19(2)	1(1)	2(2)	1(2)
C(3)	12(2)	22(2)	20(2)	5(1)	-2(1)	0(1)
C(4)	11(2)	16(2)	18(2)	-1(1)	2(1)	0(1)
C(5)	10(2)	21(2)	18(2)	-2(1)	-1(1)	-1(1)
C(6)	11(2)	19(2)	14(2)	0(1)	2(1)	2(1)
C(7)	12(2)	17(2)	15(2)	-1(1)	1(1)	0(1)
C(8)	15(2)	18(2)	15(2)	3(1)	0(1)	2(1)
C(9)	21(2)	14(2)	18(2)	1(1)	2(1)	1(1)
C(10)	16(2)	18(2)	13(2)	-2(1)	1(1)	0(1)
C(11)	18(2)	20(2)	16(2)	-4(1)	2(1)	2(1)
C(12)	21(2)	20(2)	17(2)	-3(1)	-4(1)	-2(2)
C(13)	21(2)	20(2)	14(2)	0(1)	-4(1)	2(1)
C(14)	14(2)	18(2)	13(2)	0(1)	3(1)	0(1)
C(15)	12(2)	15(2)	13(2)	-1(1)	2(1)	2(1)
C(16)	18(2)	16(2)	15(2)	-3(1)	-3(1)	0(1)
C(17)	20(2)	19(2)	18(2)	-2(1)	-1(1)	0(1)
C(18)	23(2)	24(2)	22(2)	-6(2)	-10(2)	3(2)
C(19)	34(2)	26(2)	15(2)	2(1)	-6(2)	5(2)
C(20)	34(2)	27(2)	16(2)	1(2)	2(2)	-2(2)
C(21)	21(2)	24(2)	17(2)	-2(1)	-2(1)	0(2)
C(22)	14(2)	19(2)	23(2)	0(1)	-6(1)	1(1)
C(23)	21(2)	27(2)	23(2)	3(2)	-4(2)	-4(2)
C(24)	21(2)	33(2)	35(2)	13(2)	-7(2)	-8(2)
C(25)	24(2)	20(2)	51(3)	6(2)	-10(2)	-8(2)
C(26)	22(2)	25(2)	44(2)	-11(2)	-6(2)	-2(2)
C(27)	19(2)	24(2)	23(2)	-2(2)	-1(2)	-2(2)
C(28)	16(2)	14(2)	24(2)	-1(1)	-4(1)	0(1)
C(29)	37(2)	22(2)	17(2)	1(1)	-10(2)	2(2)
C(30)	17(2)	35(2)	28(2)	-9(2)	6(2)	-2(2)
C(31)	29(2)	28(2)	30(2)	-4(2)	4(2)	0(2)
C(32)	41(3)	25(2)	38(2)	0(2)	13(2)	-1(2)
C(33)	20(2)	56(3)	21(2)	-5(2)	6(2)	3(2)
C(34)	35(3)	51(3)	35(2)	-13(2)	13(2)	-8(2)
C(35)	32(2)	58(3)	35(2)	-23(2)	7(2)	-16(2)
C(36)	30(3)	65(3)	42(3)	-19(2)	2(2)	-1(2)
C(37)	33(2)	55(3)	38(2)	-10(2)	3(2)	6(2)
C(38)	22(2)	39(2)	32(2)	-6(2)	11(2)	1(2)
C(39)	25(2)	31(2)	34(2)	1(2)	11(2)	2(2)
C(40)	35(2)	30(2)	36(2)	8(2)	13(2)	7(2)
C(41)	30(2)	53(3)	34(2)	2(2)	1(2)	-3(2)
Cl(1)	36(1)	56(1)	41(1)	-2(1)	-2(1)	5(1)
Cl(4)	50(1)	52(1)	36(1)	5(1)	0(1)	7(1)
Cl(2)	50(1)	60(1)	34(1)	-4(1)	6(1)	20(1)
Cl(3)	58(1)	50(1)	57(1)	-6(1)	-4(1)	2(1)

2. 4. 9. X-ray Crystallographic analysis for TOS3

The X-ray examination and data collection was performed on a yellow colored crystal of TOS3. The crystal was mounted on a Cryoloop with Paratone-N oil. A Bruker APEX CCD was used to collect the data using Mo K alpha radiation. The data collection temperature was 200 K. Using the integration method (SADABS), data were corrected for absorption effects. The structure was solved by direct methods. Non-hydrogen atoms were refined anisotropically by full matrix least squares on F^2. All hydrogen atoms were placed in calculated positions using appropriate riding models. Disorder of one chlorine atom (66/34 ratio) was treated using a two-part model.

Table 52: Crystal data and structure refinement for TOS3

Empirical formula	$C_{24}H_{19}Cl_2N_2O_6ReS$	
Formula weight	720.57	
Temperature	200(2) K	
Wavelength	0.71073 Å	
Crystal system	Monoclinic	
Space group	P2(1)/n	
Unit cell dimensions	a = 11.7363(18) Å	a= 90°.
	b = 14.911(2) Å	b= 110.588(3)°.
	c = 15.665(2) Å	g = 90°.
Volume	2566.4(6) Å3	
Z	4	
Density (calculated)	1.865 Mg/m3	
Absorption coefficient	5.067 mm-1	
F(000)	1400	
Crystal size	0.18 x 0.14 x 0.12 mm3	
Crystal color / habit	yellow / block	
Theta range for data collection	1.89 to 27.93°.	
Index ranges	-15<=h<=14, -19<=k<=19, -20<=l<=20	
Reflections collected	31000	
Independent reflections	6001 [R(int) = 0.0413]	
Completeness to theta = 25.00°	100.00%	
Absorption correction	multi-scan / sadabs	
Max. and min. transmission	0.5815 and 0.4624	
Refinement method	Full-matrix least-squares on F2	
Data / restraints / parameters	6001 / 2 / 331	
Goodness-of-fit on F2	1.07	
Final R indices [I>2sigma(I)]	R1 = 0.0371, wR2 = 0.0863	
R indices (all data)	R1 = 0.0516, wR2 = 0.0919	
Largest diff. peak and hole	1.562 and -1.022 e.Å-3	

Table 53: Atomic coordinates (x 10^4) and equivalent isotropic displacement parameters ($Å^2$ x 10^3) for TOS3

	x	y	z	U(eq)
Re(1)	7342(1)	3963(1)	3358(1)	38(1)
S(1)	4444(1)	3772(1)	1976(1)	40(1)
Cl(1)	2927(2)	1079(1)	5088(2)	93(1)
Cl(2)	553(7)	1838(6)	4345(5)	106(2)
Cl(2A)	221(14)	1442(10)	4125(9)	106(2)
O(1)	10083(4)	3939(3)	4400(3)	67(1)
O(2)	7672(4)	2604(3)	1986(3)	71(1)
O(3)	7560(4)	5444(3)	2053(4)	83(2)
O(4)	5380(3)	4063(2)	2865(2)	39(1)
O(5)	3290(3)	4147(3)	1922(3)	54(1)
O(6)	4826(4)	3947(2)	1215(3)	54(1)
N(1)	6969(4)	2996(3)	4251(3)	40(1)
N(2)	7041(4)	4792(3)	4398(3)	46(1)
C(1)	6972(5)	2115(4)	4183(4)	54(1)
C(2)	6627(6)	1556(4)	4786(5)	68(2)
C(3)	6290(5)	1954(5)	5440(4)	60(2)
C(4)	6279(5)	2873(4)	5554(4)	53(1)
C(5)	5976(5)	3340(4)	6272(4)	52(1)
C(6)	6079(6)	4226(5)	6325(4)	63(2)
C(7)	6430(5)	4762(4)	5727(4)	57(2)
C(8)	6562(6)	5691(4)	5762(5)	60(2)
C(9)	6908(6)	6153(4)	5169(5)	66(2)
C(10)	7153(5)	5685(4)	4482(4)	56(2)
C(11)	6704(5)	4336(4)	5001(4)	45(1)
C(12)	6643(4)	3374(4)	4926(3)	44(1)
C(13)	5601(8)	2781(6)	6930(5)	88(2)
C(14)	9049(5)	3943(4)	3991(4)	47(1)
C(15)	7545(5)	3126(4)	2492(4)	49(1)
C(16)	7494(5)	4901(4)	2548(4)	52(1)
C(17)	4355(4)	2591(3)	2090(3)	40(1)
C(18)	4664(4)	2013(3)	1522(3)	40(1)
C(19)	4624(5)	1100(3)	1647(4)	44(1)
C(20)	4302(5)	732(4)	2349(4)	44(1)
C(21)	3964(6)	1343(4)	2897(4)	56(2)
C(22)	3980(5)	2250(4)	2778(4)	52(1)
C(23)	4323(6)	-243(4)	2535(4)	57(2)
C(24)	1385(6)	856(4)	4886(5)	69(2)

Table 54: Bond lengths [Å] and angles [°] for TOS3

Re(1)-C(14)	1.898(6)
Re(1)-C(15)	1.920(6)
Re(1)-C(16)	1.939(6)
Re(1)-O(4)	2.161(3)
Re(1)-N(1)	2.159(4)
Re(1)-N(2)	2.170(4)
S(1)-O(6)	1.436(4)
S(1)-O(5)	1.440(4)
S(1)-O(4)	1.502(3)
S(1)-C(17)	1.778(5)
Cl(1)-C(24)	1.755(8)
Cl(2)-C(24)	1.797(8)
Cl(2A)-C(24)	1.704(12)
O(1)-C(14)	1.155(7)
O(2)-C(15)	1.157(7)
O(3)-C(16)	1.141(7)
N(1)-C(1)	1.319(7)
N(1)-C(12)	1.367(7)
N(2)-C(11)	1.331(7)
N(2)-C(10)	1.340(7)
C(1)-C(2)	1.422(9)
C(1)-H(1)	0.95
C(2)-C(3)	1.358(9)
C(2)-H(2)	0.95
C(3)-C(4)	1.382(9)
C(3)-H(3)	0.95
C(4)-C(12)	1.416(7)
C(4)-C(5)	1.469(8)
C(5)-C(6)	1.327(9)
C(5)-C(13)	1.507(9)
C(6)-C(7)	1.400(9)
C(6)-H(6)	0.95
C(7)-C(8)	1.393(9)
C(7)-C(11)	1.434(8)
C(8)-C(9)	1.330(10)
C(8)-H(8)	0.95
C(9)-C(10)	1.394(9)
C(9)-H(9)	0.95
C(10)-H(10)	0.95
C(11)-C(12)	1.439(8)
C(13)-H(13A)	0.98
C(13)-H(13B)	0.98
C(13)-H(13C)	0.98
C(17)-C(18)	1.375(7)
C(17)-C(22)	1.395(7)
C(18)-C(19)	1.380(7)
C(18)-H(18)	0.95
C(19)-C(20)	1.394(8)
C(19)-H(19)	0.95
C(20)-C(21)	1.401(8)
C(20)-C(23)	1.482(8)
C(21)-C(22)	1.366(8)
C(21)-H(21)	0.95
C(22)-H(22)	0.95
C(23)-H(23A)	0.98
C(23)-H(23B)	0.98
C(23)-H(23C)	0.98
C(24)-H(24A)	0.99

Table 55: Bond lengths [Å] and angles [°] for TOS3 cont'd

C(24)-H(24B)	0.99
C(14)-Re(1)-C(15)	89.3(2)
C(14)-Re(1)-C(16)	91.7(2)
C(15)-Re(1)-C(16)	86.8(3)
C(14)-Re(1)-O(4)	169.87(19)
C(15)-Re(1)-O(4)	99.98(19)
C(16)-Re(1)-O(4)	92.74(19)
C(14)-Re(1)-N(1)	93.93(19)
C(15)-Re(1)-N(1)	97.3(2)
C(16)-Re(1)-N(1)	173.1(2)
O(4)-Re(1)-N(1)	81.04(14)
C(14)-Re(1)-N(2)	92.1(2)
C(15)-Re(1)-N(2)	173.9(2)
C(16)-Re(1)-N(2)	99.1(2)
O(4)-Re(1)-N(2)	78.17(14)
N(1)-Re(1)-N(2)	76.71(17)
O(6)-S(1)-O(5)	116.2(3)
O(6)-S(1)-O(4)	112.2(2)
O(5)-S(1)-O(4)	108.0(2)
O(6)-S(1)-C(17)	108.0(2)
O(5)-S(1)-C(17)	107.6(2)
O(4)-S(1)-C(17)	104.1(2)
S(1)-O(4)-Re(1)	130.7(2)
C(1)-N(1)-C(12)	118.9(5)
C(1)-N(1)-Re(1)	127.4(4)
C(12)-N(1)-Re(1)	113.7(3)
C(11)-N(2)-C(10)	118.8(5)
C(11)-N(2)-Re(1)	114.2(4)
C(10)-N(2)-Re(1)	127.1(4)
N(1)-C(1)-C(2)	121.4(6)
N(1)-C(1)-H(1)	119.3
C(2)-C(1)-H(1)	119.3
C(3)-C(2)-C(1)	118.1(6)
C(3)-C(2)-H(2)	120.9
C(1)-C(2)-H(2)	120.9
C(2)-C(3)-C(4)	123.3(6)
C(2)-C(3)-H(3)	118.3
C(4)-C(3)-H(3)	118.3
C(3)-C(4)-C(12)	114.6(6)
C(3)-C(4)-C(5)	125.7(6)
C(12)-C(4)-C(5)	119.6(6)
C(6)-C(5)-C(4)	118.6(6)
C(6)-C(5)-C(13)	123.4(6)
C(4)-C(5)-C(13)	118.0(6)
C(5)-C(6)-C(7)	124.6(6)
C(5)-C(6)-H(6)	117.7
C(7)-C(6)-H(6)	117.7
C(8)-C(7)-C(6)	126.5(6)
C(8)-C(7)-C(11)	114.8(6)
C(6)-C(7)-C(11)	118.7(6)
C(9)-C(8)-C(7)	122.9(6)
C(9)-C(8)-H(8)	118.5
C(7)-C(8)-H(8)	118.5
C(8)-C(9)-C(10)	118.5(6)
C(8)-C(9)-H(9)	120.8

Table 56: Bond lengths [Å] and angles [°] for TOS3 cont'd

C(10)-C(9)-H(9)	120.8
N(2)-C(10)-C(9)	122.2(7)
N(2)-C(10)-H(10)	118.9
C(9)-C(10)-H(10)	118.9
N(2)-C(11)-C(7)	122.8(5)
N(2)-C(11)-C(12)	118.0(5)
C(7)-C(11)-C(12)	119.2(6)
N(1)-C(12)-C(4)	123.7(5)
N(1)-C(12)-C(11)	117.1(5)
C(4)-C(12)-C(11)	119.3(5)
C(5)-C(13)-H(13A)	109.5
C(5)-C(13)-H(13B)	109.5
H(13A)-C(13)-H(13B)	109.5
C(5)-C(13)-H(13C)	109.5
H(13A)-C(13)-H(13C)	109.5
H(13B)-C(13)-H(13C)	109.5
O(1)-C(14)-Re(1)	177.9(5)
O(2)-C(15)-Re(1)	178.2(5)
O(3)-C(16)-Re(1)	178.3(6)
C(18)-C(17)-C(22)	119.9(5)
C(18)-C(17)-S(1)	121.1(4)
C(22)-C(17)-S(1)	119.0(4)
C(17)-C(18)-C(19)	119.8(5)
C(17)-C(18)-H(18)	120.1
C(19)-C(18)-H(18)	120.1
C(18)-C(19)-C(20)	122.1(5)
C(18)-C(19)-H(19)	118.9
C(20)-C(19)-H(19)	118.9
C(19)-C(20)-C(21)	116.2(5)
C(19)-C(20)-C(23)	123.4(5)
C(21)-C(20)-C(23)	120.4(5)
C(22)-C(21)-C(20)	122.6(5)
C(22)-C(21)-H(21)	118.7
C(20)-C(21)-H(21)	118.7
C(21)-C(22)-C(17)	119.3(5)
C(21)-C(22)-H(22)	120.4
C(17)-C(22)-H(22)	120.4
C(20)-C(23)-H(23A)	109.5
C(20)-C(23)-H(23B)	109.5
H(23A)-C(23)-H(23B)	109.5
C(20)-C(23)-H(23C)	109.5
H(23A)-C(23)-H(23C)	109.5
H(23B)-C(23)-H(23C)	109.5
Cl(2A)-C(24)-Cl(1)	123.4(7)
Cl(2A)-C(24)-Cl(2)	23.7(4)
Cl(1)-C(24)-Cl(2)	106.6(5)
Cl(2A)-C(24)-H(24A)	113.2
Cl(1)-C(24)-H(24A)	110.4
Cl(2)-C(24)-H(24A)	110.4
Cl(2A)-C(24)-H(24B)	87.9
Cl(1)-C(24)-H(24B)	110.4
Cl(2)-C(24)-H(24B)	110.4
H(24A)-C(24)-H(24B)	108.6

Table 57: Anisotropic displacement parameters ($Å^2 x\ 10^3$) for TOS3

	U11	U22	U33	U23	U13	U12
Re(1)	31(1)	42(1)	41(1)	0(1)	13(1)	0(1)
S(1)	37(1)	45(1)	35(1)	-7(1)	9(1)	4(1)
Cl(1)	100(2)	85(1)	104(2)	-17(1)	49(1)	-21(1)
Cl(2)	139(4)	96(4)	90(3)	32(3)	50(3)	38(4)
Cl(2A)	139(4)	96(4)	90(3)	32(3)	50(3)	38(4)
O(1)	35(2)	83(3)	77(3)	20(2)	11(2)	-2(2)
O(2)	73(3)	93(3)	59(3)	-17(3)	39(2)	3(3)
O(3)	68(3)	81(3)	91(4)	37(3)	18(3)	-9(3)
O(4)	32(2)	47(2)	37(2)	-10(2)	10(2)	-1(1)
O(5)	36(2)	58(2)	56(2)	-18(2)	2(2)	12(2)
O(6)	70(3)	51(2)	42(2)	0(2)	20(2)	6(2)
N(1)	32(2)	48(2)	37(2)	1(2)	10(2)	3(2)
N(2)	31(2)	52(3)	49(3)	-7(2)	6(2)	4(2)
C(1)	47(3)	54(3)	64(4)	6(3)	21(3)	4(3)
C(2)	54(4)	46(3)	91(5)	13(3)	10(4)	9(3)
C(3)	43(3)	77(4)	55(4)	21(3)	13(3)	-7(3)
C(4)	32(3)	71(4)	51(3)	13(3)	8(2)	6(3)
C(5)	34(3)	80(4)	42(3)	0(3)	12(2)	0(3)
C(6)	55(4)	90(5)	47(4)	-12(3)	23(3)	-1(3)
C(7)	30(3)	73(4)	59(4)	-8(3)	4(3)	5(3)
C(8)	50(4)	66(4)	56(4)	-22(3)	8(3)	-2(3)
C(9)	57(4)	53(4)	79(5)	-21(3)	10(3)	3(3)
C(10)	44(3)	46(3)	66(4)	-9(3)	5(3)	1(3)
C(11)	31(3)	54(3)	40(3)	-10(2)	-1(2)	5(2)
C(12)	21(2)	76(4)	33(3)	8(2)	8(2)	-4(2)
C(13)	94(6)	120(7)	63(5)	9(4)	43(4)	-17(5)
C(14)	37(3)	52(3)	52(3)	6(3)	15(3)	0(2)
C(15)	44(3)	60(3)	44(3)	-1(3)	16(2)	6(3)
C(16)	42(3)	59(3)	54(3)	12(3)	14(3)	-1(3)
C(17)	30(3)	49(3)	38(3)	-8(2)	9(2)	-4(2)
C(18)	36(3)	49(3)	36(3)	-4(2)	13(2)	1(2)
C(19)	44(3)	48(3)	41(3)	-6(2)	16(2)	4(2)
C(20)	33(3)	52(3)	47(3)	-7(2)	13(2)	-5(2)
C(21)	66(4)	62(4)	47(3)	-1(3)	29(3)	-13(3)
C(22)	58(4)	59(3)	49(3)	-13(3)	31(3)	-4(3)
C(23)	54(4)	58(3)	62(4)	2(3)	22(3)	-6(3)
C(24)	81(5)	68(4)	60(4)	-8(3)	27(4)	-5(4)

2. 4. 10. X-ray Crystallographic analysis for TOS4

The X-ray examination and data collection was performed on a suitable yellow rod-shaped crystal of TOS4 with approximate dimensions of 0.11 mm × 0.03 mm × 0.02 mm. The crystal was mounted in a loop with paratone-N and transferred to the goniostat bathed in a cold stream. Intensity data were collected at 150K with a Bruker APEXII CCD detector at Beamline 11.3.1 at the Advanced Light Source (Lawrence Berkeley National Laboratory) using synchrotron radiation tuned to λ=0.7749Å. A series of 1s data

frames measured at 0.2° increments of ω were collected to calculate a unit cell. The data collection frames were measured for a duration of 1s at 0.3° intervals of ω and ϕ with a maximum θ value of ~60°. The data frames were collected using the APEX2 program and processed using the program SAINT routine within APEX2. The data were corrected for absorption and beam corrections based on the multi-scan technique in SADABS.

The structure was solved by a combination of direct methods SHELXTL v6.14 and the difference Fourier technique. It was refined by full-matrix least squares on F^2. Non-hydrogen atoms were refined with anisotropic displacement parameters. All H-atom positions were calculated and treated with a riding model in subsequent refinements. The isotropic displacement parameters for the H-atoms were defined as $a*U_{eq}$ of the adjacent atom, (a=1.5 for methyl and 1.2 for all others). The refinement converged with crystallographic agreement factors of wR2=8.87%, R1=3.77%, for 4769 reflections with I>2σ(I) (R1=4.17%, wR2=9.13% for all data) and 310 variable parameters.

Table 58: Crystal data and structure refinement for TOS4

Empirical formula	$C_{24}H_{19}N_2O_6SRe$	
Formula weight	649.67	
Temperature	150(2) K	
Wavelength	0.77490 Å	
Crystal system	Monoclinic	
Space group	$P2_1/n$	
Unit cell dimensions	a = 9.7844(9) Å	α = 90°
	b = 17.4129(17) Å	β = 104.752(1)°
	c = 13.1508(13) Å	γ = 90°
Volume	2166.7(4) $Å^3$	
Z	4	
Density (calculated)	1.992 Mg/m^3	
Absorption coefficient	7.134 mm^{-1}	
F(000)	1264	
Crystal size	0.11 x 0.03 x 0.02 mm^3	
θ range for data collection	2.54 to 31.09°	
Index ranges	$-13 \leq h \leq 13, -23 \leq k \leq 23, -17 \leq l$	
Reflections collected	27133	
Independent reflections	5360 [R_{int} = 0.0931]	
Completeness to θ = 31.09°	100.00%	
Absorption correction	Multi-scan	
Max. and min. transmission	0.8705 and 0.5075	
Refinement method	Full-matrix least-squares on F^2	
Data / restraints / parameters	5360 / 0 / 310	
Goodness-of-fit on F^2	1.033	
Final R indices [I>2σ(I)]	R1 = 0.0377, wR2 = 0.0887	
R indices (all data)	R1 = 0.0417, wR2 = 0.0913	
Largest diff. peak and hole	1.239 and -0.813 $eÅ^{-3}$	

Table 59: Atomic coordinates [x10^4] and equivalent isotropic displacement parameters [Å^{2}x10^3] for TOS4

	x	y	z	U(eq)
Re	659(1)	1956(1)	7852(1)	13(1)
S(1)	3894(1)	1590(1)	9287(1)	16(1)
O(1)	1039(4)	3422(2)	9181(3)	31(1)
O(2)	2476(4)	2914(2)	6735(3)	26(1)
O(3)	-2049(3)	2535(2)	6331(2)	27(1)
O(4)	2339(3)	1415(2)	9023(2)	16(1)
O(5)	4171(3)	2400(2)	9191(3)	23(1)
O(6)	4571(3)	1237(2)	10276(2)	21(1)
N(1)	668(3)	811(2)	7124(3)	15(1)
N(2)	-645(3)	1245(2)	8631(3)	14(1)
C(1)	843(4)	2868(2)	8687(3)	18(1)
C(2)	1806(4)	2530(2)	7141(3)	17(1)
C(3)	-1003(4)	2331(2)	6883(3)	19(1)
C(4)	1230(4)	600(2)	6331(3)	19(1)
C(5)	1387(4)	-179(2)	6110(3)	22(1)
C(6)	916(4)	-746(2)	6639(3)	21(1)
C(7)	233(4)	-546(2)	7427(3)	18(1)
C(8)	146(4)	245(2)	7652(3)	16(1)
C(9)	-410(5)	-1096(2)	7949(4)	23(1)
C(10)	-1155(4)	-877(2)	8638(4)	22(1)
C(11)	-1259(4)	-87(2)	8882(3)	17(1)
C(12)	-582(4)	468(2)	8416(3)	14(1)
C(13)	-2079(4)	165(2)	9555(3)	20(1)
C(14)	-2174(4)	930(2)	9725(3)	21(1)
C(15)	-1465(4)	1467(2)	9253(3)	17(1)
C(16)	1699(4)	1207(2)	5683(3)	20(1)
C(17)	-1658(5)	2309(3)	9441(4)	28(1)
C(18)	4519(4)	1106(2)	8311(3)	17(1)
C(19)	4461(4)	303(2)	8273(3)	20(1)
C(20)	5052(5)	-82(3)	7566(4)	24(1)
C(21)	5699(4)	317(3)	6886(3)	24(1)
C(22)	5725(5)	1116(3)	6927(4)	26(1)
C(23)	5145(5)	1506(3)	7642(3)	22(1)
C(24)	6411(5)	-100(3)	6170(4)	33(1)
H(5)	1836	-312	5574	26
H(6)	1044	-1270	6483	26
H(9)	-317	-1627	7815	28
H(10)	-1610	-1253	8960	26
H(13)	-2557	-195	9885	24
H(14)	-2733	1105	10174	25
H(16A)	2623	1407	6067	31
H(16B)	1007	1626	5545	31
H(16C)	1774	984	5015	31
H(17A)	-1811	2588	8774	42
H(17B)	-810	2508	9938	42
H(17C)	-2477	2378	9731	42
H(19)	4022	25	8725	24
H(20)	5019	-627	7541	29
H(22)	6142	1397	6464	31
H(23)	5179	2051	7669	26
H(24B)	5760	-481	5760	49
H(24C)	7256	-360	6588	49
H(24A)	6683	267	5691	49

Table 60: Bond lengths [Å] and angles [°] for TOS4

Re-C(3)	1.908(4)	Re-C(1)	1.913(4)
Re-C(2)	1.915(4)	Re-O(4)	2.162(3)
Re-N(2)	2.208(3)	Re-N(1)	2.214(3)
S(1)-O(6)	1.439(3)	S(1)-O(5)	1.448(3)
S(1)-O(4)	1.503(3)	S(1)-C(18)	1.770(4)
O(1)-C(1)	1.151(5)	O(2)-C(2)	1.158(5)
O(3)-C(3)	1.150(5)	N(1)-C(4)	1.348(5)
N(1)-C(8)	1.377(5)	N(2)-C(15)	1.341(5)
N(2)-C(12)	1.386(5)	C(4)-C(5)	1.403(6)
C(4)-C(16)	1.501(5)	C(5)-C(6)	1.354(6)
C(6)-C(7)	1.413(6)	C(7)-C(8)	1.415(5)
C(7)-C(9)	1.416(6)	C(8)-C(12)	1.425(5)
C(9)-C(10)	1.354(6)	C(10)-C(11)	1.422(6)
C(11)-C(12)	1.399(5)	C(11)-C(13)	1.408(5)
C(13)-C(14)	1.359(6)	C(14)-C(15)	1.400(5)
C(15)-C(17)	1.506(6)	C(18)-C(23)	1.383(5)
C(18)-C(19)	1.399(6)	C(19)-C(20)	1.386(6)
C(20)-C(21)	1.404(6)	C(21)-C(22)	1.391(6)
C(21)-C(24)	1.495(6)	C(22)-C(23)	1.393(6)
C(3)-Re-C(1)	92.21(18)	C(3)-Re-C(2)	90.07(16)
C(1)-Re-C(2)	82.31(16)	C(3)-Re-O(4)	171.62(13)
C(1)-Re-O(4)	90.57(15)	C(2)-Re-O(4)	98.14(14)
C(3)-Re-N(2)	90.38(14)	C(1)-Re-N(2)	100.41(14)
C(2)-Re-N(2)	177.22(14)	O(4)-Re-N(2)	81.34(11)
C(3)-Re-N(1)	96.68(15)	C(1)-Re-N(1)	170.48(16)
C(2)-Re-N(1)	101.02(14)	O(4)-Re-N(1)	80.16(11)
N(2)-Re-N(1)	76.21(12)	O(6)-S(1)-O(5)	116.23(18)
O(6)-S(1)-O(4)	109.15(16)	O(5)-S(1)-O(4)	112.29(17)
O(6)-S(1)-C(18)	106.62(18)	O(5)-S(1)-C(18)	107.13(18)
O(4)-S(1)-C(18)	104.59(18)	S(1)-O(4)-Re	128.09(16)
C(4)-N(1)-C(8)	118.2(3)	C(4)-N(1)-Re	128.8(3)
C(8)-N(1)-Re	112.6(2)	C(15)-N(2)-C(12)	118.1(3)
C(15)-N(2)-Re	128.9(3)	C(12)-N(2)-Re	113.0(2)
O(1)-C(1)-Re	175.7(3)	O(2)-C(2)-Re	176.1(4)
O(3)-C(3)-Re	176.2(3)	N(1)-C(4)-C(5)	120.7(4)
N(1)-C(4)-C(16)	119.4(4)	C(5)-C(4)-C(16)	119.8(3)
C(6)-C(5)-C(4)	121.9(4)	C(5)-C(6)-C(7)	118.9(4)
C(6)-C(7)-C(8)	117.3(4)	C(6)-C(7)-C(9)	122.7(4)
C(8)-C(7)-C(9)	119.9(4)	N(1)-C(8)-C(7)	122.8(3)
N(1)-C(8)-C(12)	118.4(3)	C(7)-C(8)-C(12)	118.7(3)
C(10)-C(9)-C(7)	121.0(4)	C(9)-C(10)-C(11)	120.3(4)
C(12)-C(11)-C(13)	118.0(4)	C(12)-C(11)-C(10)	120.0(4)
C(13)-C(11)-C(10)	121.9(4)	N(2)-C(12)-C(11)	122.3(3)
N(2)-C(12)-C(8)	117.8(3)	C(11)-C(12)-C(8)	119.8(4)
C(14)-C(13)-C(11)	118.9(4)	C(13)-C(14)-C(15)	121.3(4)
N(2)-C(15)-C(14)	121.3(4)	N(2)-C(15)-C(17)	120.0(3)
C(14)-C(15)-C(17)	118.7(3)	C(23)-C(18)-C(19)	120.1(4)
C(23)-C(18)-S(1)	120.8(3)	C(19)-C(18)-S(1)	119.0(3)
C(20)-C(19)-C(18)	119.2(4)	C(19)-C(20)-C(21)	121.4(4)
C(22)-C(21)-C(20)	118.5(4)	C(22)-C(21)-C(24)	120.2(4)
C(20)-C(21)-C(24)	121.2(4)	C(21)-C(22)-C(23)	120.5(4)
C(18)-C(23)-C(22)	120.4(4)		

Table 61: Anisotropic displacement parameters [$Å^2 x10^3$] for TOS4

	U11	U22	U33	U23	U13	U12
Re	15(1)	11(1)	15(1)	1(1)	7(1)	0(1)
S(1)	16(1)	14(1)	18(1)	1(1)	5(1)	-1(1)
O(1)	43(2)	17(2)	34(2)	-4(1)	14(2)	-2(1)
O(2)	29(2)	25(2)	26(2)	4(1)	11(2)	-9(1)
O(3)	23(2)	26(2)	29(2)	11(1)	4(1)	4(1)
O(4)	17(1)	14(1)	19(2)	3(1)	7(1)	-2(1)
O(5)	26(2)	14(1)	30(2)	0(1)	8(1)	-4(1)
O(6)	19(1)	25(2)	17(2)	2(1)	2(1)	2(1)
N(1)	13(2)	18(2)	14(2)	-2(1)	4(1)	1(1)
N(2)	15(2)	15(2)	14(2)	-1(1)	6(1)	-1(1)
C(1)	22(2)	14(2)	19(2)	1(2)	9(2)	-1(2)
C(2)	21(2)	16(2)	15(2)	-2(2)	5(2)	-2(1)
C(3)	22(2)	15(2)	23(2)	4(2)	11(2)	-2(2)
C(4)	15(2)	22(2)	20(2)	-2(2)	6(2)	2(2)
C(5)	23(2)	23(2)	19(2)	-4(2)	5(2)	3(2)
C(6)	23(2)	15(2)	24(2)	-6(2)	2(2)	4(2)
C(7)	17(2)	13(2)	23(2)	2(2)	3(2)	-2(1)
C(8)	17(2)	14(2)	16(2)	-1(2)	4(2)	-1(1)
C(9)	27(2)	10(2)	32(2)	2(2)	6(2)	2(2)
C(10)	21(2)	18(2)	25(2)	4(2)	5(2)	-5(2)
C(11)	13(2)	17(2)	19(2)	5(2)	1(2)	-1(1)
C(12)	13(2)	14(2)	16(2)	2(2)	4(2)	-1(1)
C(13)	15(2)	27(2)	17(2)	6(2)	4(2)	-4(2)
C(14)	21(2)	25(2)	19(2)	2(2)	9(2)	-2(2)
C(15)	18(2)	19(2)	14(2)	1(2)	5(2)	3(1)
C(16)	24(2)	22(2)	19(2)	-3(2)	13(2)	-2(2)
C(17)	35(3)	28(2)	30(3)	-4(2)	24(2)	4(2)
C(18)	21(2)	17(2)	15(2)	-1(2)	7(2)	1(1)
C(19)	18(2)	21(2)	23(2)	0(2)	8(2)	-2(2)
C(20)	21(2)	25(2)	26(2)	-6(2)	5(2)	-2(2)
C(21)	13(2)	38(3)	20(2)	-7(2)	4(2)	1(2)
C(22)	23(2)	35(2)	20(2)	3(2)	9(2)	-4(2)
C(23)	20(2)	25(2)	22(2)	6(2)	7(2)	0(2)
C(24)	23(2)	51(3)	26(2)	-9(2)	8(2)	5(2)

2. 4. 11. X-ray Crystallographic analysis for TOS5

The X-ray examination and data collection was performed on single cryatals of TOS5 obtained as yellow rods and plates with approximate dimensions of 0.20 mm × 0.05 mm × 0.04 mm. The crystal was mounted in a Cryo-loop with Paratone-N and transferred to the goniostat bathed in a cold stream. A SMART6000 CCD diffractometer using graphite-monochromated Cu Kα radiation, λ=1.54178Å was used to collect the X-ray intensity data. The data collection temperature was 150 K. The detector was set at 5.17 cm from the crystal. A series of 5s data frames measured at 0.3º increments of ω were collected to calculate a unit cell. The data collection frames were measured for a duration of 5s at 0.3º intervals of ω with a maximum θ value of ~130º. The SAINT program was used to process the data frames. The data were corrected for decay, Lorentz and polarization effects as well as absorption and beam corrections based on the multi-scan technique used in SADABS.

A combination of direct methods SHELXTL v6.14 and the difference Fourier technique was used to solve the structure. The structure was refined by full-matrix least squares on F^2 out to 0.85Å resolution. Non-hydrogen atoms were refined with anisotropic displacement parameters. Weights were assigned as $w^{-1} = [\sigma^2(F_o^2) + (0.0290P)^2 + 0.5659P]$ where $P = 0.33333F_o^2+0.66667F_c^2$. A riding model was used to treat all hydrogen atoms. The hydrogen atoms were either located directly or calculated based on geometric criteria. The isotropic displacement parameters for the H-atoms were defined as $a*U_{eq}$ (a =1.5 for $–CH_3$ and 1.2 for all others). The refinement converged with crystallographic agreement factors of wR2 = 5.43%, R1 = 2.18%. This was for 3587

reflections with I>2σ(I) (R1 = 2.23%, wR2 = 5.48% for all data) and 307 variable parameters.

Table 62: Crystal data and structure refinement for TOS5

Empirical formula	$C_{24}H_{19}N_2O_3SRe$	
Formula weightn	649.67	
Temperature	150(2) K Wavelength	
	1.54178 Å Crystal system	
	Triclinic Space group	
	P-1	
Unit cell dimensions:	a = 9.9148(2) Å	α = 81.141(1)°
	b = 10.0847(2) Å	β = 88.235(1)°
	c = 12.2133(2) Å	γ = 68.280(1)°
Volume, Z	1120.49(4) $Å^3$, 2	
Density (calculated)	1.926 Mg/m^3	
Absorption coefficient	11.872 mm^{-1}	
F(000)	632	
Crystal size	0.20 x 0.05 x 0.04 mm	
θ range for data collection	3.66 to 65.11°	
Limiting indices	-11 < h < 11, -11 < k < 11, -14 < l < 14	
Reflections collected	8377	
Independent reflections	3667 (R_{int} = 0.0269)	
Completeness to θ = 65.11°	95.9 %	
Absorption correction	multi-scan	
Max. and min. transmission	0.6481and 0.1999	
Refinement method	Full-matrix least-squares on F^2	
Data / restraints / parameters	3667 / 0 / 307	
Goodness-of-fit on F^2	1.071	
Final R indices [I>2σ(I)]	R1 = 0.0218, wR2 = 0.0543	
R indices (all data)	R1 = 0.0223, wR2 = 0.0548	
Largest diff. peak and hole	0.730 and -0.630 $eÅ^{-3}$	

Table 63: Atomic coordinates [x 10^4] and equivalent isotropic displacement parameters [$Å^2$ x 10^3] for TOS5

	x	y	z	U(eq)
Re	1836(1)	424(1)	7721(1)	19(1)
S(1)	3775(1)	2185(1)	6412(1)	23(1)
O(1)	817(3)	3083(3)	8913(2)	38(1)
O(2)	-372(3)	2018(3)	5798(2)	39(1)
O(3)	-630(3)	-293(3)	8893(3)	45(1)
O(4)	3711(2)	787(2)	6991(2)	22(1)
O(5)	2998(3)	3376(3)	6992(2)	33(1)
O(6)	5276(3)	1974(3)	6196(2)	34(1)
N(1)	2909(3)	-1598(3)	7074(2)	20(1)
N(2)	3449(3)	-922(3)	8991(2)	20(1)
C(1)	1192(3)	2121(4)	8438(3)	26(1)
C(2)	481(3)	1442(4)	6502(3)	26(1)
C(3)	317(4)	-54(4)	8445(3)	28(1)
C(4)	2578(4)	-1932(4)	6127(3)	24(1)
C(5)	3354(4)	-3255(4)	5786(3)	26(1)
C(6)	4502(3)	-4245(3)	6411(3)	25(1)
C(7)	4912(3)	-3937(3)	7414(3)	22(1)
C(8)	4063(3)	-2584(3)	7702(2)	19(1)
C(9)	6101(3)	-4936(3)	8136(3)	25(1)
C(10)	6356(3)	-4597(4)	9136(3)	26(1)
C(11)	5461(3)	-3220(3)	9462(3)	23(1)
C(12)	4347(3)	-2221(3)	8739(2)	20(1)
C(13)	5611(3)	-2821(4)	10494(3)	27(1)
C(14)	4688(4)	-1524(4)	10753(3)	29(1)
C(15)	3618(4)	-590(4)	9985(3)	25(1)
C(16)	7017(4)	-6330(4)	7726(3)	34(1)
C(17)	7538(4)	-5600(4)	9953(3)	33(1)
C(18)	2842(4)	2515(4)	5122(3)	25(1)
C(19)	3089(4)	1388(4)	4517(3)	31(1)
C(20)	2349(5)	1648(4)	3515(3)	39(1)
C(21)	1346(5)	3012(4)	3112(3)	39(1)
C(22)	1129(4)	4127(4)	3734(3)	37(1)
C(23)	1869(4)	3883(4)	4727(3)	30(1)
C(24)	504(7)	3305(5)	2046(4)	64(1)

Table 64: Bond lengths [Å] and angles [º] for TOS5

Re-C(3)	1.900(3)	Re-C(2)	1.925(3)
Re-C(1)	1.929(3)	Re-O(4)	2.165(2)
Re-N(2)	2.169(3)	Re-N(1)	2.180(3)
S(1)-O(5)	1.443(2)	S(1)-O(6)	1.445(2)
S(1)-O(4)	1.498(2)	S(1)-C(18)	1.775(3)
O(1)-C(1)	1.143(4)	O(2)-C(2)	1.148(4)
O(3)-C(3)	1.155(4)	N(1)-C(4)	1.336(4)
N(1)-C(8)	1.365(4)	N(2)-C(15)	1.339(4)
N(2)-C(12)	1.360(4)	C(4)-C(5)	1.392(5)
C(5)-C(6)	1.361(5)	C(6)-C(7)	1.416(5)
C(7)-C(8)	1.405(4)	C(7)-C(9)	1.447(4)
C(8)-C(12)	1.434(4)	C(9)-C(10)	1.373(5)
C(9)-C(16)	1.516(5)	C(10)-C(11)	1.453(5)
C(10)-C(17)	1.509(5)	C(11)-C(12)	1.406(4)
C(11)-C(13)	1.408(5)	C(13)-C(14)	1.368(5)
C(14)-C(15)	1.393(5)	C(18)-C(23)	1.381(5)
C(18)-C(19)	1.393(5)	C(19)-C(20)	1.385(5)
C(20)-C(21)	1.390(6)	C(21)-C(22)	1.401(6)
C(21)-C(24)	1.498(5)	C(22)-C(23)	1.378(5)
C(3)-Re-C(2)	87.47(15)	C(3)-Re-C(1)	87.17(14)
C(2)-Re-C(1)	90.69(14)	C(3)-Re-O(4)	174.52(11)
C(2)-Re-O(4)	97.48(11)	C(1)-Re-O(4)	95.07(11)
C(3)-Re-N(2)	93.31(13)	C(2)-Re-N(2)	173.62(11)
C(1)-Re-N(2)	95.67(12)	O(4)-Re-N(2)	81.51(9)
C(3)-Re-N(1)	97.27(12)	C(2)-Re-N(1)	98.24(12)
C(1)-Re-N(1)	170.18(11)	O(4)-Re-N(1)	79.77(9)
N(2)-Re-N(1)	75.39(10)	O(5)-S(1)-O(6)	115.56(15)
O(5)-S(1)-O(4)	112.06(13)	O(6)-S(1)-O(4)	108.49(14)
O(5)-S(1)-C(18)	106.95(15)	O(6)-S(1)-C(18)	108.21(14)
O(4)-S(1)-C(18)	104.97(14)	S(1)-O(4)-Re	127.31(13)
C(4)-N(1)-C(8)	118.2(3)	C(4)-N(1)-Re	126.7(2)
C(8)-N(1)-Re	115.1(2)	C(15)-N(2)-C(12)	118.3(3)
C(15)-N(2)-Re	126.0(2)	C(12)-N(2)-Re	115.74(19)
O(1)-C(1)-Re	176.6(3)	O(2)-C(2)-Re	176.6(3)
O(3)-C(3)-Re	177.5(3)	N(1)-C(4)-C(5)	121.9(3)
C(6)-C(5)-C(4)	120.2(3)	C(5)-C(6)-C(7)	120.2(3)
C(8)-C(7)-C(6)	115.9(3)	C(8)-C(7)-C(9)	120.4(3)
C(6)-C(7)-C(9)	123.7(3)	N(1)-C(8)-C(7)	123.7(3)
N(1)-C(8)-C(12)	116.8(3)	C(7)-C(8)-C(12)	119.5(3)
C(10)-C(9)-C(7)	120.0(3)	C(10)-C(9)-C(16)	123.2(3)
C(7)-C(9)-C(16)	116.7(3)	C(9)-C(10)-C(11)	120.3(3)
C(9)-C(10)-C(17)	123.3(3)	C(11)-C(10)-C(17)	116.4(3)
C(12)-C(11)-C(13)	116.6(3)	C(12)-C(11)-C(10)	119.7(3)
C(13)-C(11)-C(10)	123.7(3)	N(2)-C(12)-C(11)	123.2(3)
N(2)-C(12)-C(8)	116.6(3)	C(11)-C(12)-C(8)	120.1(3)
C(14)-C(13)-C(11)	120.0(3)	C(13)-C(14)-C(15)	119.8(3)
N(2)-C(15)-C(14)	122.1(3)	C(23)-C(18)-C(19)	120.3(3)
C(23)-C(18)-S(1)	119.9(3)	C(19)-C(18)-S(1)	119.7(3)
C(20)-C(19)-C(18)	119.5(3)	C(19)-C(20)-C(21)	121.0(3)
C(20)-C(21)-C(22)	118.1(3)	C(20)-C(21)-C(24)	121.8(4)
C(22)-C(21)-C(24)	120.0(4)	C(23)-C(22)-C(21)	121.3(3)
C(22)-C(23)-C(18)	119.7(3)		

Table 65: Anisotropic displacement parameters [$Å^2 x10^3$] for TOS5

	U11	U22	U33	U23	U13	U12
Re	19(1)	20(1)	18(1)	-5(1)	-2(1)	-7(1)
S(1)	29(1)	25(1)	17(1)	-2(1)	-3(1)	-13(1)
O(1)	41(1)	33(1)	42(1)	-19(1)	7(1)	-12(1)
O(2)	30(1)	44(2)	35(1)	-5(1)	-12(1)	-5(1)
O(3)	39(1)	55(2)	56(2)	-22(1)	18(1)	-29(1)
O(4)	23(1)	23(1)	19(1)	-1(1)	0(1)	-8(1)
O(5)	50(1)	29(1)	22(1)	-6(1)	-2(1)	-17(1)
O(6)	34(1)	43(1)	29(1)	0(1)	-2(1)	-23(1)
N(1)	24(1)	21(1)	18(1)	-3(1)	-2(1)	-10(1)
N(2)	23(1)	22(1)	18(1)	-2(1)	-2(1)	-11(1)
C(1)	23(2)	27(2)	29(2)	-3(1)	-2(1)	-10(1)
C(2)	22(2)	27(2)	27(2)	-6(1)	-3(1)	-7(1)
C(3)	28(2)	29(2)	30(2)	-10(1)	4(1)	-12(1)
C(4)	27(2)	28(2)	18(1)	-4(1)	-4(1)	-10(1)
C(5)	33(2)	30(2)	21(1)	-7(1)	-3(1)	-15(1)
C(6)	26(2)	25(2)	26(2)	-10(1)	7(1)	-9(1)
C(7)	22(1)	22(2)	24(1)	-1(1)	2(1)	-12(1)
C(8)	20(1)	22(1)	17(1)	-1(1)	1(1)	-11(1)
C(9)	23(2)	23(2)	29(2)	1(1)	1(1)	-10(1)
C(10)	22(2)	28(2)	28(2)	0(1)	0(1)	-11(1)
C(11)	22(1)	28(2)	21(1)	2(1)	-4(1)	-13(1)
C(12)	23(1)	23(2)	18(1)	-2(1)	-1(1)	-14(1)
C(13)	29(2)	34(2)	20(2)	5(1)	-8(1)	-17(1)
C(14)	39(2)	37(2)	18(1)	-1(1)	-5(1)	-23(2)
C(15)	30(2)	29(2)	20(1)	-5(1)	2(1)	-16(1)
C(16)	31(2)	25(2)	40(2)	-4(2)	2(2)	-5(1)
C(17)	27(2)	35(2)	33(2)	0(2)	-3(1)	-7(1)
C(18)	29(2)	31(2)	18(1)	-1(1)	-3(1)	-13(1)
C(19)	37(2)	27(2)	26(2)	-6(1)	-5(1)	-8(1)
C(20)	57(2)	34(2)	27(2)	-9(2)	-8(2)	-16(2)
C(21)	58(2)	34(2)	28(2)	0(2)	-13(2)	-21(2)
C(22)	46(2)	27(2)	35(2)	4(2)	-12(2)	-14(2)
C(23)	41(2)	26(2)	25(2)	-3(1)	-3(1)	-15(2)
C(24)	103(4)	49(3)	44(2)	7(2)	-41(3)	-36(3)

2. 5. DNA Binding Studies

2. 5. 1. Electronic absorption spectroscopy

The interactions of the 1NS, 2NS and TOS complexes with CT-DNA (Calf Thymus DNA) were studied using UV-Vis spectroscopy in order to determine the possible binding modes. 25 μM solution (except for a 75 μM solution 1NS7) of each complex was prepared in DMSO and then titrated against varied amounts of DNA stock solution. The DNA stock concentrations used for different compounds are shown in Table 1 below.

The titrations were carried out using two cuvettes. One of the cuvettes contained the reference and the other (sample cuvette) contained the compounds to be analyzed. 3000 μL of Tris buffer saline (5 mM Tris–HCl, 50 mM NaCl, pH 7.2) was added to both the reference and the sample cuvette. Following this, a calculated amount of the complex in DMSO solution was added to the 3000 μL of Tris buffer in the sample cuvette to make 25 μM solution (except for a 75 μM solution 1NS7). An equal amount of neat DMSO solution as was used in the sample cuvette was also added to the 3000 μL of Tris buffer in the reference cuvette. The content of the reference cuvette was used as a blank and the absorption spectra of the complexes were recorded in the range of 225–700 nm.

The titrations started by recording the absorption spectra of the complex by itself, followed by the absoption spectra of the complex plus varied amounts of DNA. The solutions in the cuvettes were mixed by repeated inversion and then incubated for 10 min before the absorption spectra was recorded. The change in concentration of the complexes due to each titration was negligible.

Table 66: Concentration of stock DNA used for the UV-Vis titrations of each compound

Concentration (μM)	Compound
1555.76	1NS1
	1NS2
	1NS10
	2NS1
	2NS2
	2NS5
	2NS7
1692.71	1NS6
	1NS7
	2NS6
	TOS6
	TOS7
1944.70	1NS9
	2NS9
	2NS10
2333.64	1NS3
	1NS4
	1NS5
	2NS3
	2NS4
	TOS1
	TOS2
	TOS3
	TOS4
	TOS5
	TOS8
	TOS9
	TOS10

2. 5. 2. Cyclic Voltammetry

The interactions of the sulfonato complexes with CT-DNA were also investigated using cyclic voltammetry. The changes observed in the cyclic voltammogram of the complexes upon addtion of CT-DNA were monitored. The electrochemical studies were carried out using a CH Instrument Electrochemical analyzer in a single compartmental cell. A three-electrode configuration was used comprising a Platinum wire as the auxiliary electride, Ag/AgCl as the reference electrode and a glassy carbon electrode as the working electrode. The experiment started with sample preparation.

First, 0.1M (50 mL) solution of the supporting electrolyte tetrabutylammonium perchlorate (TBN) in either dimethylformamide (DMF) or acetonitrile was prepared in a 50 mL centrifuge tube. This TBN solution served as the solvent that was used to prepare

a 2mM (1.2mL) solution of the complexes. Dimethylformamide was the solvent used for most complexes since most of the complexes either partially dissolved or did not dissolve in acetonitrile. However, acetonitrile supporting electrolyte solution was used to dissolve 2NS6, 2NS7 and 2NS10 since these complexes dissolved better in it.

Following this a 1:1 (400:400 μL) mixture of complex solution (in TBN) and Tris buffer (5 mM Tris–HCl, 50 mM NaCl, pH 7.2) was prepared. The cyclic voltammogram of this mixture was then recorded. The cyclic voltammogram of the mixture upon addition of 10 μL of DNA was also recorded.

2. 5. 3. Ethidium bromide displacement assay

Ethidium bromide (EtBr) fluorescence displacement experiments were carried out to further investigate the interaction modes of the sulfonato complexes with DNA. The experiment was carried out by recording the fluorescence spectra of EtBr bound to DNA, and then monitoring the changes in the EtBr-DNA spectra with increasing concentration of complex. First, 3500 μL stock solution of EtBr in Tris buffer (1 mM) was prepared. Following this, calculated volumes of 12.3 μM EB-Tris solution and 100 μM CT-DNA were diluted with Tris buffer (5 mM Tris–HCl, 50 mM NaCl, pH 7.2) to give a total volume of 2500 μL in a cuvette. The fluorescence spectrum of this solution was recorded. The fluorescence spectra of the EtBr + DNA + complex were then recorded with increasing concentrations of complex as follows: 12.3 μM, 24.4 μM, 36.5 μM, 48.5 μM, and 60.4 μM. The complexes were mixed by repeated inversion and then incubated for 15 min before each fluorescence spectra was recorded.

2. 5. 4. Gel Electrophoresis

The interaction mode of the sufonato complexes with DNA was further investigated using gel electrophoresis. Since some of our compounds are fluorescent, their binding to DNA can be investigated via their ability to stain DNA in agarose gels. The procedure involved incubating the compounds in a microfuge tube with lambda bacteriophage HindIII DNA ladder at room temperature for 1 hr. Following this, the 6X gel loading buffer (65% sucrose, 10 mM Tris– HCl, 10 mM EDTA, 0.3% bromophenol blue, pH 7.5) was added to the tube. Electrophoresis was conducted by casting the agarose gels in 1X Tris-acetate-EDTA (TAE) buffer (40 mmM Tris.HCl, pH 8.0, 20 mM acetic acid, and 1 mM EDTA). Electrophoresis was carried out for 2 hrs at 8 volts/cm constant voltage. After the electrophoresis step, the gels were preimaged using a VersaDoc molecular imager (BioRad), stained with Ethidium bromide for 1 hr and then washed with water under a shaker for another 10 mins.

2. 5. 5. Viscosity

The interaction of the sulfonato complexes with CT-DNA was studied by measuring the change in viscosity of CT-DNA upon addition of the complexes to it. CT-DNA was dissolved in 10X Phosphate Buffered Saline (PBS) buffer to make a stock solution of 1mg/mL. The stock solution was diluted to make a working solution (0.025 mg/mL and 0.05 mg/mL). The absorbance of this working solution was measured using a Nanodrop UV spectrophotometer at 260 nm. The absorbance was measured in duplicates and the average absorbance was calculated for each working solution. The concentration in molarity was calculated for each working solution. The average concentration was used for the rest of the experiment.

After the concentration was calculated, the stock solution of DNA was sheared using a sonicating water bath for pulses of 120 s on/30 s off for 60 min. The sheared DNA was confirmed by running a gel. A constant concentration (200 μM) of DNA was then used for the binding studies. Binding of CT-DNA to each sulfonato complex or Ethidium bromide (EtBr) was tested using 48 μM, 96 μM and 200 μM solutions of complex and EtBr after 30 min incubation at room temperature. Viscosities of DNA/complex or DNA/EB were measured using a 3156 viscometer (Q Glass Company Inc.) and a digital stop watch was used to measure the flow time. For the control, the flow rate of buffer alone and the flow rate of buffer plus DNA was measured. Each measurement was done in triplicate and the average flow rate was calculated.

The relative viscosities of DNA in the presence and absence of the sulfonato complex were calculated using the following relation: $\eta \alpha (t - t_o)$, where t is the observed flow time of DNA solutions and t_o is the flow time of the PBS buffer alone. The data was graphed as $(\eta/\eta_o)^{1/3}$ versus [complex]/[DNA] where η is the viscosity of DNA in the presence of the complex. η_o is the viscosity of DNA alone. [complex] = concentration of sulfonato complex. [DNA] is the concentration of DNA.

2. 6. Cytotoxicity Studies

Alamar blue assay wasTo determine the cytotoxicity of the sulfonato complexes, we used the Alamar blue assay. The anticancer activity studies of the sulfonato complexes against breast cancer cells (MCF-7, MDA-MB-231, and MCF-10A) was carried out by Wilder and his group and the procedure was described in a previously published article.[9]

The cytotoxicity studies of the sulfonato complexes against lymphoma cells was carried out in our lab and is described as thus: First, the lymphoma cells (U937) were counted using a hemocytometer. After cells were counted, the cells were diluted to a concentration of 150,000 cells/mL. 200 μL of the 150,000 cells/mL concentration were plated per well in a 96-well plate. The first three wells contained just cells to serve as control. Another three wells contained cells plus DMSO. The remaining 90 wells contained the cells plus several concentrations of the compounds (dissolved in DMSO) to be tested. The concentrations used were 0.001 μM, 0.01 μM, 0.1 μM, 1 μM and 10 μM. Each concentration was added in triplicate for each compound tested on the 96-well plate.

Next, the plate was placed in an incubator at 37 ^{o}C for 72 hours (3 days). Following this, 20 μL of Alamar blue was added to each well after which the plate was placed in an incubator at 37 ^{o}C for another 4 hours. When incubation period was over, the plate was placed in a UV spectrophotometer microplate reader to read the absorbance at 595 nm. The absorbance data was transferred to excel, and the average absorbance was calculated for each compound and control. The graph of concentration of compound vs. cell viability was plotted. Cell viability is calculated as thus: [Absorbance of compound/Absorbance of control] x 100 = % cell survival. The experiment was done in triplicate. The average cell viability (% cell survival) was calculated for each compound after which the standard deviation was calculated.

CHAPTER III: RESULTS AND DISCUSSION

A series of sulfonato rhenium complexes of the type $XRe(CO)_3Z$ [X = α-diimines and Z = tosylate, 1-naphthalenesulfonate and 2-naphthalenesulfonate] were synthesized. The first step of the synthesis was the conversion of $Re_2(CO)_{10}$ to a series of novel *fac*-tricarbonyl (pentylcarbonato) (α-diimine) rhenium complexes (PC) in the presence of α-diimine, CO_2 and 1-pentanol under reflux conditions. The α-diimines we considered are 2,2'-bipyridyl, 1,10-phenanthroline, 5-methyl-1,10-phenanthroline, neocuproin, 5,6-dimethyl-1,10-phenanthroline, bathophenanthroline, bathocuproin, 4,7-dimethyl-1,10-phenanthroline, 3,4,7,8-tetramethyl-1,10-phenanthroline and 4-methyl-1,10-phenanthroline. Figure 4 is a schematic representation of this step. The protocol for this first step was developed in the mandal lab and published for the first 7 PC compounds.[49]

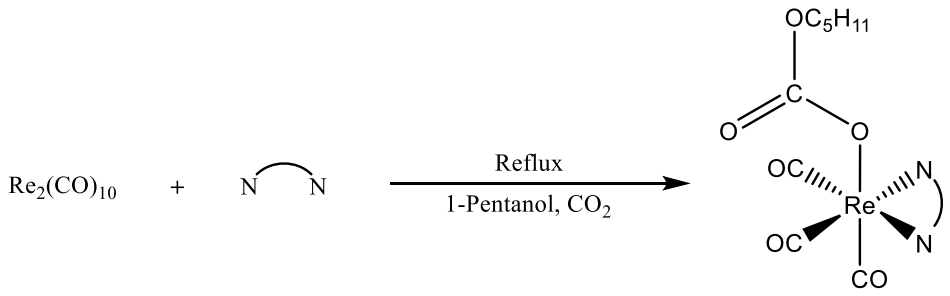

N ⌒ N = α-diimine **PC**

Figure 5: Synthesis of Pentylcarbonato complex

After completion of the first step of the synthesis, a second step was carried out. This step is the synthesis of 30 sulfonato complexes by treating the pentylcarbonato complex with the corresponding p-toluenesulfonic acid, 1-naphthalenesulfonic acid or 2-naphthalenesulfonic acid in dichloromethane at room temperature. Figure 5 is a

schematic representation of this step. The yield and purity of these complexes will also be determined.

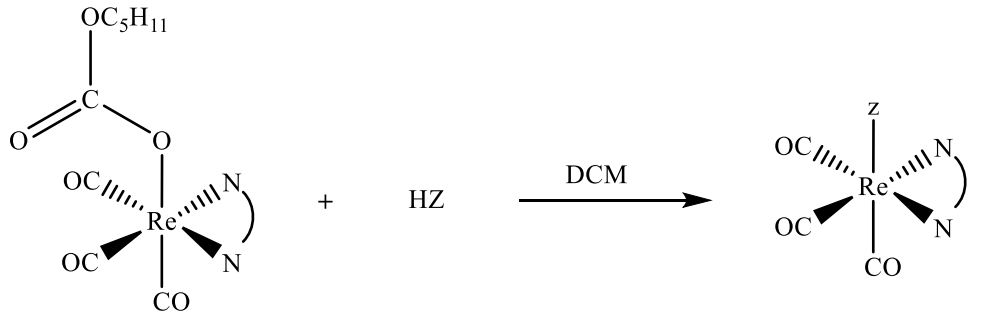

PC **Sulfonato complex**

Z = Sulfonate
HZ = Sulfonic Acid

Figure 6: Synthesis of Sulfonato complexes

After succefully synthesizing and purifying the pentylcarbonato and sulfonato complexes, these compounds were characterized using Infrared IR, ^{1}H NMR, and X-ray crystallography (in some cases). The proposed mechanisms and results for all reactions are discussed below.

3. 1. Mechanism of Reactions

The proposed mechanisms of the reactions for step 1 and step 2 of the synthesis of the sulfonato complexes are shown in Scheme 1 and 2 below. We did not study the mechanisms of the reactions in this project, however, it is possible that the reactions follow the pathways in Scheme 1 and 2 below.

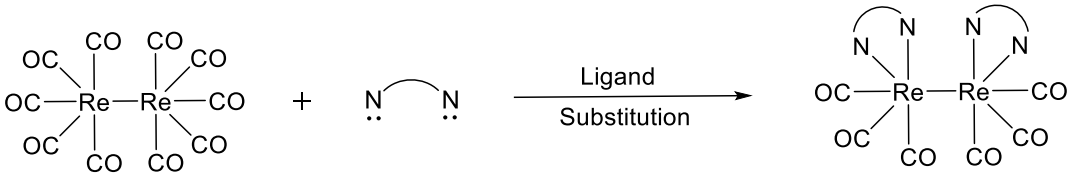

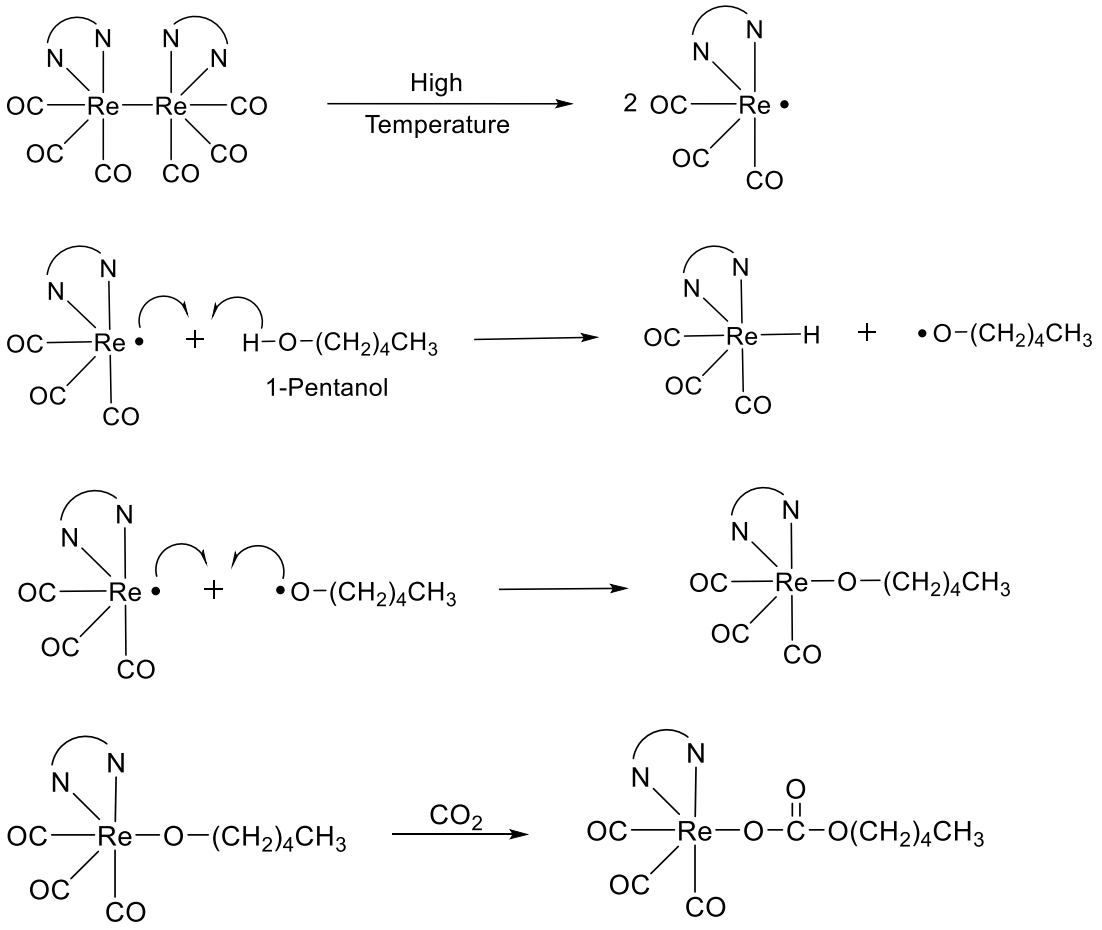

Scheme 1: Proposed step-by-step mechanism of PC synthesis reaction

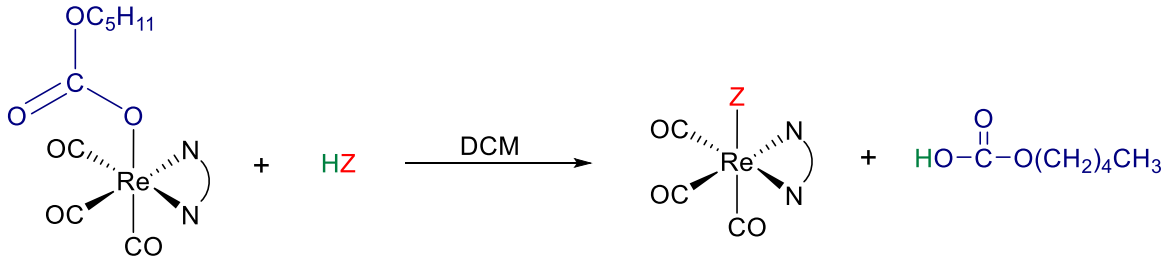

Z = sulfonate
HZ = sulfonic acid

Scheme 2: Proposed mechanism of sulfonato synthesis reaction

3. 2. Synthesis

3. 2. 1. Synthesis of *fac*-tricarbonyl (pentylcarbonato) (α-diimine) rhenium complexes

3. 2. 1. 1. *fac*-$(CO)_3$(4,7-dimethyl-1,10-phenanthroline) $ReOC(O)OC_5H_{11}$ (PC8)

PC8 was synthesized from a one-pot reflux reaction of dirhenium decacarbonyl ($Re_2(CO)_{10}$), 4,7-dimethyl-1,10-phenanthroline, 1-Pentanol, and CO_2 gas according to Scheme 3 below. The yellow crystals (78%) of PC8 were characterized using IR and ^1H NMR.

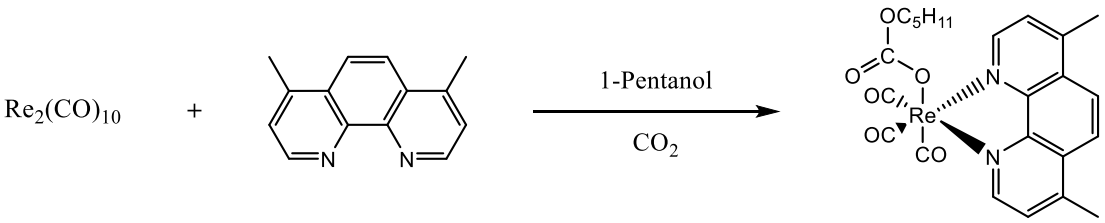

PC8

Scheme 3: Synthesis of PC8

As expected, the IR spectrum (Figure 7) of **PC8** exhibits three strong υ(C≡O)'s at 2022(s), 1916(s) and 1892(s) cm^{-1} and a υ(C=O) at 1660 (m) cm^{-1}. The ^1H NMR spectrum (see, Figure 8) accounts for the phenanthroline ligand's and pentyl group's protons. In the ^1H NMR spectrum of **PC8**, the phenanthroline ligand attachment is symmetrical. As a result, the phenantholine doublet at 9.08 ppm represents two similar protons (CH=N) each. The singlet at 8.17 ppm represents the similar protons on position 5 and 6 of the phenanthroline ring. The doublet at 7.74 ppm represents the similar protons on position 3 and 8 of the phenathroline ring. The triplet at 3.18 ppm represents the OCH_2 protons. The singlet at 2.71 ppm represents the methyl group protons on the phenathroline ring. The protons on three aliphatic methylene groups show up as

multiplets between 0.91–0.82 ppm and 0.77–0.61 ppm representing six protons altogether. The aliphatic CH_3 protons show up as a triplet at 0.51 ppm. Similar IR and NMR data were also obtained for PC1–PC8 complexes.[49]

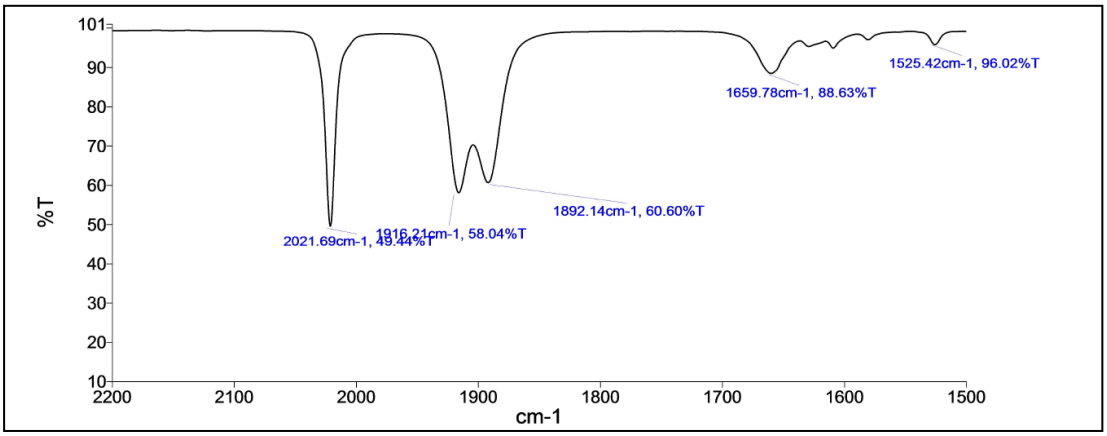

Figure 7: IR spectrum of PC8

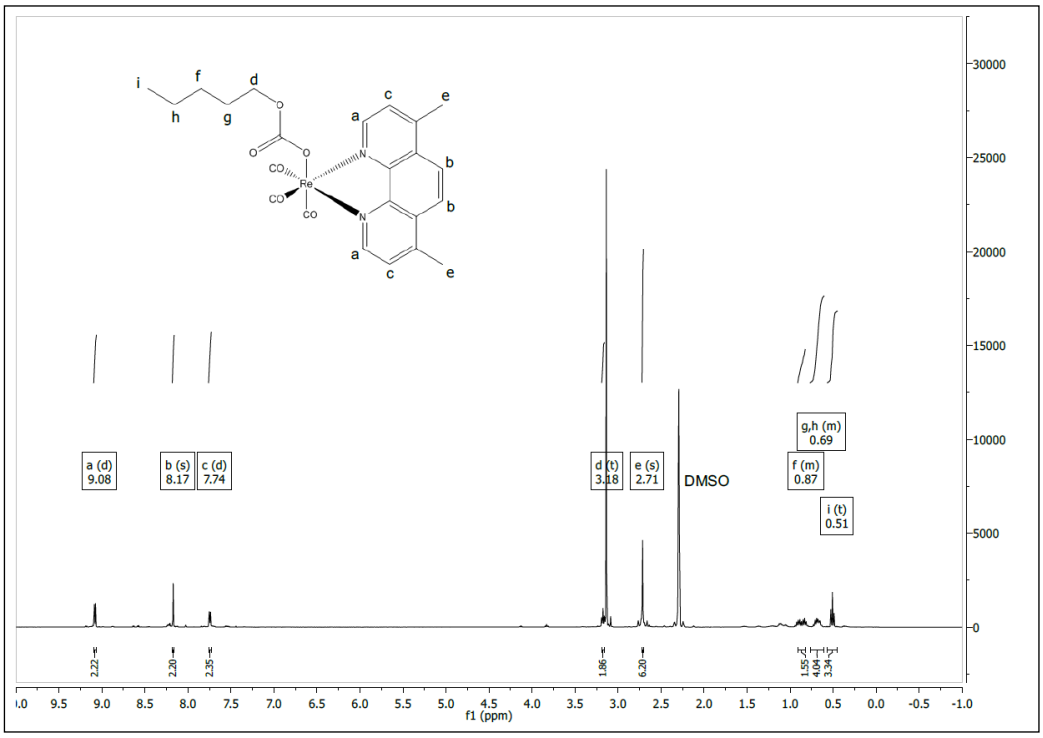

Figure 8: ^{1}H NMR spectrum of PC8

3. 2. 1. 2. *fac*-$(CO)_3$(3,4,7,8-tetramethyl-1,10-phenanthroline) $ReOC(O)OC_5H_{11}$ (PC9)

PC9 was synthesized from a one-pot reflux reaction of dirhenium decacarbonyl ($Re_2(CO)_{10}$), 3,4,7,8-tetramethyl-1,10-phenanthroline, 1-Pentanol, and CO_2 gas according to Scheme 4 below. The yellow crystals (76%) of PC9 were characterized using ^1H NMR.

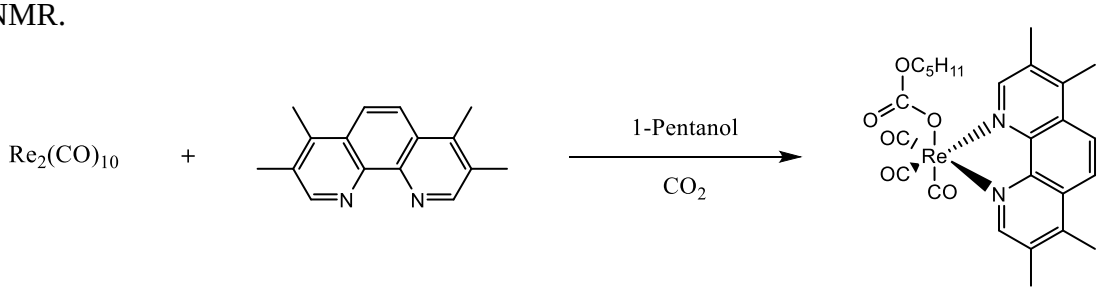

PC9

Scheme 4: Synthesis of PC9

Figures 9 and 10 show the IR and ^1H NMR spectra of **PC9**, respectively. The spectral data for **PC9** is very similar to the spectral data for **PC8**. The IR spectrum shows three strong υ(C≡O)'s at 2021, 1915 and 1890 cm^{-1} characteristic for a facial geometry and an expected medium intensity υ(C=O) at 1660 cm^{-1}.

The 1H NMR spectrum accounts for all protons. In the ^1H NMR spectrum of **PC9**, the phenanthroline ligand attachment is symmetrical. As a result, the phenantholine singlet at 9.18 ppm represents two similar protons (CH=N). The singlet at 8.14 ppm represents the similar protons on position 5 and 6 of the phenanthroline ring. The triplet at 3.75 ppm represents the OCH_2 protons. The singlet at 2.79 ppm represents the methyl group protons at position 3 and 8 of the phenanthroline ring. The singlet at 2.63 ppm represents the methyl group protons at position 4 and 7 of the phenanthroline ring. The protons on three aliphatic methylene groups show up as multiplets between 1.52–1.41

ppm and 1.27–1.11 ppm representing six protons altogether. The aliphatic CH_3 protons show up as a triplet at 0.81 ppm.

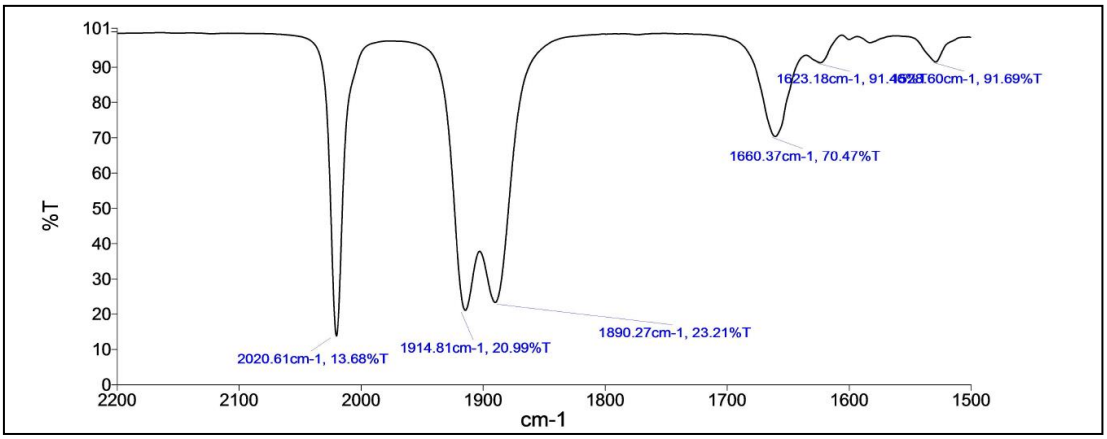

Figure 9: IR spectrum of PC9

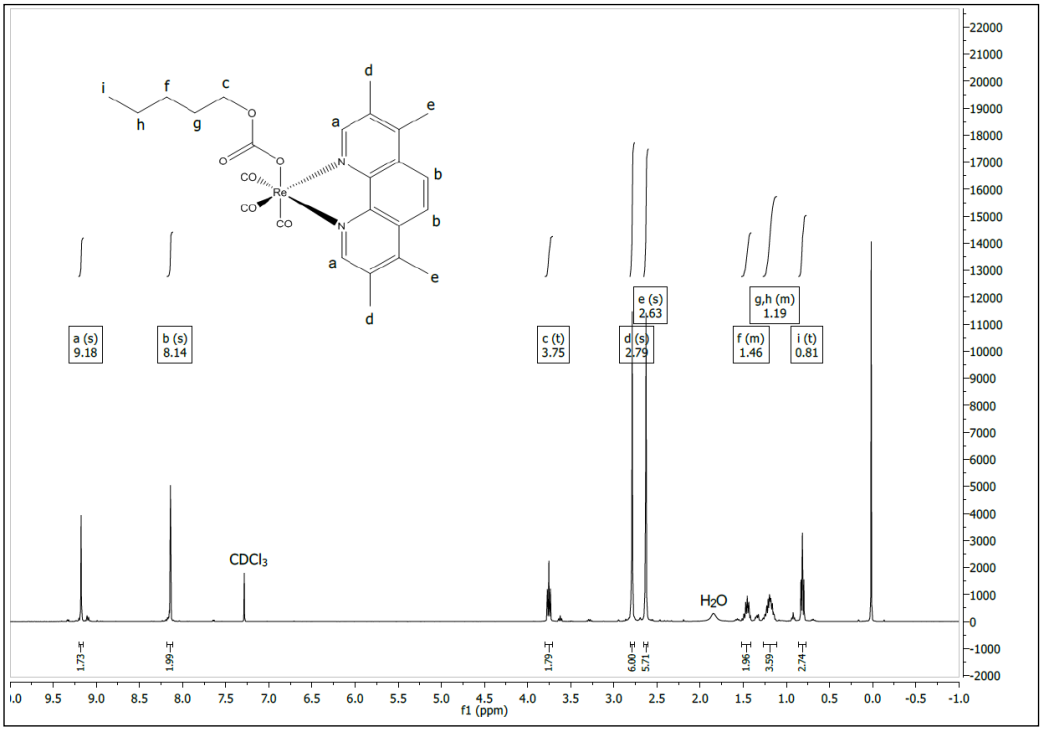

Figure 10: ^{1}H NMR spectrum of PC9

3. 2. 1. 3. *fac*-$(CO)_3$(4-methyl-1,10-phenanthroline) $ReOC(O)OC_5H_{11}$ (PC10)

PC10 was synthesized from a one-pot reflux reaction of dirhenium decacarbonyl ($Re_2(CO)_{10}$), 4-methyl-1,10-phenanthroline, 1-Pentanol, and CO_2 gas according to Scheme 5 below. The grey crystals (74%) of PC10 were characterized using ^1H NMR.

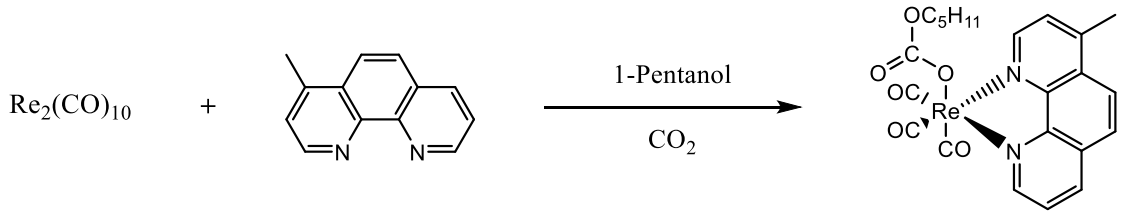

PC10

Scheme 5: Synthesis of PC10

The IR spectrum (Figure 11) and ^1H NMR spectrum (Figure 12) of **PC10** exhibit spectral characteristics similar to those of **PC8** and **PC9**. In the IR spectrum of PC10, the three peaks at 2022.43, 1917.48 and 1893.12 cm^{-1} represent the three CO bonds attached to the Re center. The peak at 1660.13 cm^{-1} represent the carbonyl (C=O) group.

In the ^1H NMR spectrum of **PC10**, the doublet of doublets at 9.31 ppm represents the phenantholine proton (CH=N) at position 9 of the phenanthroline ring. The doublet at 9.15 ppm represents the proton (CH=N) at position 2 of the phenanthroline ring. The doublet of doublets at 8.48 ppm represents the proton at position 8 of the phenanthroline ring. The doublets at 8.06 and 7.93 ppm represent the protons at position 5 and 6. The proton at postion 7 of the phenanthroline ring appears as a doublet of doublets at 7.75 ppm. The proton at postion 3 of the phenanthroline ring appears as a doublet at 7.60 ppm. The triplet at 3.44 ppm represents the OCH_2 protons. The singlet at 2.79 ppm represents the methyl group proton at position 4 of the phenanthroline ring. The protons on three aliphatic methylene groups show up as multiplets between 1.23–1.11 ppm and 1.09–0.89

ppm representing six protons altogether. The aliphatic CH_3 protons show up as a triplet at 0.65 ppm.

As expected, the ^{13}C NMR spectrum (Figure 13) shows a total of 12 aromatic and six (6) aliphatic carbons and C=O resonance at δ158.67. In the phenanthroline ligand component of the PC10 structure, there are 13 distinct carbon types on the ligand representing the 13 carbons on the ring and represented as peaks in the ^{13}C NMR spectra. One of those peaks (28.84 ppm) represents the methyl group carbon on the phenanthroline ligand. The OCH_3 carbon on the aliphatic chain of the PC10 structure appears as a peak at 65.84 ppm. The CH_3 carbon on the aliphatic chain appears as a peak at 13.72 ppm. The three CH_2 carbons appear at 28.05, 22.36 and 19.05 ppm.

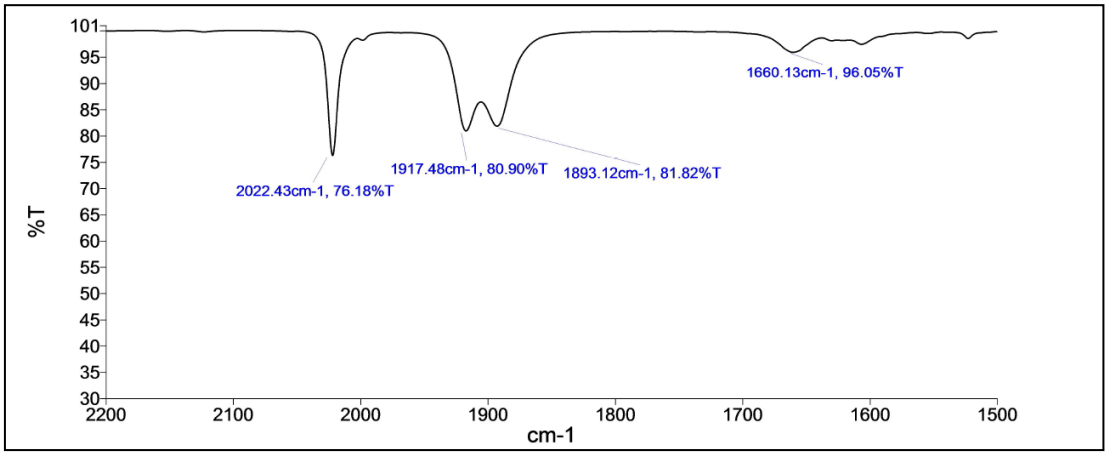

Figure 11: IR spectrum of PC10

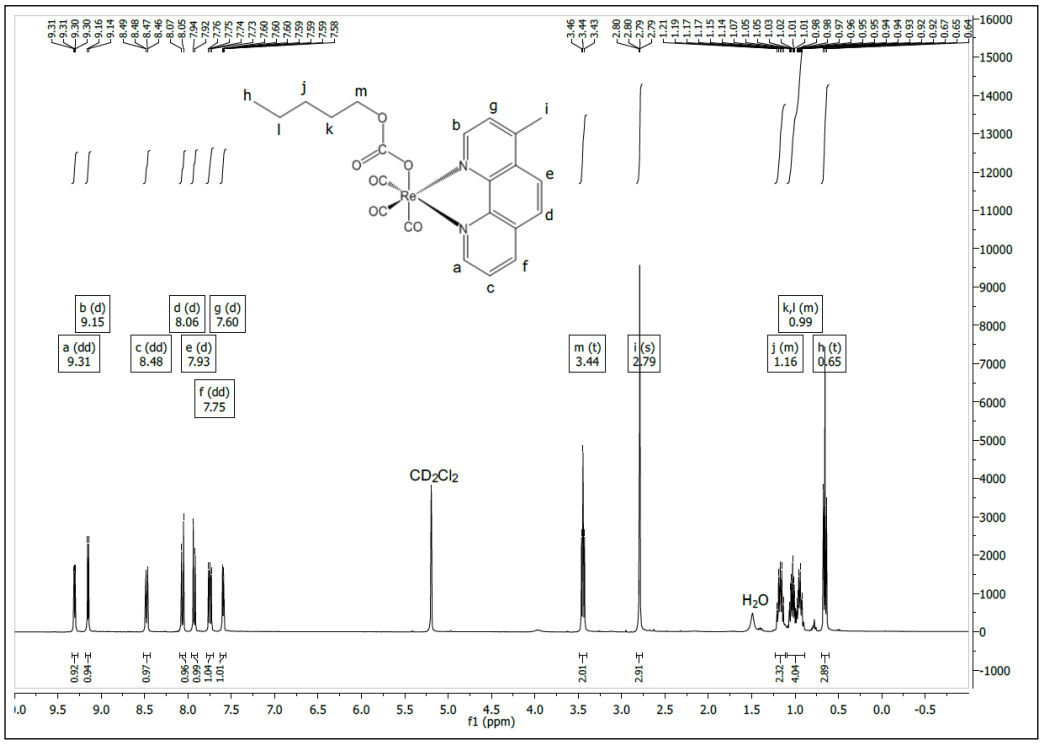

Figure 12: ^{1}H NMR spectrum of PC10

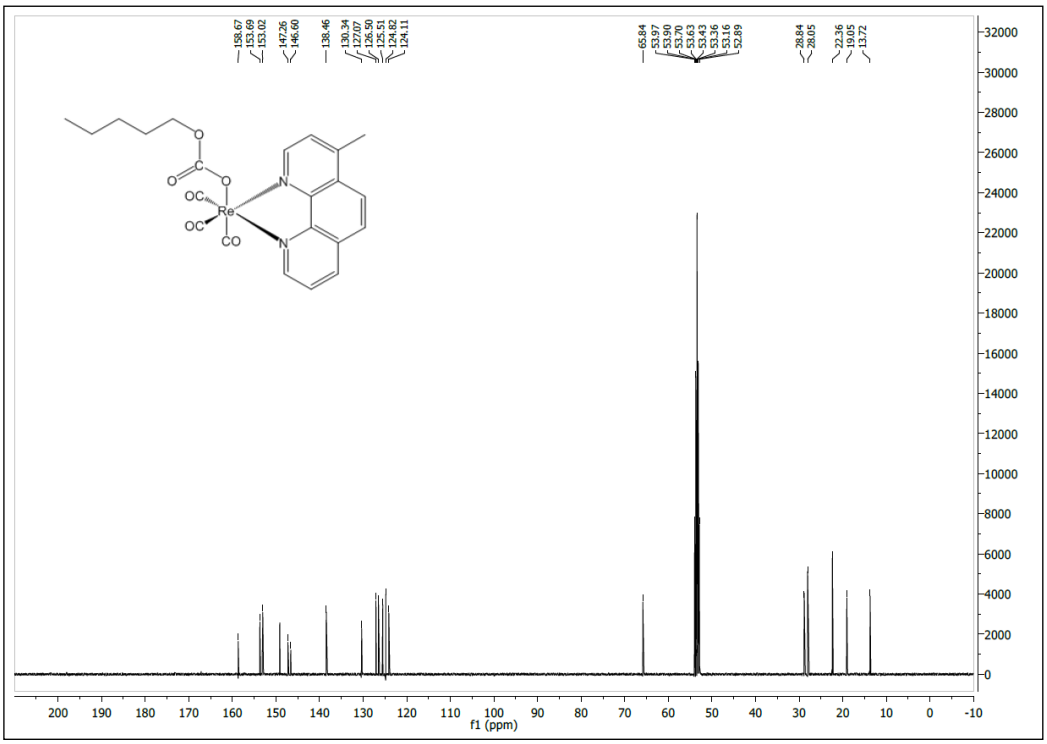

Figure 13: ^{13}C NMR spectrum of PC10

3. 2. 2. Synthesis of *fac*-tricarbonyl (pentylcarbonato) (α-diimine) rhenium complexes

3. 2. 2. 1. *fac*-$(CO)_3$(2,2'-bipyridyl) $ReOS(O_2)C_{10}H_7$ (1NS1)

1NS1 was synthesized from a one-pot reaction of PC1 and 1-Naphthalenesulfonic acid in dichloromethane solvent according to Scheme 6 below. The yellow crystals (94%) of 1NS1 were characterized using ^{1}H NMR.

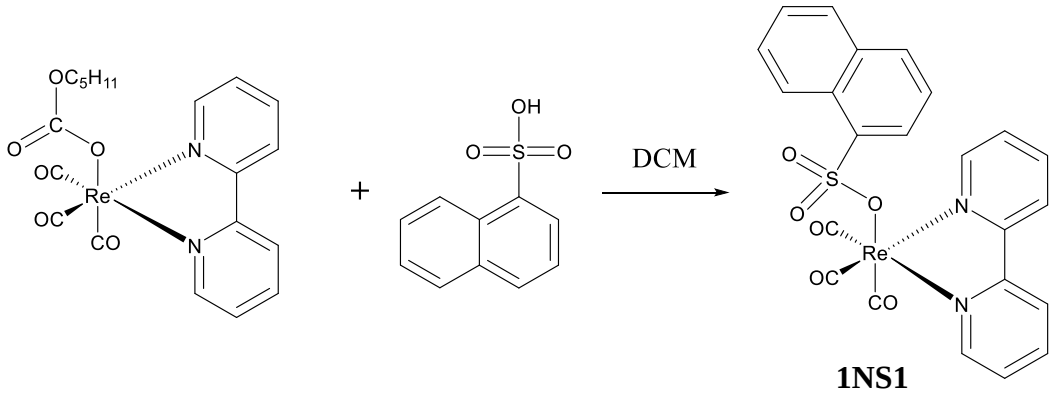

1NS1

Scheme 6: Synthesis of 1NS1

1NS1 has been characterized spectroscopically. The IR spectrum (Figure 14) exhibits three strong υ(C≡O)'s at 2031(s), 1928(s) and 1906(s) characteristic of an organometallic complex of the type, *Fac*-$(CO)_3$(N~N)M-OS(=O)OR, where, N~N is a polypyridyl, M is either Mn or Re, and R is an aryl group. The ^{1}H NMR spectrum (Figure 15) shows a doublet of doublets at 8.64 ppm representing two similar protons (CH=N). All the other protons on the bipyridyl ring and the proton on position 2 of the naphthalene ring appear as a multiplet at 7.96–7.68 ppm. The protons at positions 3, 4, 5 and 7 of the naphthalene ring appear as a multiplet at 7.39–7.23 ppm. The multiplet at 7.13–7.05 ppm represents the proton on position 6 of the naphthalene ring.

Although the ^{1}H NMR does not provide much information, the structure was established through X-ray crystallography. As expected, the X-ray structure of 1NS1

(Figure 16) shows the Re atom is octahedrally coordinated to three terminal carbonyls in *Facial* arrangement (i.e., three CO's are cis to each other), one bidentate 2,2'-dipyridyl ligand and the anion, 1-naphthalenesulfonate.

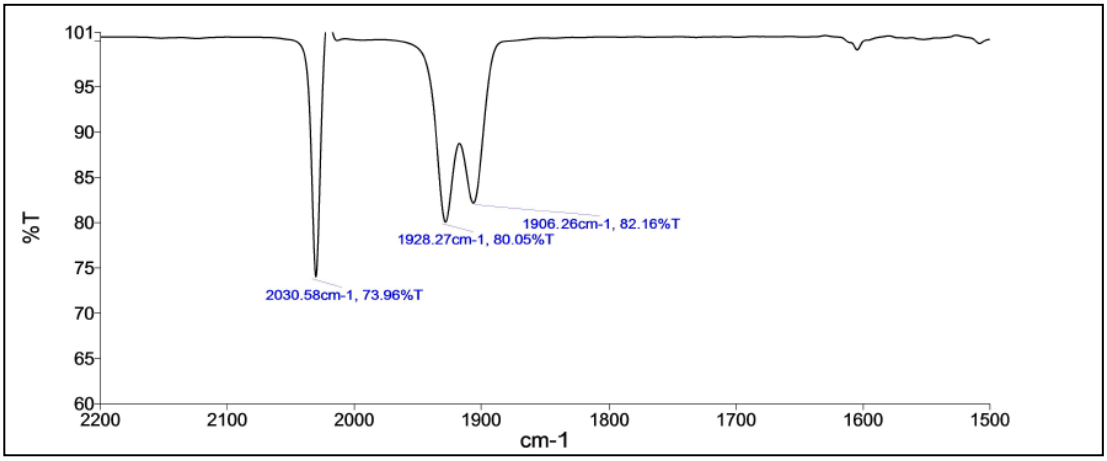

Figure 14: IR spectrum of 1NS1

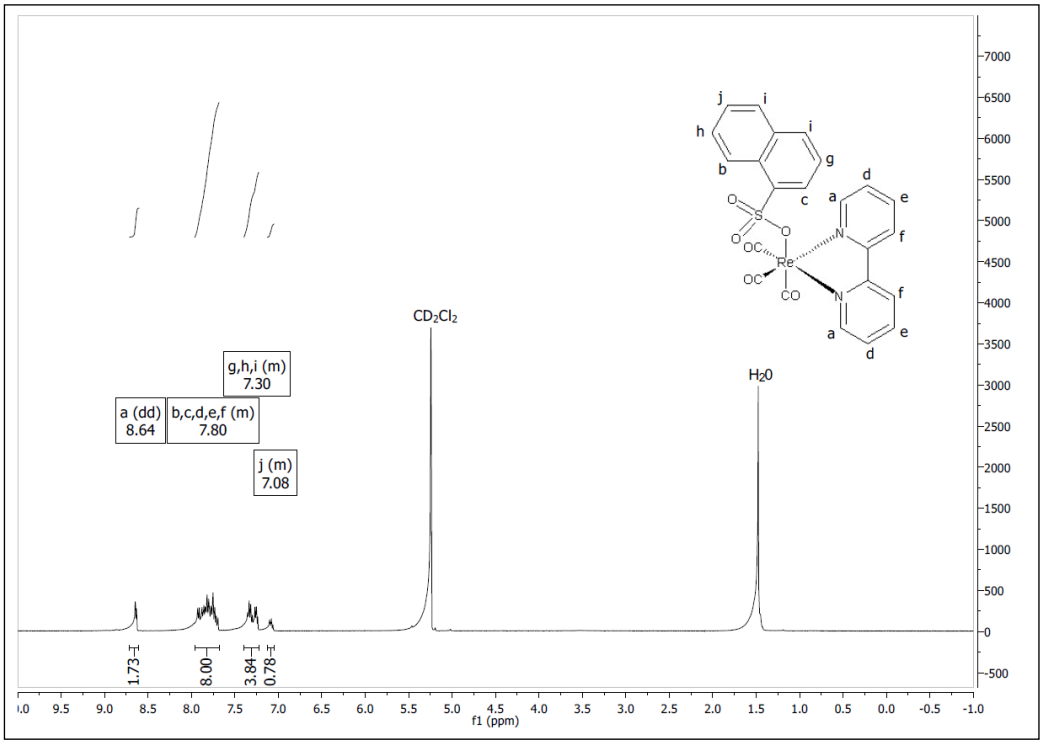

Figure 15: ^{1}H NMR spectrum of 1NS1

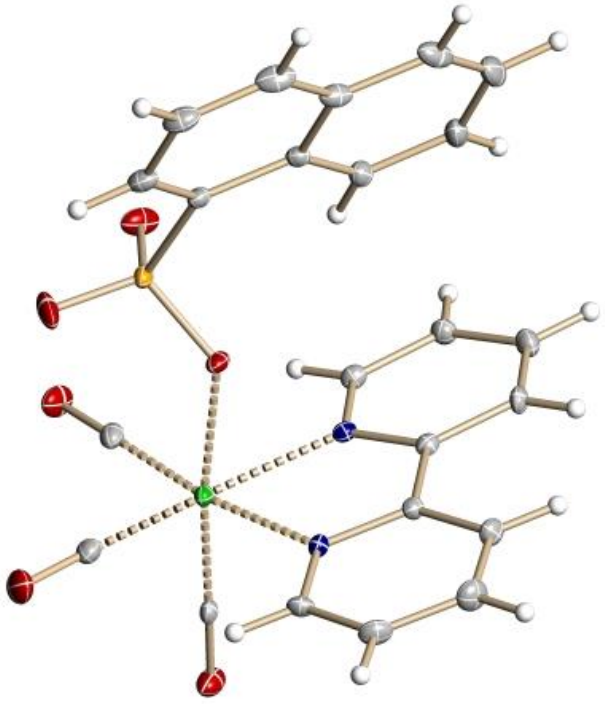

Figure 16: X-ray structure of 1NS1

3. 2. 2. 2. *fac*-$(CO)_3$(1,10-phenanthroline) $ReOS(O_2)C_{10}H_7$ (1NS2)

1NS2 was synthesized from a one-pot reaction of PC2 and 1-Naphthalenesulfonic acid in dichloromethane solvent according to Scheme 7 below. The yellow crystals (95%) of 1NS2 were characterized using ^{1}H NMR.

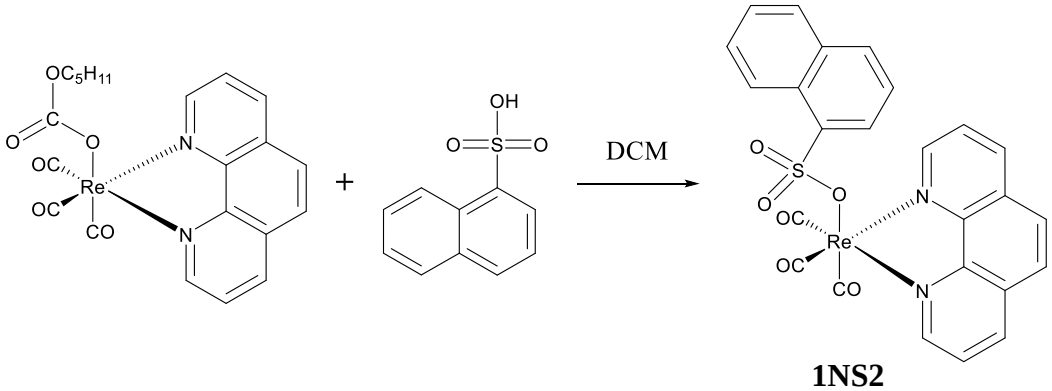

1NS2

Scheme 7: Synthesis of 1NS2

INS2 has been characterized spectroscopically and crystallographically. The IR spectrum (Figure 17) shows strong υ(C≡O)'s at 2031(s), 1928(s) and 1906 cm^{-1} characteristic of fac geometry.

In the ^{1}H NMR spectrum (Figure 18) of **1NS2**, the phenanthroline ligand attachment is symmetrical. As a result, the phenantholine doublet of doublets at 8.97 ppm represents two similar protons (CH=N). The doublet of doublets at 8.26 ppm represents the two similar protons on positions 3 and 8. The doublet of doublets at 7.80 ppm represents the proton on position 8 of the naphthalene ring. The protons on positions 5 and 6 of the phenanthroline ring appear as a singlet at 7.70 ppm. The multiplets at 7.69–7.65 ppm represent the proton on position 3 of the naphthalene ring. The multiplets at 7.62–7.55 ppm represent the proton on position 7 of the naphthalene ring. The doublet of doublets at 7.55 ppm represent the protons on positions 4 and 7 of the phenanthroline ring. The proton on position 2 of the napthalene ring appearas a doublet of doublets at 7.39 ppm. The multiplet at 7.29–7.15 ppm represents naphthalene protons at position 4 and 5. The proton at 6.67 ppm represents the naphthalene proton at position 6.

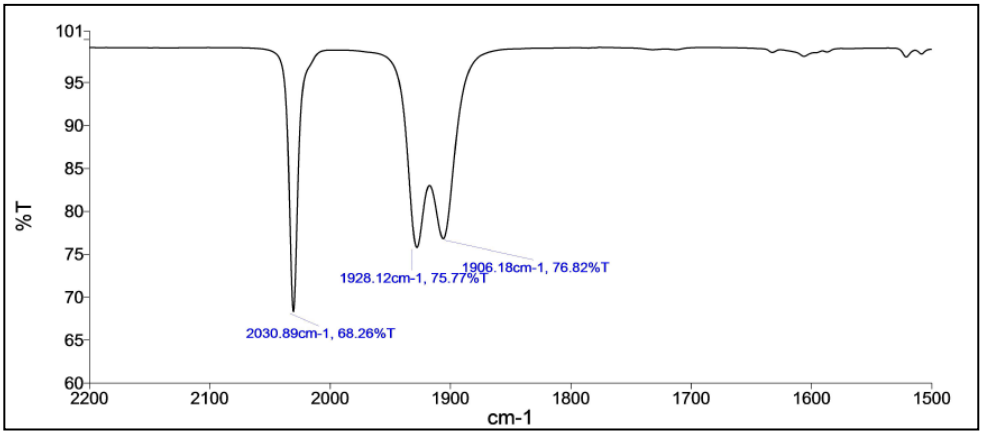

Figure 17: IR spectrum of 1NS2

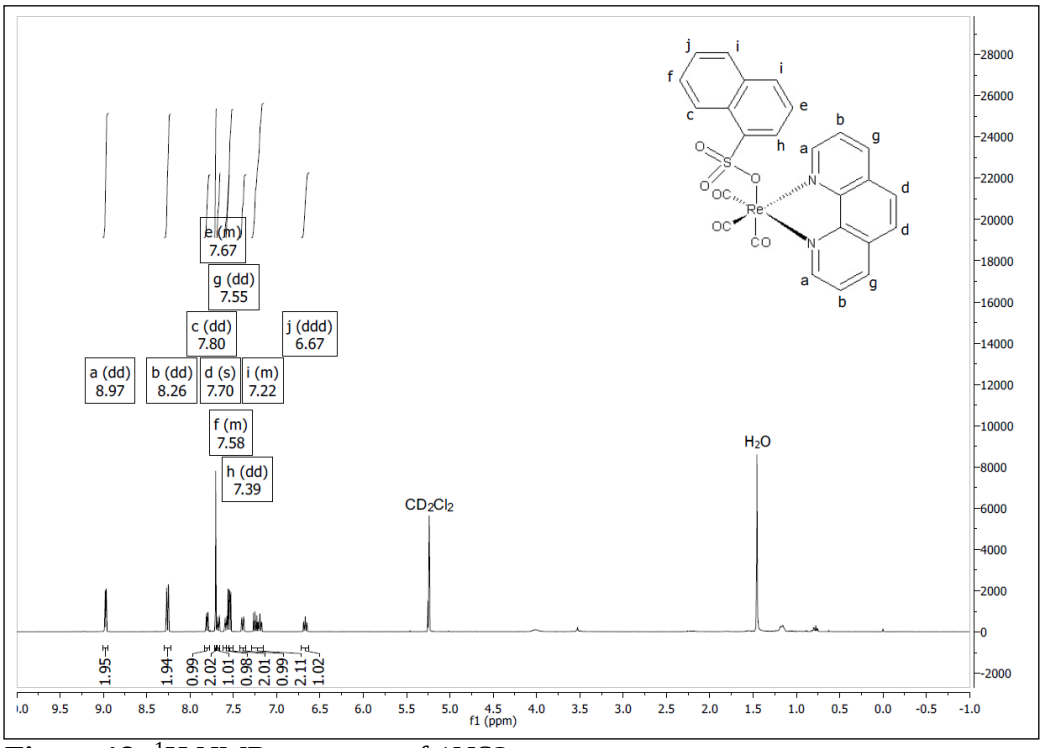

Figure 18: ^{1}H NMR spectrum of 1NS2

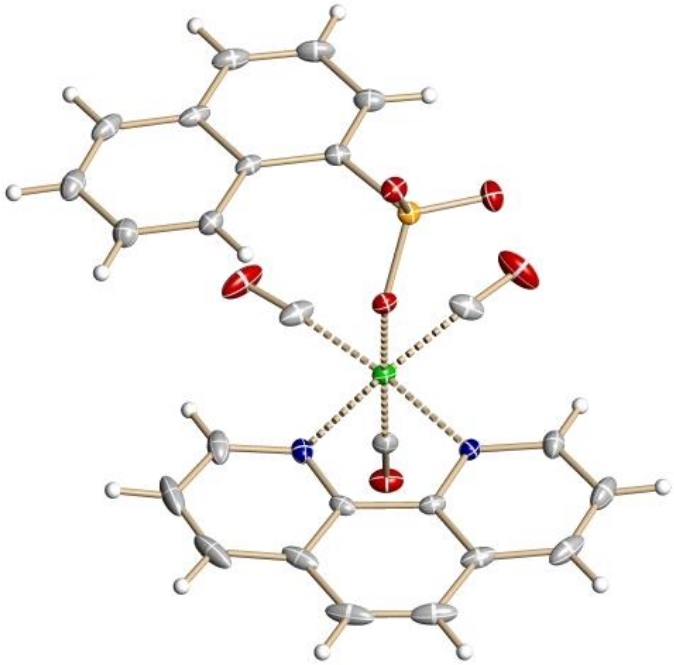

Figure 19: X-ray structure of 1NS2

As seen in Figure 19, the rhenium atom is octahedrally coordinated to three facial CO's, two N atoms of the bidentate 1,10-phenanthroline ligand and a 1-naphthalenesulfonic acid anion.

3. 2. 2. 3. *fac*-(CO)$_3$(5-methyl-1,10-phenanthroline) ReOS(O$_2$)C$_{10}$H$_7$ (1NS3)

1NS3 was synthesized from a one-pot reaction of PC3 and 1-Naphthalenesulfonic acid in dichloromethane solvent according to Scheme 8 below. The yellow crystals (75%) of 1NS3 were characterized using ^{1}H NMR.

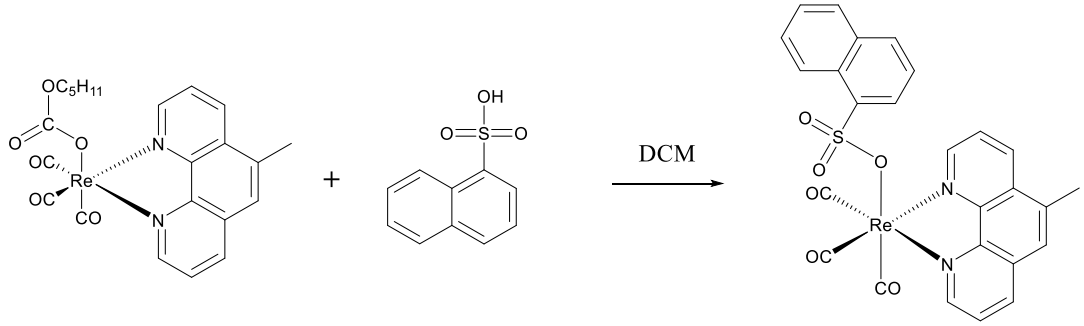

1NS3

Scheme 8: Synthesis of 1NS3

INS3 have been characterized through spectroscopic techniques. The IR spectrum (Figure 20) shows three characteristic υ(C≡O)'s at 2030, 1928 and 1906 cm^{-1}. The ^{1}H NMR peak assignments are shown in Figure 21 below. The doublet of doublets at 8.96 ppm represents the phenantholine protons (CH=N) at position 2 and 9 of the phenanthroline ring. The doublet of doublets at 8.28 ppm represents the proton at position 8 of the phenanthroline ring. The doublet of doublets at 8.15 ppm represents the proton at position 3 of the phenanthroline ring. The doublet of doublets at 7.74 ppm represents the proton at position 8 of the naphthalene ring. The doublet of doublets at 7.64 ppm represents the proton at position 2 of the naphthalene ring. The naphthalene protons at position 3, 6 and 7 appear as a multiplet at 7.60–7.48 ppm. The naphthalene protons at

position 4 and 5 appear as a multiplet at 7.25–7.14 ppm. The phenanthroline proton at position 6 appears as a multiplet at 6.70–6.61 ppm. The singlet at 2.63 ppm represents the methyl group protons at position 5 of the phenanthroline ring.

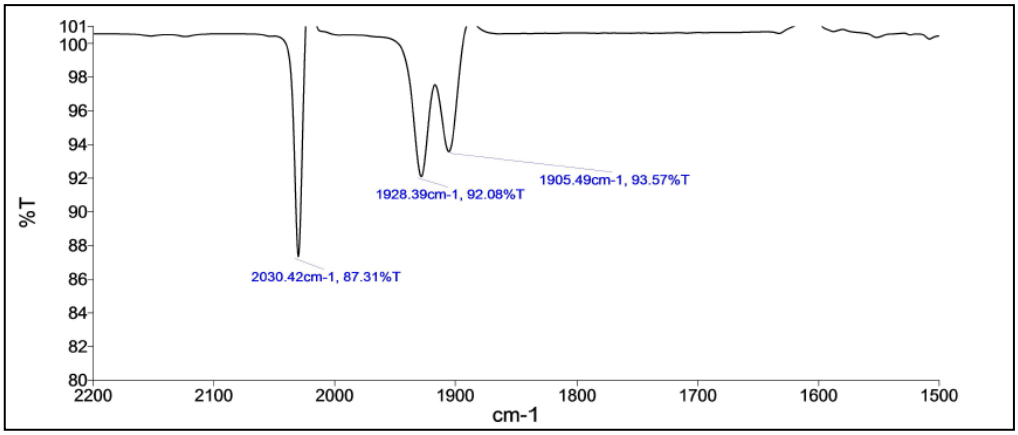

Figure 20: IR spectrum of 1NS3

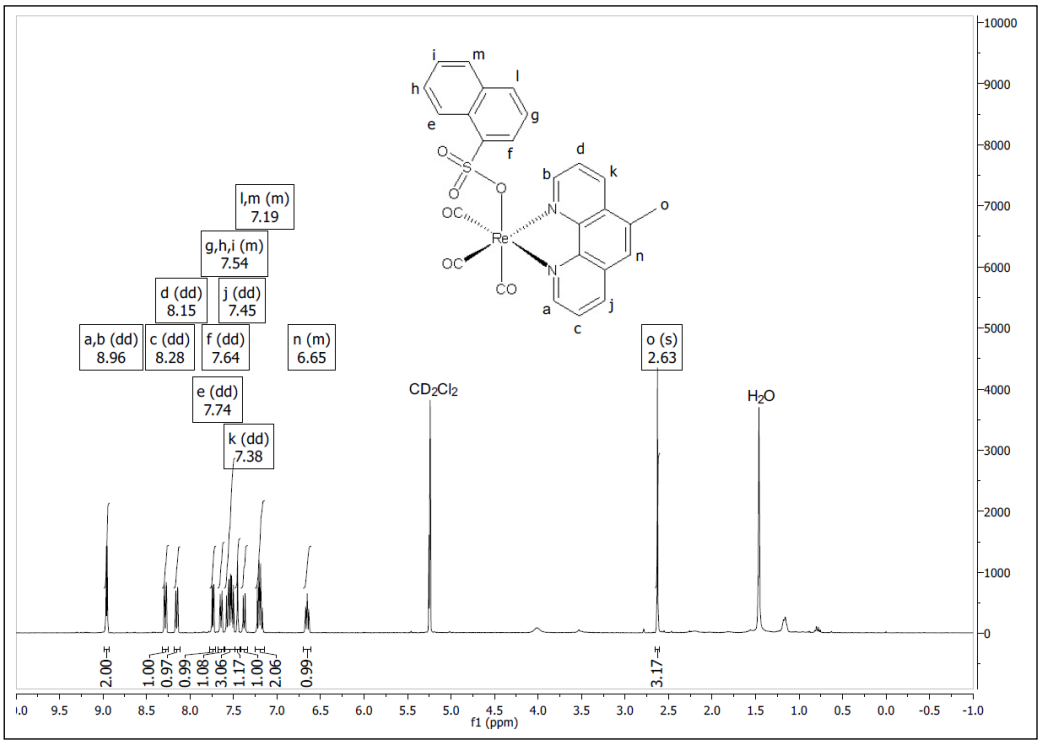

Figure 21: ^{1}H NMR spectrum of 1NS3

3. 2. 2. 4. *fac*-(CO)$_3$(2,9-Dimethyl-1,10-phenanthroline) ReOS(O$_2$)C$_{10}$H$_7$ (1NS4)

1NS4 was synthesized from a one-pot reaction of PC4 and 1-Naphthalenesulfonic acid in dichloromethane solvent according to Scheme 9 below. The yellow crystals (86%) of 1NS4 were characterized using ^{1}H NMR.

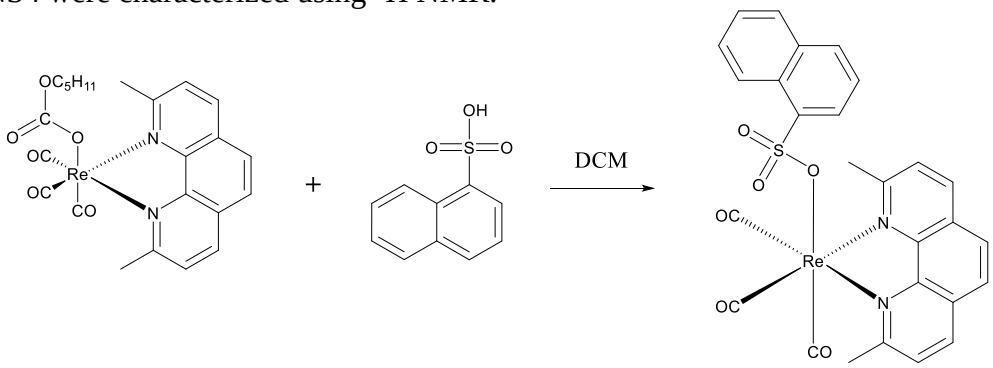

1NS4

Scheme 9: Synthesis of 1NS4

The IR spectrum of INS4 (Figure 22) shows three expected strong υ(C≡O)'s at 2030, 1925, and 1905 cm^{-1}. The ^{1}H NMR peak assignments are shown in Figure 23 below. In the ^{1}H NMR spectrum of **1NS4**, the doublet at 8.15 ppm represents the similar phenantholine protons at positions 3 and 8. The doublet of doublets at 7.85 ppm represents the proton at position 8 of the naphthalene ring. The doublet at 7.69 ppm represents the similar protons at position 7 of the phenanthroline ring. The singlet at 7.65 ppm represents protons at positions 5 and 6 of the phenanthroline ring. The naphthalene ring protons appear as multiplets at 7.61–7.41 ppm and 7.21–7.18 ppm. The singlet at 3.19 ppm represents the methly group protons at positions 2 and 9 of the phenanthroline ring. The structure of 1NS4 (Figure 24) was finally solved through X-ray crystal structure determination. As expected, the Re atom is octahedrally coordinated to three facial CO's, two N atoms of the neocuproine ligand and 1-naphthalenesulfonate anion.

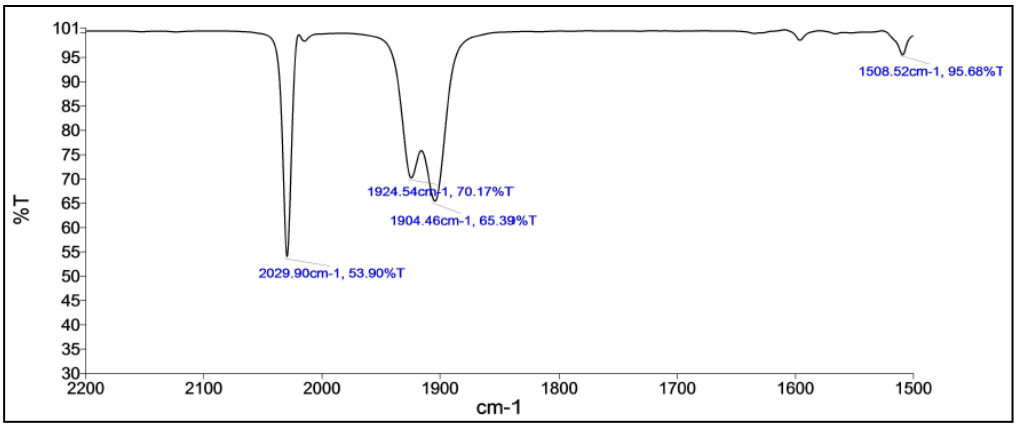

Figure 22: IR spectrum of 1NS4

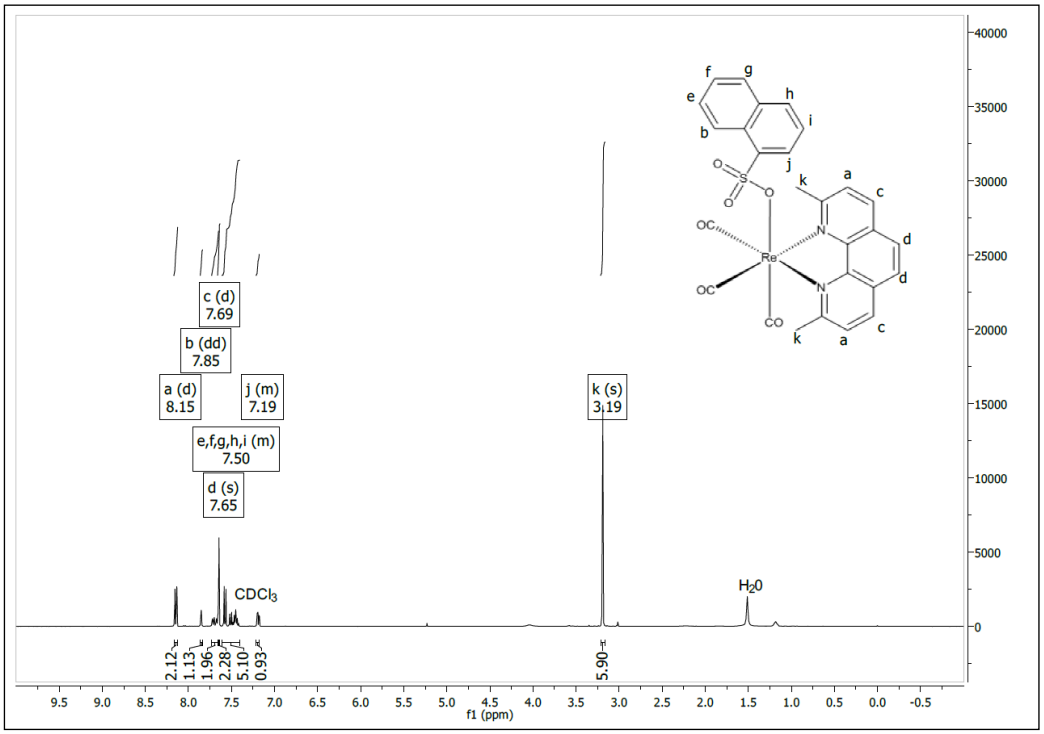

Figure 23: ^{1}H NMR spectrum of 1NS4

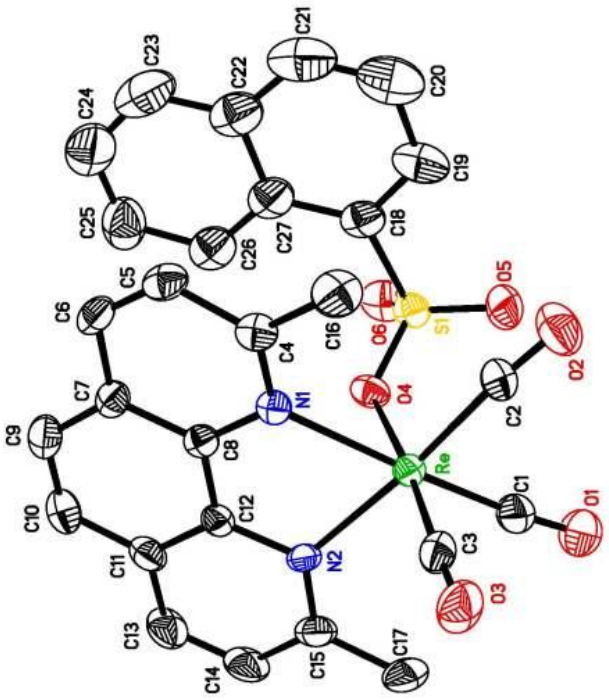

Figure 24: X-ray structure of 1NS4

3. 2. 2. 5. *fac*-(CO)$_3$(5,6-dimethyl-1,10-phenanthroline) ReOS(O$_2$)C$_{10}$H$_7$ (1NS5)

1NS5 was synthesized from a one-pot reaction of PC5 and 1-Naphthalenesulfonic acid in dichloromethane solvent according to Scheme 10 below. The yellow crystals (80%) of 1NS5 were characterized using ^{1}H NMR.

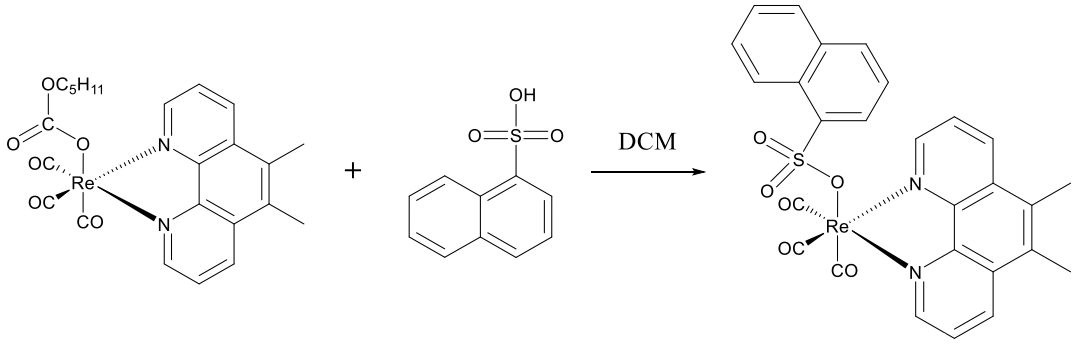

1NS5

Scheme 10: Synthesis of 1NS5

As expected, the IR spectrum of **1NS5** (Figure 25) shows three υ(C≡O)'s at 2030(s), 1927(s), and 1905(s) cm^{-1}. The ^{1}H NMR peak assignments are shown in Figure 26 below. The doublet of doublets at 8.96 ppm represents the similar phenanthroline protons at positions 2 and 9. The doublet of doublets at 8.64 ppm represents the proton at position 8 of the naphthalene ring. The doublet of doublets at 8.32 ppm represents the similar protons at position 3 and 8 of the phenanthroline ring. The multiplet at 7.80 ppm represents protons at positions 4 and 7 of the phenanthroline ring. The proton on position 2 of the naphthalene ring appears as a doublet of doublet of doublets at 6.70 ppm. The remaining naphthalene ring protons appear as a multiplet at 7.60–7.46 ppm. The singlet at 2.54 ppm represents the methyl group protons at positions 5 and 6 of the phenanthroline ring. However, several other peaks are also observed in the upfield region possibly due to the instability of **1NS5** in $CDCl_3$.

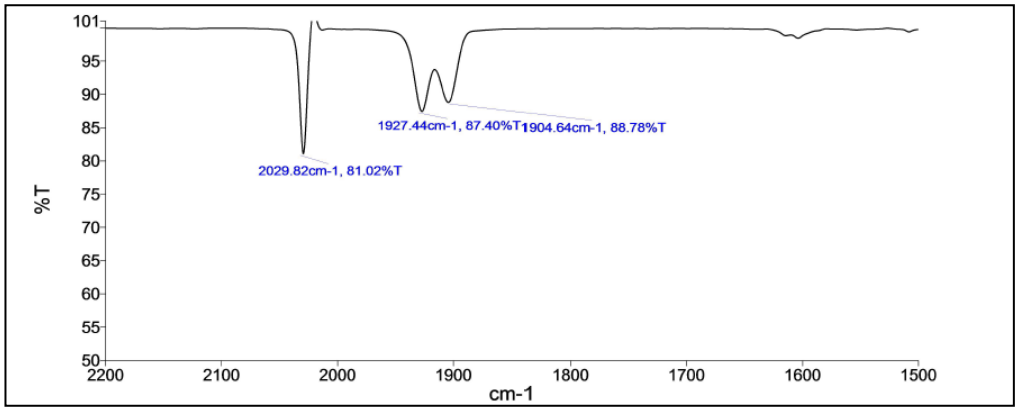

Figure 25: IR spectrum of 1NS5

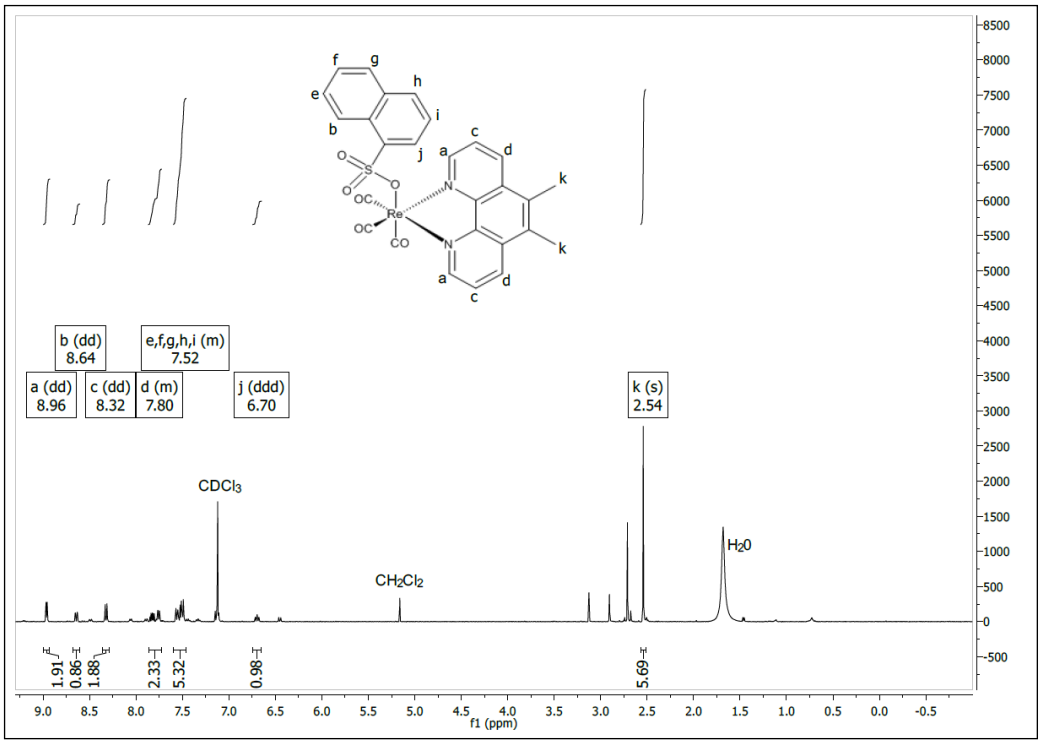

Figure 26: ^{1}H NMR spectrum of 1NS5

3. 2. 2. 6. *fac*-(CO)$_3$(4,7-diphenyl-1,10-phenanthroline) ReOS(O$_2$)C$_{10}$H$_7$ (1NS6)

1NS6 was synthesized from a one-pot reaction of PC6 and 1-Naphthalenesulfonic acid in dichloromethane solvent according to Scheme 11 below. The yellow crystals (70%) of 1NS6 were characterized using ^{1}H NMR.

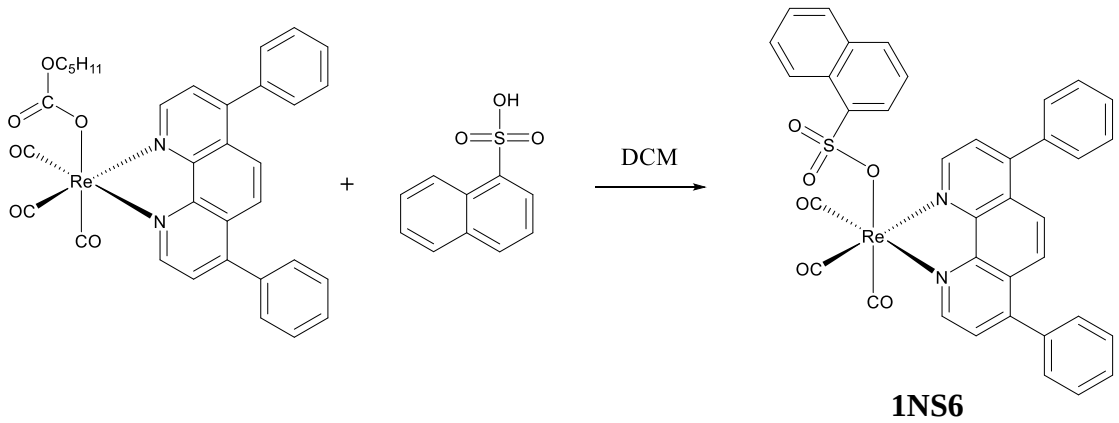

Scheme 11: Synthesis of 1NS6

1NS6 have been characterized spectroscopically. The IR spectrum of **1NS6** (Figure 27) exhibits the three expected strong υ(C≡O)'s at 2029, 1927, and 1904 cm^{-1}. The ^{1}H NMR peak assignments are shown in Figure 28. The doublet at 9.03 ppm represents the similar phenanthroline protons (CH=N) at positions 2 and 9. The doublet of doublets at 7.87 ppm represents the proton at position 8 of the naphthalene ring. The singlet at 7.76 ppm represents the similar protons at position 5 and 6 of the phenanthroline ring. The multiplet at 7.69–7.43 ppm represents an overlap of the benzen rings attached at positions 4 and 7 of the phenanthroline ring, the protons on positions 3 and 8 of the phenanthroline ring and the position 2, 4 and 5 protons on the naphthalene ring. The proton on position 3 of the naphthalene ring appears as a doublet of doublets at 7.25 ppm. The proton on position 7 of the naphthalene ring appears as a doublet of doublets at 7.11 ppm. The proton on position 6 of the naphthalene ring appears as a doublet of doublet of doublets at 6.77 ppm.

As expected, the ^{13}C NMR spectrum (Figure 29) shows two highly deshielded carbons with intensity ratio of 2:1 for the three CO's and 20 aromatic carbons. In the phenanthroline ligand component of the 1NS6 structure there are 12 carbon types on the ligand represented as peaks in the ^{13}C NMR spectra. The ten carbons on the naphthalene ring appear as distinct peaks in the spectra. The peaks at 197.08 and 192.62 ppm represent the CO carbons connected to the Re center.

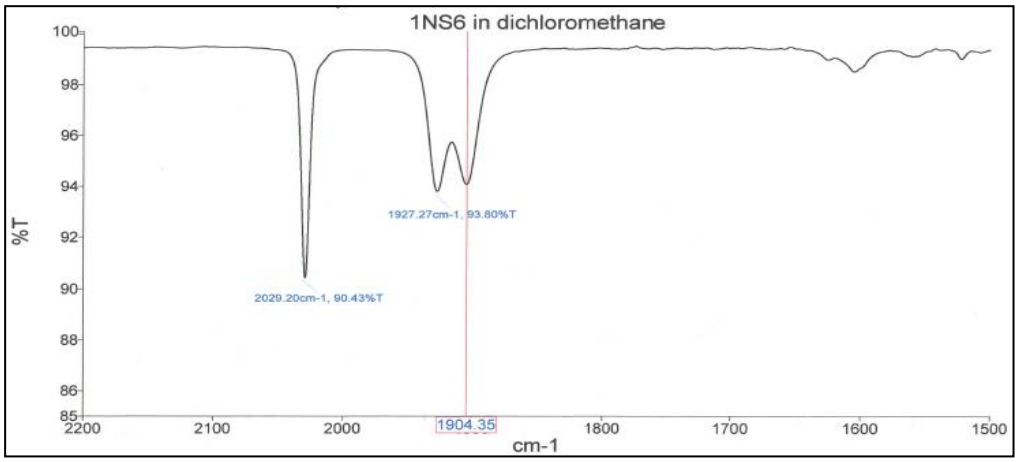

Figure 27: ^{1}H NMR spectrum of 1NS6

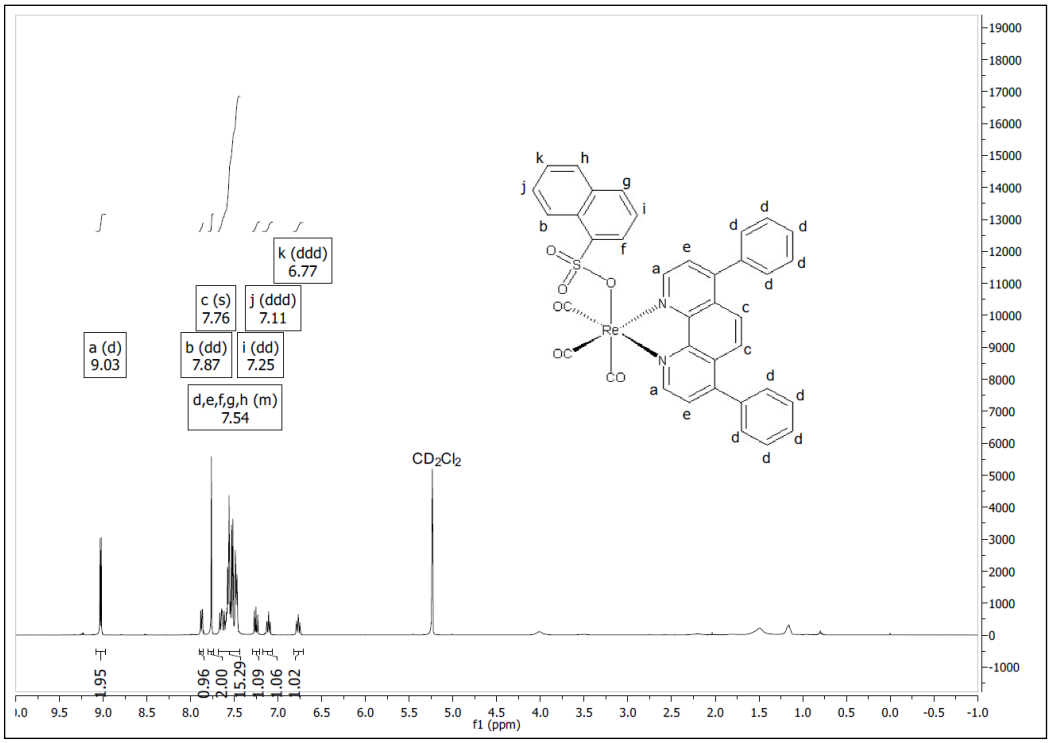

Figure 28: ^{1}H NMR spectrum of 1NS6

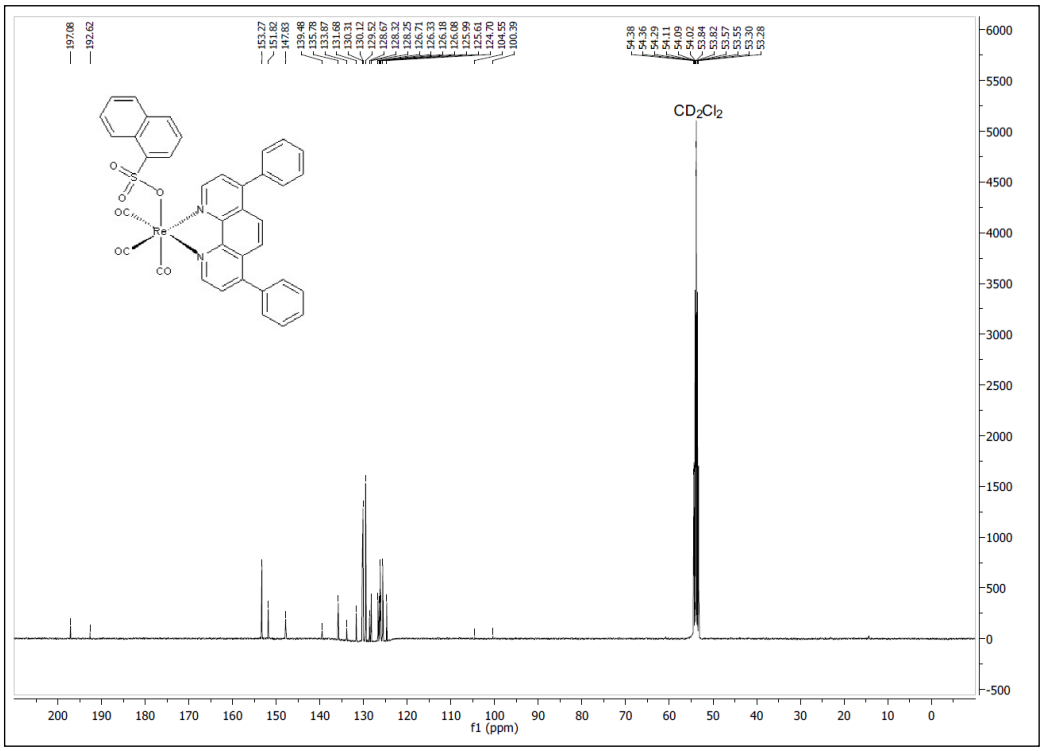

Figure 29: ^{13}C NMR spectrum of 1NS6

3. 2. 2. 7. *fac*-$(CO)_3$(2,9-dimethyl-4,7-diphenyl-1,10-phenanthroline) $ReOS(O_2)C_{10}H_7$ (1NS7)

1NS7 was synthesized from a one-pot reaction of PC7 and 1-Naphthalenesulfonic acid in dichloromethane solvent according to Scheme 12 below. The yellow crystals (75%) of 1NS7 were characterized using ^1H NMR.

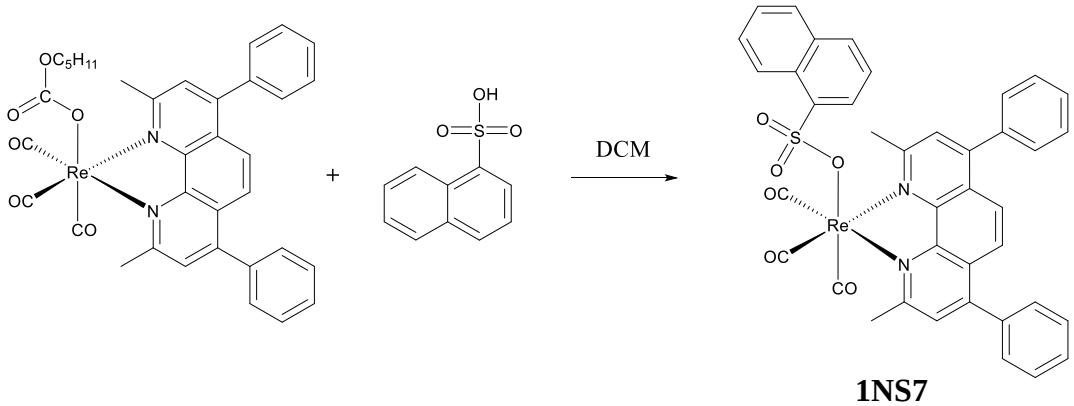

1NS7

Scheme 12: Synthesis of 1NS7

1NS7 have been characterized spectroscopically and crystallographically. The IR spectrum (Figure 30) shows three strong υ(C≡O)'s at 2029, 1923, and 1904 cm^{-1} characteristic of facial geometry. The ^{1}H NMR spectrum (Figure 31) exhibits the two methyl groups of the phenanthroline ligand at δ3.06 which is somewhat deshielded due to the N atoms. The ^{13}C NMR spectrum (Figure 32) shows two downfield resonances at δ 196.47 and 192.24 with intensity a ratio of 2:1 due to the three terminal CO's. A total of 20 resonances are observed for the expected 20 aromatic carbons. In the phenanthroline ligand component of the 1NS7 structure there are 13 carbon types on the ligand represented as peaks in the ^{13}C NMR spectra. One of those peaks (31.56 ppm) represents the aliphatic carbons. The ten carbons on the naphthalene ring appear as distinct peaks in the spectra. The peaks at 196.47 and 192.24 ppm represent the CO carbons connected to the Re center. The X-ray structure of **1NS7** (Figure 33) suggests that the Re atom is coordinated octahedrally through three facial CO's, two N atoms of the bathocuproine ligand and the 1-naphthalenesulfonate anion.

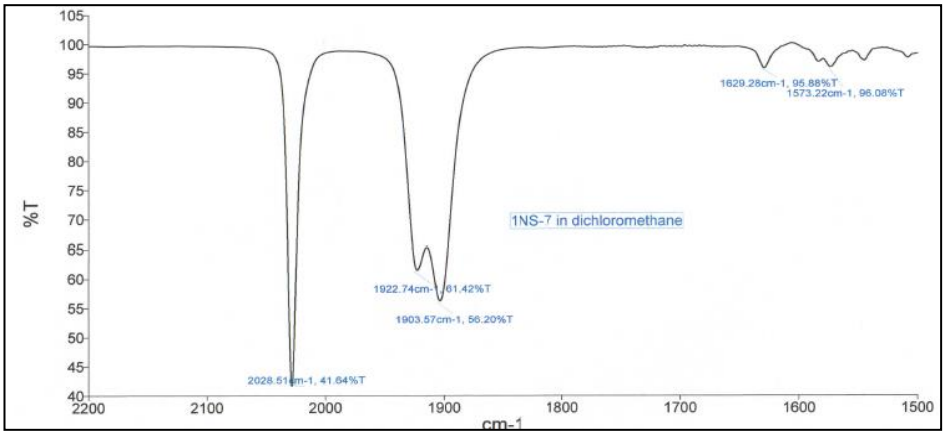

Figure 30: IR spectrum of 1NS7

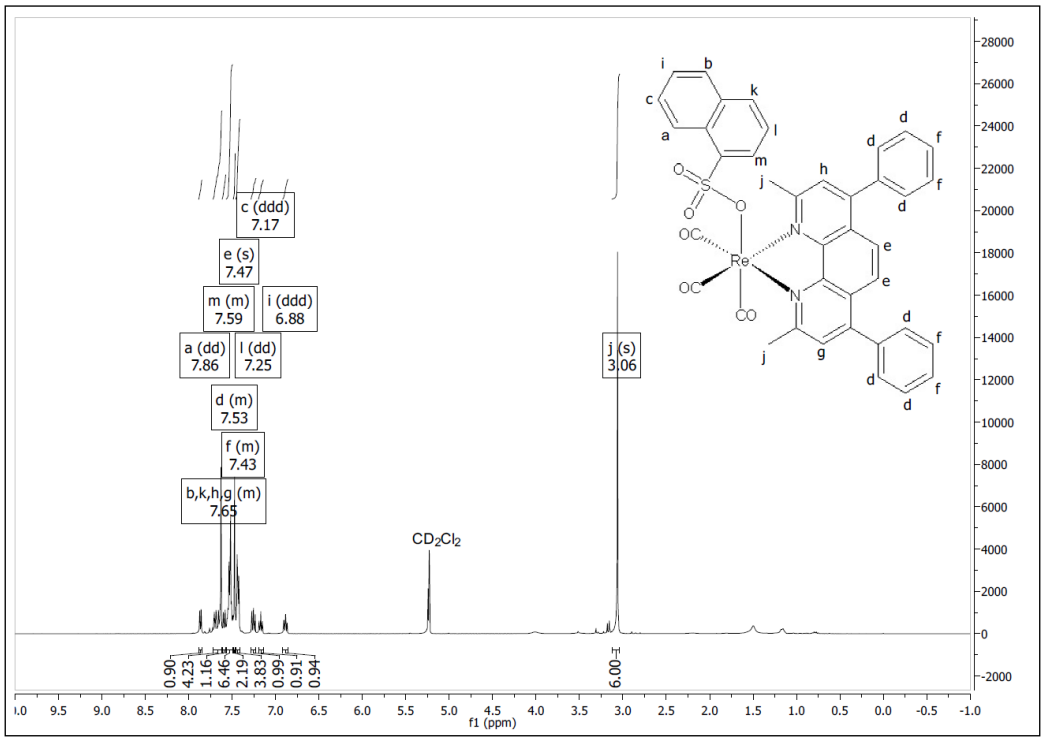

Figure 31: ^{1}H NMR spectrum of 1NS7

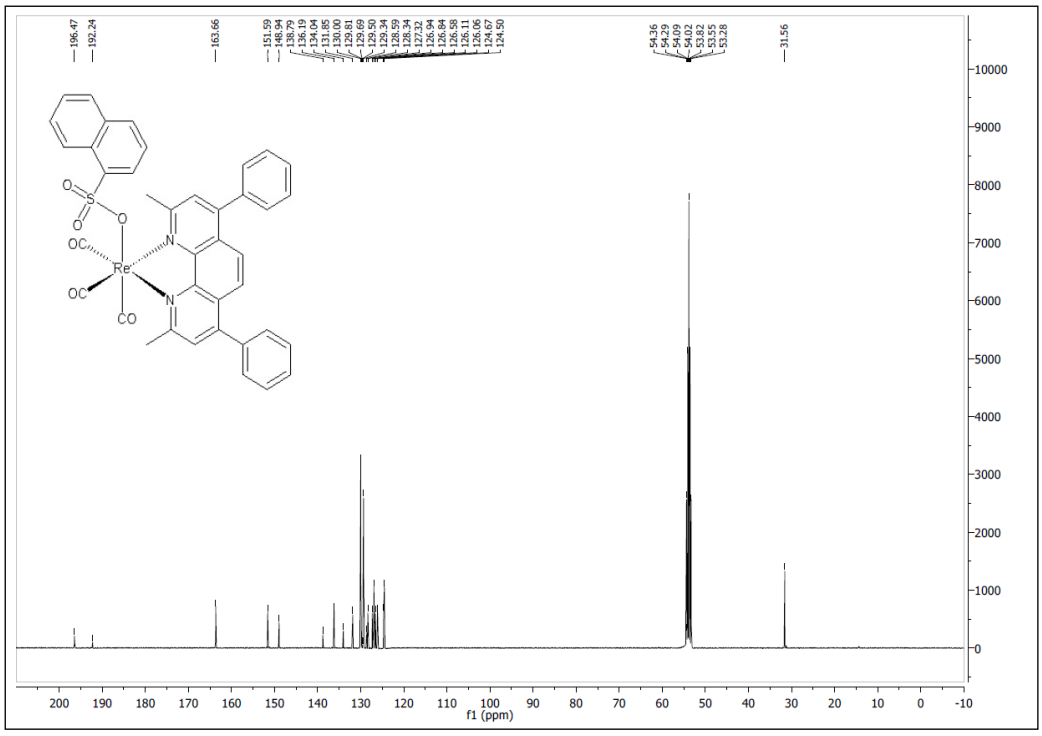

Figure 32: ^{13}C NMR spectrum of 1NS7

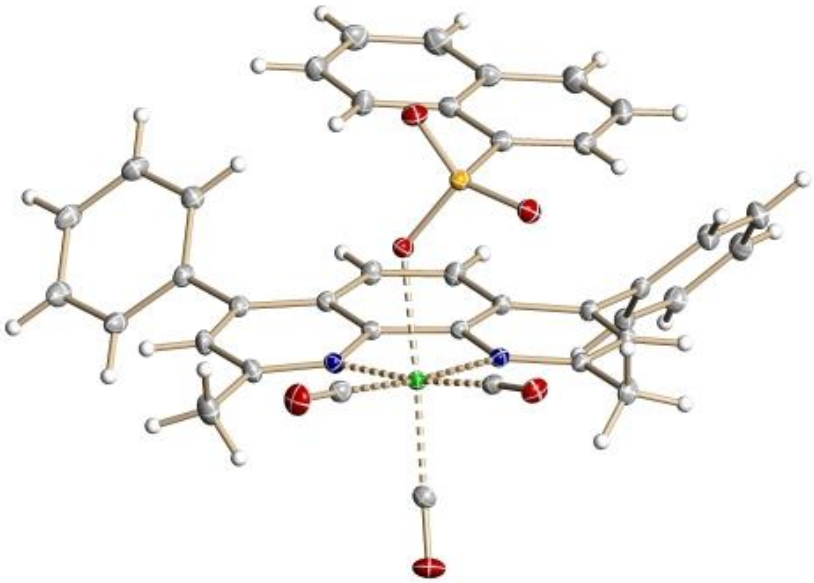

Figure 33: X-ray structure of 1NS7

3. 2. 2. 8. *fac*-(CO)$_3$(4,7-dimethyl-1,10-phenanthroline) ReOS(O$_2$)C$_{10}$H$_7$ (1NS8)

1NS8 was synthesized from a one-pot reaction of PC8 and 1-Naphthalenesulfonic acid in dichloromethane solvent according to Scheme 13 below. The yellow crystals (80%) of 1NS8 were characterized using ^{1}H NMR.

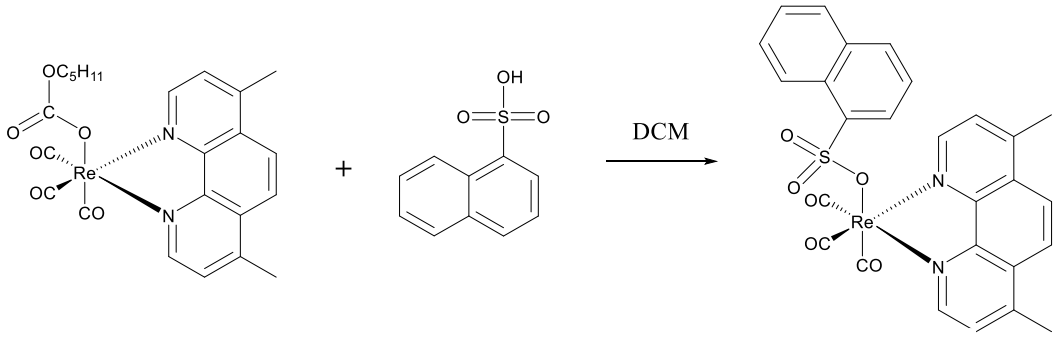

1NS8

Scheme 13: Synthesis of 1NS8

1NS8 have been characterized spectroscopically using IR and NMR techniques. Each of the IR (Figure 34) and ^{1}H NMR (Figure 35) spectrum exhibits the expected spectral characteristics. It seems the compound decomposes in DMSO-d^6.

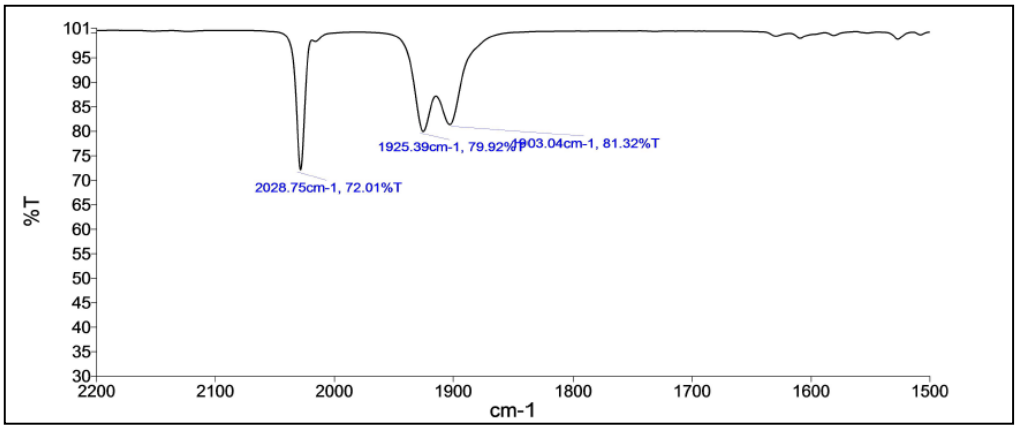

Figure 34: IR spectrum of 1NS8

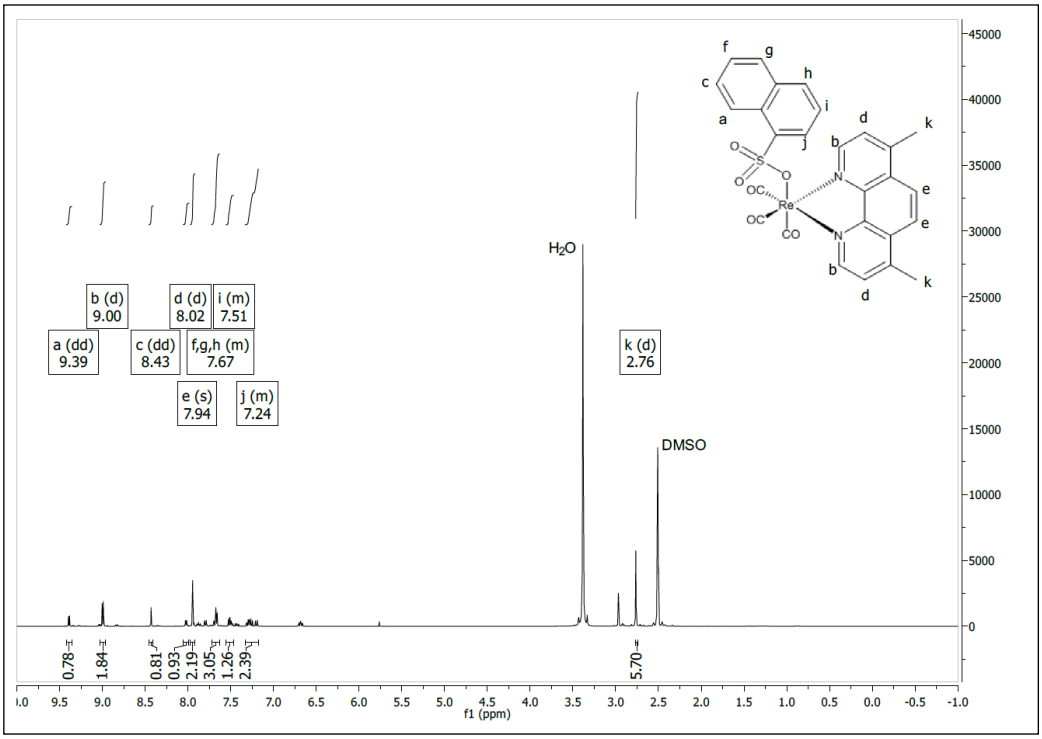

Figure 35: ^{1}H NMR spectrum of 1NS8

3. 2. 2. 9. *fac*-(CO)$_3$(3,4,7,8-tetramethyl-1,10-phenanthroline) ReOS(O$_2$)C$_{10}$H$_7$ (1NS9)

1NS9 was synthesized from a one-pot reaction of PC9 and 1-Naphthalenesulfonic acid in dichloromethane solvent according to Scheme 14 below. The yellow crystals (78%) of 1NS9 were characterized using ^{1}H NMR.

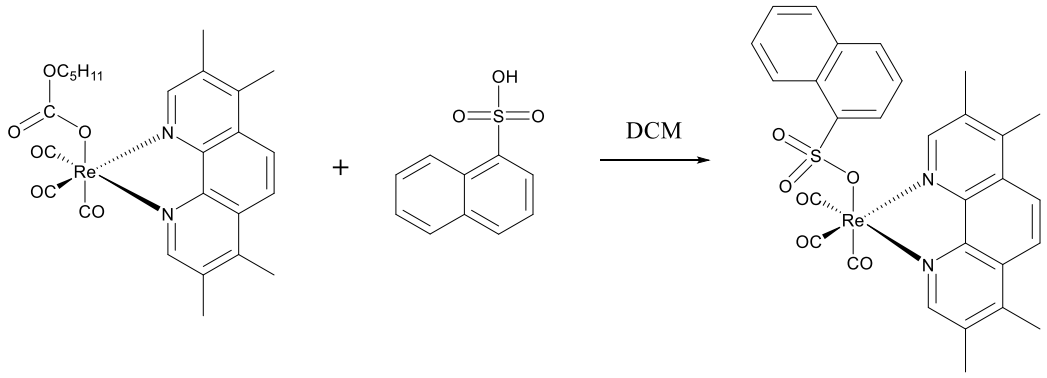

1NS9

Scheme 14: Synthesis of 1NS9

1NS9 have been characterized spectroscopically. The IR spectrum (Figure 36) shows three characteristic υ(C≡O)'s at 2028(s), 1924(s), and 1902 cm^{-1} due to the three facial carbonyls. The ^{1}H NMR spectrum (Figure 37) exhibits the two downfield singlets at δ 8.57 and 7.77 due to the protons adjacent to the N atoms and the protons in the 4 and 7 positions of the phenanthroline ligand. The two methyl groups are observed at δ2.52 and 2.32.

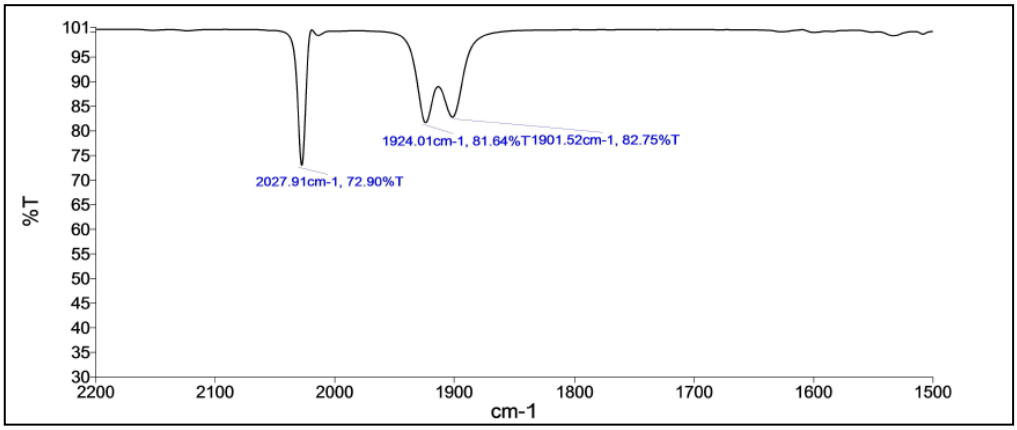

Figure 36: IR spectrum of 1NS9

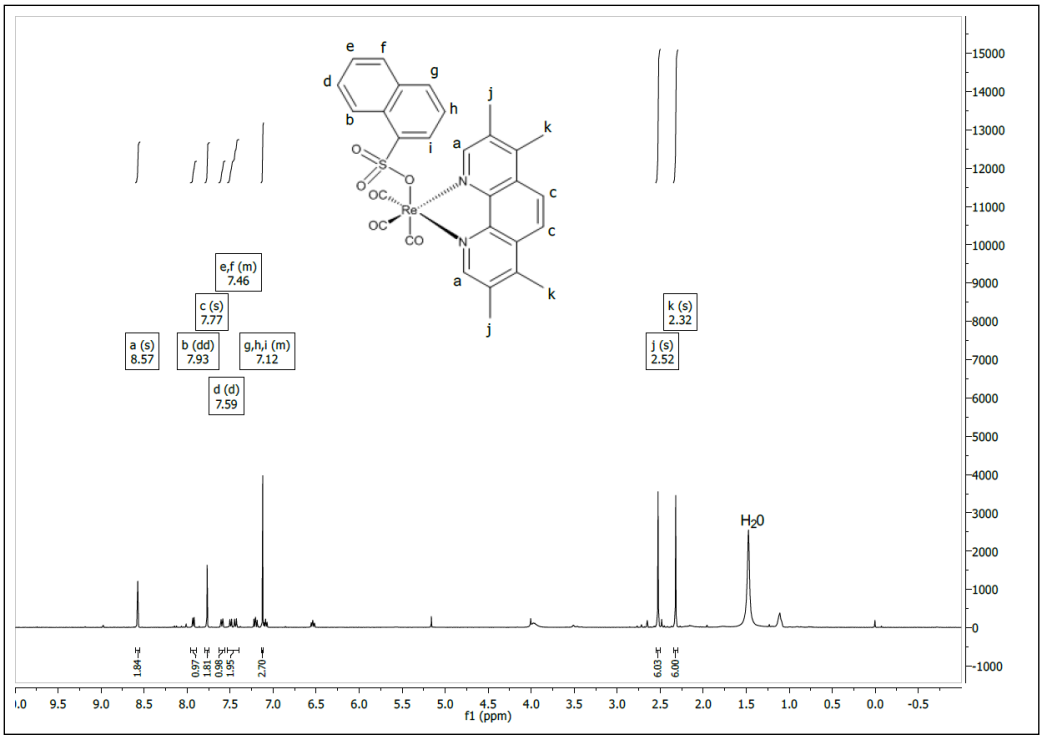

Figure 37: ^{1}H NMR spectrum of 1NS9

3. 2. 2. 10. *fac*-(CO)$_3$(4-methyl-1,10-phenanthroline) ReOS(O$_2$)C$_{10}$H$_7$ (1NS10)

1NS10 was synthesized from a one-pot reaction of PC10 and 1-Naphthalenesulfonic acid in dichloromethane solvent according to Scheme 15 below. The yellow crystals (72%) of 1NS10 were characterized using ^{1}H NMR.

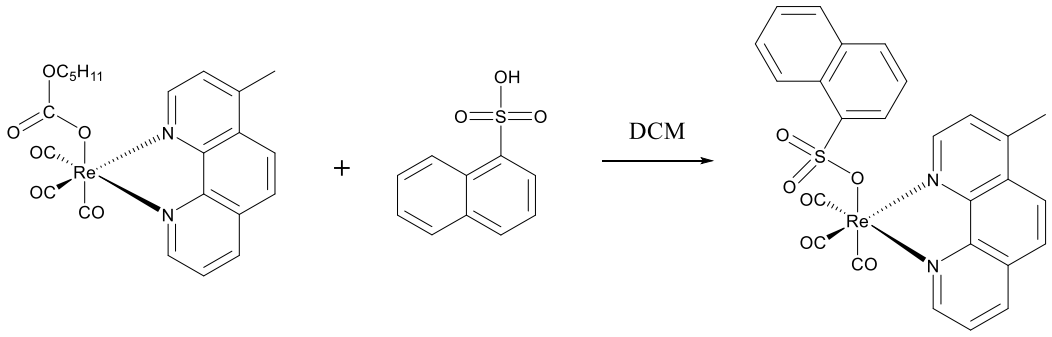

1NS10

Scheme 15: Synthesis of 1NS10

1NS10 have been characterized through IR and NMR spectroscopic techniques. The IR spectrum (Figure 38) shows three υ(C≡O)'s at 2030(s), 1927(s), and 1905 cm^{-1}

due to the three facial carbonyls. The ^{1}H NMR spectrum (Figure 39) shows 14 aromatic protons and three aliphatic protons with an integration ratio of 14:3. As expected, the ^{13}C NMR spectrum shows 22 aromatic carbons and one aliphatic carbon. In the phenanthroline ligand component of the 1NS10 structure, there are 13 distinct carbon types on the ligand representing the 13 carbons on the ring and represented as peaks in the ^{13}C NMR spectra. One of those peaks (19.01 ppm) represents the methyl group carbon on the phenanthroline ligand. The ten carbons on the naphthalene ring appear as distinct peaks in the ^{13}C NMR spectra.

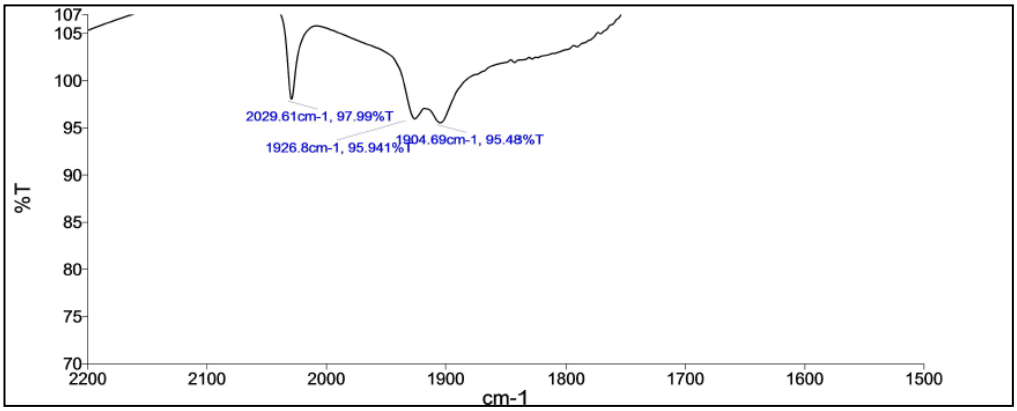

Figure 38: IR spectrum of 1NS10

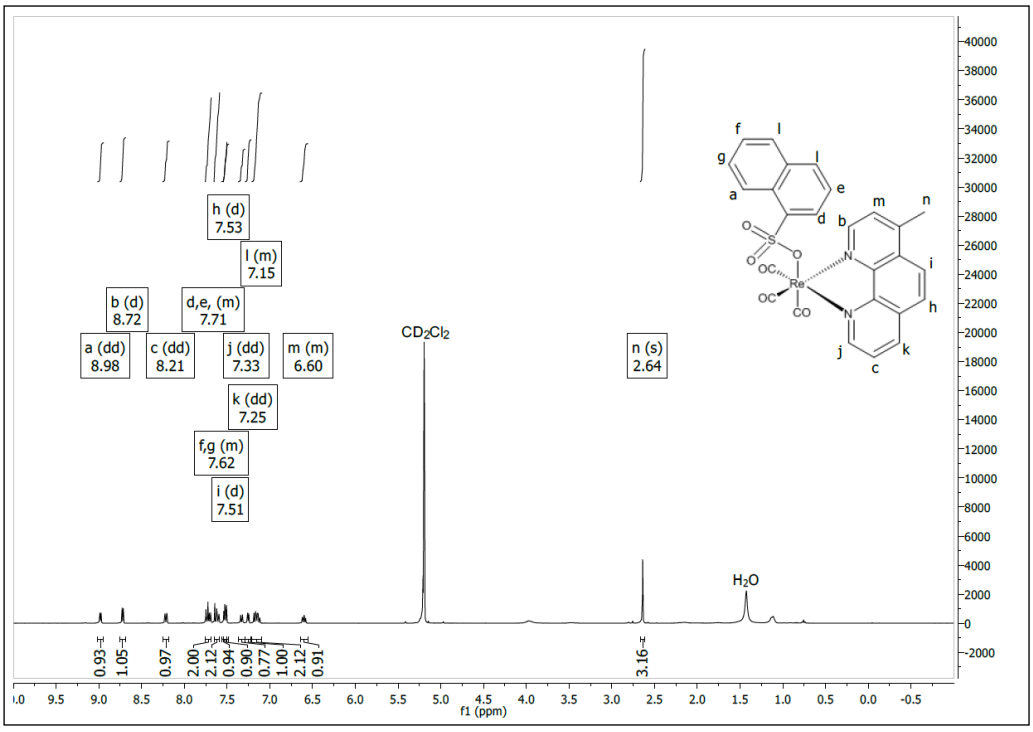

Figure 39: ^{1}H NMR spectrum of 1NS10

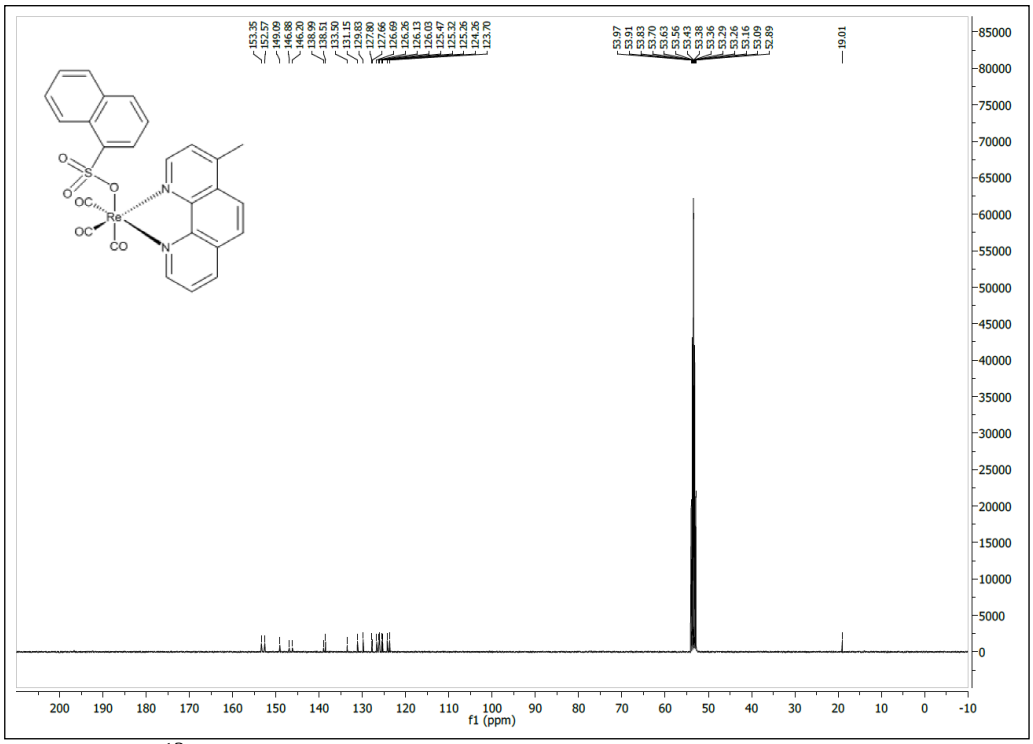

Figure 40: ^{13}C NMR spectrum of 1NS10

3. 2. 2. 11. *fac*-$(CO)_3$(2,2'-bipyridyl) $ReOS(O_2)C_{10}H_7$ (2NS1)

2NS1 was synthesized from a one-pot reaction of PC1 and 2-Naphthalenesulfonic acid in dichloromethane solvent according to Scheme 16 below. The yellow crystals (99%) of 2NS1 were characterized using ^{1}H NMR.

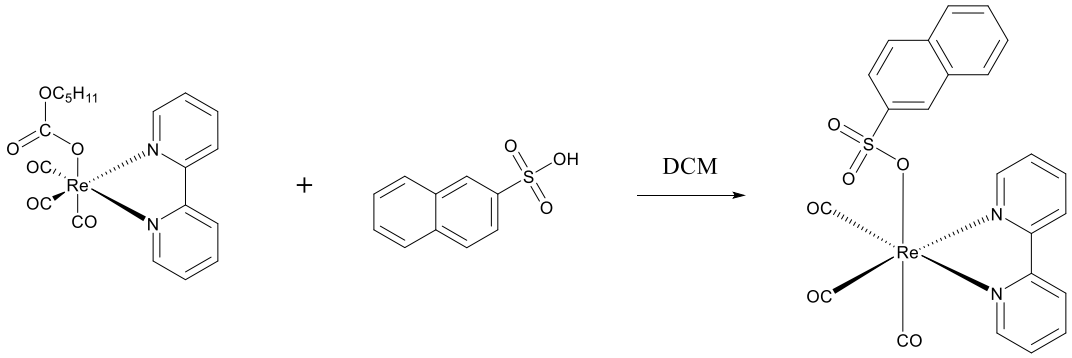

2NS1

Scheme 16: Synthesis of 2NS1

Both the IR (Figure 41) and NMR (Figure 42) spectra show the expected spectral characteristics as observed previously for analogous 1-naphthalenesulfonato complexes **1NS1**-**1NS10**. In the ^{1}H NMR spectrum, the bipyridyl ligand attachment is symmetrical. As a result, the bipyridyl doublet of doublets at 8.97 ppm represents two similar protons (CH=N). All the other protons on the bipyridyl ring appear as a multiplet at 8.18–8.05 ppm. The proton at position 3 on the naphthalene ring and the bipyridyl proton at position 5 overlap and appear as a multiplet at 7.93–7.83 ppm. The multiplet at 7.79–7.73 ppm represents the proton on position 4 of the naphthalene ring. The protons at positions 5, 6, 7, 8 and 1 of the naphthalene ring appear as a multiplet at 7.65–7.45 ppm.

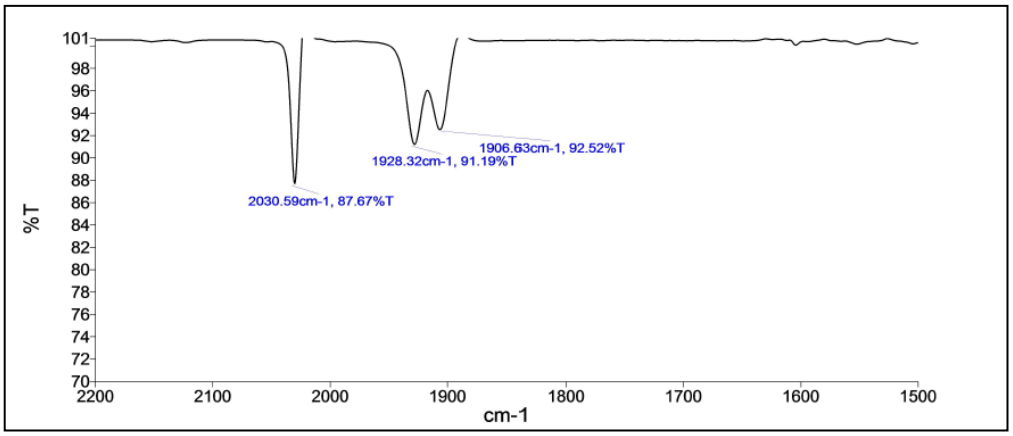

Figure 41: IR spectrum of 2NS1

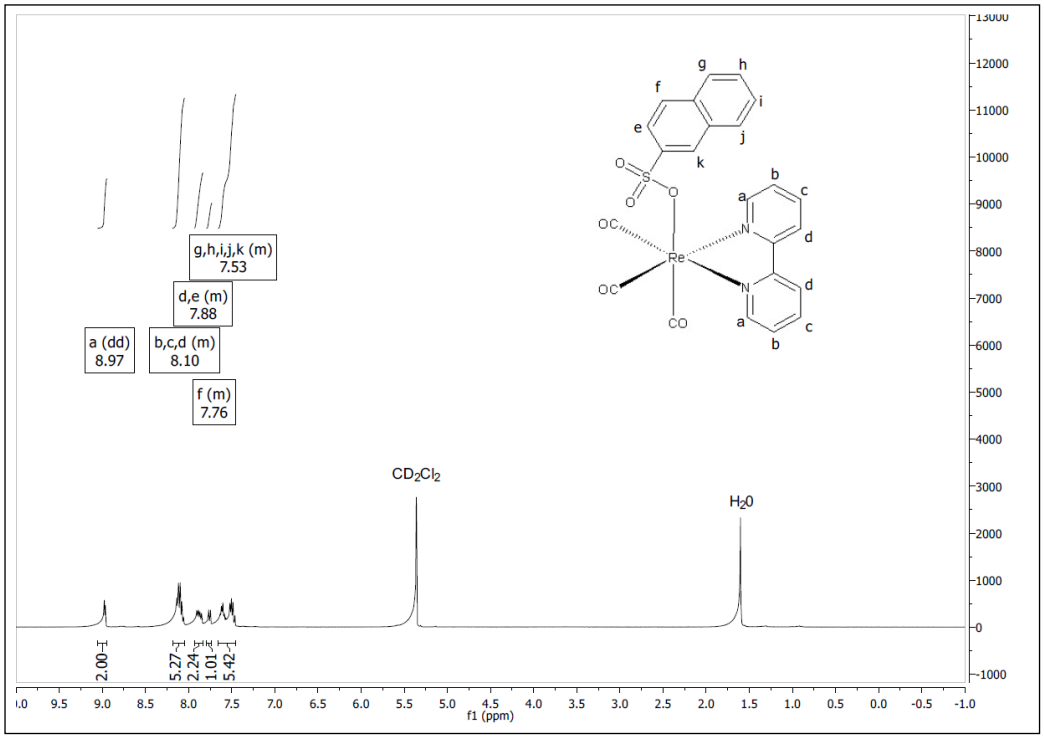

Figure 42: ^{1}H NMR spectrum of 2NS1

3. 2. 2. 12. *fac*-$(CO)_3$(1,10-phenanthroline) $ReOS(O_2)C_{10}H_7$ (2NS2)

2NS2 was synthesized from a one-pot reaction of PC2 and 2-Naphthalenesulfonic acid in dichloromethane solvent according to Scheme 17 below. The yellow crystals (90%) of 2NS2 were characterized using ^{1}H NMR.

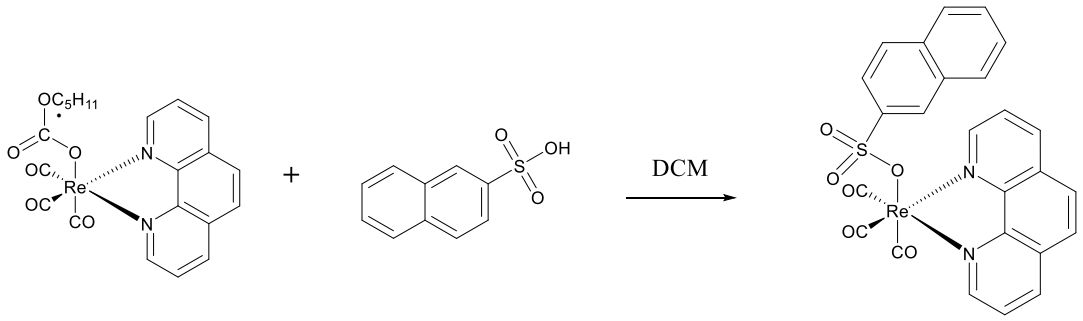

Scheme 17: Synthesis of 2NS2

2NS2 have been characterized spectroscopically. A very similar IR (Figure 43) and ^{1}H NMR (Figure 44) spectral data are obtained as is observed for **1NS2** complex. The phenanthroline ligand attachment is symmetrical. As a result, the phenanthroline doublet of doublets at 9.37 ppm represents two similar protons (CH=N). The doublet of doublets at 8.50 ppm represents the two similar protons on positions 3 and 8. The multiplet at 8.10 – 8.04 ppm represents the proton on position 3 of the naphthalene ring. The protons on positions 5 and 6 of the phenanthroline ring appear as a singlet at 7.91 ppm. The multiplet at 7.87–7.74 ppm represent an overlap of the protons on positions 4 and 7 of the phenanthroline ring, and 4 and 5 of the naphthalene ring. The doublet at 7.63 ppm represent the proton on position 1 of the naphthalene ring. The doublet of doublet of doublets at 7.55 ppm represents the protons on positions 6 and 7 of the naphthalene ring. The proton on position 8 of the napthalene ring appears as a doublet of doublets at 7.43 ppm.

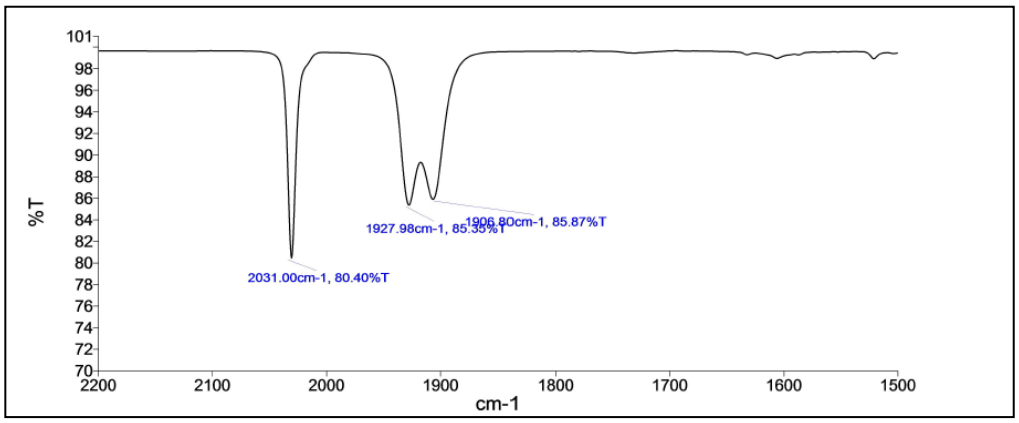

Figure 43: IR spectrum of 2NS2

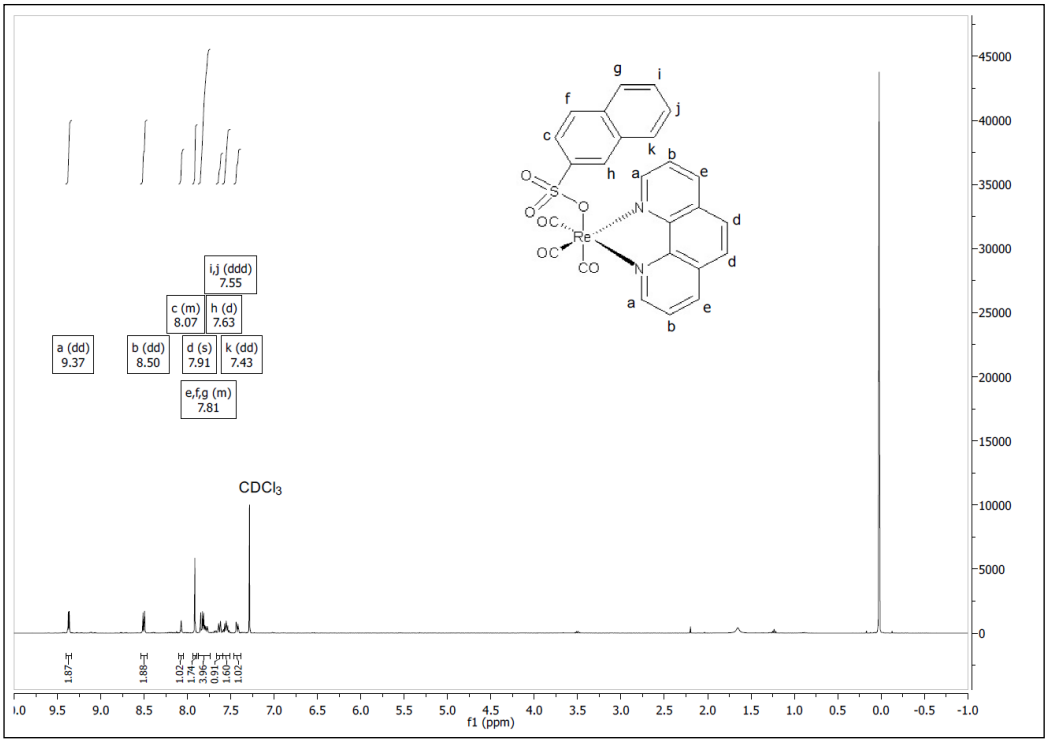

Figure 44: ^{1}H NMR spectrum of 2NS2

3. 2. 2. 13. *fac*-$(CO)_3$(5-methyl-1,10-phenanthroline) $ReOS(O_2)C_{10}H_7$ (2NS3)

2NS3 was synthesized from a one-pot reaction of PC3 and 2-Naphthalenesulfonic acid in dichloromethane solvent according to Scheme 18 below. The yellow crystals (71%) of 2NS3 were characterized using ^{1}H NMR.

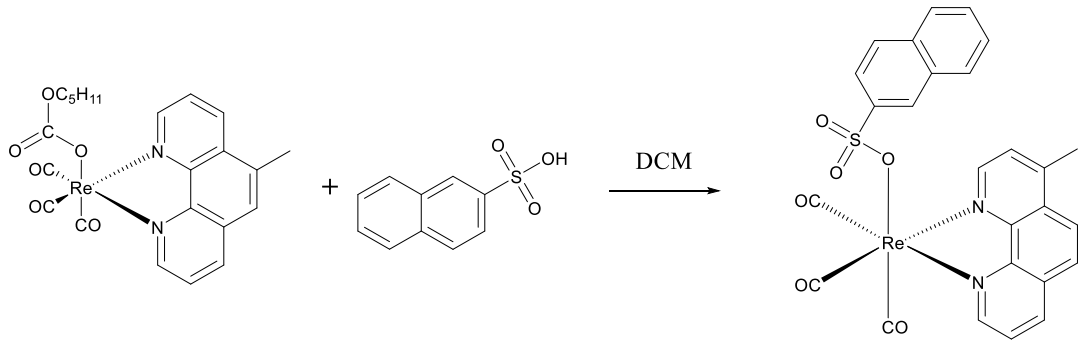

2NS3

Scheme 18: Synthesis of 2NS3

The spectral properties of **2NS3** and **1NS3** are very similar to each other. The IR spectrum of **2NS3** (Figure 45) shows three υ(C≡O)'s at 2031(s), 1928(s), and 1906 cm^{-1} due to the three facial carbonyls. In the ^{1}H NMR spectrum (Figure 46), the doublet of doublets at 9.37 ppm represents the phenantholine proton (CH=N) at position 9 of the phenanthroline ring. The doublet of doublets at 9.27 ppm represents the phenantholine proton at position 8 of the phenanthroline ring. The doublet of doublets at 8.52 ppm represents the proton at position 7 of the phenanthroline ring. The doublet of doublets at 8.38 ppm represents the proton at position 3 of the naphthalene ring. The doublet at 7.94 ppm represents the proton at position 6 of the phenanthroline ring. The multiplet at 7.88–7.68 ppm represents the protons at positions 4, 5, 6 and 7 of the naphthalene ring. The doublet at 7.64 ppm represents the proton at position 5 of the phenanthroline ring. The multiplet at 7.59–7.48 ppm represents an overlap of proton 8 on the naphthalene ring and

protons 2 and 3 at on the phenanthroline ring. The singlet at 7.28 ppm represents the proton at position 1 of the naphthalene ring. The singlet at 2.69 ppm represents the methyl group protons at position 4 of the phenanthroline ring.

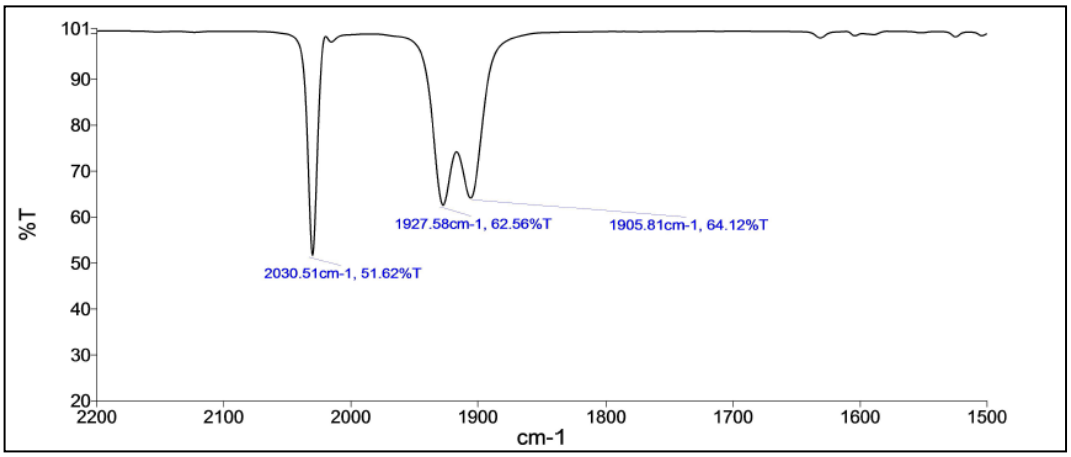

Figure 45: IR spectrum of 2NS3

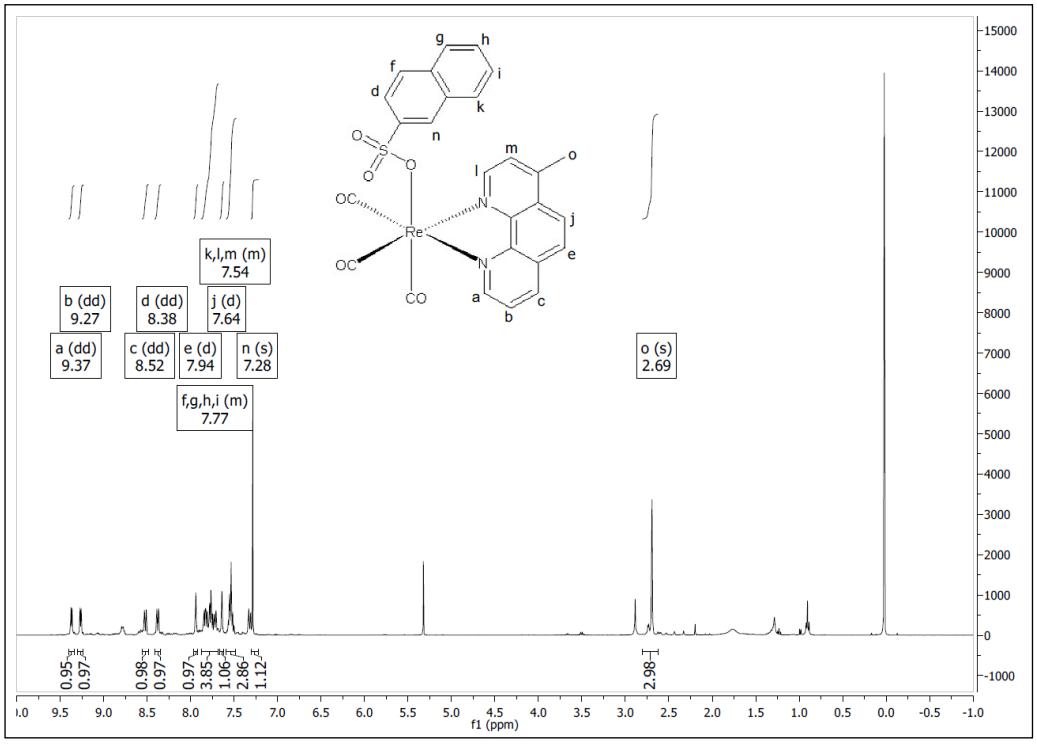

Figure 46: ^{1}H NMR spectrum of 2NS3

3. 2. 2. 14. *fac*-$(CO)_3$(2,9-Dimethyl-1,10-phenanthroline) $ReOS(O_2)C_{10}H_7$ (2NS4)

2NS4 was synthesized from a one-pot reaction of PC4 and 2-Naphthalenesulfonic acid in dichloromethane solvent according to Scheme 19 below. The yellow crystals (82%) of 2NS4 were characterized using ^{1}H NMR.

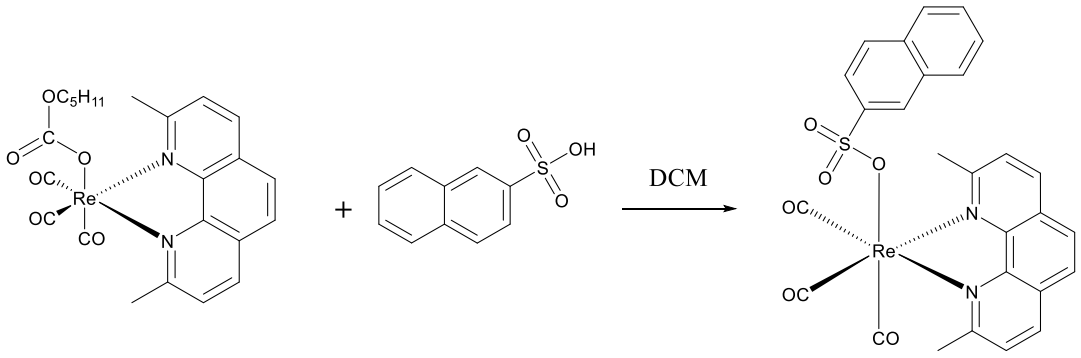

Scheme 19: Synthesis of 2NS4

2NS4 have been characterized spectroscopically and crystallographically. The IR spectrum (Figure 47) exhibits the three characteristic υ(C≡O)'s at 2030(s), 1925(s), and 1905 cm^{-1} for a facial geometry. The ^{1}H NMR peak assignments are shown in Figure 48. The doublet at 8.08 ppm represents the similar phenantholine protons at positions 3 and 8. The multiplet at 7.79–7.75 ppm represents the proton at position 3 of the naphthalene ring. The multiplet at 7.59–7.57 ppm represents an overlap of similar protons 5 and 6 on the phenanthroline ring and the proton at position 4 of the naphthalene ring. The doublet at 7.50 ppm represents the similar protons at position 4 and 7 of the phenanthroline ring. The multiplet at 7.46–7.34 ppm represents the protons at positions 5, 6, 7, 8 of the naphthalene ring. The singlet at 7.16 ppm represents the proton at position 1 of the naphthalene ring. The methyl group protons on positions 2 and 9 of the phenanthroline ring appear as a singlet at 3.11 ppm. The X-ray structure of **2NS4** (Figure 49) establishes its octahedral geometry where the central Re atom is coordinated to three facial

carbonyls, two N atoms of the chelated phenanthroline ligand and the 2-naphthalenesulfonate anion.

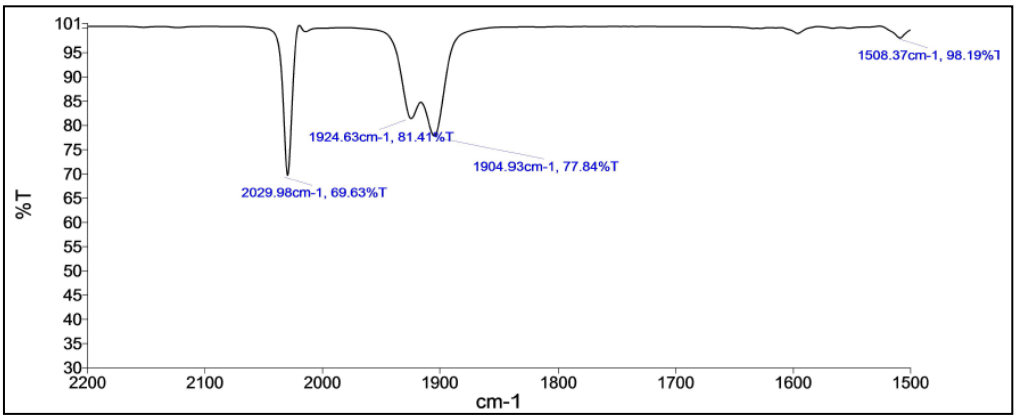

Figure 47: IR spectrum of 2NS4

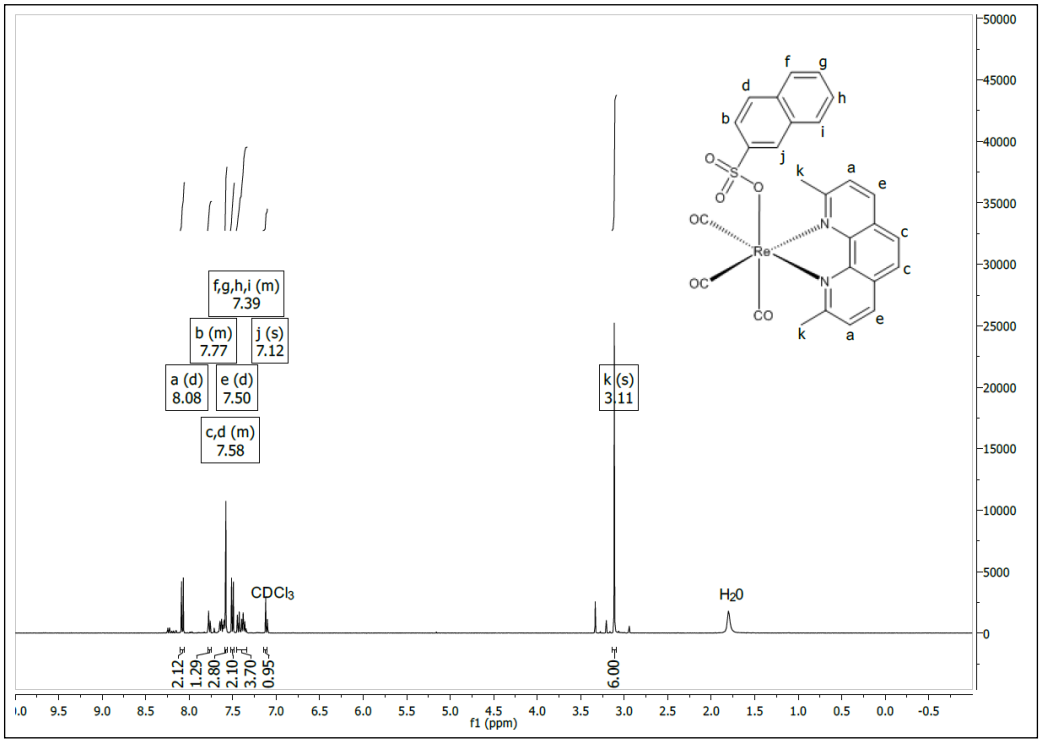

Figure 48: ^{1}H NMR spectrum of 2NS4

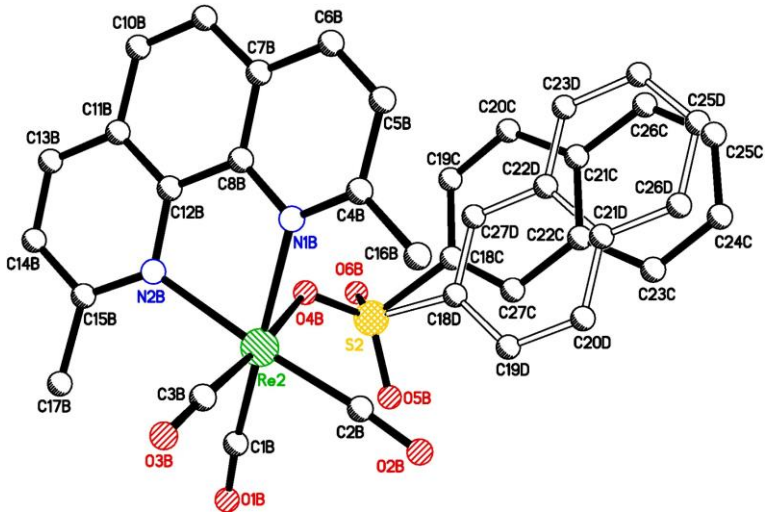

Figure 49: X-ray structure of 2NS4

3. 2. 2. 15. *fac*-(CO)$_3$(5,6-dimethyl-1,10-phenanthroline) ReOS(O$_2$)C$_{10}$H$_7$ (2NS5)

2NS5 was synthesized from a one-pot reaction of PC5 and 2-Naphthalenesulfonic acid in dichloromethane solvent according to Scheme 20 below. The yellow crystals (70%) of 2NS5 were characterized using ^{1}H NMR.

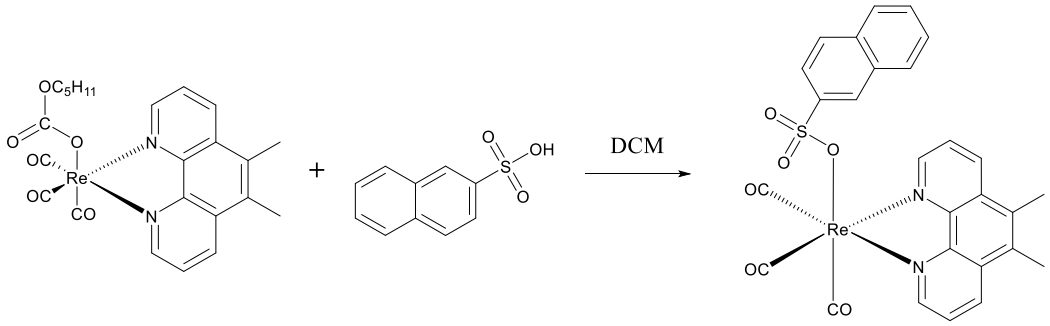

2NS5

Scheme 20: Synthesis of 2NS5

2NS5 has been characterized through IR and ^{1}H NMR spectroscopic techniques and X-ray crystallography. As expected, the IR spectrum of **2NS5** (Figure 50) exhibits three strong υ(C≡O)'s at 2030(s), 1928(s), and 1905 cm^{-1} suggesting a facial geometry of

the complex. The ^{1}H NMR peak assignments are shown in Figure 51. The doublet of doublets at 9.48 ppm represents the similar phenanthroline protons at positions 2 and 9. The doublet of doublets at 9.14 ppm represents the similar protons at positions 3 and 8 of the phenanthroline ring. The multiplet at 8.20–8.10 ppm represents the protons at positions 3, 4 and 5 of the naphthalene ring. The doublet of doublets at 7.94 ppm represents the proton at position 6 of the naphthalene ring. The multiplet at 7.90–7.80 ppm represents the similar protons at positions 4 and 7 of the phenanthroline ring. The proton on position 7 of the naphthalene ring appears as a doublet of doublets at 7.70 ppm. The naphthalene ring protons 1 and 8 appear as a doublet of doublets at 7.49 ppm. The singlet at 2.79 ppm represents the methyl group protons at positions 5 and 6 of the phenanthroline ring.

Figure 52 shows the X-ray structure of **2NS5**. The six coordination positions of the octahedral geometry are occupied by three facial CO's, two N atoms of the chelated phenanthroline ligand and a 2-naphthalenesulfonate anion. The X-ray structure clearly demonstrates the planarity of the phenanthroline ligand.

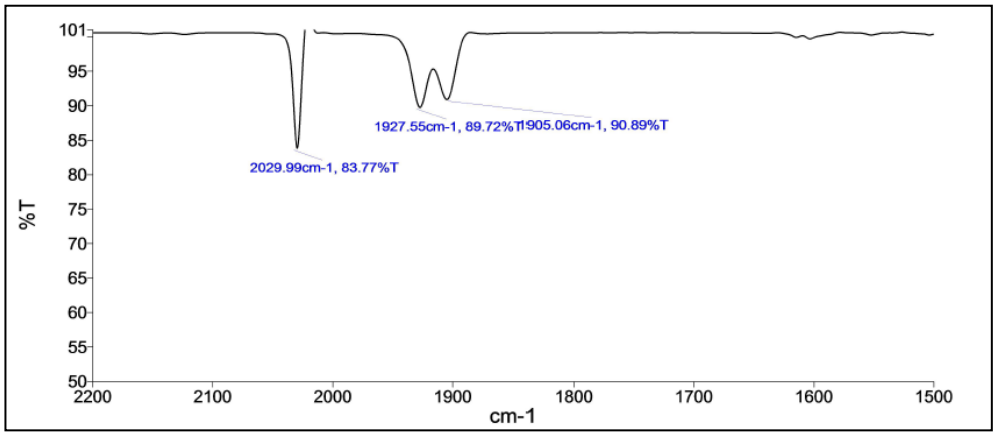

Figure 50: IR spectrum of 2NS5

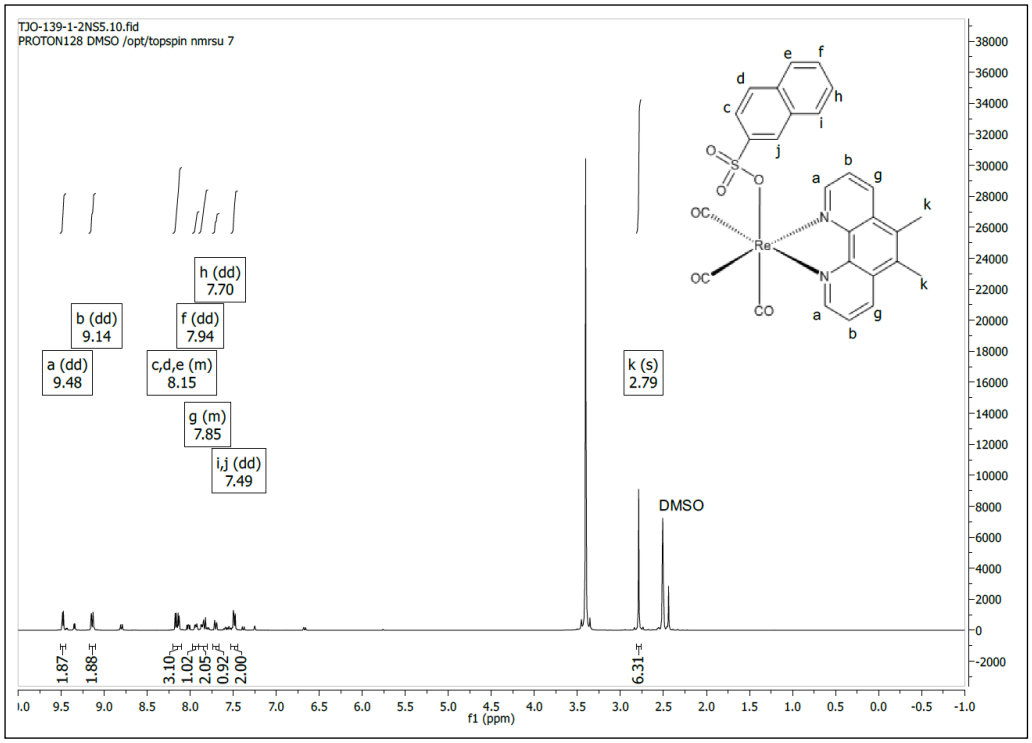

Figure 51: ^{1}H NMR spectrum of 2NS5

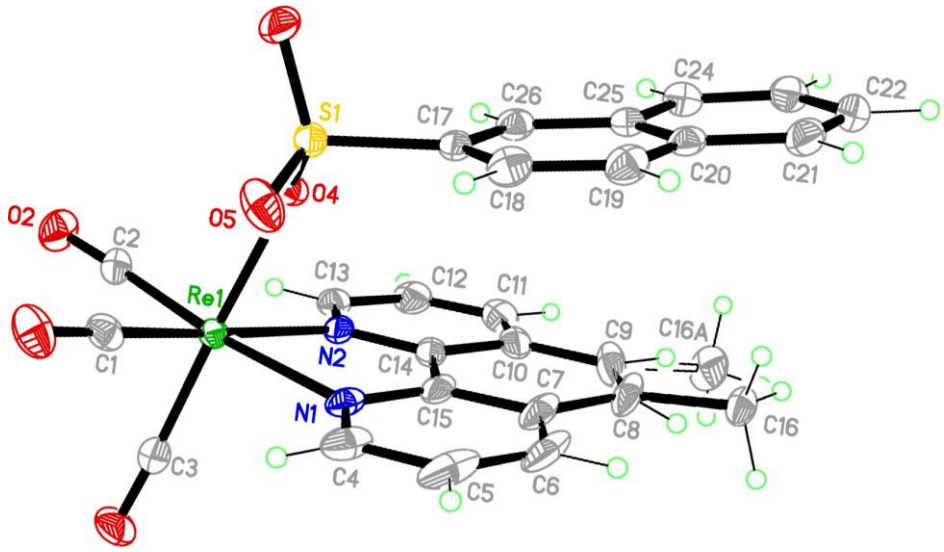

Figure 52: X-ray structure of 2NS5

3. 2. 2. 16. *fac*-$(CO)_3$(4,7-diphenyl-1,10-phenanthroline) $ReOS(O_2)C_{10}H_7$ (2NS6)

2NS6 was synthesized from a one-pot reaction of PC6 and 2-Naphthalenesulfonic acid in dichloromethane solvent according to Scheme 21 below. The yellow crystals (73%) of 2NS6 were characterized using ^{1}H NMR.

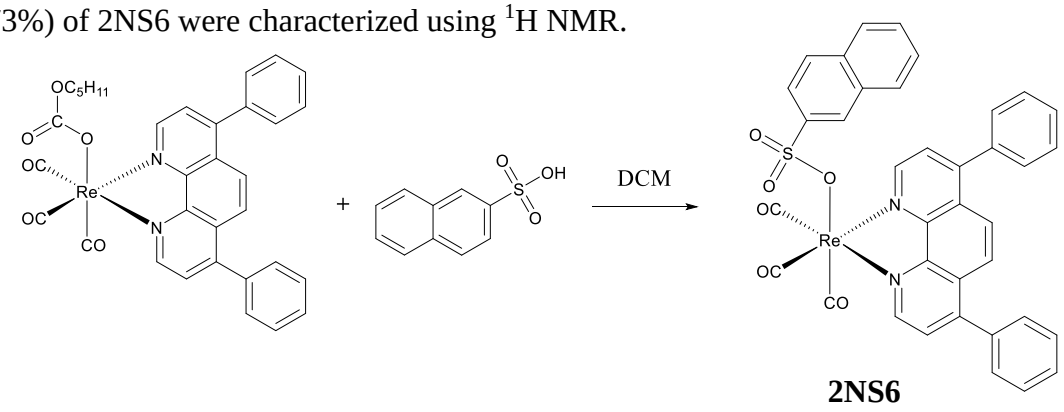

2NS6

Scheme 21: Synthesis of 2NS6

2NS6 has been characterized spectroscopically using IR, ^{1}H NMR and ^{13}C NMR. The molecular structure is confirmed through X-ray crystal structure determination. The IR spectrum (Figure 53) shows three υ(C≡O)'s at 2029(s), 1927(s) and 1905(s) cm^{-1} which establishes the facial geometry of the complex. In the ^{1}H NMR spectrum (Figure 54), the doublet at 9.20 ppm represents the similar phenanthroline protons (CH=N) at positions 2 and 9. The singlet at 7.81 ppm represents the similar protons at position 5 and 6 of the phenanthroline ring. The multiplet at 7.64–7.57 ppm represents 4 of the benzene ring protons attached at positions 4 and 7 of the phenanthroline ring. The multiplet at 7.54–7.49 ppm represents the remaining benzene ring protons attached at positions 4 and 7 of the phenanthroline ring. The multiplet at 7.46–7.31 ppm represents an overlap of the phenanthroline ring protons 3 and 8 and protons 3, 4, 5, 6, 7, and 8 on the naphthalene ring. The proton on position 1 of the naphthalene ring appears as a doublet of doublets at 7.16 ppm.

The ^{13}C NMR spectrum (Figure 55) shows two downfield resonances at δ197 and 193, with an intensity ratio of 2:1, due to the three carbonyls. 20 resonances in the aromatic region accounts for 20 aromatic carbons. In the phenanthroline ligand component of the 2NS6 structure there are 12 carbon types on the ligand represented as peaks in the ^{13}C NMR spectra. The ten carbons on the naphthalene ring appear as distinct peaks in the spectra. The peaks at 197.19 and 192.60 ppm represent the CO carbons connected to the Re center. Finally, the molecular structure (Figure 56) of the complex was established through X-ray crystallography. As expected, the Re center is coordinated to three facial CO's, two N atoms of the chelated ligand and the 2-naphthalenesulfonate anion.

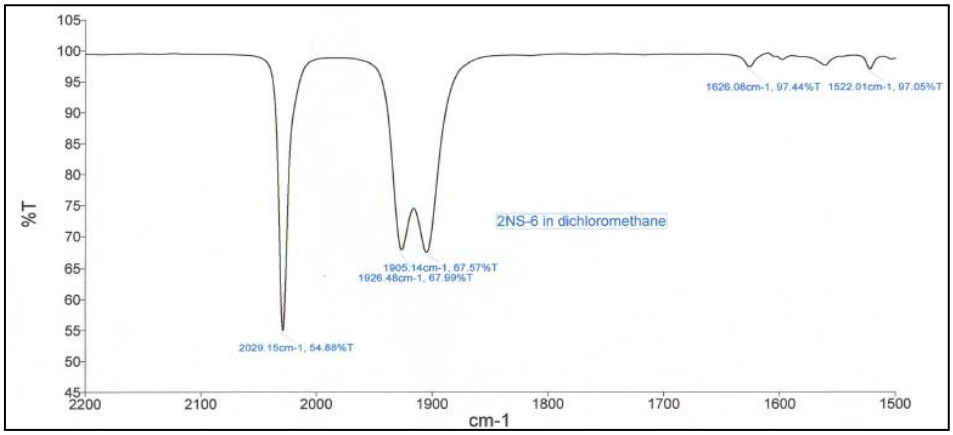

Figure 53: IR spectrum of 2NS6

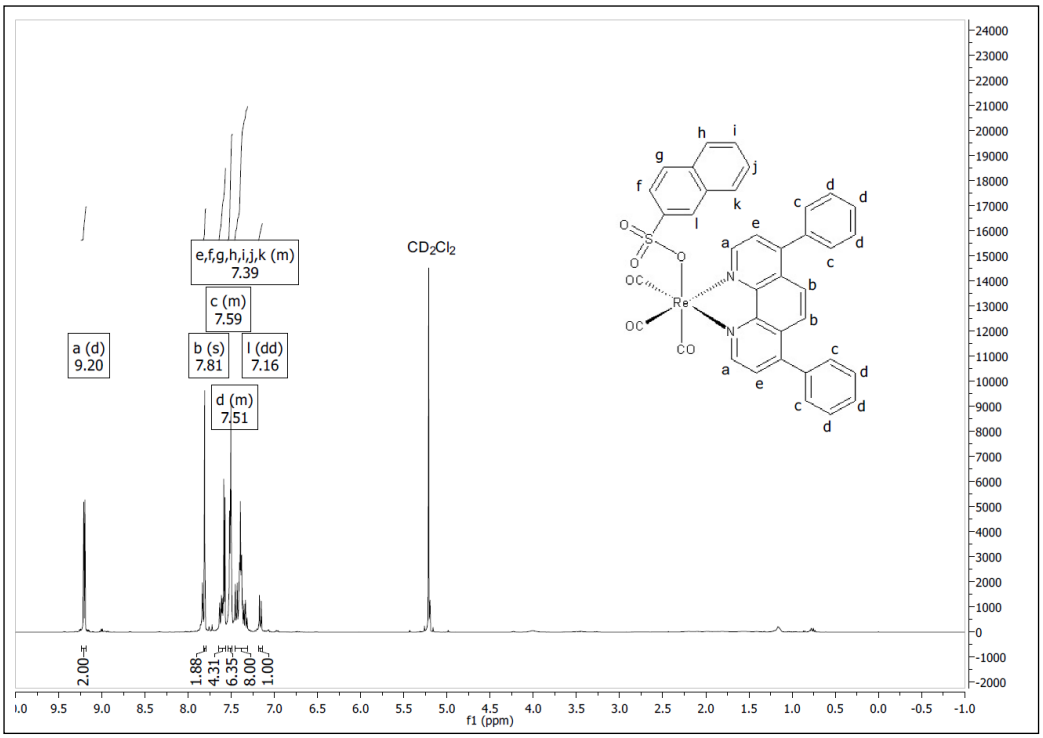

Figure 54: ^{1}H NMR spectrum of 2NS6

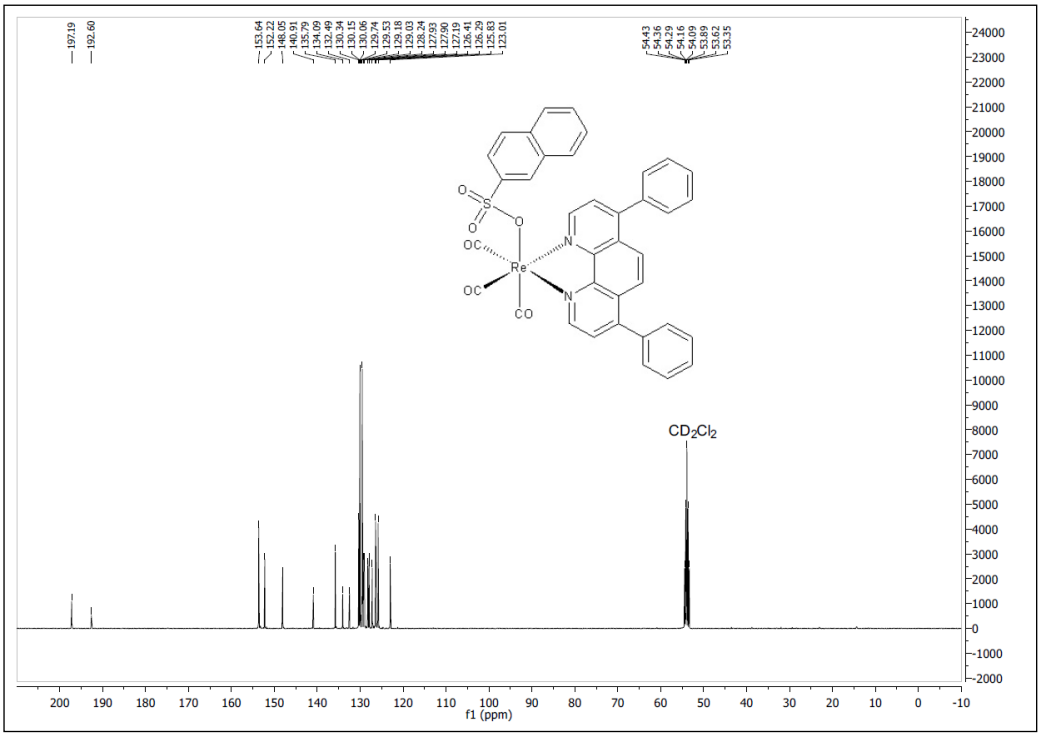

Figure 55: ^{13}C NMR spectrum of 2NS6

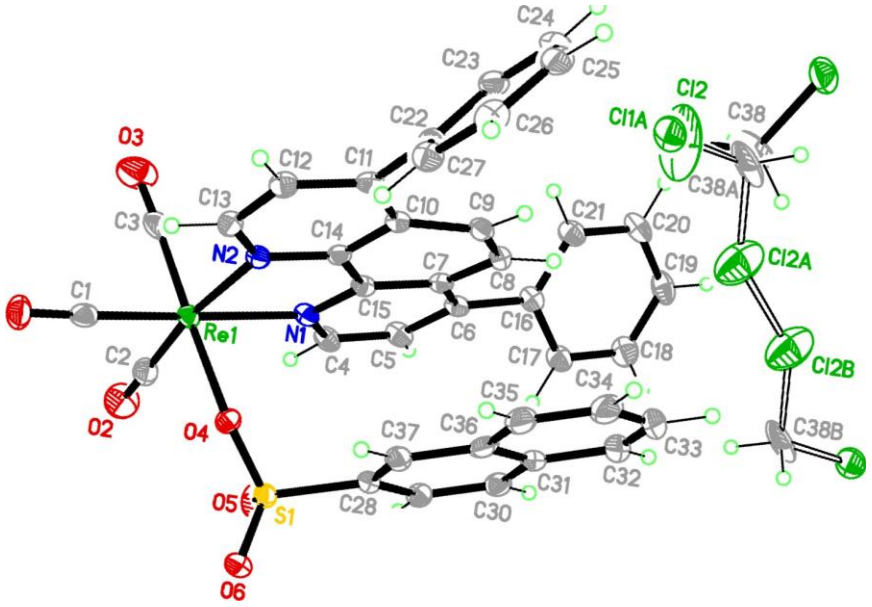

Figure 56: X-ray structure of 2NS6

3. 2. 2. 17. *fac*-$(CO)_3$(2,9-dimethyl-4,7-diphenyl-1,10-phenanthroline) $ReOS(O_2)C_{10}H_7$ (2NS7)

2NS7 was synthesized from a one-pot reaction of PC7 and 2-Naphthalenesulfonic acid in dichloromethane solvent according to Scheme 22 below. The yellow crystals (74%) of 2NS7 were characterized using ^{1}H NMR.

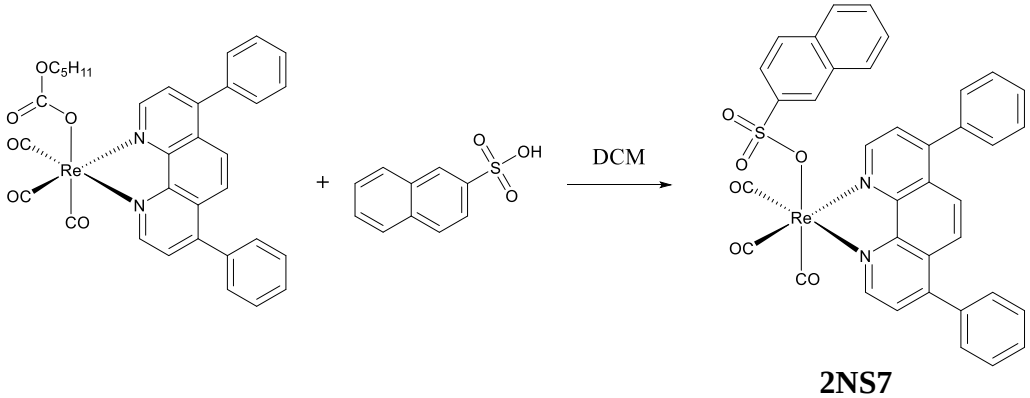

2NS7

Scheme 22: Synthesis of 2NS7

The IR spectrum of 2NS7 (Figure 57) shows three υ(C≡O)'s at peaks at 2028(s), 1923(s) and 1904(s) cm^{-1} representing a facial geometry of the complex. In the ^{1}H NMR spectrum (Figure 58), the doublet of doublets at 8.15 ppm represents the proton at position 3 of the naphthalene ring. The singlet at 7.84 ppm represents the protons on positions 5 and 6 of the phenanthroline ring. The multiplet at 7.67–7.45 ppm represents an overlap of the naphthalene ring protons at positions 4, 5, 6, 7 and 8, and the benzene ring protons attached to the phenanthroline ring at positions 5 and 6. The doublet of doublet of doublets at 7.40 ppm represents the proton at position 1 of the naphthalene ring. The methyl group protons on positions 2 and 9 of the phenanthroline ring appear as a singlet at 3.30 ppm. The X-ray crystal structure (Figure 59) demonstrate the octahedral geometry of the complex coordinating with three facial CO's, two N atoms of the ligand and the sulfonate anion.

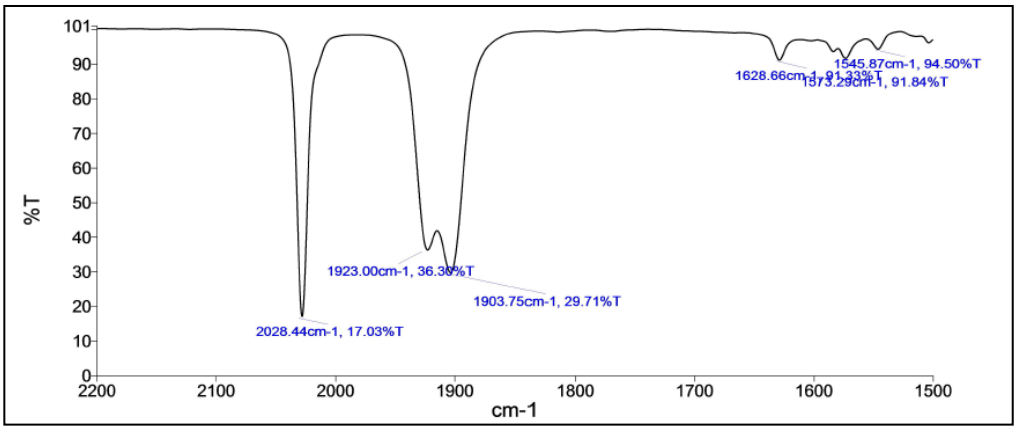

Figure 57: IR spectrum of 2NS7

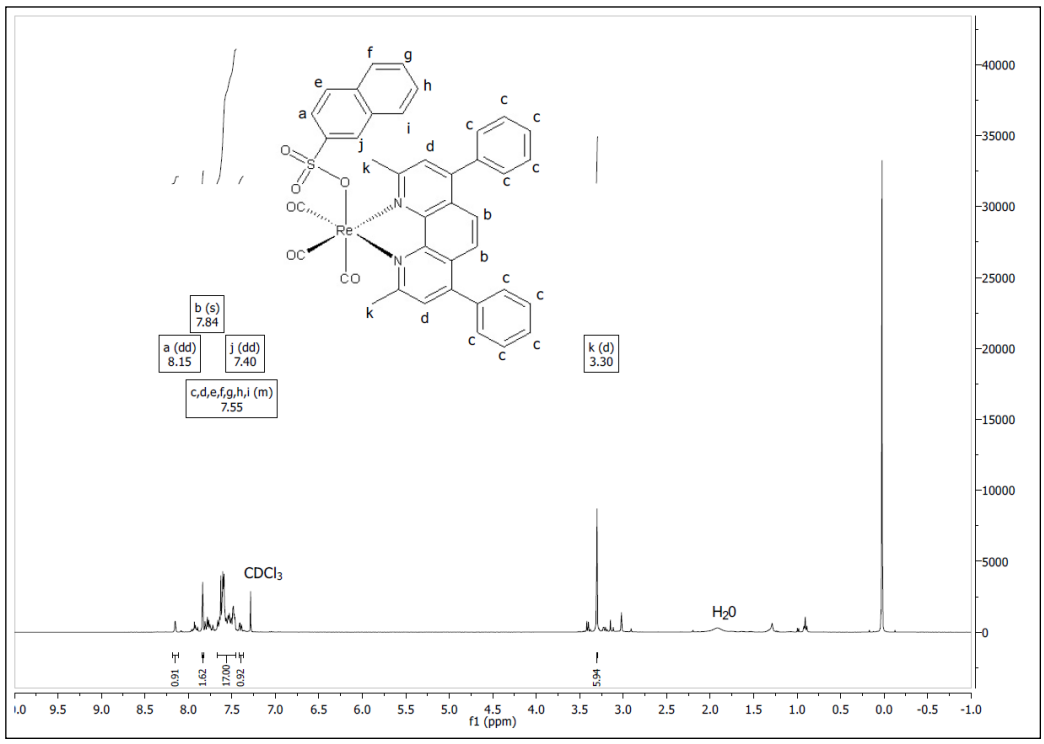

Figure 58: ^{1}H NMR spectrum of 2NS7

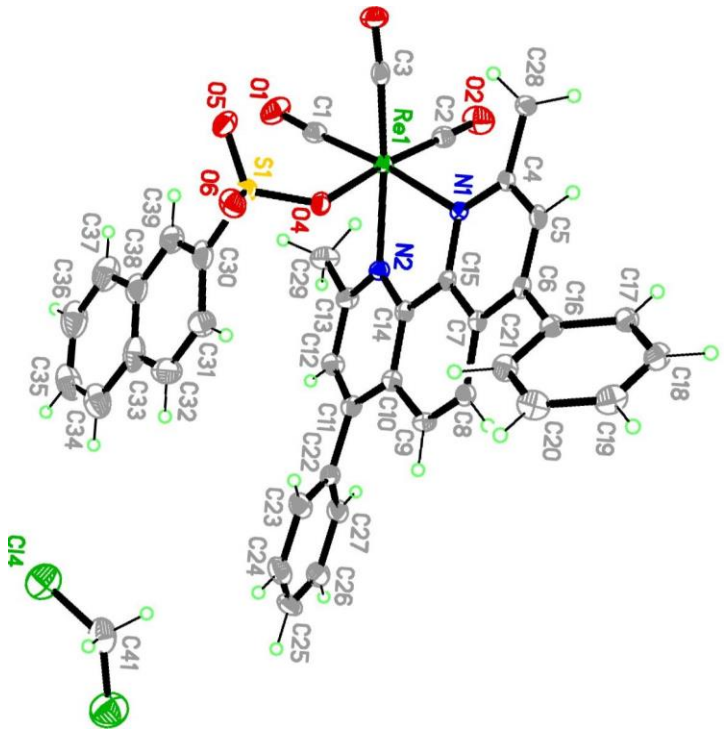

Figure 59: X-ray structure of 2NS7

3. 2. 2. 18. *fac*-$(CO)_3$(4,7-dimethyl-1,10-phenanthroline) $ReOS(O_2)C_{10}H_7$ (2NS8)

2NS8 was synthesized from a one-pot reaction of PC8 and 2-Naphthalenesulfonic acid in dichloromethane solvent according to Scheme 23 below. The yellow crystals (77%) of 2NS8 were characterized using ^{1}H NMR.

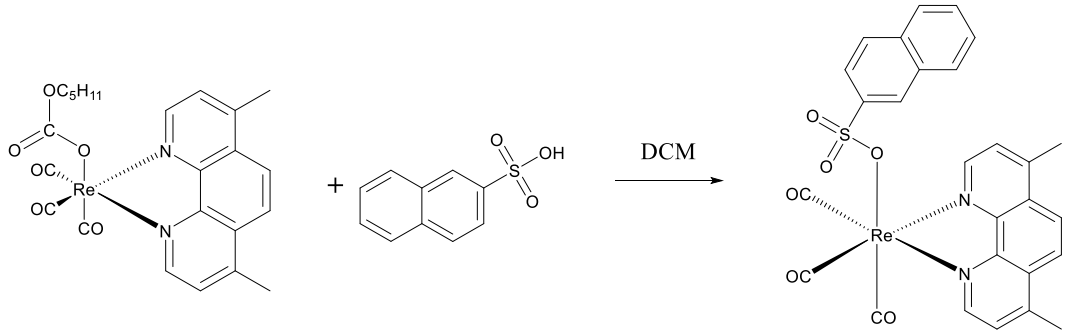

2NS8

Scheme 23: Synthesis of 2NS8

As expected, the IR spectrum (Figure 60) of **2NS8** shows three strong υ(C≡O)'s at 2028, 1924 and 1902 cm^{-1} suggesting a facial geometry of the complex. In the ^{1}H NMR spectrum (Figure 61), the doublet at 9.20 ppm represents the similar protons at positions 2 and 9 of the phenanthroline ring. The singlet at 8.04 ppm represents the similar protons at position 5 and 6 of the phenanthroline ring. The doublet at 7.81 ppm represents the similar protons at position 3 and 8 of the phenanthroline ring. The multiplet at 7.63–7.55 ppm represents the protons at positions 3 and 4 of the naphthalene ring. The multiplet at 7.49–7.41 ppm represents the protons at positions 5 and 6 of the naphthalene ring. The doublet of doublets at 6.72 ppm represents the proton at position 7 of the naphthalene ring. The doublet at 5.76 ppm represents the protons at positions 1 and 8 of the naphthalene ring. The singlet at 2.73 ppm represents the methyl group protons at positions 4 and 7 of the phenanthroline ring.

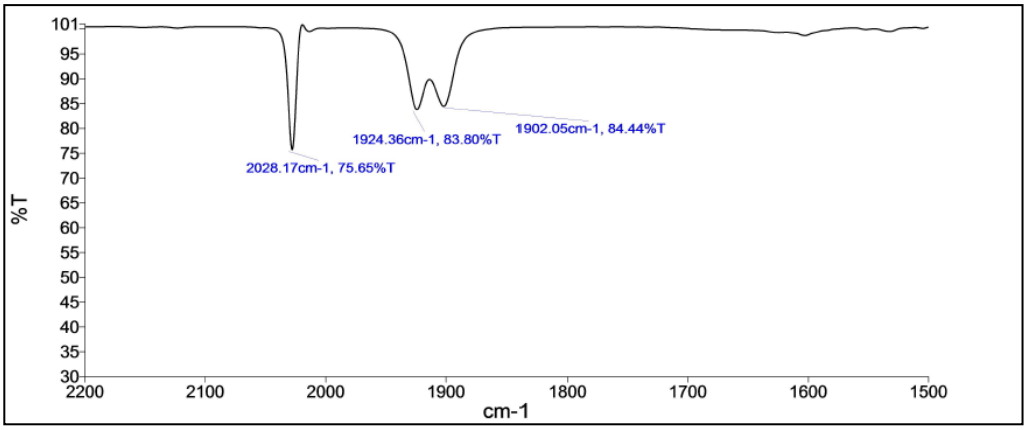

Figure 60: IR spectrum of 2NS8

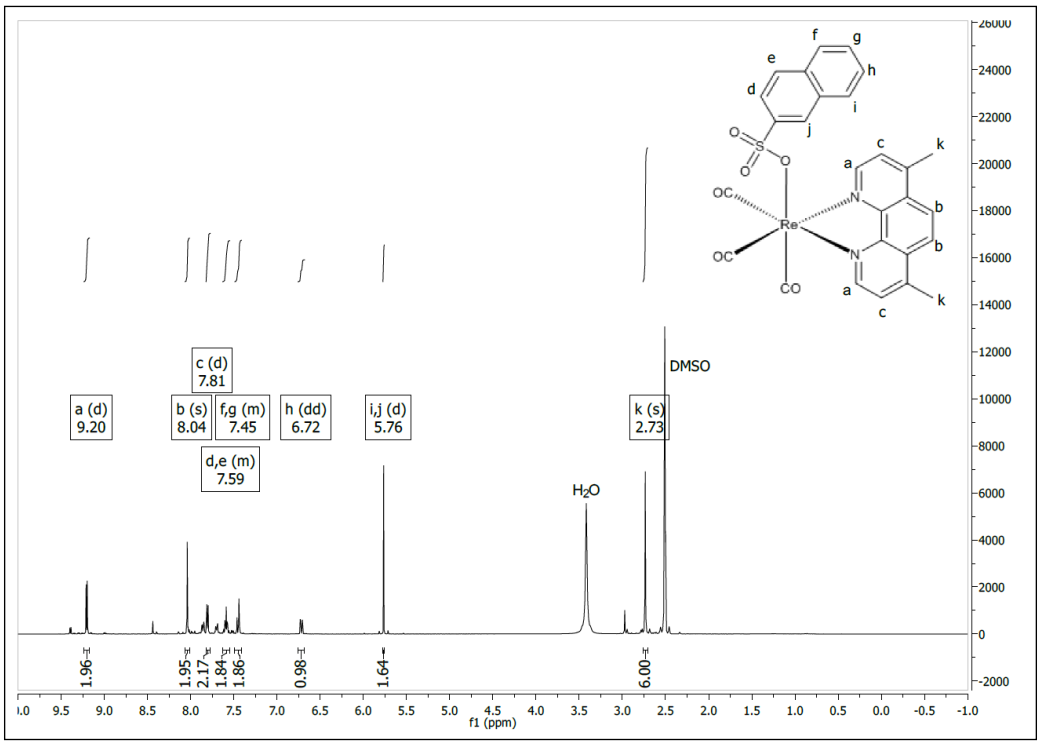

Figure 61: ^{1}H NMR spectrum of 2NS8

3. 2. 2. 19. *fac*-(CO)$_3$(3,4,7,8-tetramethyl-1,10-phenanthroline)ReOS(O$_2$)C$_{10}$H$_7$ (2NS9)

2NS9 was synthesized from a one-pot reaction of PC9 and 2-Naphthalenesulfonic acid in dichloromethane solvent according to Scheme 24 below. The yellow crystals (76%) of 2NS9 were characterized using ^{1}H NMR.

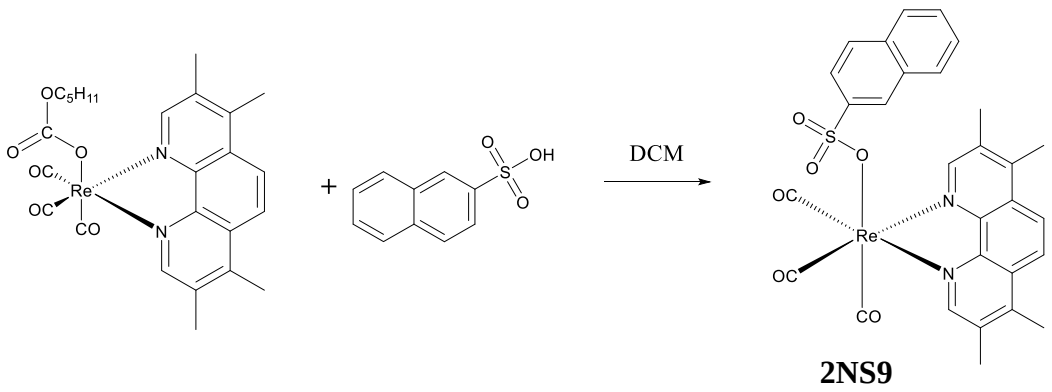

2NS9

Scheme 24: Synthesis of 2NS9

The IR spectrum of **2NS9** (Figure 62) exhibits three strong υ(C≡O)'s at 2028, 1924 and 1902 cm^{-1} confirming a facial geometry. In the ^{1}H NMR spectrum (Figure 63), the singlet at 9.08 ppm represents the naphthalene proton at position 3. The singlet at 9.00 ppm represents the similar phenanthroline protons at positions 2 and 9. The singlet at 7.99 ppm represents the similar phenanthroline protons at positions 5 and 6. The multiplet at 7.93–7.88 ppm represents the proton at position 4 of the naphthalene ring. The multiplet at 7.83–7.66 ppm represents the protons at positions 5 and 6 of the naphthalene ring. The multiplet at 7.59–7.51 ppm represents the proton at position 7 of the naphthalene ring. The multiplet at 7.47–7.41 ppm represents the proton at position 8 of the naphthalene ring. The doublet of doublets at 7.19 ppm represents the proton at position 1 of the naphthalene ring. The singlet at 2.62 ppm represents the methyl group protons at positions 3 and 8 of the phenanthroline ring. The singlet at 2.48 ppm represents the methyl group protons at positions 4 and 7 of the phenanthroline ring.

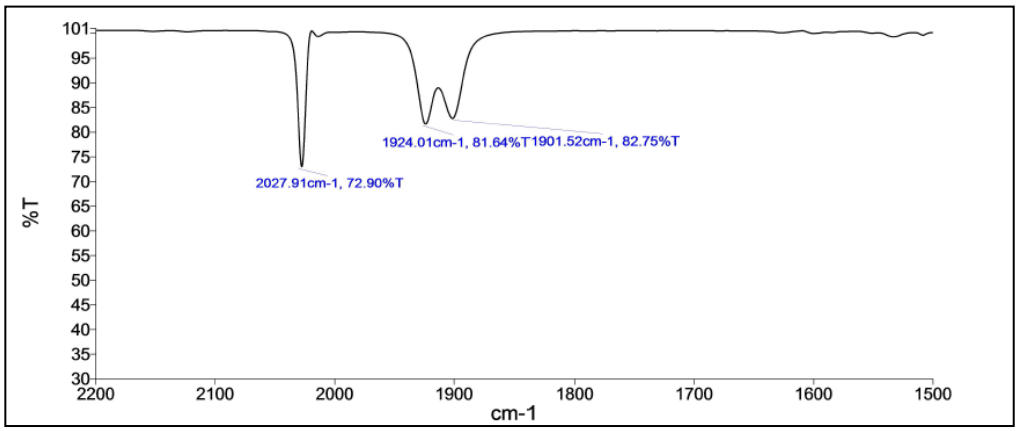

Figure 62: IR spectrum of 2NS9

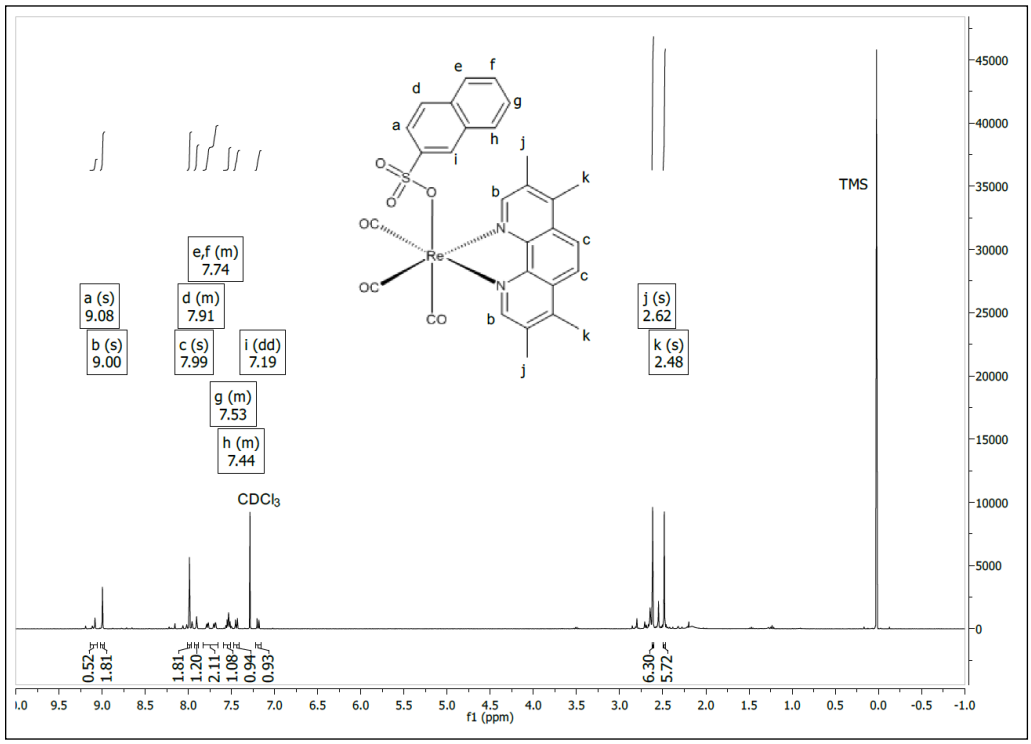

Figure 63: ^{1}H NMR spectrum of 2NS9

3. 2. 2. 20. *fac*-(CO)$_3$(4-methyl-1,10-phenanthroline) ReOS(O$_2$)C$_{10}$H$_7$ (2NS10)

2NS10 was synthesized from a one-pot reaction of PC10 and 2-Naphthalenesulfonic acid in dichloromethane solvent according to Scheme 25 below. The yellow crystals (70%) of 2NS10 were characterized using ^{1}H NMR.

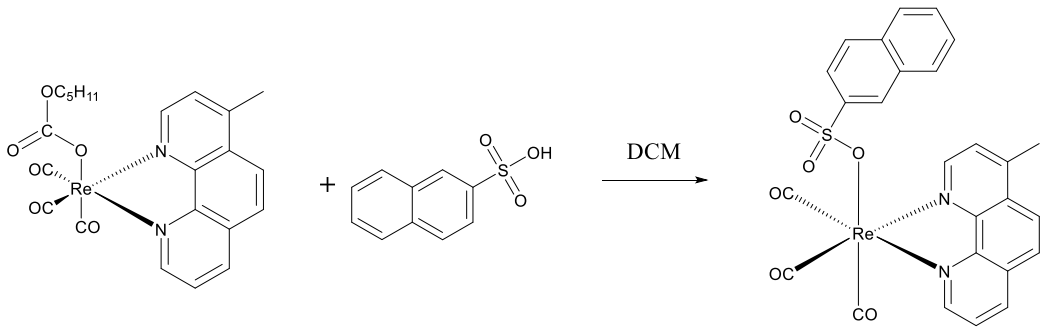

2NS10

Scheme 25: Synthesis of 2NS10

Figures 64 exhibits three strong υ(C≡O)'s at 2030, 1926 and 1906 cm^{-1} in the IR spectrum of **2NS10** representing a facial geometry of **2NS10**. In the ^{1}H NMR spectrum (Figure 65), the doublet of doublets at 9.22 ppm represents the proton at position 9 of the phenanthroline ring. The doublet at 9.04 ppm represents the phenanthroline proton at position 2. The doublet of doublets at 8.37 ppm represents the phenanthroline proton at position 8. The doublet at 7.84 ppm represents the phenanthroline protons at positions 5 and 6. The multiplet at 7.72–7.50 ppm represents an overlap of the phenathroline proton 7 and the protons at positions 3, 4 and 5 of the naphthalene ring. The multiplet at 7.46–7.34 ppm represents an overlap of the phenathroline proton 3 and the protons at positions 6, 7 and 8 of the naphthalene ring. The singlet at 7.12 ppm represents the proton at position 1 of the naphthalene ring. The singlet at 2.64 ppm represents the methyl group protons at position 4 of the phenanthroline ring.

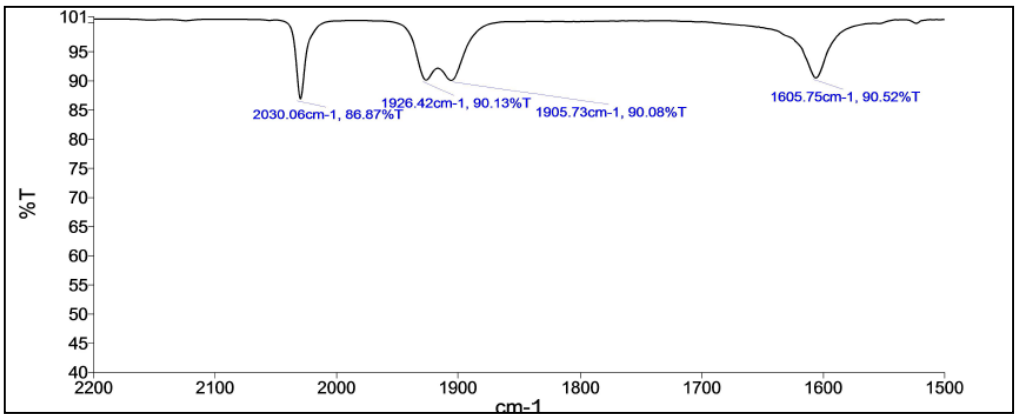

Figure 64: IR spectrum of 2NS10 in dichloromethane

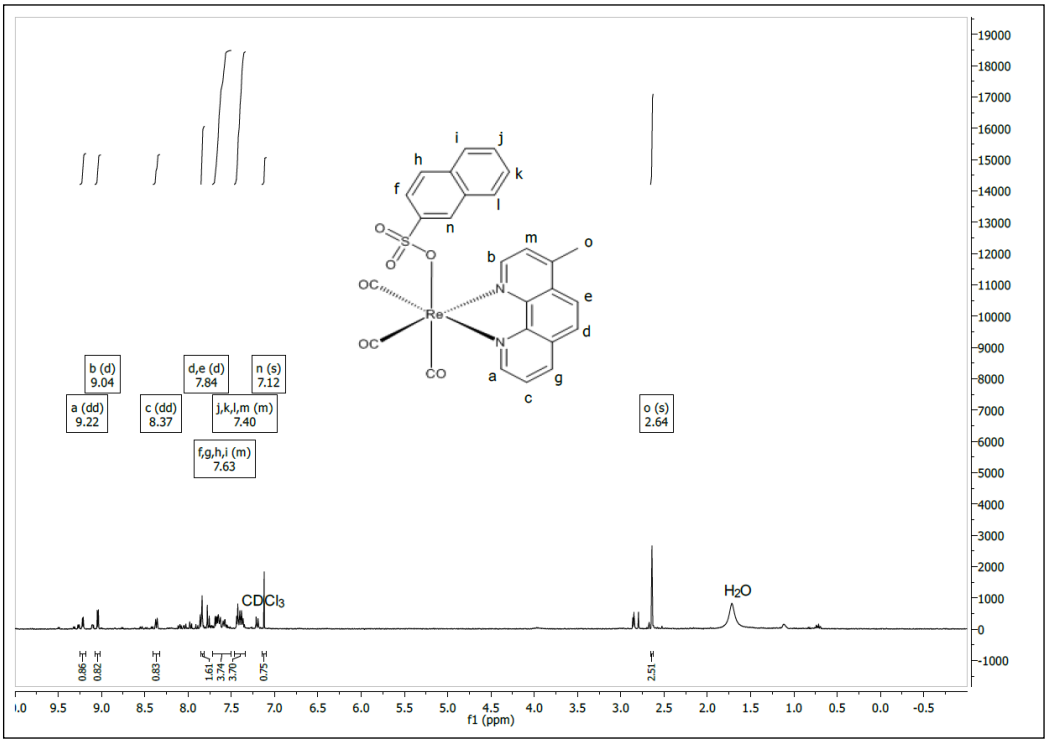

Figure 65: ^{1}H NMR spectrum of 2NS10

3. 2. 2. 21. *fac*-$(CO)_3$(2,2'-bipyridyl) $ReOS(O_2)C_7H_7$ (TOS1)

TOS1 was synthesized from a one-pot reaction of PC1 and *p*-Toluenesulfonic acid in dichloromethane solvent according to Scheme 26 below. The yellow crystals (84%) of TOS1 were characterized using ^{1}H NMR.

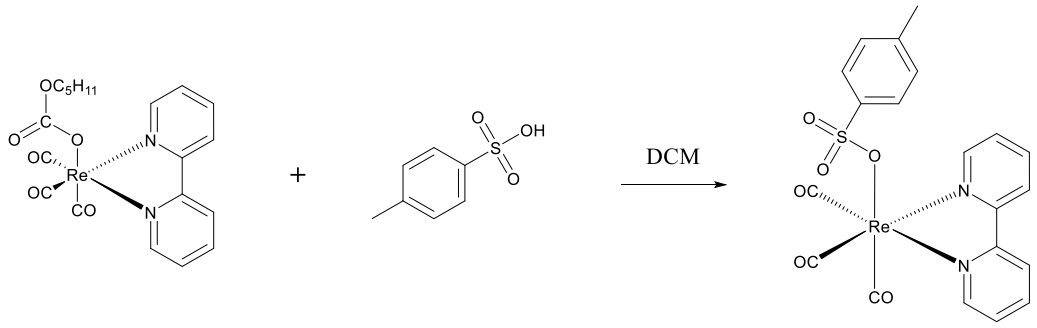

TOS1

Scheme 26: Synthesis of TOS1

The IR spectrum (Figure 66) of **TOS1** shows three υ(C≡O)'s at 2030(s), 1927(s) and 1907(s) cm^{-1} establishing **TOS1** as a facial complex. In the ^{1}H NMR spectrum (Figure 67) of **TOS1**, the multiplet at 9.01 pm represents an overlap of ortho and meta toluene protons. The multiplet at 8.18 ppm represents the similar protons at positions 2 and 9 of the bipyridyl ring. The multiplet at 7.60 ppm represents the similar protons at positions 3 and 8 of the bipyridyl ring. The multiplet at 7.41 ppm represents the similar protons at positions 4 and 7 of the bipyridyl ring. The similar protons on positions 5 and 6 of the bipyridyl ring appear as a singlet at 7.14 ppm. The singlet at 2.39 ppm represents the methyl group protons on the toluene ring.

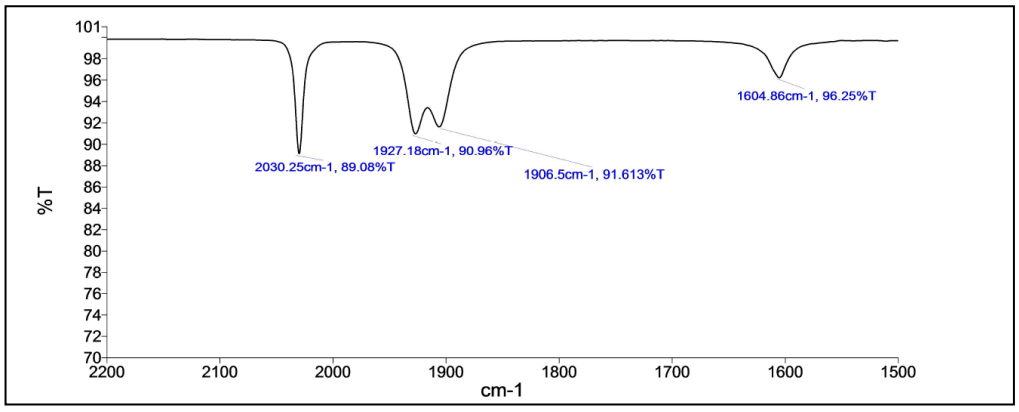

Figure 66: IR spectrum of TOS1 in dichloromethane

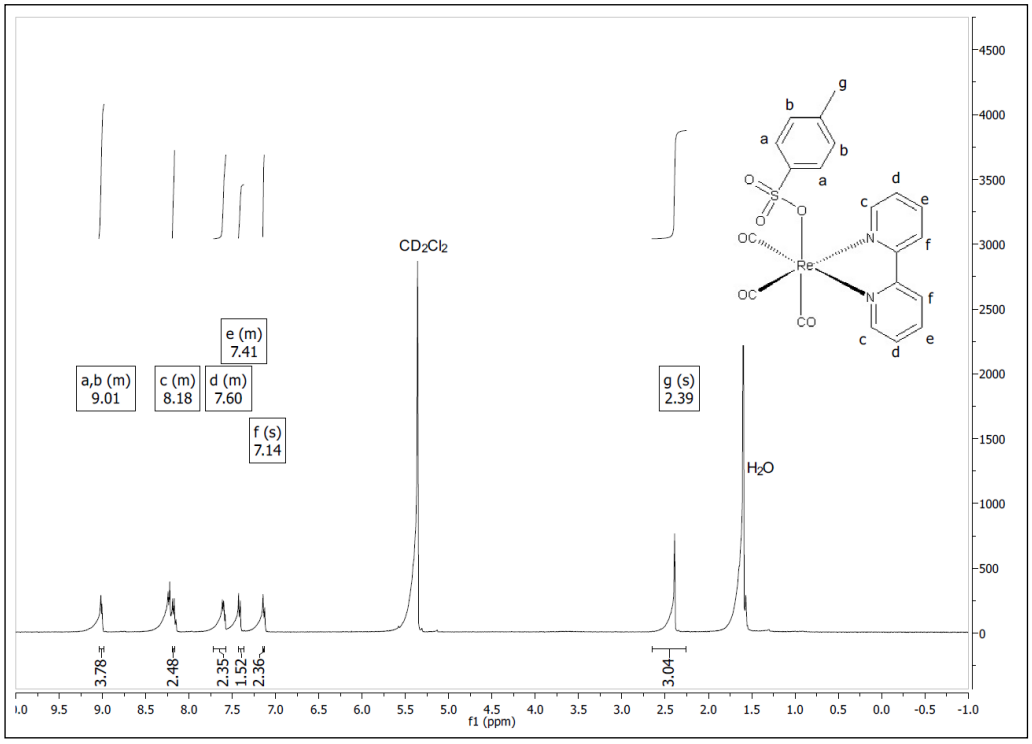

Figure 67: ^{1}H NMR spectrum of TOS1

3. 2. 2. 22. *fac*-(CO)$_3$(1,10-phenanthroline) ReOS(O$_2$)C$_7$H$_7$ (TOS2)

TOS2 was synthesized from a one-pot reaction of PC2 and *p*-Toluenesulfonic acid in dichloromethane solvent according to Scheme 27 below. The yellow crystals (90%) of TOS2 were characterized using ^{1}H NMR.

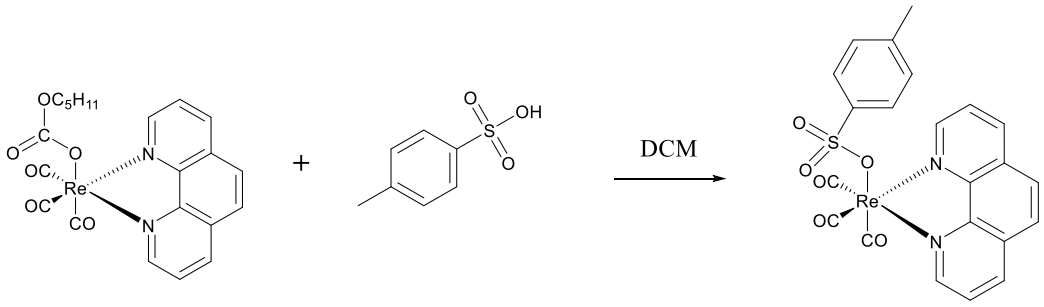

TOS2

Scheme 27: Synthesis of TOS2

TOS2 has been characterized through IR and NMR spectroscopic techniques. Figures 68, 69 and 70 show the IR, ^{1}H NMR and ^{13}C NMR spectra respectively. The IR spectrum exhibits three $\upsilon(C\equiv O)$'s at 2031(s), 1927(s) and 1906(s) cm^{-1} confirming a facial geometry of the complex. In the ^{1}H NMR spectrum, the doublet of doublets at 9.35 ppm represents the similar protons at positions 2 and 9 of the phenanthroline ring. The doublet of doublets at 8.57 ppm represents the similar protons at positions 4 and 7 of the phenanthroline ring. The singlet at 7.99 ppm represents the similar protons at positions 5 and 6 of the phenanthroline ring. The doublet of doublets at 7.85 ppm represents the similar protons at positions 3 and 8 of the phenanthroline ring. The doublet at 7.47 ppm represents the similar meta toluene protons. The doublet at 7.07 ppm represents the similar ortho toluene protons. The singlet at 2.34 ppm represents the methyl group protons on the toluene ring.

The ^{13}C NMR spectrum shows two characteristic downfield resonances due to the three facial CO's, 10 expected aromatic carbons and an aliphatic carbon. In the phenanthroline ligand component of the TOS2 structure, there are 6 carbon types on the ligand represented as peaks in the ^{13}C NMR spectra. There are two carbon types on the toluene ring that represent four carbons and appear as two distinct peaks in the ^{13}C spectra. The two quaternary carbons on that ring appear as two distinct peaks and the methyl carbon appears as a peak at 21.38 ppm. The peaks at 196.09 and 191.88 ppm represent the CO carbons connected to the Re center.

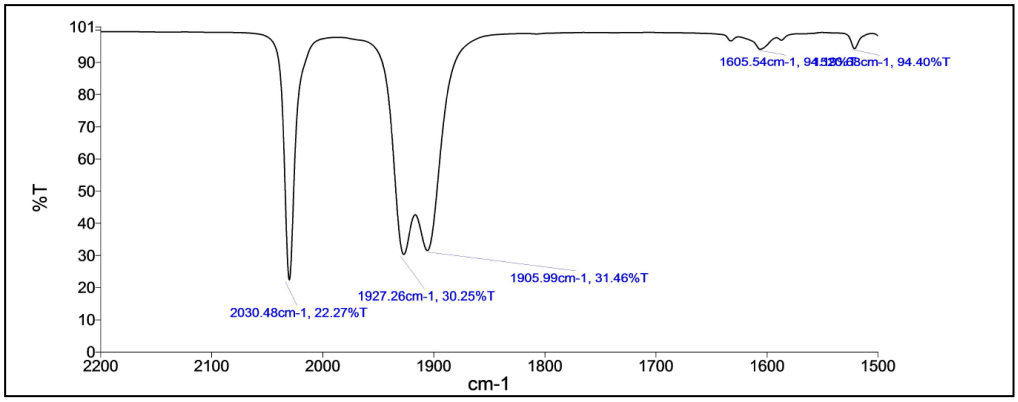

Figure 68: IR spectrum of TOS2 in dichloromethane

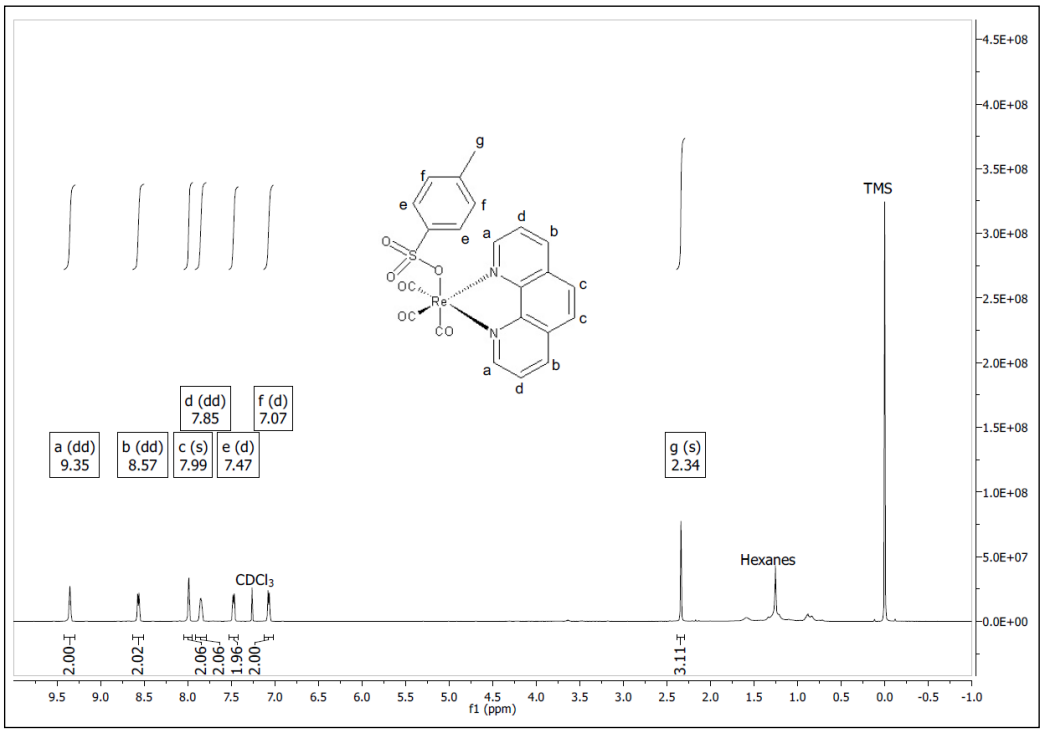

Figure 69: ^{1}H NMR spectrum of TOS2

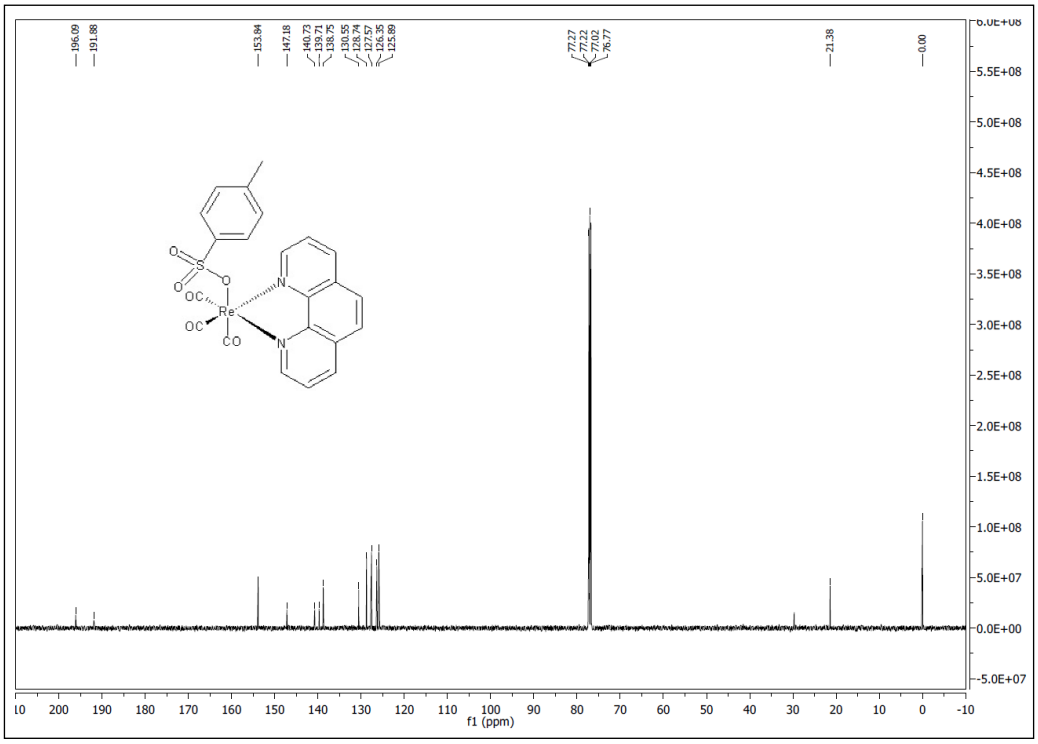

Figure 70: ^{13}C NMR spectrum of TOS2

3. 2. 2. 23. *fac*-(CO)$_3$(5-methyl-1,10-phenanthroline) ReOS(O$_2$)C$_7$H$_7$ (TOS3)

TOS3 was synthesized from a one-pot reaction of PC3 and *p*-Toluenesulfonic acid in dichloromethane solvent according to Scheme 28 below. The yellow crystals (85%) of TOS3 were characterized using ^{1}H NMR.

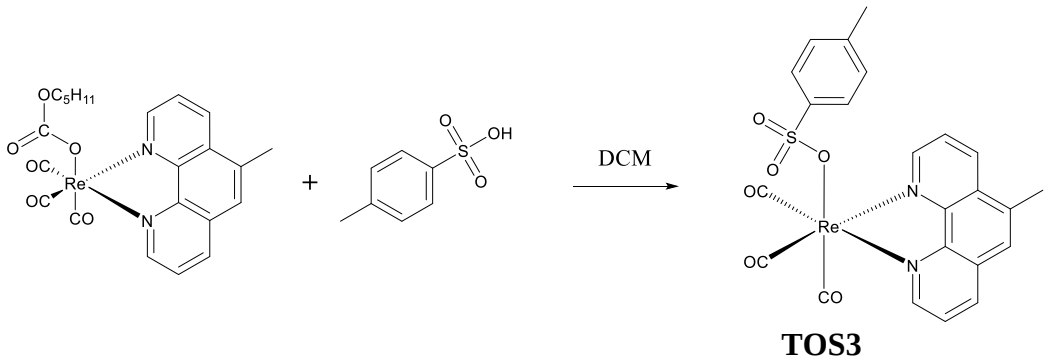

Scheme 28: Synthesis of TOS3

Figures 71, 72 and 73 show the IR, ^{1}H NMR and ^{13}C NMR of **TOS3** respectively. In the IR spectrum, the three peaks at 2030(s), 1927(s) and 1905(s) cm^{-1} represent the three υ(C≡O)'s, suggesting a facial geometry of the complex. The ^{1}H NMR peak assignments are shown in Figure 72 below. The doublet of doublets at 9.39 ppm represents the proton at position 2 of the phenanthroline ring. The doublet of doublets at 9.29 ppm represents the proton at position 9 of the phenanthroline ring. The doublet of doublets at 8.69 ppm represents the proton at position 3 of the phenanthroline ring. The doublet of doublets at 8.47 ppm represents the proton at position 8 of the phenanthroline ring. The doublet of doublets at 7.90 ppm represents the proton at position 7 of the phenanthroline ring. The multiplet 7.85–7.80 ppm represents the protons at positions 4 and 6 of the phenanthroline ring. The doublet at 7.47 ppm represents the similar meta toluene protons. The doublet at 7.07 ppm represents the similar ortho toluene protons. The singlet at 2.87 ppm represents the methyl group protons on the toluene ring. The singlet at 2.34 ppm represents the methyl group protons on position 5 of the phenanthroline ring.

The ^{13}C NMR spectrum shows the expected two downfield resonances at δ196 and 191, 16 aromatic carbons and two aliphatic carbons. In the phenanthroline ligand component of the TOS3 structure, there are 13 distinct carbon types on the ligand representing the 13 carbons on the ring and represented as peaks in the ^{13}C NMR spectra. One of those peaks (18.81 ppm) represents the methyl group carbon on the phenanthroline ligand. There are two carbon types on the toluene ring that represent four carbons and appear as two distinct peaks in the ^{13}C spectra. The two quaternary carbons on that ring appear as two distinct peaks and the methyl carbon appears as a peak at 21.38

ppm. The peaks at 196.19 and 191.99 ppm represent the CO carbons connected to the Re center. The X-ray structure of TOS3 conclusively establishes the octahedral geometry of the complex, where, the central Re atom is coordinated to three facial CO's, two N atoms and the tosylate anion.

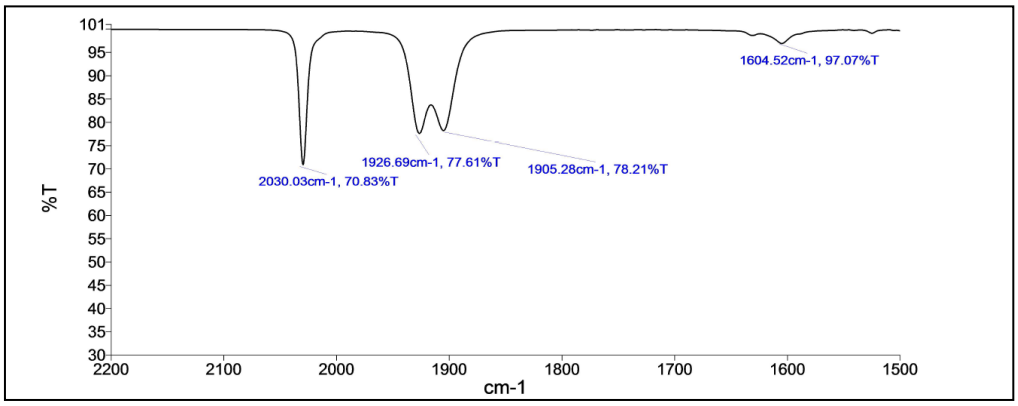

Figure 71: IR spectrum of TOS3 in dichloromethane

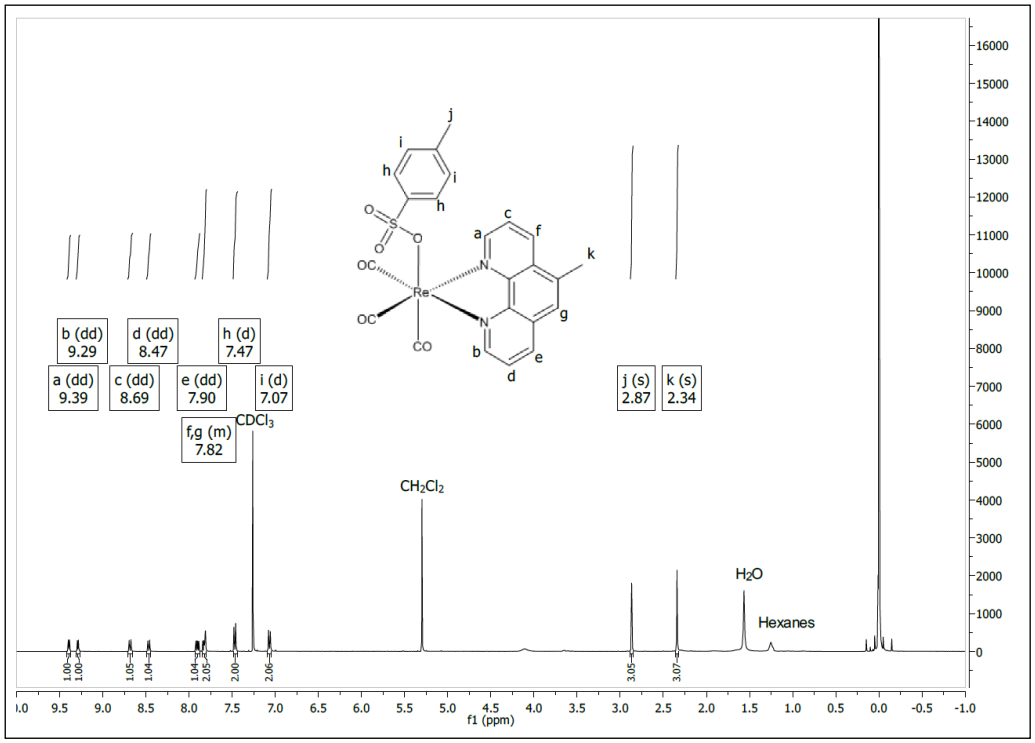

Figure 72: ^{1}H NMR spectrum of TOS3

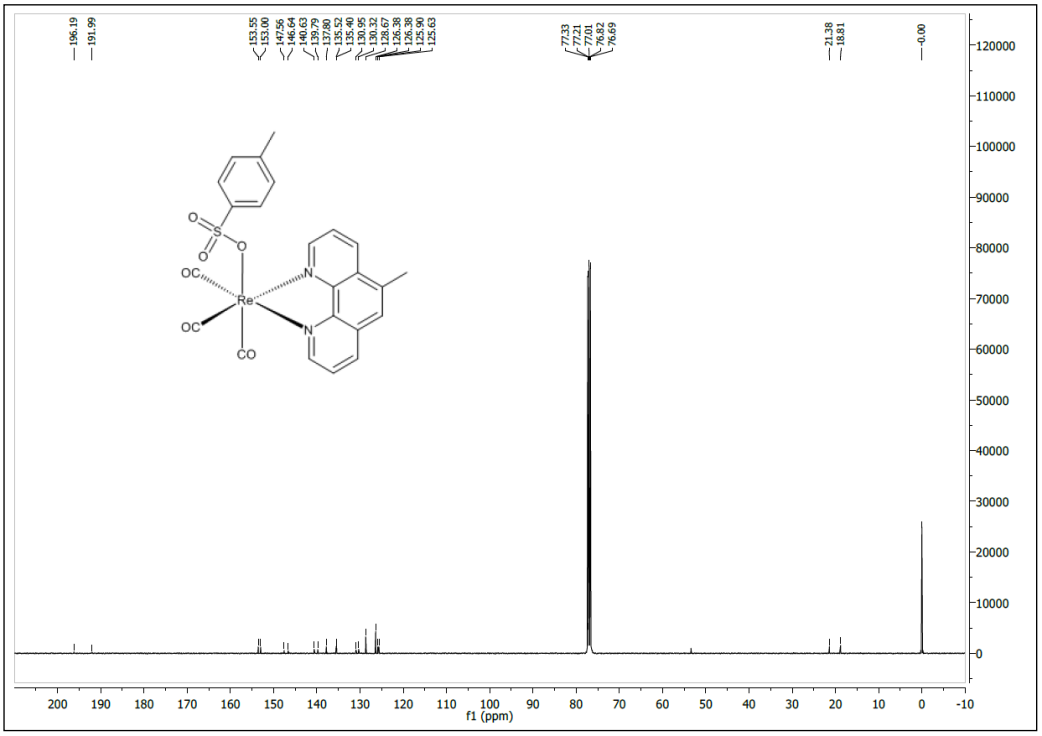

Figure 73: ^{13}C NMR spectrum of TOS3

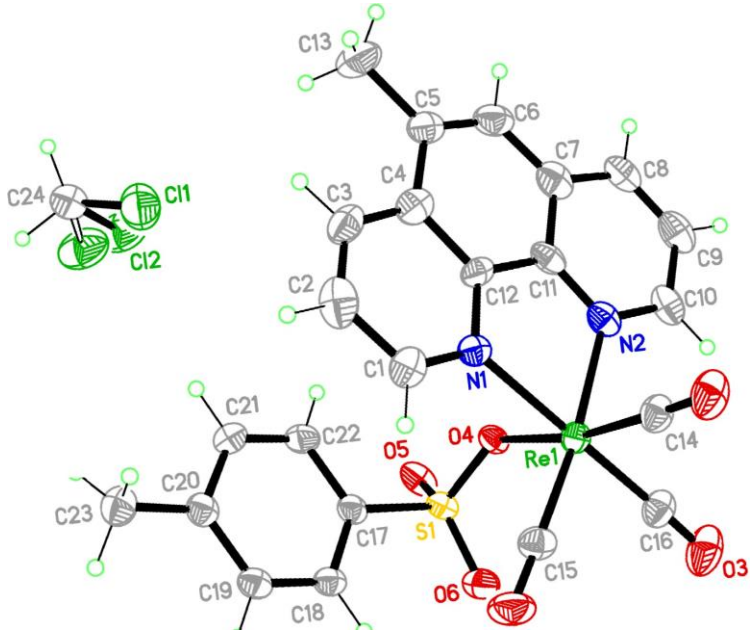

Figure 74: X-ray structure of TOS3

3. 2. 2. 24. *fac*-$(CO)_3$(2,9-Dimethyl-1,10-phenanthroline) $ReOS(O_2)C_7H_7$ (TOS4)

TOS4 was synthesized from a one-pot reaction of PC4 and *p*-Toluenesulfonic acid in dichloromethane solvent according to Scheme 29 below. The yellow crystals (87%) of TOS4 were characterized using ^1H NMR.

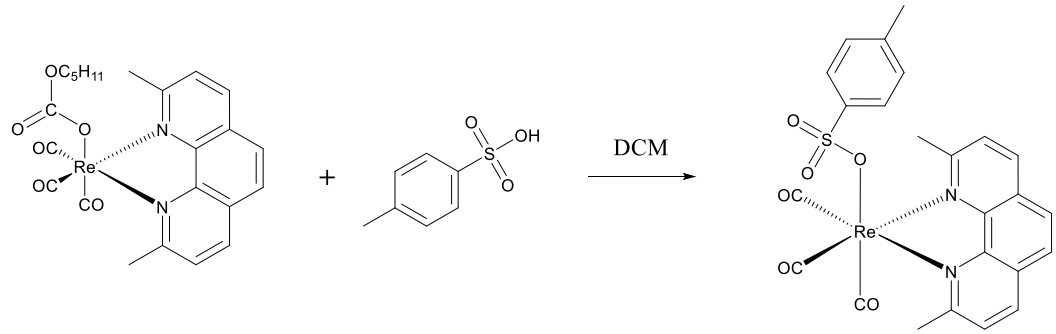

TOS4

Scheme 29: Synthesis of TOS4

Figures 75 and 76 below show the IR and ^1H NMR of TOS4. In the IR spectrum (Figure 75) of **TOS4**, the three υ(C≡O)'s at 2030(s), 1923(s) and 1904(s) cm^{-1} confirms the fac geometry of the complex. In the ^1H NMR spectrum (Figure 76), the doublet at 8.21 ppm represents the similar meta toluene protons. The singlet at 7.72 ppm represents the similar protons at positions 5 and 6 of the phenanthroline ring. The doublet at 7.60 ppm represents the similar ortho toluene protons. The doublet at 7.19 ppm represents the similar protons at positions 3 and 8 of the phenanthroline ring. The doublet of doublets at 6.90 ppm represents the similar protons at positions 4 and 7 of the phenanthroline ring. The singlet at 3.14 ppm represents the methyl group protons on positions 2 and 9 of the phenanthroline ring. The singlet at 2.19 ppm represents the methyl group protons on the toluene ring. The molecular structure (Figure 77) of the complex has been conclusively established through X-ray crystallography. As expected, the central Re atom is

coordinated to three facial CO's, two N atoms of the chelated ligand and the tosylate anion.

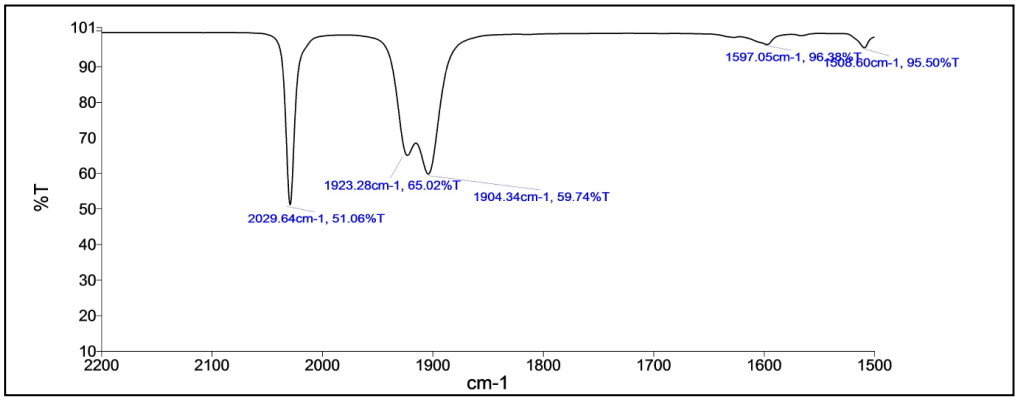

Figure 75: IR spectrum of TOS4 in dichloromethane

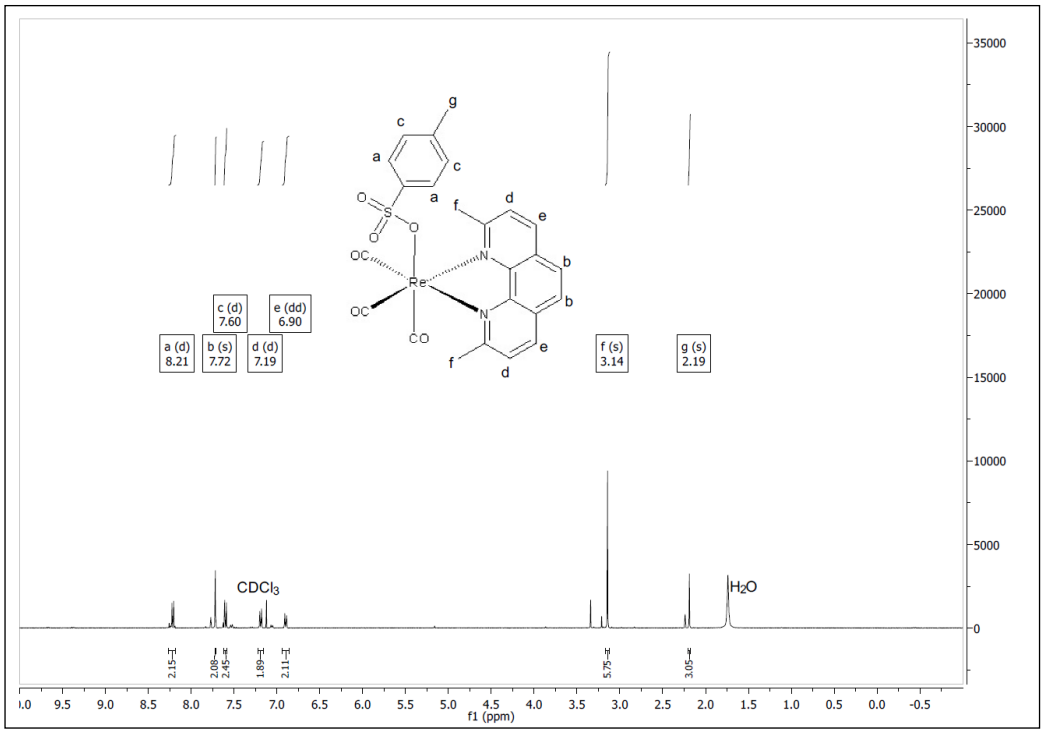

Figure 76: ^{1}H NMR spectrum of TOS4

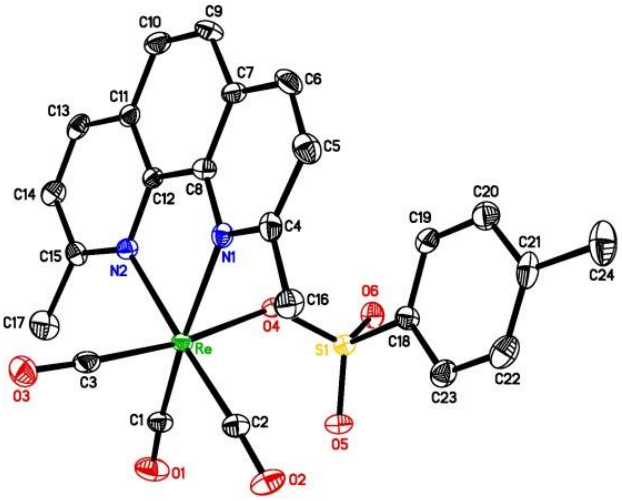

Figure 77: X-ray structure of TOS4

3. 2. 2. 25. *fac*-$(CO)_3$(5,6-dimethyl-1,10-phenanthroline) $ReOS(O_2)C_7H_7$ (TOS5)

TOS5 was synthesized from a one-pot reaction of PC5 and *p*-Toluenesulfonic acid in dichloromethane solvent according to Scheme 30 below. The yellow crystals (72%) of TOS5 were characterized using ^{1}H NMR.

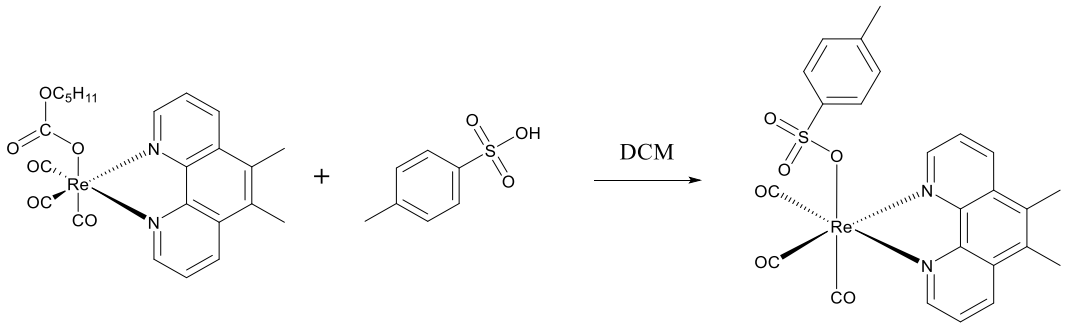

TOS5

Scheme 30: Synthesis of TOS5

TOS5 has been characterized through spectroscopic and crystallographic determinations. The IR spectrum (Figure 78) exhibits three υ(C≡O)'s at 2029(s), 1926(s) and 1905(s) cm^{-1} representing a facial geometry of the complex. In the ^{1}H NMR spectrum (Figure 79) of **TOS5**, the doublet of doublets at 9.17 ppm represents the similar protons

at positions 2 and 9 of the phenanthroline ring. The doublet of doublets at 8.59 ppm represents the similar protons at positions 3 and 8 of the phenanthroline ring. The doublet of doublets at 7.73 ppm represents the similar protons at positions 4 and 7 of the phenanthroline ring. The doublet at 7.31 ppm represents the similar meta toluene protons. The doublet at 6.92 ppm represents the similar ortho toluene protons. The singlet at 2.67 ppm represents the methyl group protons on positions 5 and 6 of the phenanthroline ring. The singlet at 2.20 ppm represents the methyl group protons on the toluene ring. The X-ray structure (Figure 80) of **TOS5** exhibits three facial CO's, two N atoms of the chelated ligand and the tosylate anion coordinated to the central Re atom.

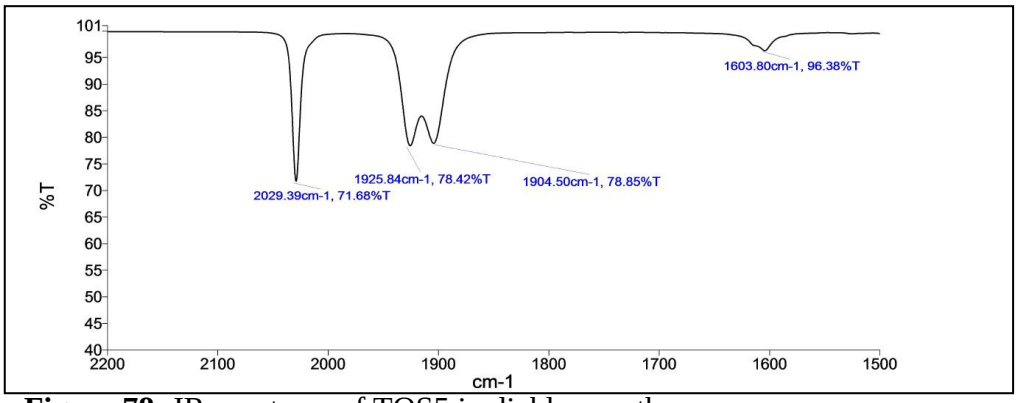

Figure 78: IR spectrum of TOS5 in dichloromethane

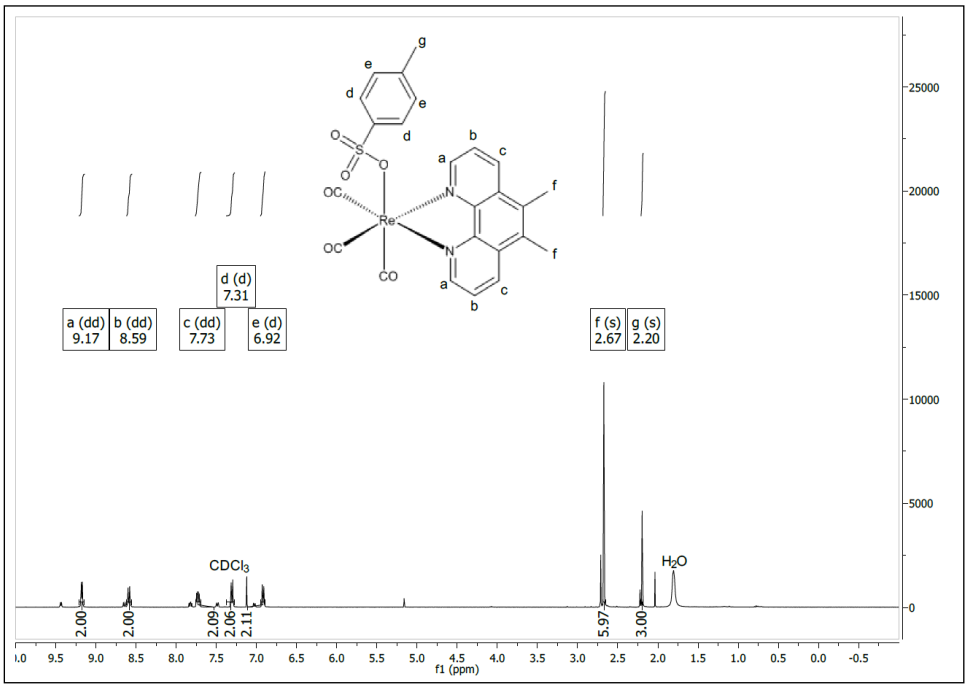

Figure 79: ^{1}H NMR spectrum of TOS5

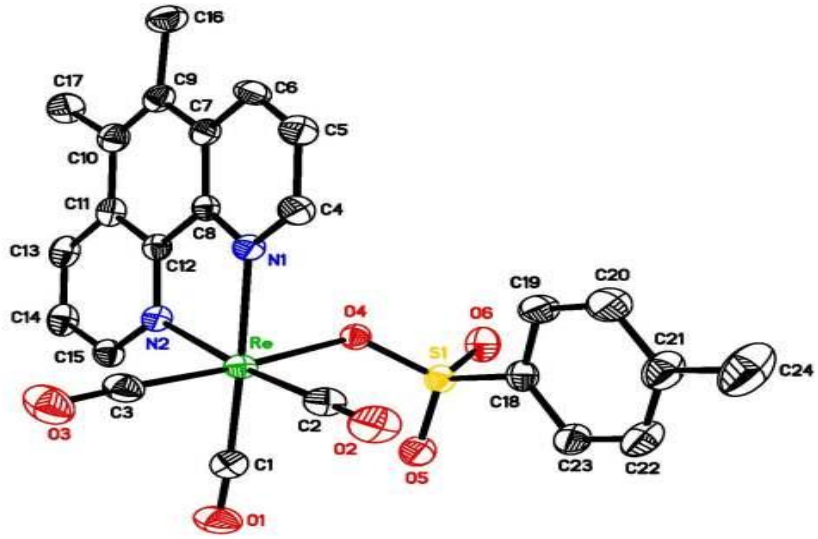

Figure 80: X-ray structure of TOS5

3. 2. 2. 26. *fac*-(CO)$_3$(4,7-diphenyl-1,10-phenanthroline) ReOS(O$_2$)C$_7$H$_7$ (TOS6)

TOS6 was synthesized from a one-pot reaction of PC6 and *p*-Toluenesulfonic acid in dichloromethane solvent according to Scheme 31 below. The yellow crystals (78%) of TOS6 were characterized using ^{1}H NMR.

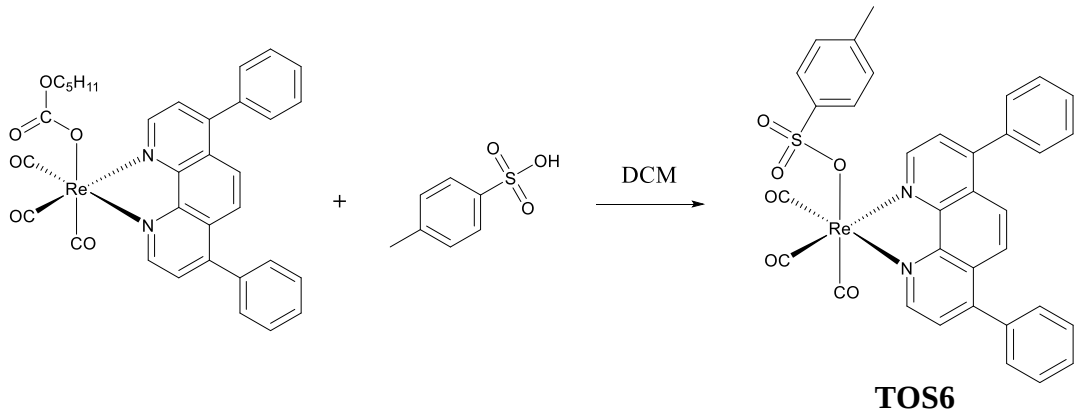

TOS6

Scheme 31: Synthesis of TOS6

Figures 81, 82 and 83 below show the IR, ^{1}H NMR and ^{13}C NMR of **TOS6**. The IR spectrum (Figure 81) of the complex exhibit three υ(C≡O)'s at 2029(s), 1927(s) and 1905(s) cm^{-1} confirming a facial geometry of **TOS6**. In the ^{1}H NMR spectrum (Figure 82) of **TOS6**, the doublet at 9.39 ppm represents the similar meta toluene protons. The singlet at 8.04 ppm represents the similar protons at positions 5 and 6 of the phenanthroline ring. The doublet at 7.78 ppm represents the similar ortho toluene protons. The multiplet at 7.65–7.55 ppm represents the overlap of similar protons at positions 3 and 8 of the phenanthroline ring and the benzene ring protons attached to positions 4 and 7 of the phenanthroline ring. The doublet at 7.12 ppm represents the similar protons at positions 2 and 9 of the phenanthroline ring. The singlet at 2.34 ppm represents the methyl group protons on the toluene ring.

The ^{13}C NMR spectrum (Figure 83) accounts for the three terminal CO's (as two singlets), 14 aromatic carbons and one methyl carbon. In the phenanthroline ligand component of the TOS6 structure, there are 12 carbon types on the ligand represented as peaks in the ^{13}C NMR spectra. There are two carbon types on the toluene ring that represent four carbons and appear as two distinct peaks in the ^{13}C spectra. The two

quaternary carbons on that ring appear as two distinct peaks and the methyl carbon appears as a peak at 21.41 ppm. The peaks at 196.34 and 192.24 ppm represent the CO carbons connected to the Re center.

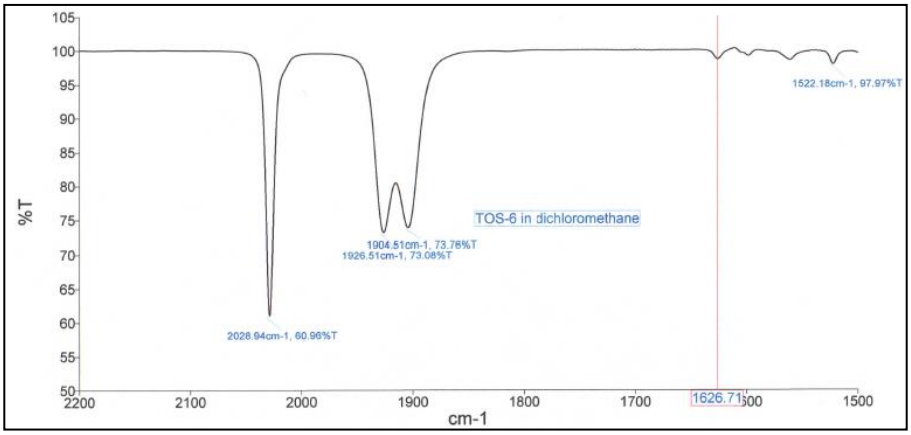

Figure 81: IR spectrum of TOS6 in dichloromethane

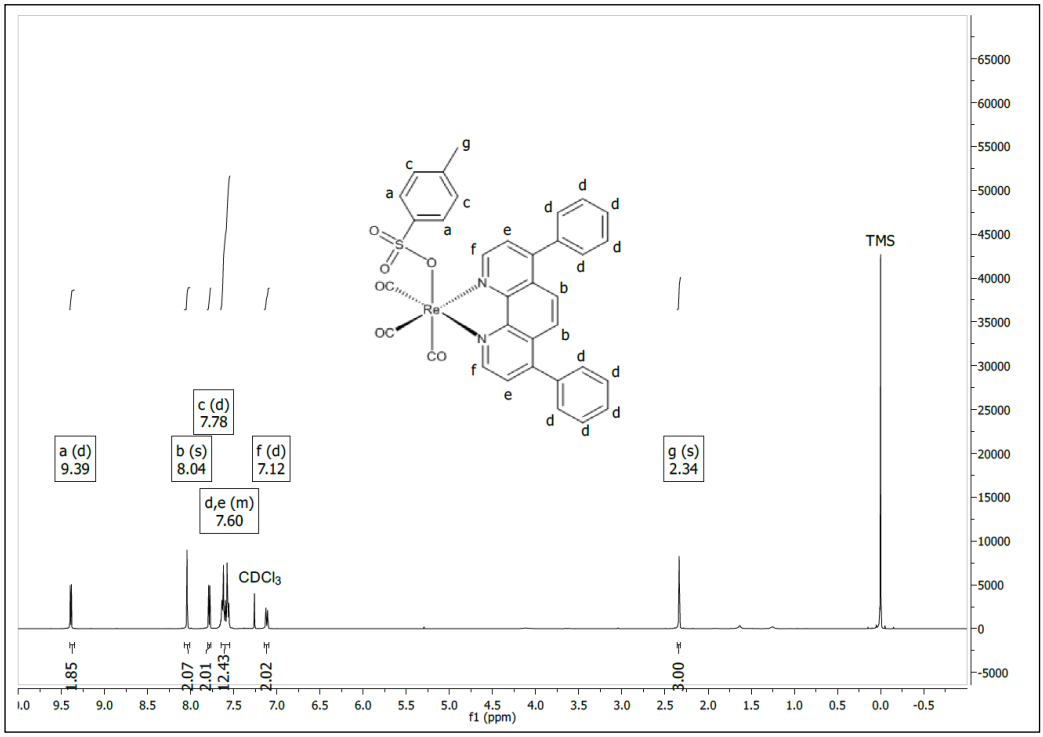

Figure 82: ^{1}H NMR spectrum of TOS6

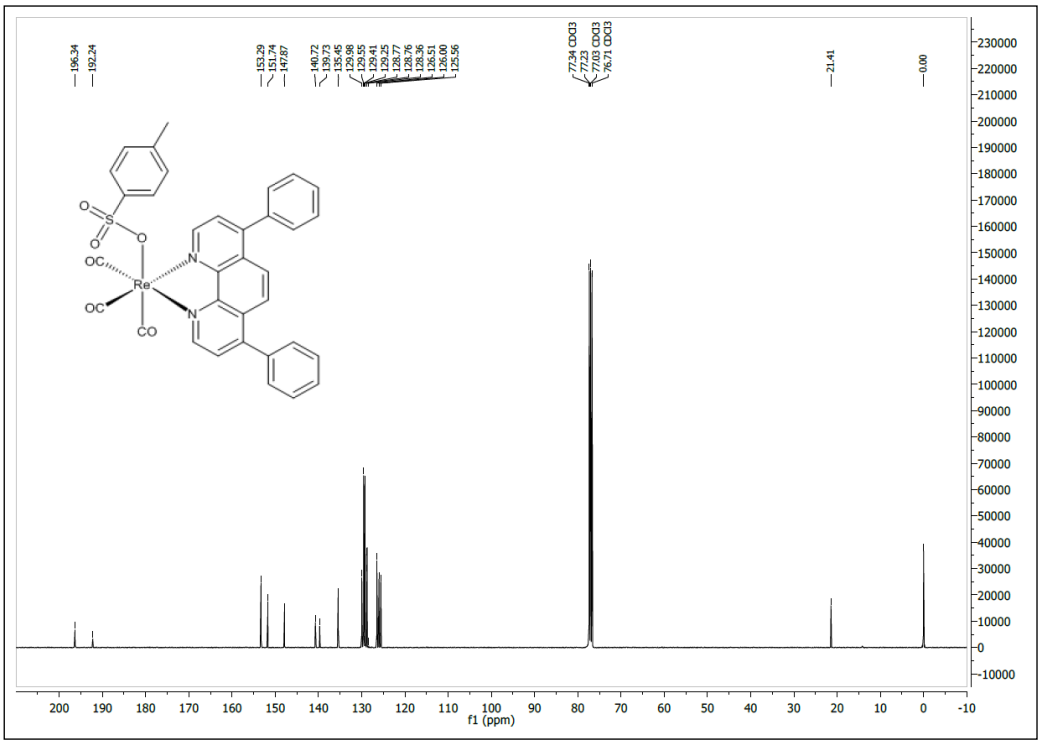

Figure 83: ^{13}C NMR spectrum of TOS6

3. 2. 2. 27. *fac*-$(CO)_3$(2,9-dimethyl-4,7-diphenyl-1,10-phenanthroline) $ReOS(O_2)C_7H_7$ (TOS7)

TOS7 was synthesized from a one-pot reaction of PC7 and *p*-Toluenesulfonic acid in dichloromethane solvent according to Scheme 32 below. The yellow crystals (80%) of TOS7 were characterized using ^{1}H NMR.

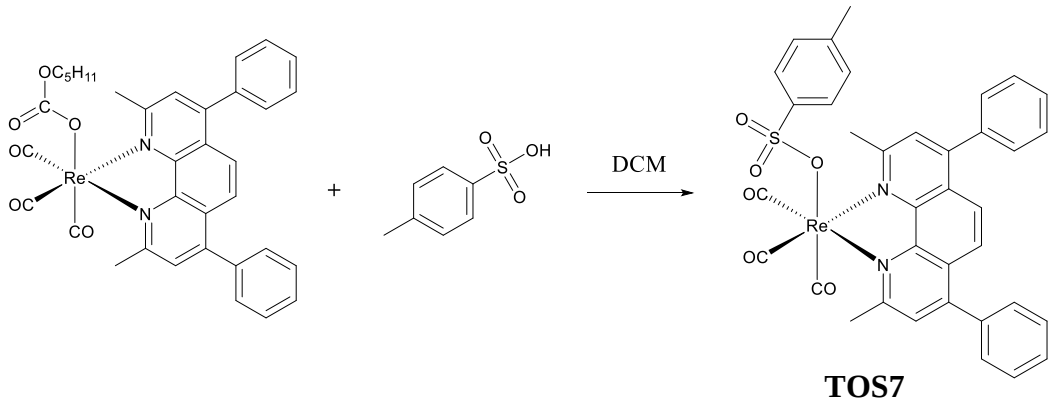

Scheme 32: Synthesis of TOS7

TOS7 has been characterized spectroscopically using IR and NMR spectroscopic techniques. In the IR spectrum (Figure 84) of **TOS7**, the three υ(C≡O)'s at 2028(s), 1923(s) and 1903(s) cm^{-1} represent the three terminal CO's bonded facially to the Re center. In the ^{1}H NMR spectrum (Figure 85) of **TOS7**, the singlet at δ7.86 represents the similar protons at positions 3 and 8 of the phenanthroline ring. The singlet at δ7.67 represents the similar protons at positions 5 and 6 of the phenanthroline ring. The multiplet at δ7.61 – 7.56 represents 6 similar protons on the benzene ring attached to positions 4 and 7 of the phenanthroline ring. The multiplet at δ7.54–7.50 represents 4 similar protons on the benzene ring attached to positions 4 and 7 of the phenanthroline ring. The doublet at δ7.43 represents the similar meta toluene protons. The doublet at δ 7.06 represents the similar ortho toluene protons. The singlet at δ3.31 represents the methyl group protons on positions 2 and 9 of the phenanthroline ring. The singlet at δ2.30 represents the methyl group protons on the toluene ring.

In the ^{13}C NMR spectrum (Figure 86), the three terminal CO's are observed as two singlets at δ196 and 192. The expected 14 aromatic carbons are observed in the region δ163–124. The methyl group attached to the phenanthroline ligand is observed at δ31 and the methyl group attached to the para position of tolyl group is relatively shielded and is observed at δ21.

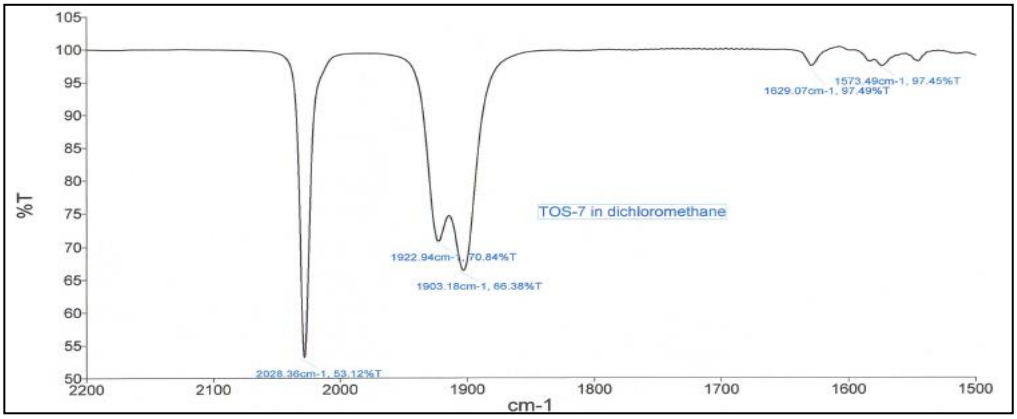

Figure 84: IR spectrum of TOS7 in dichloromethane

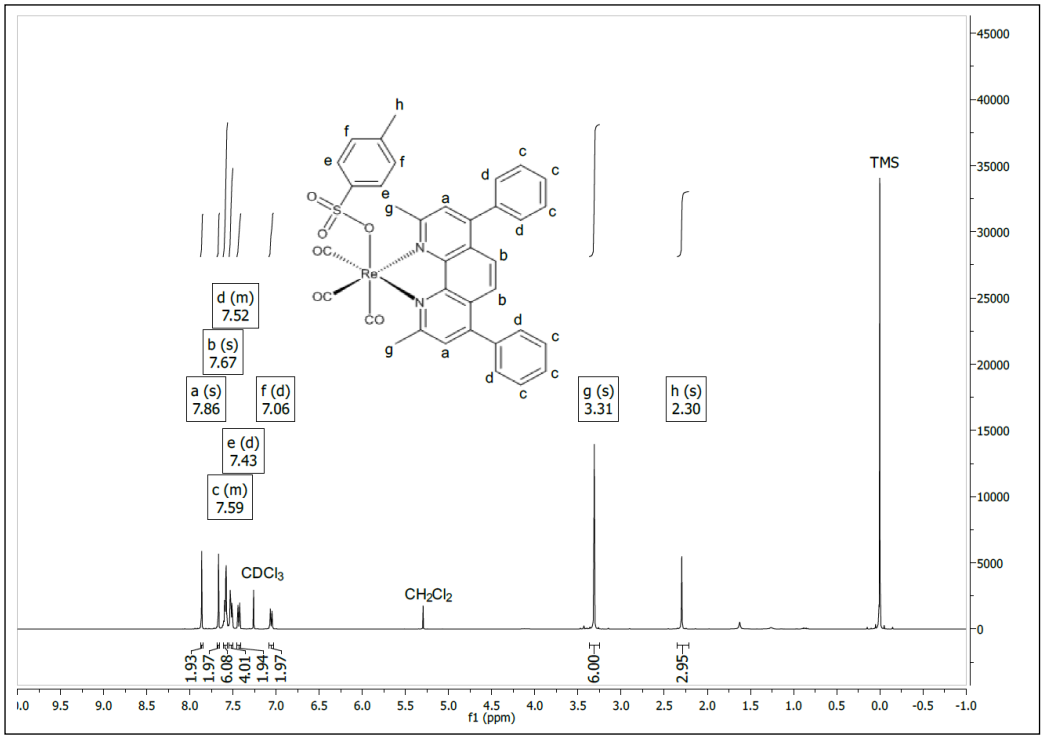

Figure 85: ^{1}H NMR spectrum of TOS7

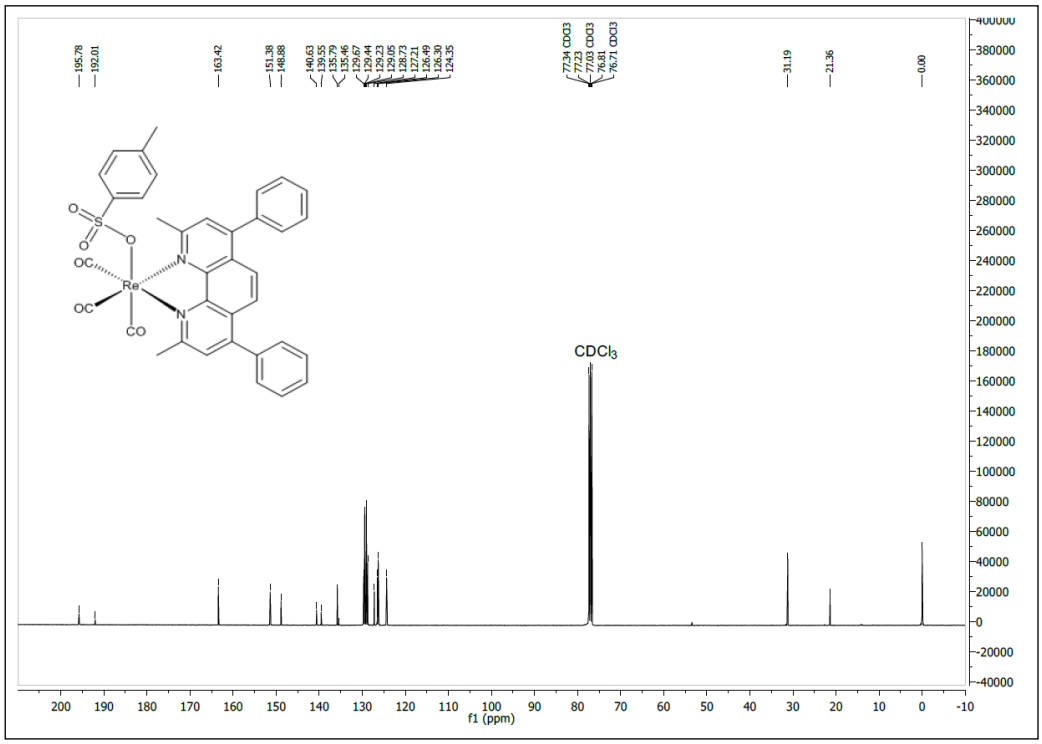

Figure 86: ^{13}C NMR spectrum of TOS7

3. 2. 2. 28. *fac*-(CO)$_3$(4,7-dimethyl-1,10-phenanthroline) ReOS(O$_2$)C$_7$H$_7$ (TOS8)

TOS8 was synthesized from a one-pot reaction of PC8 and *p*-Toluenesulfonic acid in dichloromethane solvent according to Scheme 33 below. The yellow crystals (75%) of TOS8 were characterized using ^{1}H NMR.

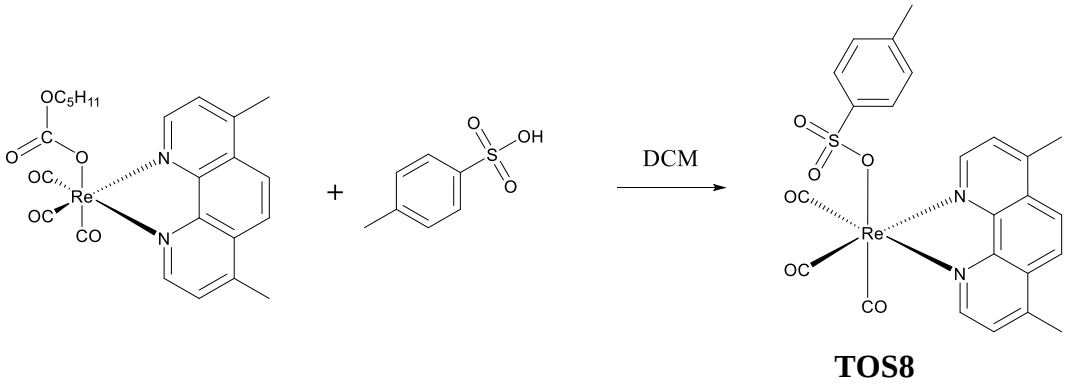

Scheme 33: Synthesis of TOS8

TOS8 has been characterized spectroscopically. In the IR spectrum (Figure 87), the υ(C≡O)'s are observed at 2029(s), 1925(s) and 1903(s) cm^{-1} confirming the facial geometry of the complex. In the ^{1}H NMR spectrum (Figure 88) of **TOS8**, the doublet at 9.07 ppm represents the similar protons at positions 2 and 9 of the phenanthroline ring. The singlet at 8.02 ppm represents the similar protons at positions 5 and 6 of the phenanthroline ring. The doublet at 7.53 ppm represents the similar meta toluene protons. The doublet at 7.33 ppm represents the similar protons at positions 3 and 8 of the phenanthroline ring. The doublet at 6.93 ppm represents the similar ortho toluene protons. The singlet at 2.80 ppm represents the methyl group protons on positions 4 and 7 of the phenanthroline ring. The singlet at 2.21 ppm represents the methyl group protons on the toluene ring.

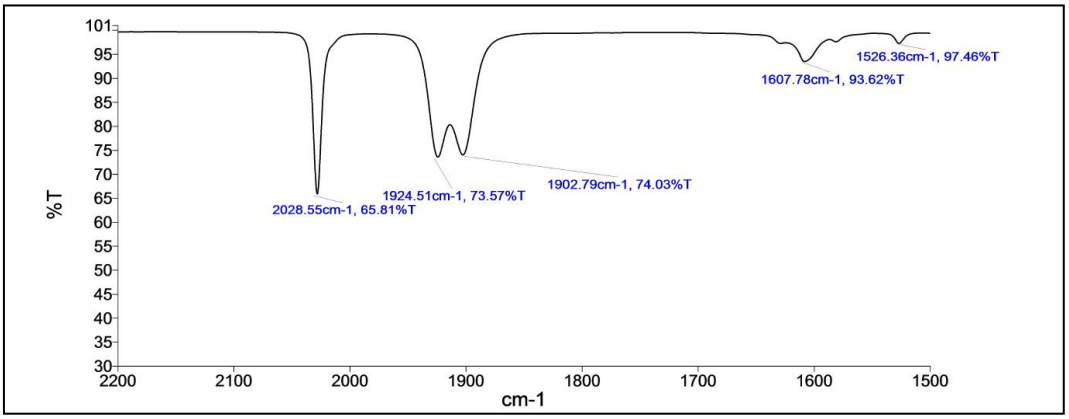

Figure 87: IR spectrum of TOS8 in dichloromethane

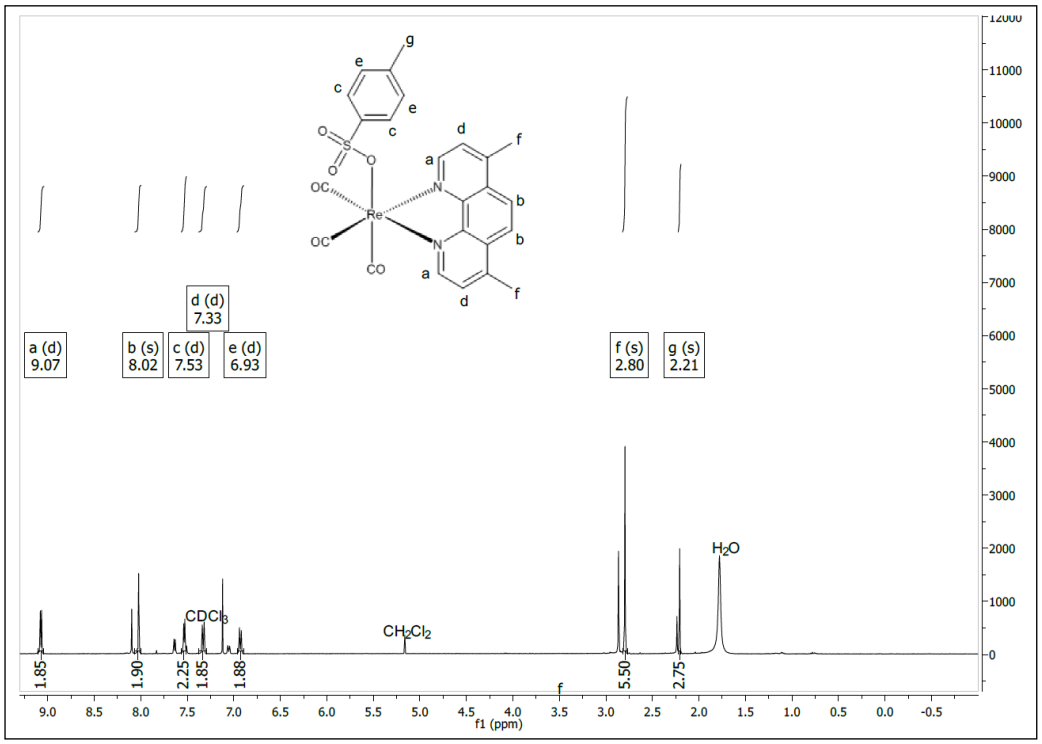

Figure 88: ^{1}H NMR spectrum of TOS8

3. 2. 2. 29. *fac*-(CO)$_3$(3,4,7,8-tetramethyl-1,10-phenanthroline) ReOS(O$_2$)C$_7$H$_7$ (TOS9)

TOS9 was synthesized from a one-pot reaction of PC9 and *p*-Toluenesulfonic acid in dichloromethane solvent according to Scheme 34 below. The yellow crystals (80%) of TOS9 were characterized using ^{1}H NMR.

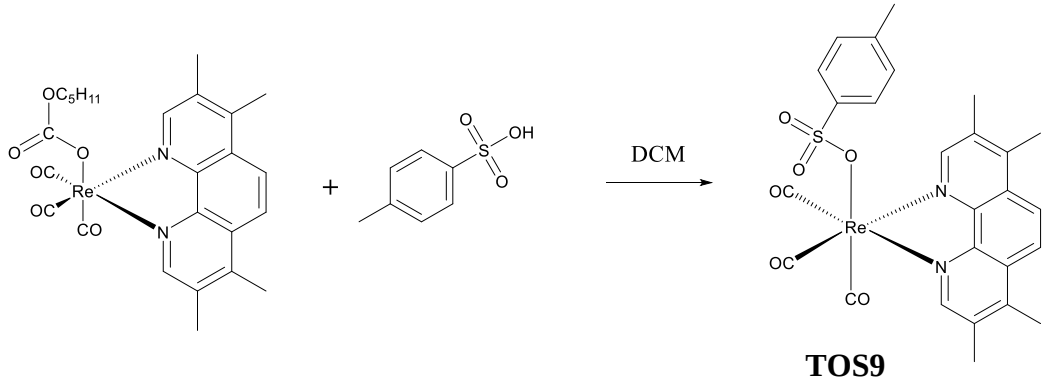

TOS9

Scheme 34: Synthesis of TOS9

TOS9 has been characterized through IR and ^{1}H NMR spectroscopic techniques. The IR spectrum (Figure 89) shows three strong $\upsilon(C\equiv O)$'s at 2028, 1923 and 1901 cm^{-1} suggesting a facial geometry of the complex. In the ^{1}H NMR spectrum (Figure 90), the doublet at 9.11 ppm represents the similar meta toluene protons. The doublet at 8.39 ppm represents the similar ortho toluene protons. The singlet at 6.89 ppm represents the similar protons at positions 2 and 9 of the phenanthroline ring. The singlet at 6.87 ppm represents the similar protons at positions 5 and 6 of the phenanthroline ring. The singlet at 5.63 ppm represents the similar methyl group protons at positions 3 and 8 of the phenanthroline ring. The singlet at 2.68 ppm represents the methyl group protons on positions 4 and 7 of the phenanthroline ring. The singlet at 2.30 ppm represents the methyl group protons on the toluene ring.

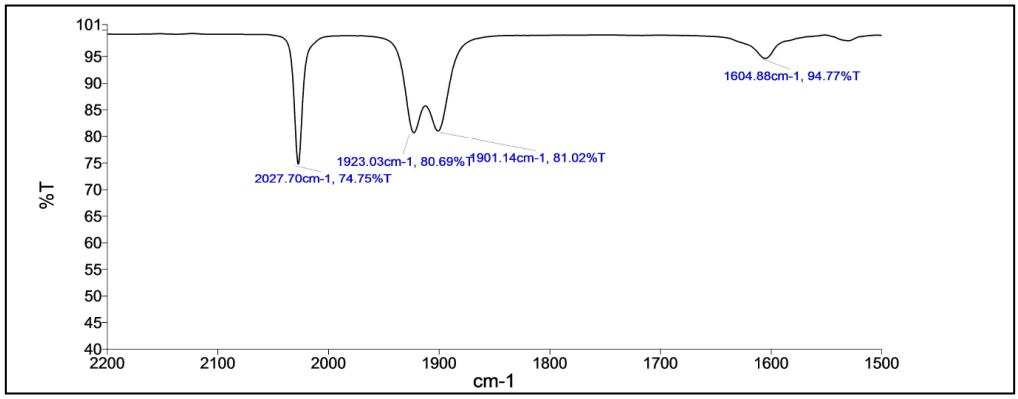

Figure 89: IR spectrum of TOS9 in dichloromethane

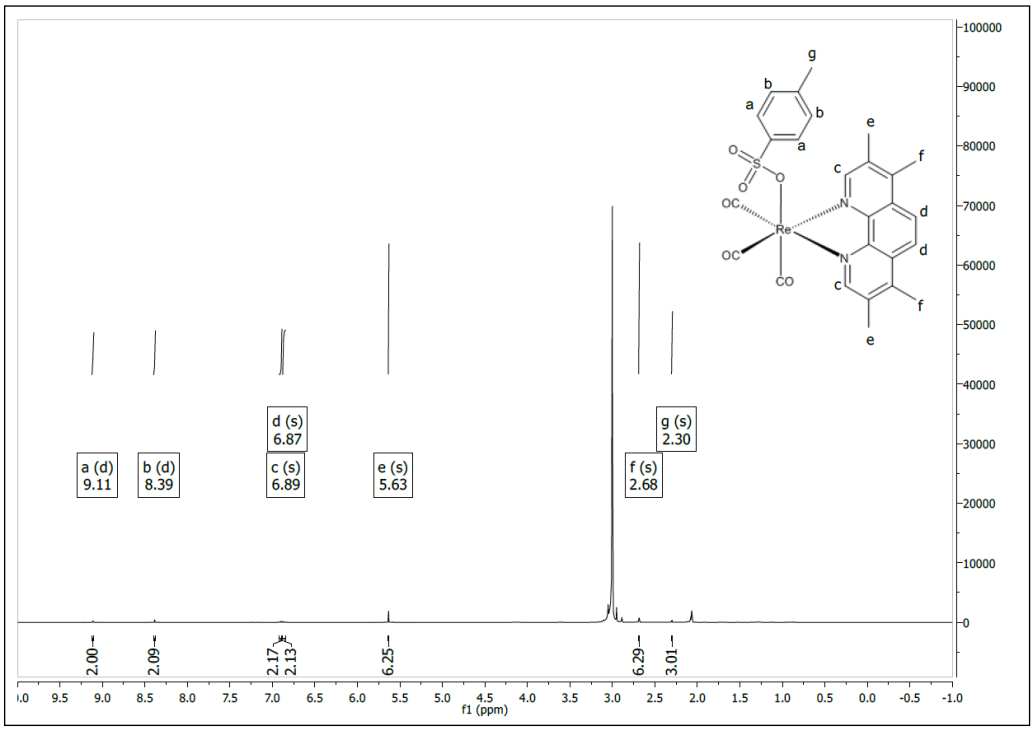

Figure 90: ^{1}H NMR spectrum of TOS9

3. 2. 2. 30. *fac*-(CO)$_3$(4-methyl-1,10-phenanthroline) ReOS(O$_2$)C$_7$H$_7$ (TOS10)

TOS10 was synthesized from a one-pot reaction of PC10 and *p*-Toluenesulfonic acid in dichloromethane solvent according to Scheme 35 below. The yellow crystals (75%) of TOS10 were characterized using ^{1}H NMR.

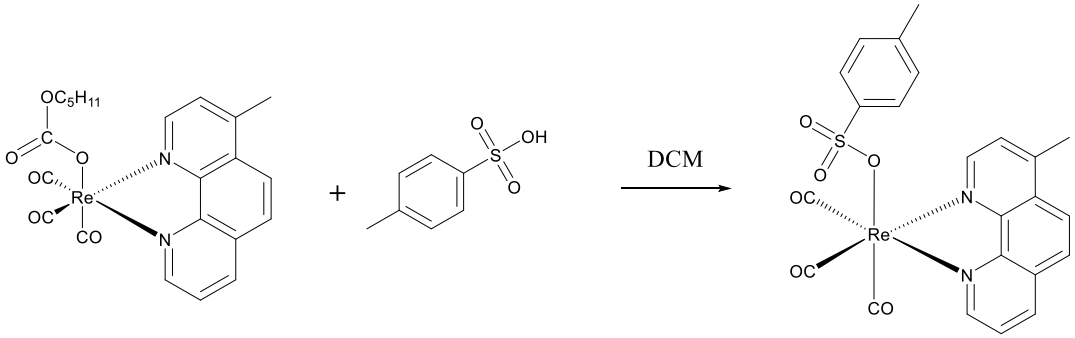

TOS10

Scheme 35: Synthesis of TOS10

Figures 91 and 92 below show the IR and ^{1}H NMR of **TOS10**. In the IR spectrum (Figure 91) of **TOS10**, the three peaks at 2030(s), 1926(s) and 1904(s) cm^{-1} corresponds

to the three υ(C≡O)'s of the three terminal carbonyls. In the ^{1}H NMR spectrum (Figure 92), the doublet of doublets at 9.24 ppm represents the proton at position 9 of the phenanthroline ring. The doublet at 9.08 ppm represents the proton at position 2 of the phenanthroline ring. The multiplet at 8.50–8.41 ppm represents the proton at position 8 of the phenanthroline ring. The multiplet at 8.13–7.94 ppm represents the proton at position 7 of the phenanthroline ring. The doublet at 7.74 ppm represents the proton at position 3 of the phenanthroline ring. The doublet at 7.55 ppm represents the similar meta toluene protons. The doublet at 7.12 ppm represents the similar ortho toluene protons. The doublet at 6.93 ppm represents the protons at positions 5 and 6 of the phenanthroline ring. The singlet at 2.80 ppm represents the methyl group protons on position 4 of the phenanthroline ring. The singlet at 2.21 ppm represents the methyl group protons on the toluene ring.

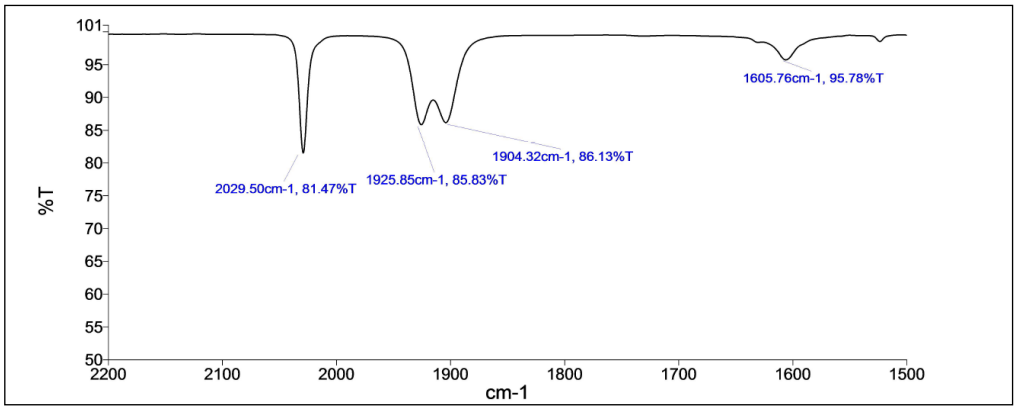

Figure 91: IR spectrum of TOS10 in dichloromethane

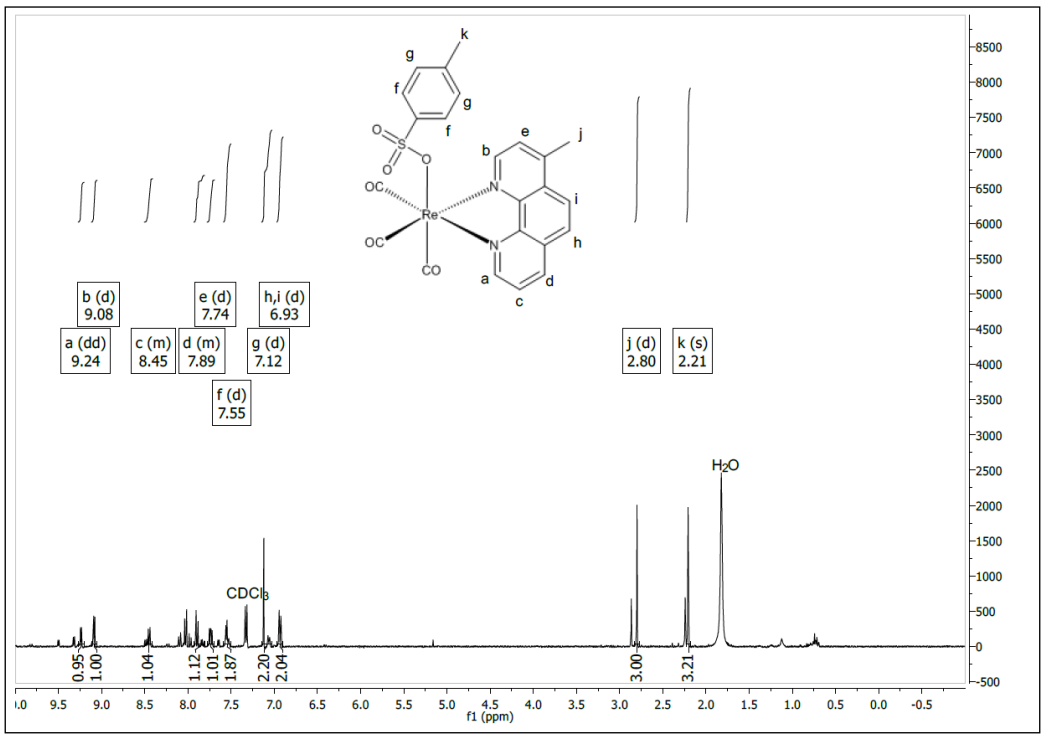

Figure 92: ^{1}H NMR spectrum of TOS10

3. 3. Cytotoxicity Studies

The cytotoxicity studies of the sulfonato complexes (1NS1–1NS8, 2NS1–2NS8, TOS1–TOS8) against breast cancer cells (MCF-7, MDA-MB-231) and normal cell (MCF 10A) were carried out in Wilder's lab[59] as part of a collaboration with our lab. The studies were carried out using Alamar blue assay. Figures 93–96 show the graphs for MCF-7 cell viability studies. As seen from these figures, the graphs show a decreasing trend for the % cell viability.

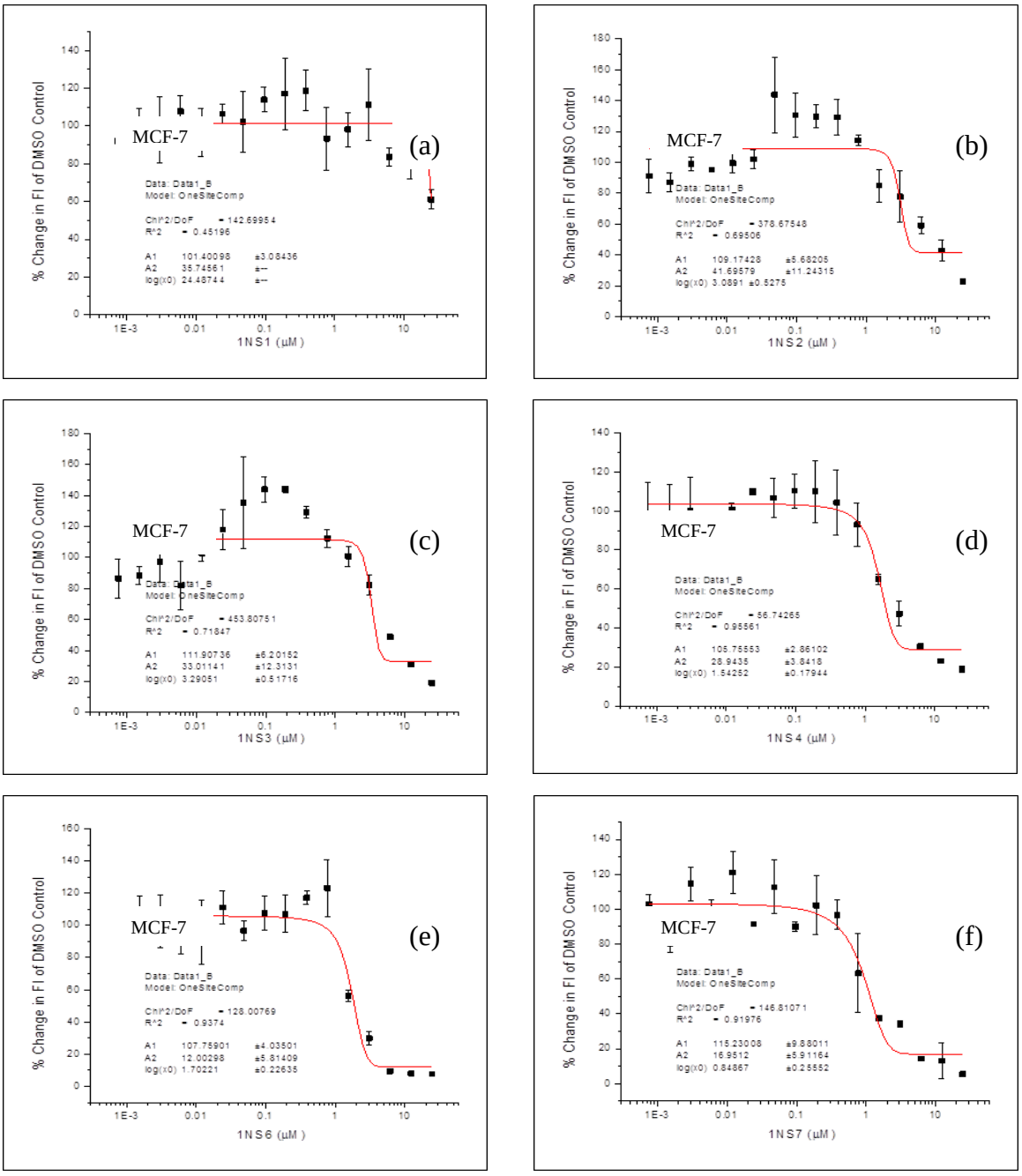

Figure 93: Change in fluorescence intensity after 72-h treatment of MCF-7 breast cancer cells with various concentrations of (a) 1NS1; (b) 1NS2; (c) 1NS3; (d) 1NS4; (e) 1NS6; (f) 1NS7

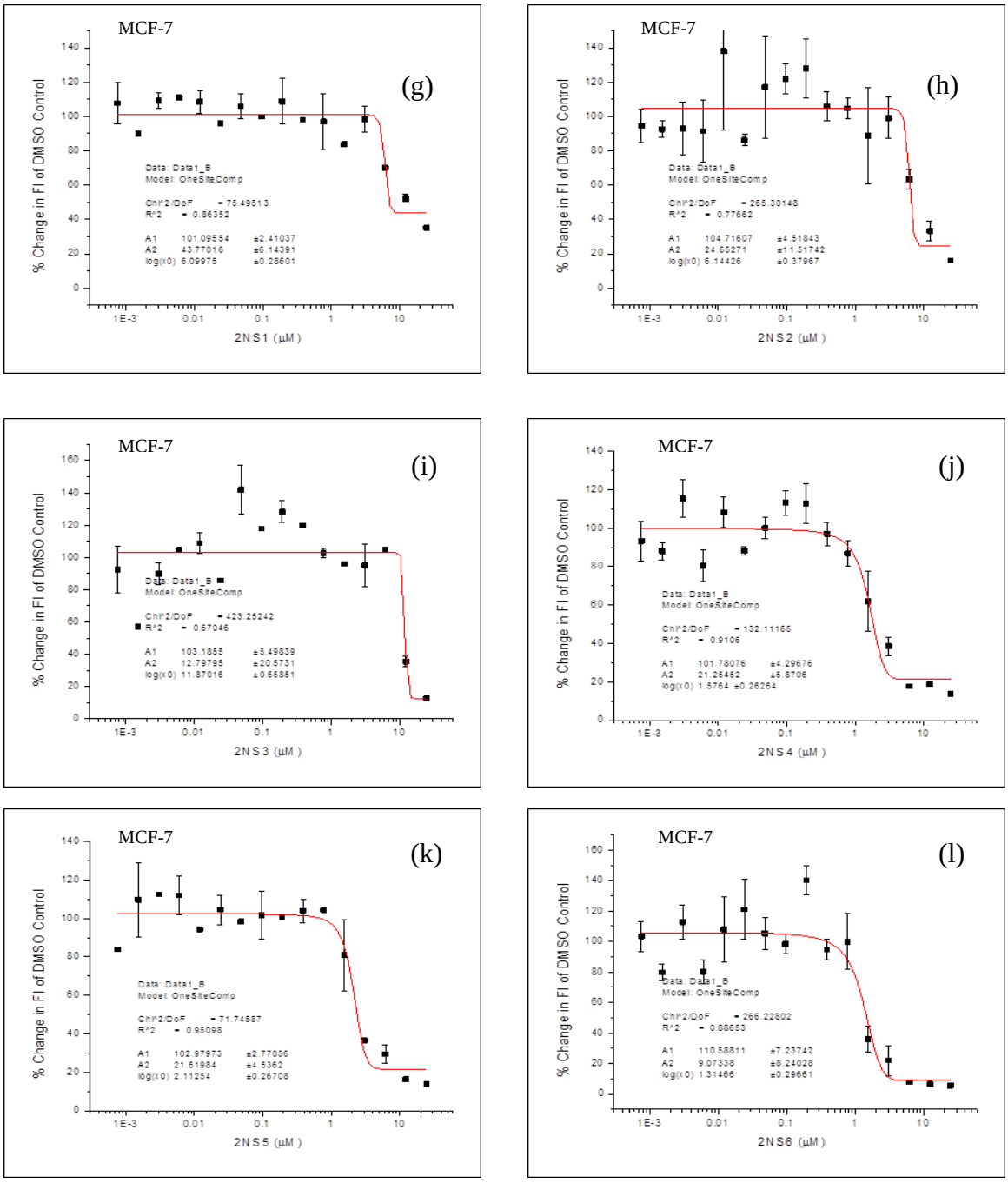

Figure 94: Change in fluorescence intensity after 72-h treatment of MCF-7 breast cancer cells with various concentrations of (g) 2NS1; (h) 2NS2; (i) 2NS3; (j) 2NS4; (k) 2NS5; (l) 2NS6

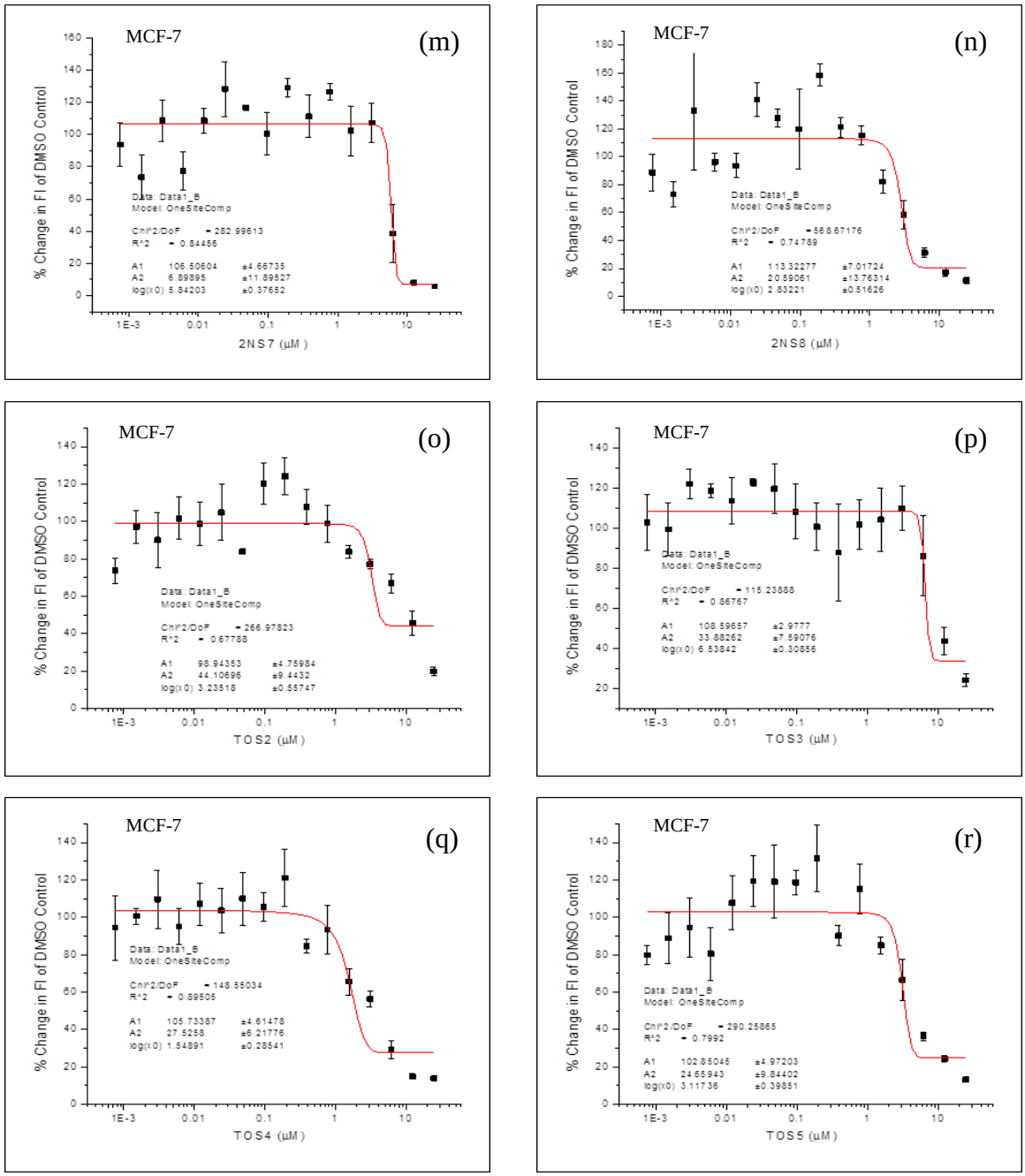

Figure 95: Change in fluorescence intensity after 72-h treatment of MCF-7 breast cancer cells with various concentrations of (m) 2NS7; (n) 2NS8; (o) TOS2; (p) TOS3; (q) TOS4; (r) TOS5

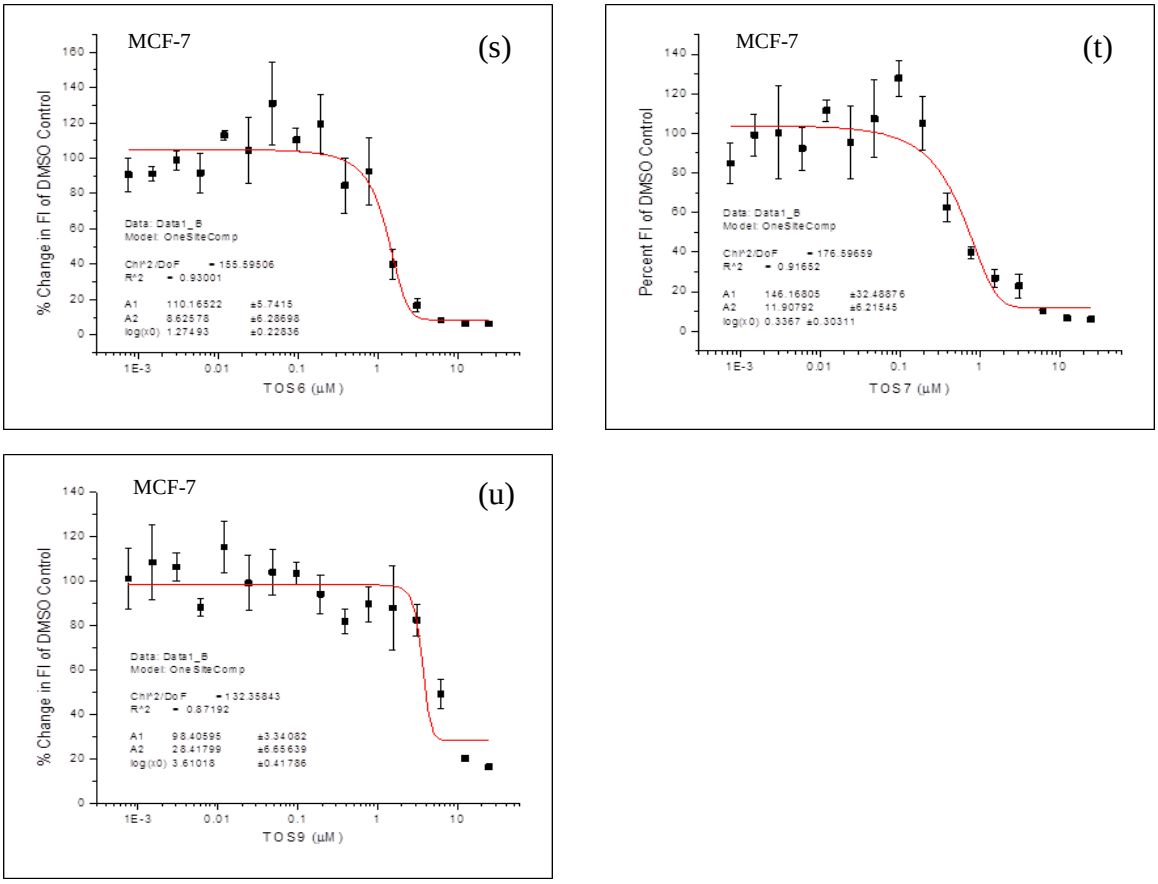

Figure 96: Change in fluorescence intensity after 72-h treatment of MCF-7 breast cancer cells with various concentrations of (s) TOS6; (t) TOS7; (u) TOS9

Figures 97–100 show the graphs for MDA-MB-231 cell viability studies. As seen from these figures, the graphs also show a decreasing trend for the % cell viability (% change in fluorescence compared to control) with increasing concentration.

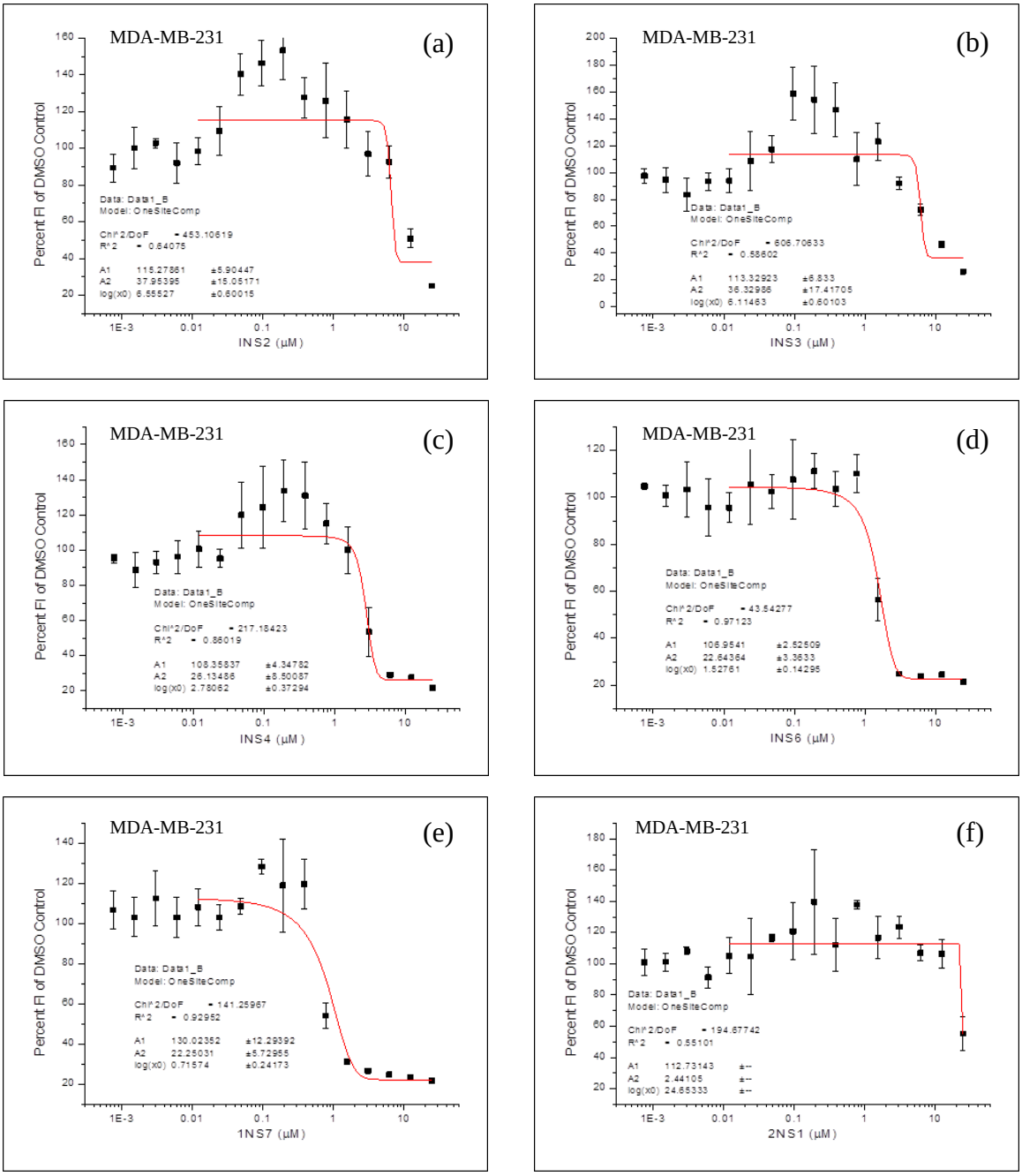

Figure 97: Change in fluorescence intensity after 72-h treatment of MDA-MB-231 breast cancer cells with various concentrations of (a) 1NS2; (b) 1NS3; (c) 1NS4; (d) 1NS6; (e) 1NS7; (f) 2NS1

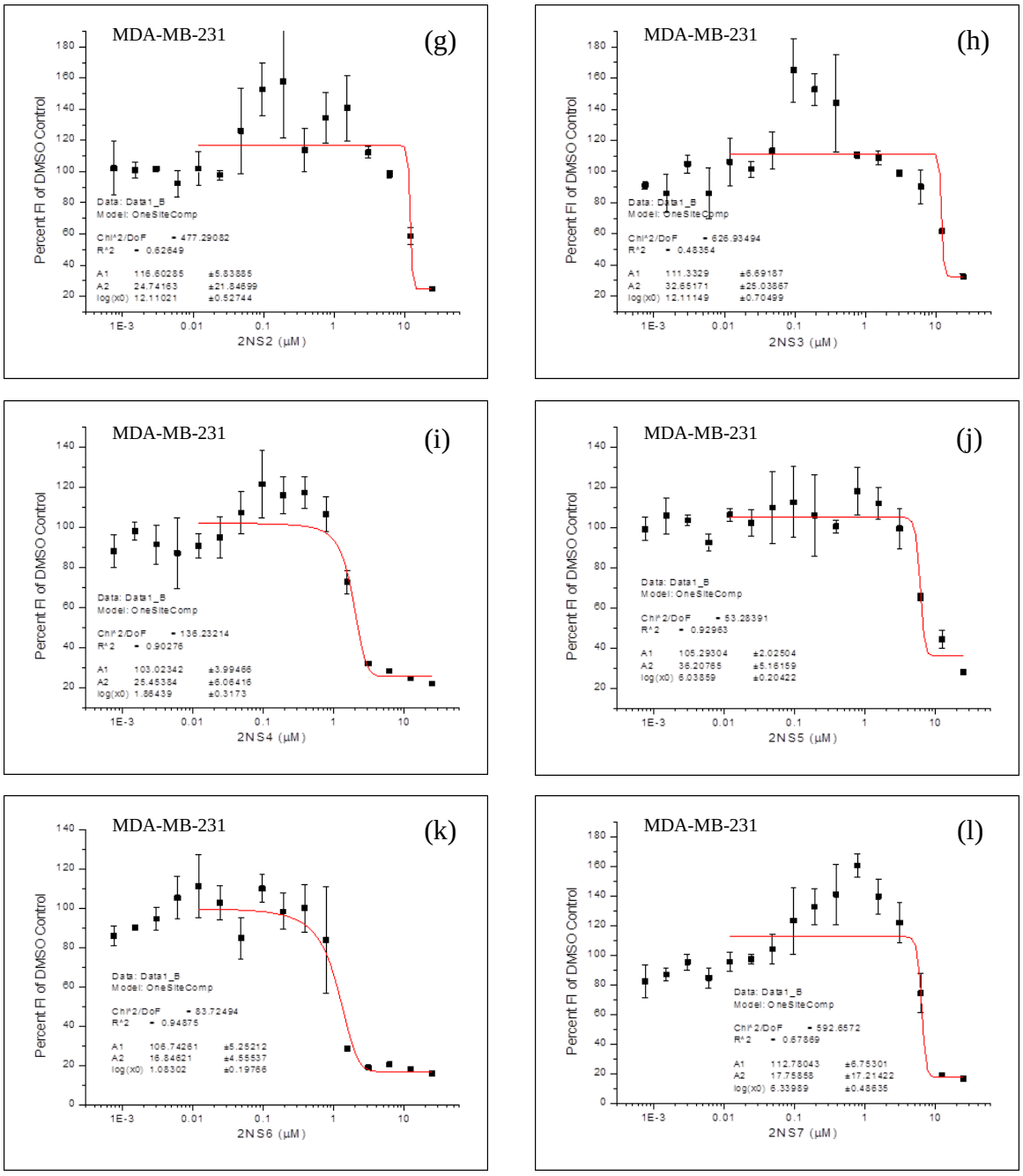

Figure 98: Change in fluorescence intensity after 72-h treatment of MDA-MB-231 breast cancer cells with various concentrations of (g) 2NS2; (h) 2NS3; (i) 2NS4; (j) 2NS5; (k) 2NS6; (l) 2NS7

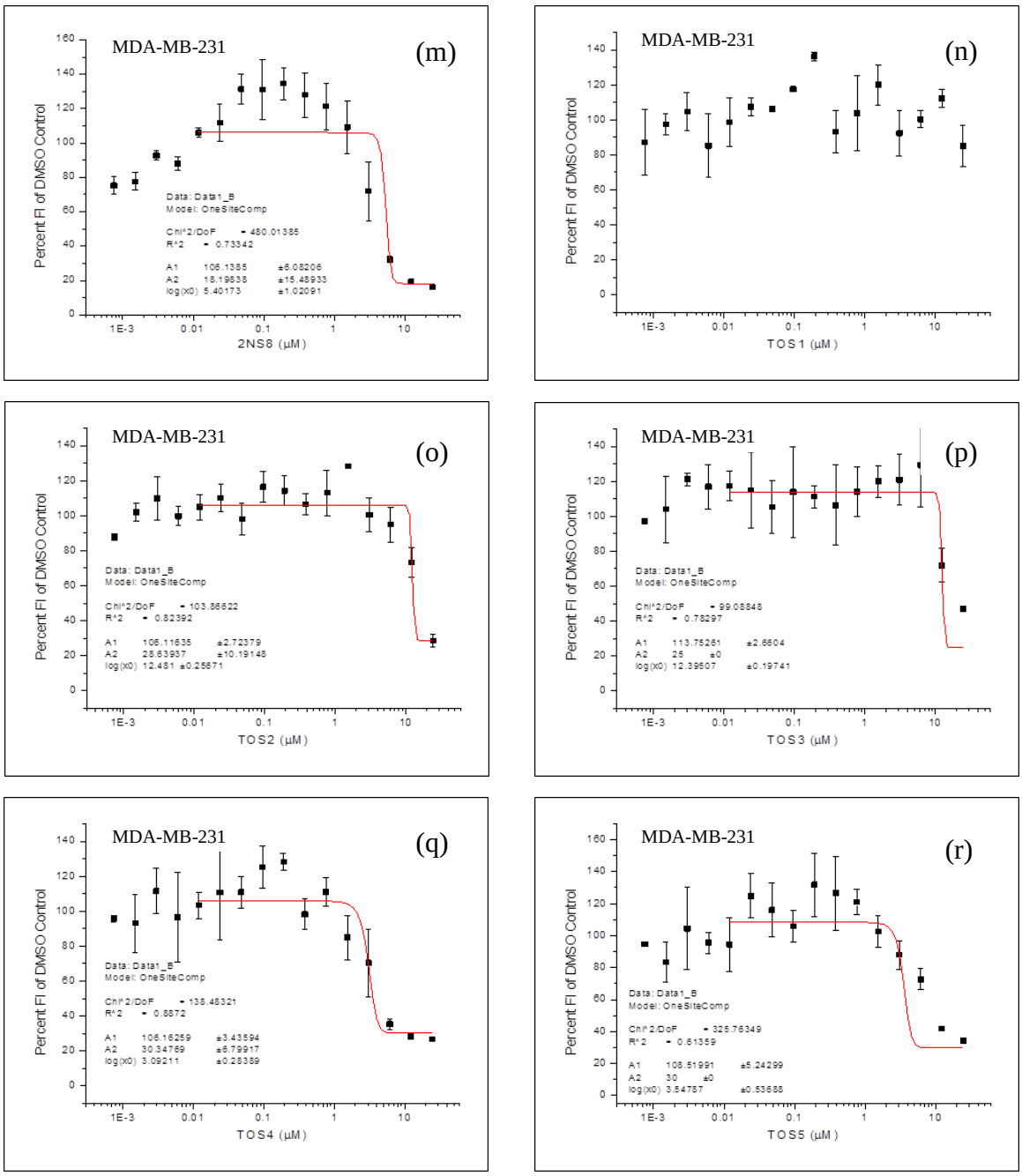

Figure 99: Change in fluorescence intensity after 72-h treatment of MDA-MB-231 breast cancer cells with various concentrations of (m) 2NS8; (n) TOS1; (o) TOS2; (p) TOS3; (q) TOS4; (r) TOS5

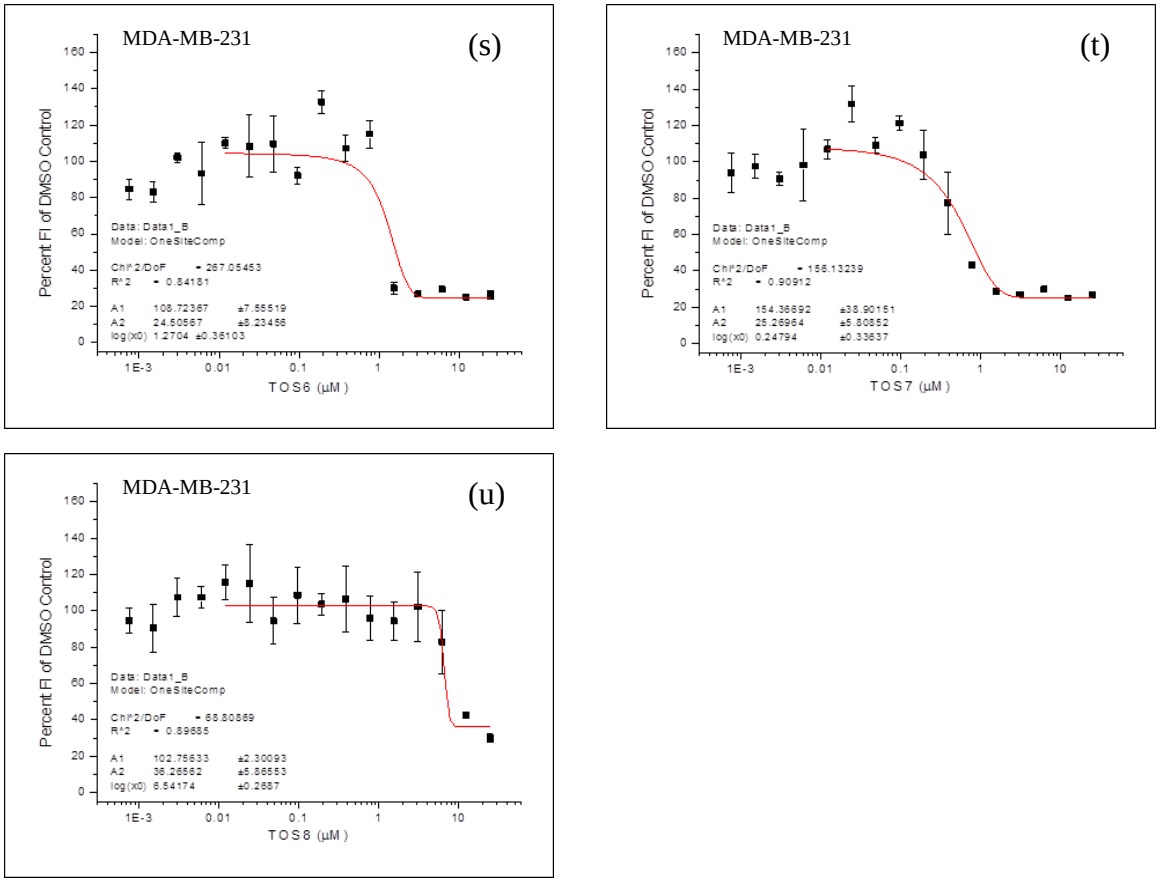

Figure 100: Change in fluorescence intensity after 72-h treatment of MDA-MB-231 breast cancer cells with various concentrations of (s) TOS6; (t) TOS7; (u) TOS8

Figures 101–104 show the viability studies for the human breast epithelial cell line (MCF 10A). As seen from these figures, the graphs also show a decreasing trend for the % cell viability (% change in fluorescence compared to control) with increasing concentration.

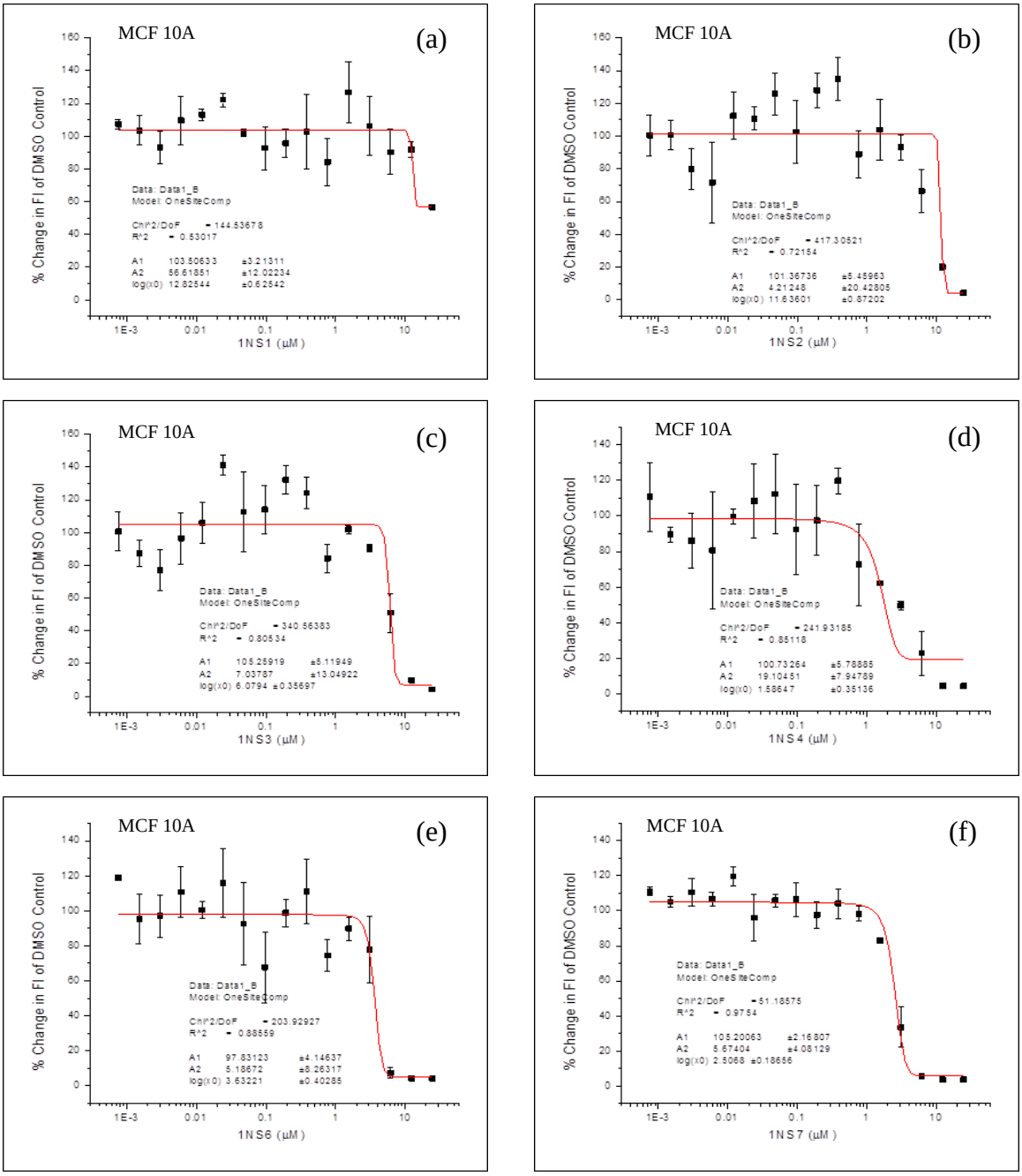

Figure 101: Change in fluorescence intensity after 72-h treatment of MCF 10A breast cells with various concentrations of (a) 1NS1; (b) 1NS2; (c) 1NS3; (d) 1NS4; (e) 1NS6; (f) 1NS7

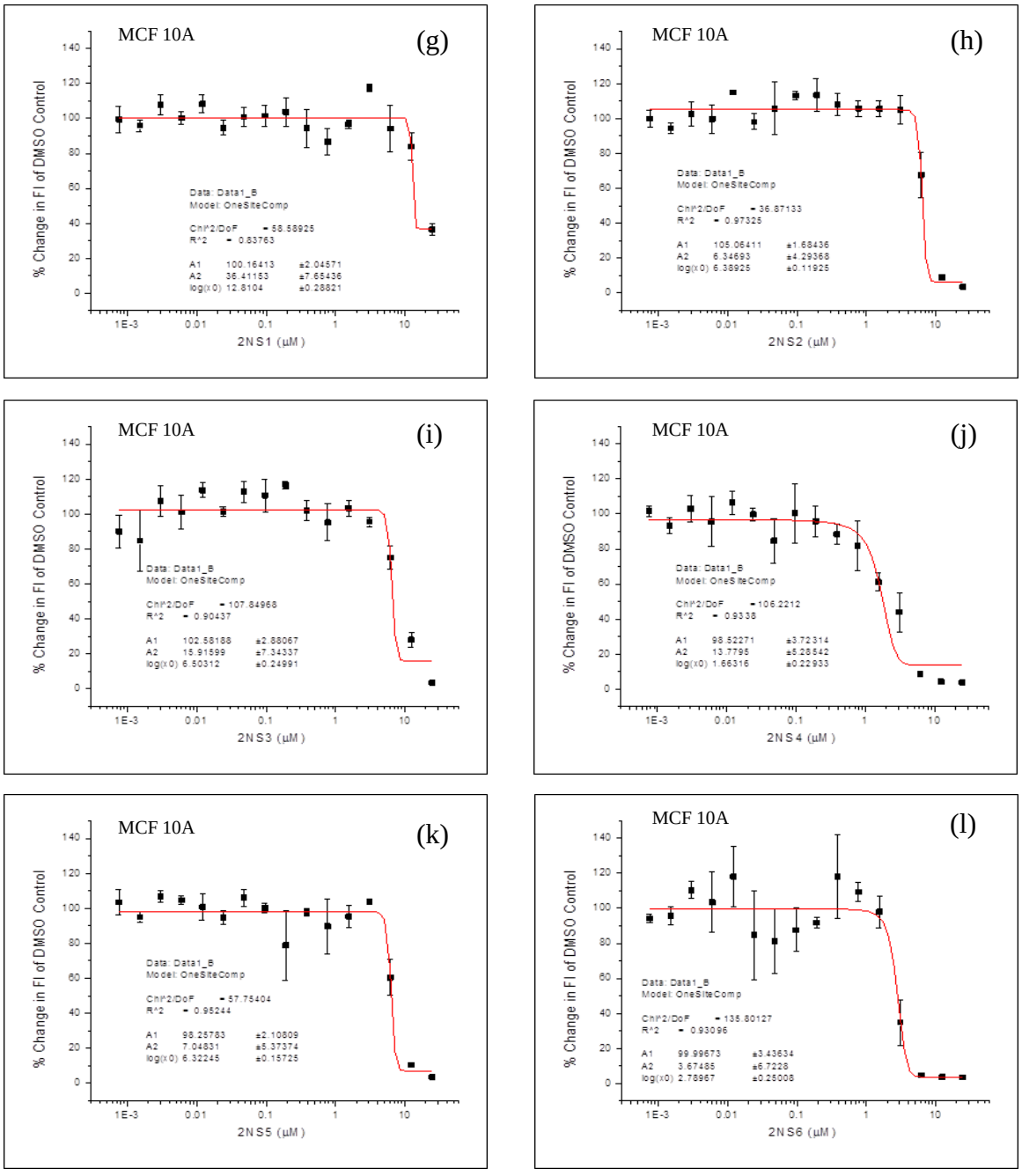

Figure 102: Change in fluorescence intensity after 72-h treatment of MCF 10A breast cells with various concentrations of (g) 2NS1; (h) 2NS2; (i) 2NS3; (j) 2NS4; (k) 2NS5; (l) 2NS6

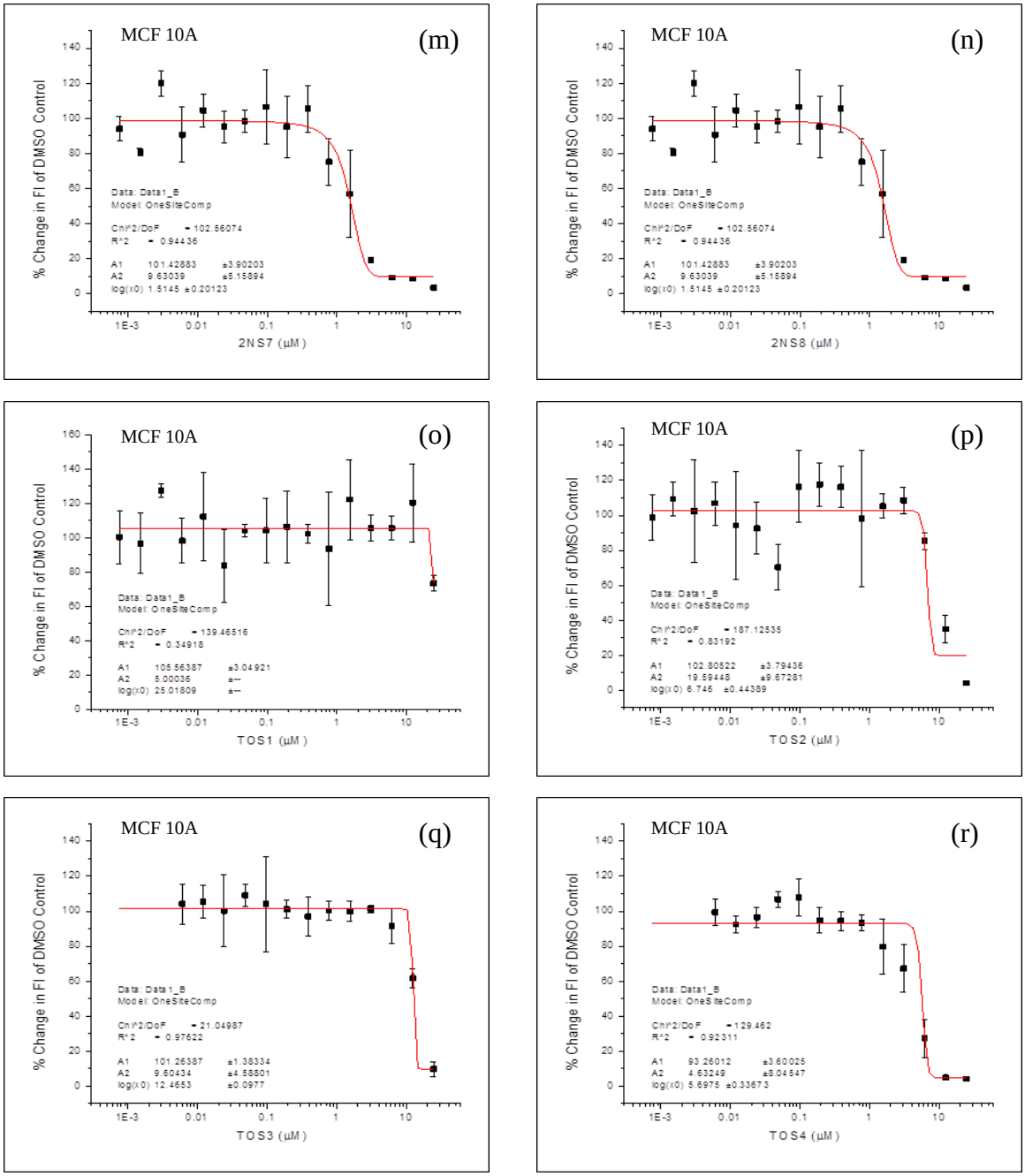

Figure 103: Change in fluorescence intensity after 72-h treatment of MCF 10A breast cells with various concentrations of (m) 2NS7; (n) 2NS8; (o) TOS1; (p) TOS2; (q) TOS3; (r) TOS4

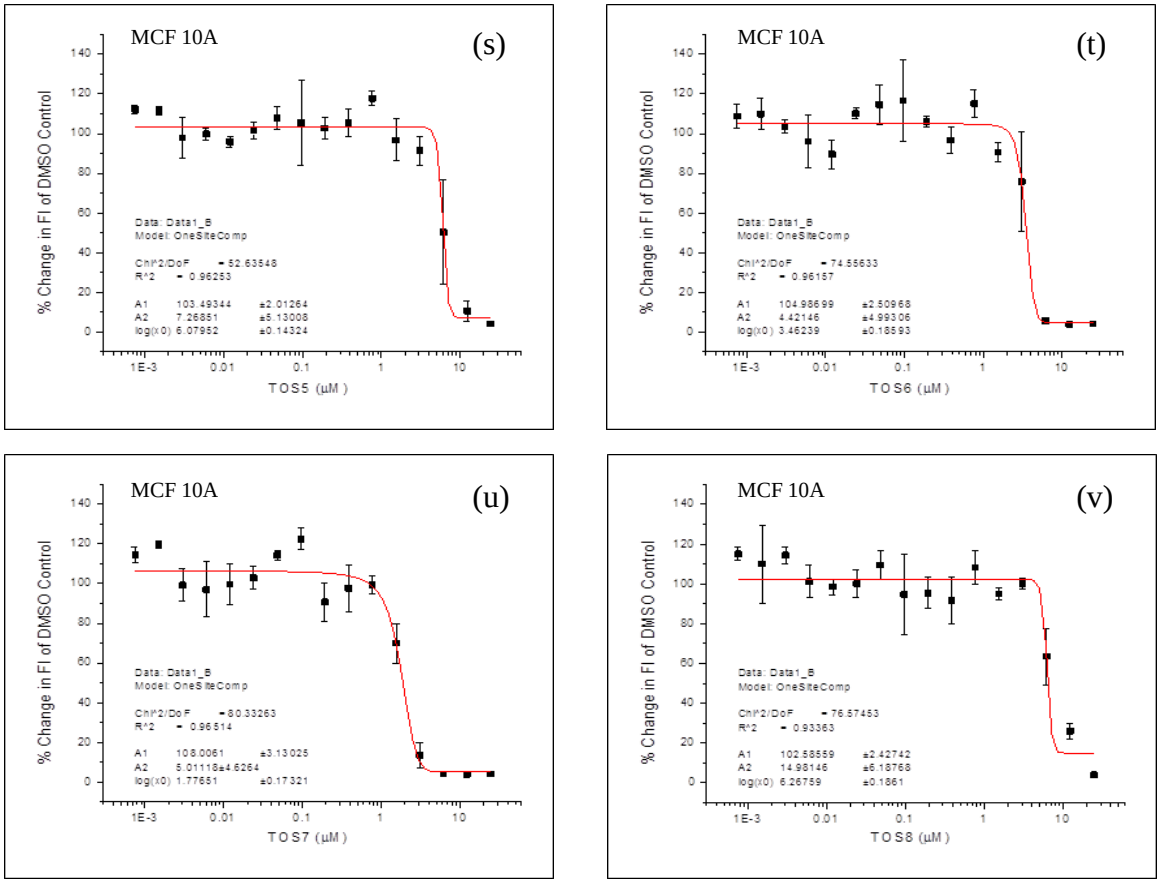

Figure 104: Change in fluorescence intensity after 72-h treatment of MCF 10A breast cells with various concentrations of (s) TOS5; (t) TOS6; (u) TOS7; (v) TOS8

Tables 67 and 68 below show the potent compounds (IC_{50} < 5 µM) against MCF-7A and MDA-MB-231 breast cancer cell lines. These tables also show the activity of the same compounds on normal human breast epithelial cell line (MCF-10A). It is apparent that of all the compounds tested TOS7 seemed to be highly cytotoxic (IC_{50} < 0.500 µM) against breast cancer cell lines MCF-7A and MDA-MB-231. Tables 69 and 70 show the IC_{50} values for all the sulfonato compounds tested on MCF-7A and MDA-MB-231 breast cancer cell lines.

Compound	MCF-7A IC_{50} Error (±)	MCF-10A IC_{50} Error (±)
TOS7	0.337 ± 0.303	1.78 ± 0.173
1NS7	0.849 ± 0.255	2.51 ± 0.187
TOS6	1.27 ± 0.228	3.46 ± 0.186
2NS6	1.31 ± 0.297	2.79 ± 0.250
1NS4	1.54 ± 0.179	1.59 ± 0.351
TOS4	1.55 ± 0.285	5.70 ± 0.337
2NS4	1.58 ± 0.263	1.66 ± 0.229
1NS6	1.70 ± 0.226	3.63 ± 0.403
2NS5	2.11 ± 0.267	6.32 ± 0.157
2NS8	2.83 ± 0.516	1.51 ± 0.201
1NS2	3.09 ± 0.528	11.6 ± 0.872
TOS5	3.12 ± 0.399	6.08 ± 0.143
TOS2	3.24 ± 0.557	6.75 ± 0.444
1NS3	3.29 ± 0.517	6.08 ± 0.357
TOS8	3.61 ± 0.418	6.27 ± 0.186

Table 67: The IC_{50} values (μM) values (in increasing order) of potent (< 5.000 μM) organorhenium complexes on MCF-7A breast cancer cell line

Compound	MDA-MB-231 IC_{50} Error (±)	MCF-10A IC_{50} Error (±)
TOS7	0.248 ± 0.336	1.78 ± 0.173
1NS7	0.716 ± 0.242	2.51 ± 0.187
2NS6	1.08 ± 0.198	3.46 ± 0.186
TOS6	1.27 ± 0.361	2.79 ± 0.250
1NS6	1.53 ± 0.143	1.59 ± 0.351
2NS4	1.86 ± 0.318	5.70 ± 0.337
1NS4	2.78 ± 0.373	1.66 ± 0.229
TOS4	3.09 ± 0.284	3.63 ± 0.403
TOS5	3.55 ± 0.537	6.32 ± 0.157

Table 68: The IC_{50} (μM) values (in increasing order) of potent (< 5.000 μM) organorhenium complexes on MDA-MB-231 breast cancer cell line

Compound	**MCF-7A IC_{50}** Error (±)	**MCF-10A IC_{50}** Error (±)
TOS7	0.337 ± 0.303	1.78 ± 0.173
1NS7	0.849 ± 0.255	2.51 ± 0.187
TOS6	1.27 ± 0.228	3.46 ± 0.186
2NS6	1.31 ± 0.297	2.79 ± 0.250
1NS4	1.54 ± 0.179	1.59 ± 0.351
TOS4	1.55 ± 0.285	5.70 ± 0.337
2NS4	1.58 ± 0.263	1.66 ± 0.229
1NS6	1.70 ± 0.226	3.63 ± 0.403
2NS5	2.11 ± 0.267	6.32 ± 0.157
2NS8	2.83 ± 0.516	1.51 ± 0.201
1NS2	3.09 ± 0.528	11.6 ± 0.872
TOS5	3.12 ± 0.399	6.08 ± 0.143
TOS2	3.24 ± 0.557	6.75 ± 0.444
1NS3	3.29 ± 0.517	6.08 ± 0.357
TOS8	3.61 ± 0.418	6.27 ± 0.186
2NS7	5.84 ± 0.377	1.51 ± 0.201
2NS1	6.10 ± 0.286	12.8 ± 0.288
2NS2	6.14 ± 0.380	6.40 ± 0.120
TOS3	6.54 ± 0.309	12.5 ± 0.098
2NS3	12.1 ± 0.705	6.50 ± 0.250
1NS1	> 24	12.8 ± 0.625
TOS1	NA	> 24

Table 69: The IC_{50} (μM) values (in increasing order) of all organorhenium sulfonato complexes tested on MCF-7A breast cancer cell line

Compound	MDA-MB-231 IC_{50} Error (±)	MCF-10A IC_{50} Error (±)
TOS7	0.248 ± 0.336	1.78 ± 0.173
1NS7	0.716 ± 0.242	2.51 ± 0.187
2NS6	1.08 ± 0.198	3.46 ± 0.186
TOS6	1.27 ± 0.361	2.79 ± 0.250
1NS6	1.53 ± 0.143	1.59 ± 0.351
2NS4	1.86 ± 0.318	5.70 ± 0.337
1NS4	2.78 ± 0.373	1.66 ± 0.229
TOS4	3.09 ± 0.284	3.63 ± 0.403
TOS5	3.55 ± 0.537	6.32 ± 0.157
2NS8	5.40 ± 1.021	1.51 ± 0.201
2NS5	6.04 ± 0.204	6.32 ± 0.157
1NS3	6.11 ± 0.601	6.08 ± 0.357
2NS7	6.34 ± 0.486	1.51 ± 0.201
TOS8	6.54 ± 0.269	6.27 ± 0.186
1NS2	6.56 ± 0.600	11.6 ± 0.872
2NS2	12.1	6.40 ± 0.120
2NS3	12.1	6.50 ± 0.250
TOS3	12.4	12.5 ± 0.098
TOS2	12.5	6.75 ± 0.444
2NS1	> 24	12.8 ± 0.288

Table 70: The IC_{50} values (μM) values (in increasing order) of all organorhenium sulfonato complexes tested on MDA-MB-231 breast cancer cell line

The cell viability studies of a few sulfonato complexes (TOS1, TOS2, TOS3, TOS4, TOS5, TOS6, TOS8 and TOS9) against U-937 lymphoma cells was carried out in our lab using the MTT assay. Figures 105–112 below show the results for the studies. The IC_{50} values are also compiled in Table 71 below. It is apparent that all the compounds except TOS4 (IC_{50} = 4.83 ± 0.151 µM) had IC_{50} values greater than 5 µM and are thus not very active against U937 lymphoma cell line.

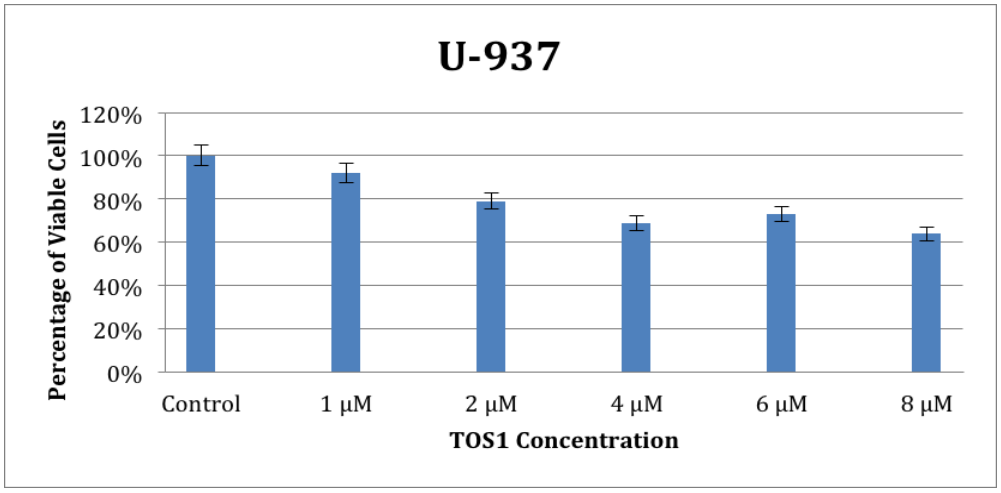

Figure 105: Percent of Viable cells after 72-h treatment of U937 lymphoma cells with various concentrations of TOS1

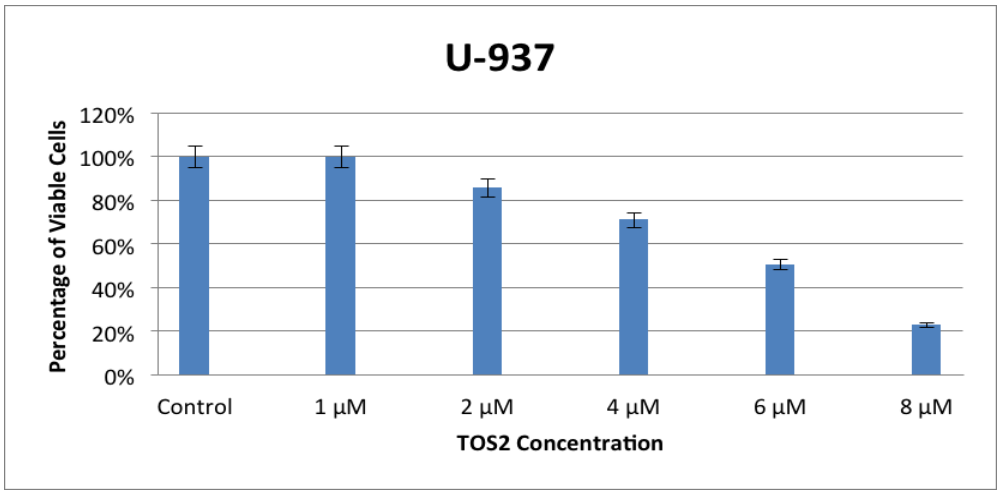

Figure 106: Percent of Viable cells after 72-h treatment of U937 lymphoma cells with various concentrations of TOS2

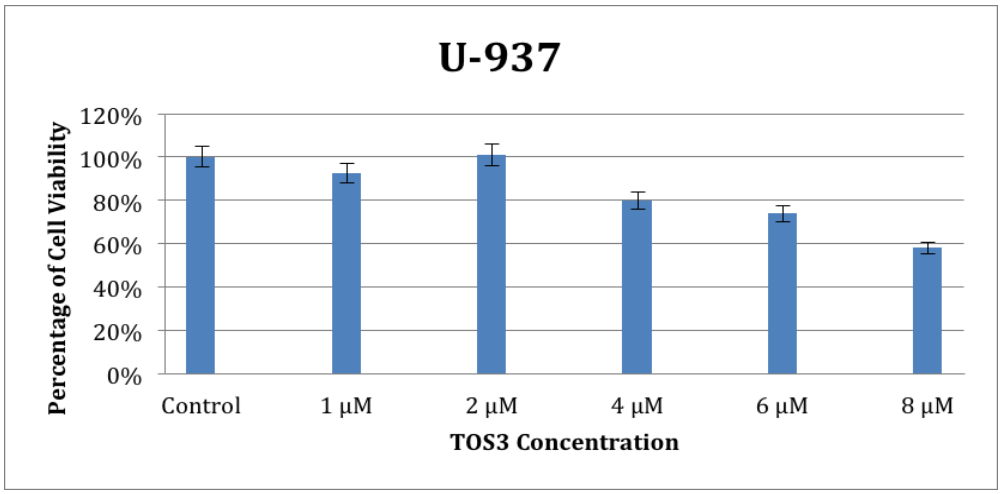

Figure 107: Percent of Viable cells after 72-h treatment of U937 lymphoma cells with various concentrations of TOS3

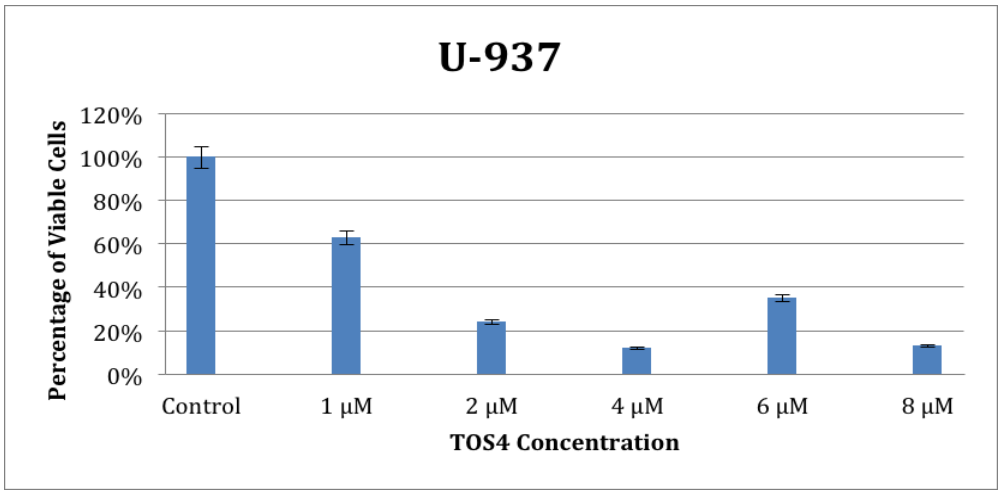

Figure 108: Percent of Viable cells after 72-h treatment of U937 lymphoma cells with various concentrations of TOS4

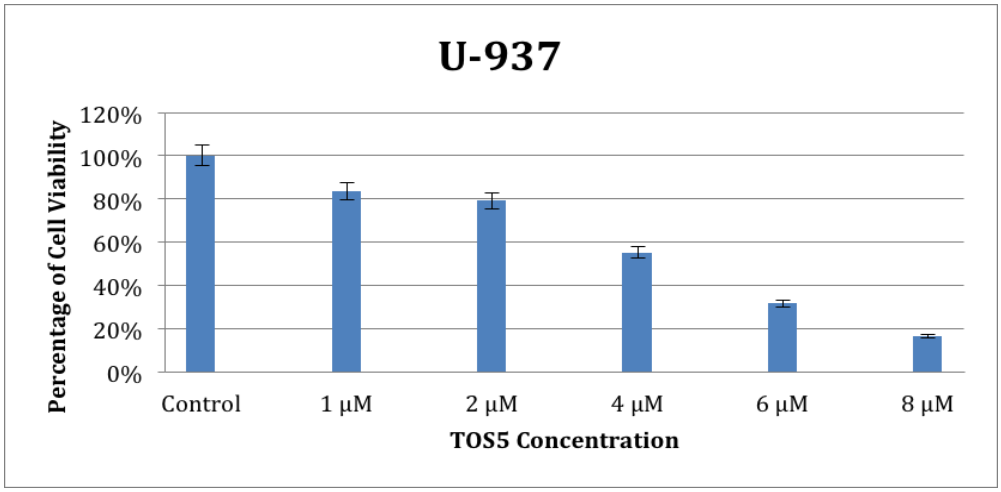

Figure 109: Percent of Viable cells after 72-h treatment of U937 lymphoma cells with various concentrations of TOS5

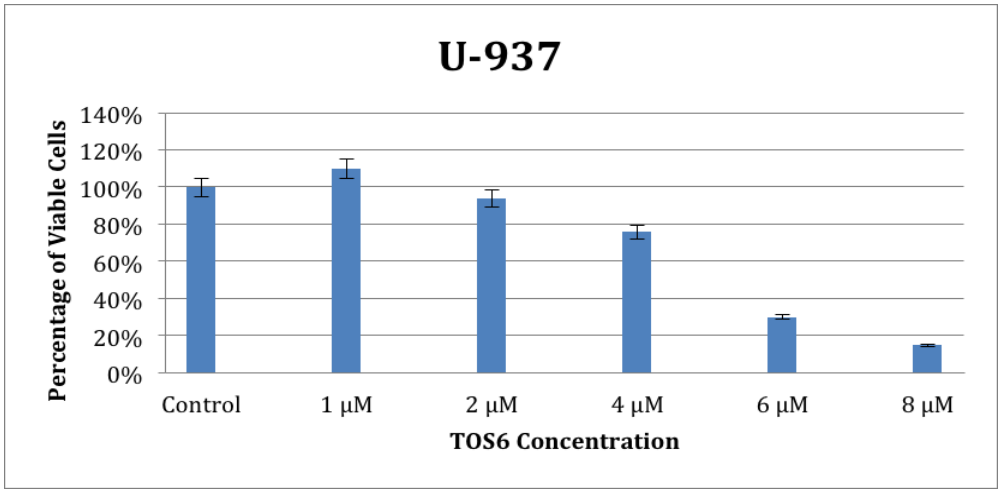

Figure 110: Percent of Viable cells after 72-h treatment of U937 lymphoma cells with various concentrations of TOS6

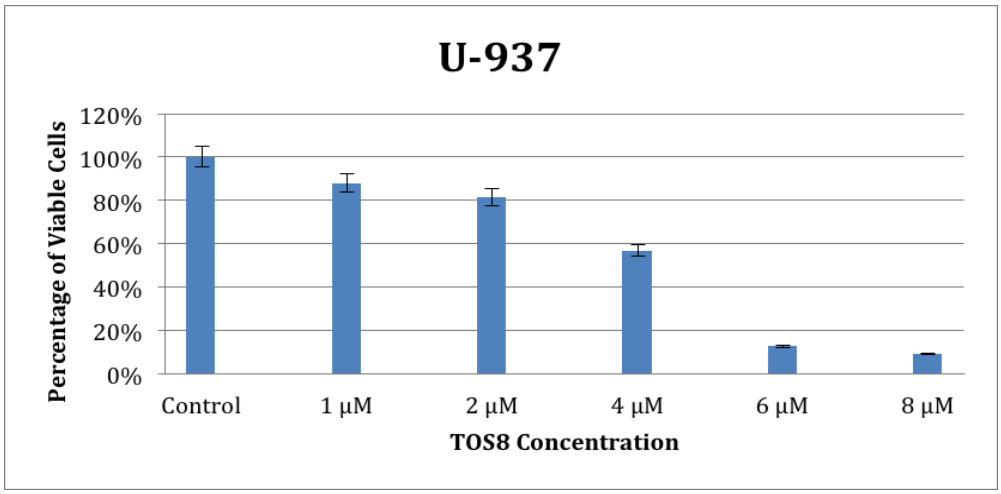

Figure 111: Percent of Viable cells after 72-h treatment of U937 lymphoma cells with various concentrations of TOS8

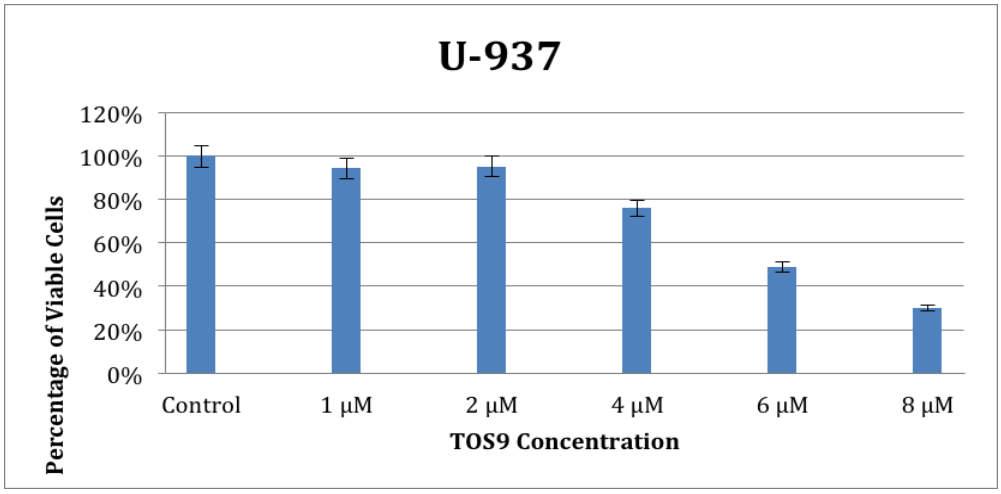

Figure 112: Percent of Viable cells after 72-h treatment of U937 lymphoma cells with various concentrations of TOS9

Compound	U937 IC_{50} Error (±)
TOS1	14.3 ± 0.277
TOS2	8.70 ± 0.171
TOS3	14.4 ± 0.224
TOS4	4.83 ± 0.151
TOS5	7.30 ± 0.107
TOS6	8.13 ± 0.201
TOS8	6.80 ± 0.174
TOS9	9.33 ± 0.207

Table 71: The IC_{50} values (in μM) of TOS1, TOS2, TOS3, TOS4, TOS5, TOS6, TOS8 and TOS9 on U937 lymphoma cell line

3. 4. DNA Binding Studies

UV-Visible (UV-Vis) absorption spectroscopy is a very effective method for examining the interaction of metal complexes with DNA. It is used to study the binding mode and binding strength metal complexes with DNA. It is also used to examine the stability of DNA when bound to these complexes. The study of the interaction of metal complexes with DNA using UV-Vis absorption spectroscopy involves monitoring the changes in absorption properties of these complexes. The aromatic molecules that are commonly used as ligands show a distinctive absorption band in the visible region of the electromagnetic spectrum. Therefore, to determine if there is any interaction between the complex and DNA, the shifting of the position of the maximum of this band from when the ligand is free in solution to when the ligand is bound to DNA can be examined.[52] The magnitude of this shifting can be interpreted as an indication of the strength of the interaction of the ligand with DNA.[52]

The interaction of ligands with DNA can be studied by comparing the UV-Vis absorption spectra of the free ligand with that of the ligand-DNA complex. The ligands

could bind covalently to DNA as is the case with cisplatin or they could bind non-covalently. When complexes bind to DNA covalently, this generally result in hyperchromism and a bathochromic shift. The hyperchromic shift results from breakage of the DNA secondary structure. The bathochromic shift results from the coordination of the metal complex with the N7 position of guanine in DNA.

The non-covalent modes of binding include intercalation, groove binding and electrostatic binding. The intercalative mode of binding to DNA involves a strong stacking interaction between an aromatic chromophore and the base pairs of DNA.[60] In a UV-vis absorption spectroscopiy experiment, the absoption spectra that represents intercalative binding to DNA usually results in hypochromism (decrease in absorption) and bathochromism (red shift or shift to longer wavelength).[61-62] The bathochromism results from the π^* orbital of the intercalating ligand coupling with the π orbital of the DNA base pairs thereby decreasing the $\pi \rightarrow \pi^*$ transition energy.[60] However, since the coupling π orbital is partially filled by electrons, this decreases the transition probabilities, thereby resulting in hypochromism.[60] The extent of hypochromism and bathochromism is commonly consistent with the strength of intercalative binding.[63]

Biver et al. showed that groove binders show a similar trend (hypochromism and bathochromism) in their absorption spectrum as with intercalators. The only difference observed was that the red shift was greater with groove binders than intercalators.[64] In the case of electrostatic binding, the absorption spectra of metal complexes exhibit hyperchromism, but no bathochromic shift.[65-66] The hyperchromism might be because of the complex uncoiling the helical structure of DNA thereby making more bases

embedded in DNA exposed. In this study, the titration graphs for all the 1NS, 2NS and TOS graphs are shown in Figures. 113–117 below.

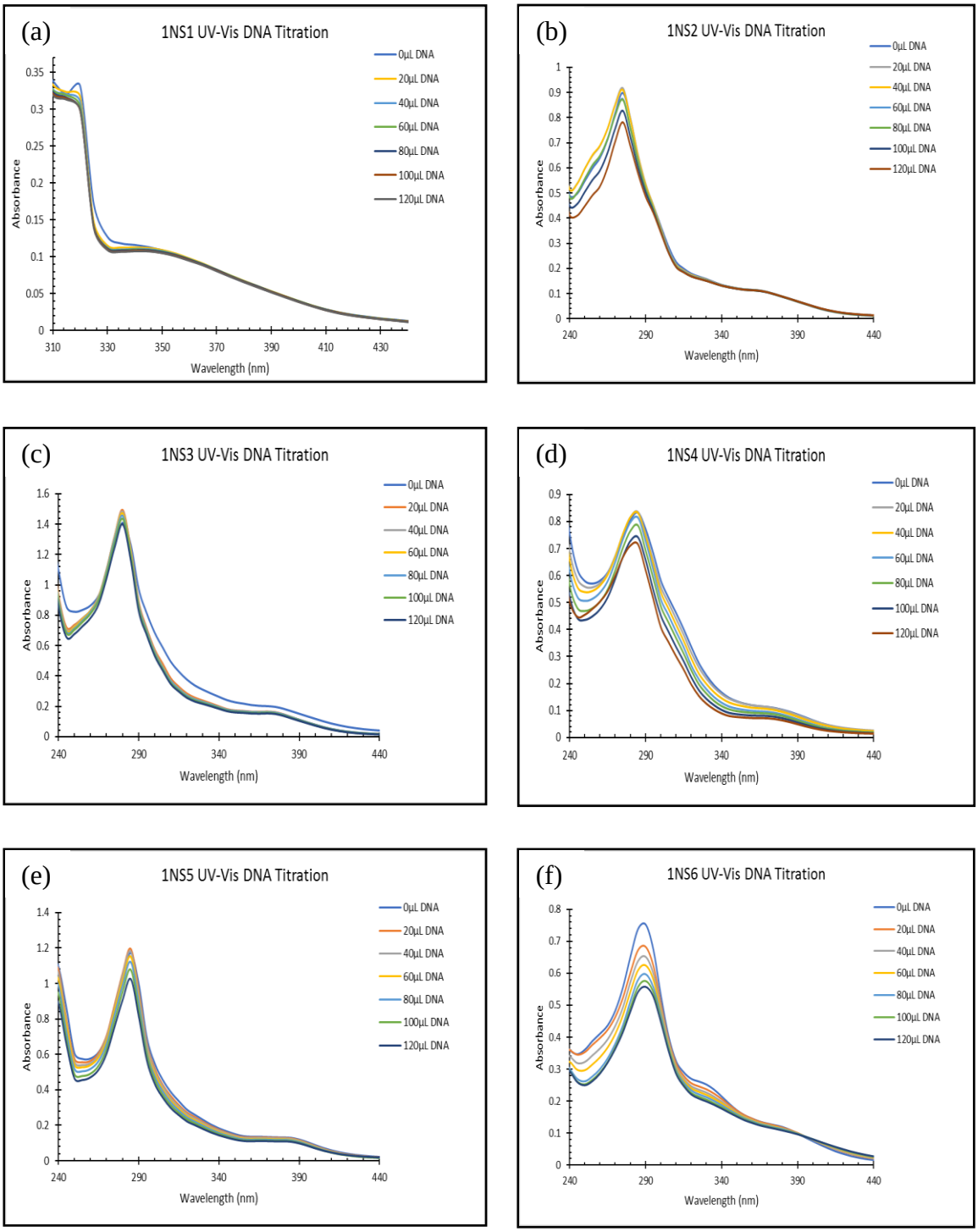

Figure 113: Electronic absorption spectra in the absence and presence of varied amount of DNA for the titration of 25 µM of (a) 1NS1; (b) 1NS2; (c) 1NS3; (d) 1NS4; (e) 1NS5; and (f) 1NS6. The concentration of the stock solution of DNA was 1693 µM

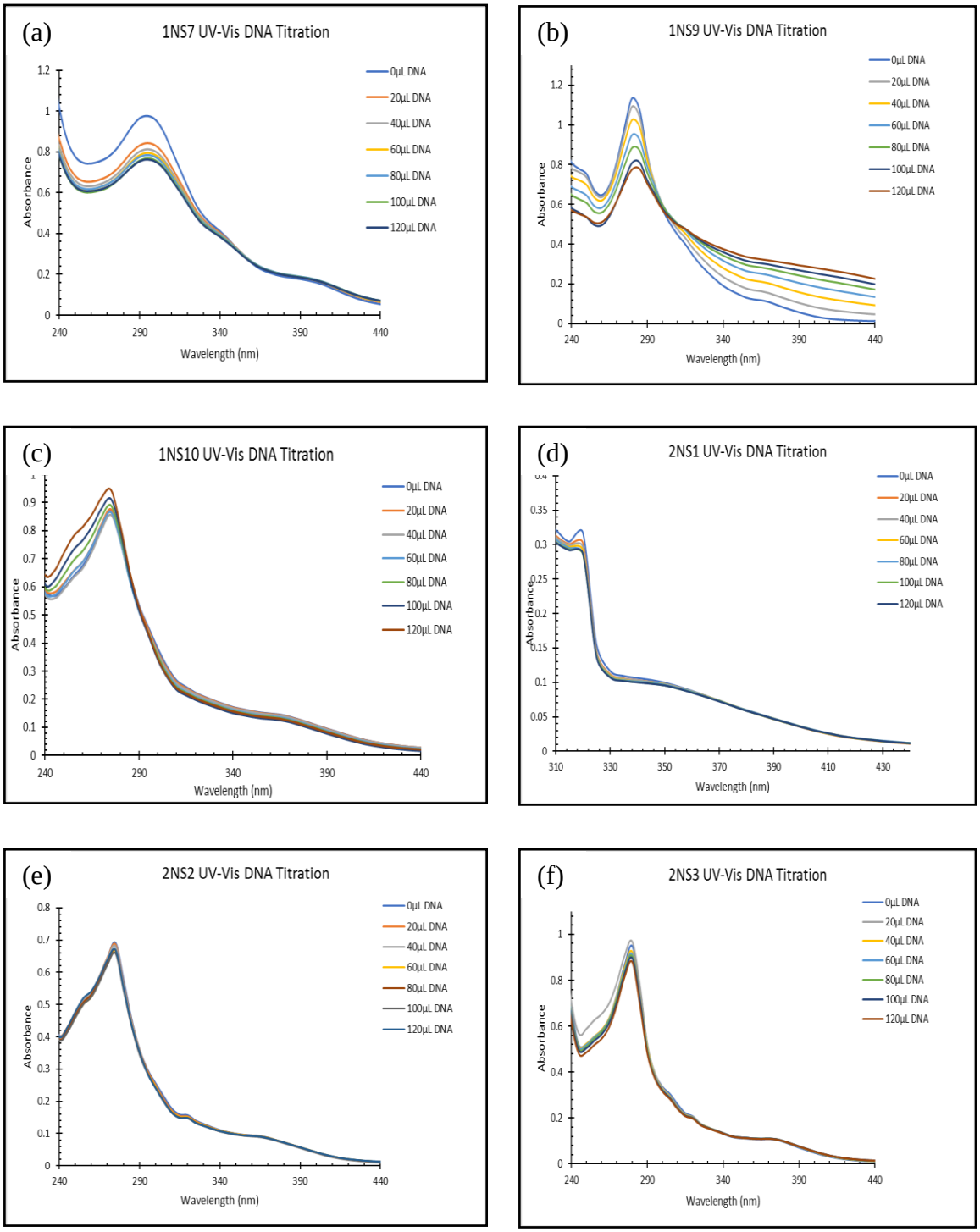

Figure 114: Electronic absorption spectra in the absence and presence of varied amount of DNA for the titration of 25 µM of (a) 1NS7; (b) 1NS9; (c) 1NS10; (d) 2NS1; (e) 2NS2; and (f) 2NS3. The concentration of the stock solution of DNA was 1693 µM

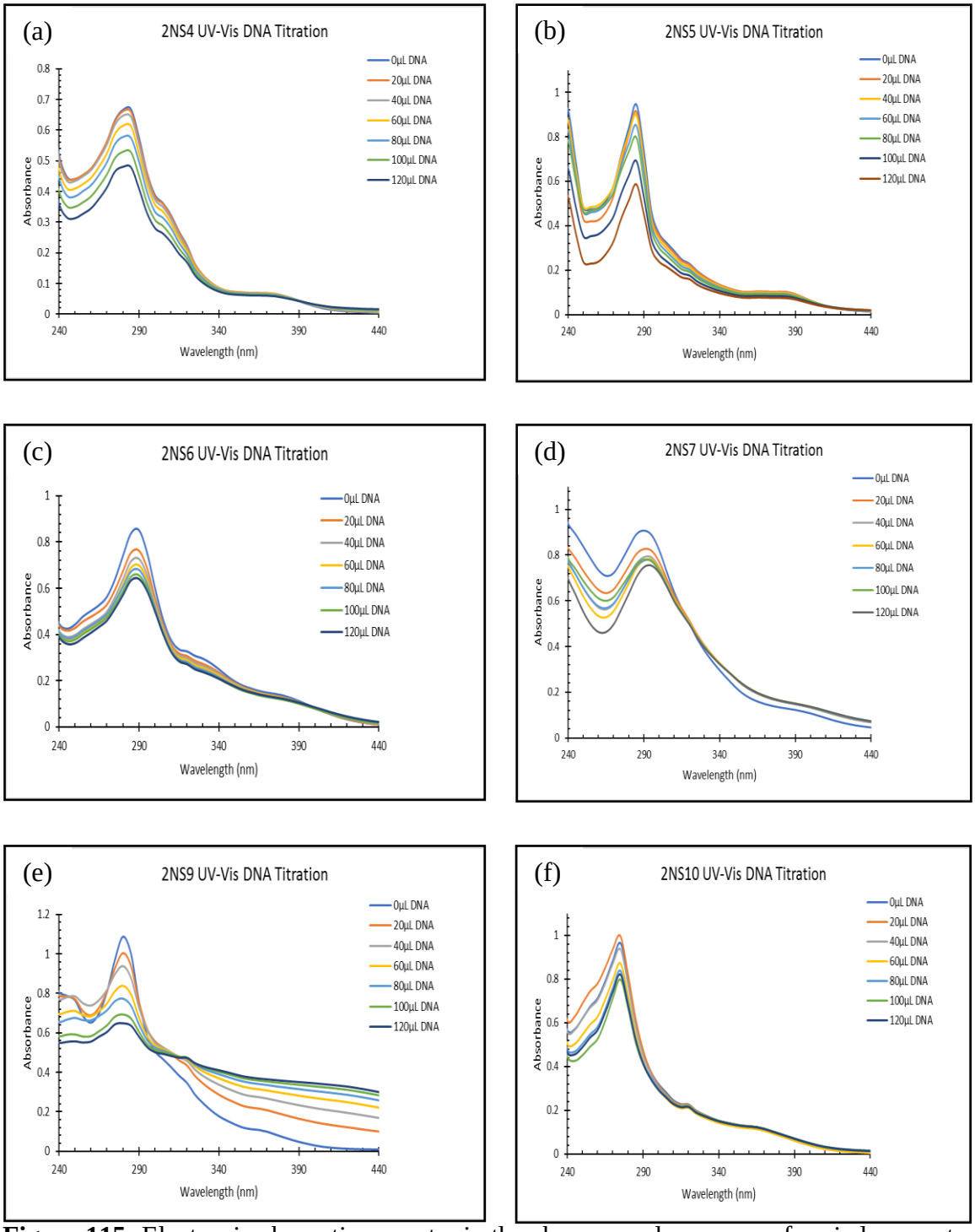

Figure 115: Electronic absorption spectra in the absence and presence of varied amount of DNA for the titration of 25 µM of (a) 2NS4; (b) 2NS5; (c) 2NS6; (d) 2NS7; (e) 2NS9; and (f) 2NS10. The concentration of the stock solution of DNA was 1693 µM

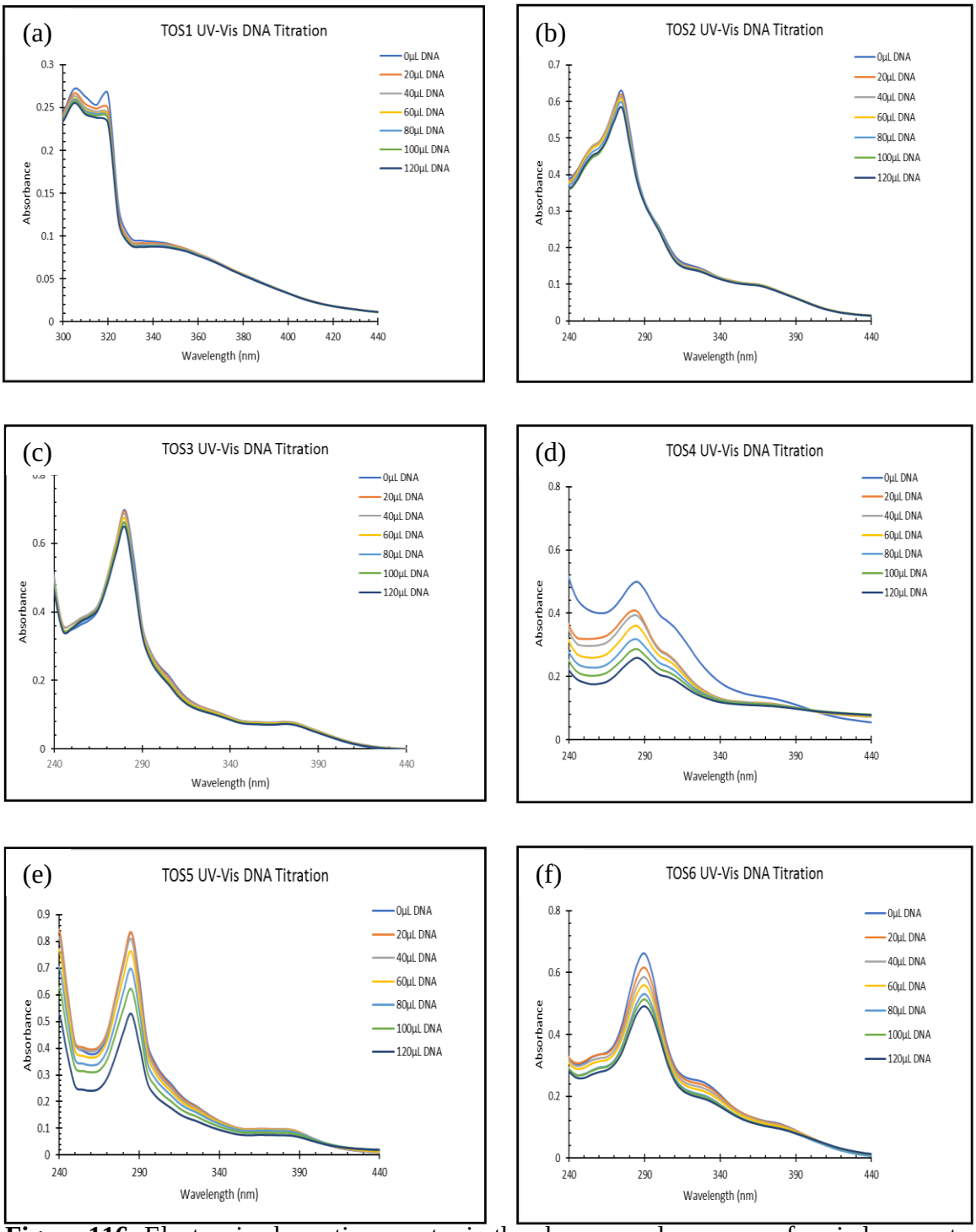

Figure 116: Electronic absorption spectra in the absence and presence of varied amount of DNA for the titration of 25 µM of (a) TOS1; (b) TOS2; (c) TOS3; (d) TOS4; (e) TOS5; and (f) TOS6. The concentration of the stock solution of DNA was 1693 µM

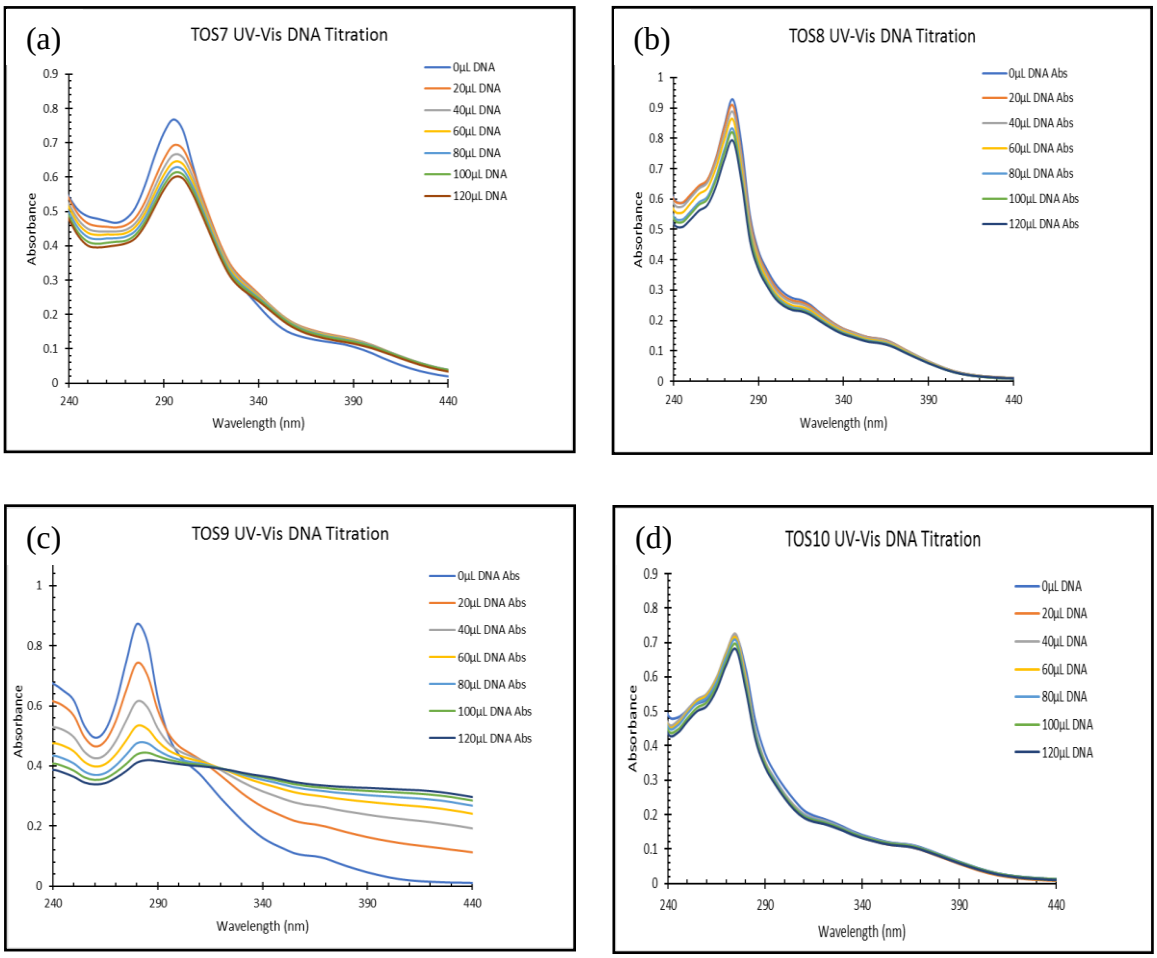

Figure 117: Electronic absorption spectra in the absence and presence of varied amount of DNA for the titration of 25 µM of (a) TOS7; (b) TOS8; (c) TOS9; (d) TOS10. The concentration of the stock solution of DNA was 1693 µM

In the UV-Vis graphs above, hypochromism was observed for each compound. However, bathochromism was not observed in any of the graphs. These results suggest that the compounds potentially follow moderate intercalation with DNA. The absence of a bathochromic shift also suggests that the mode of interaction with DNA could possibly be groove-binding mechanism.

In general, UV-Vis spectroscopy does not give conclusive results about the mode of binding of molecules to DNA. This is apparent in the similarity of abosprtion spectra

observed with intercalators and groove binders.[64] In addition, in some cases, intercalation and groove binding can be non-mutually exclusive.[64] For example, in some systems, one part of the molecule can bind to DNA intercalatively while another part binds with the grooves.[67-69] Also, some molecules can be partial intercalators, partial minor and/or major groove binders depending on the experimental conditions.[64, 70-71] As a result, more studies are needed to confirm the mode of binding of our sulfonato complexes with DNA.

The interaction of the sulfonato complexes with DNA was also studied using cyclic voltammetry. The interactions were investigated by monitoring the changes observed in the cyclic voltammogram of the complexes upon addition of DNA. There is a change in the peak potential and peak current of the complex in the presence of DNA if the complex interacts with DNA.[52] The shift in peak potential is used to confirm the mode of interaction.[52] Studies have shown that as DNA is added incrementally to the metal complexes, a shift in the potential peak to a more positive value indicates intercalative mode of binding. However, a shift in the potential to a more negative value is indicative of electrostatic binding. A decay in the peak current (I_p) of the redox process indicates the formation of an adduct and is used to determine the binding constant and binding site size. [52]

Figures 118–122 show the cyclic voltammograms of the 1NS, 2NS and TOS compounds in the absence and presence of DNA. Additions of DNA to all the complexes (except 2NS4 and 2NS6) show no decrease in the oxidation peak intensity, indicating that there is little or no interactions between the complexes and DNA. To 2NS4 and 2NS6, addition of DNA reduces the peak intensity suggesting interactions between the complexes and DNA.

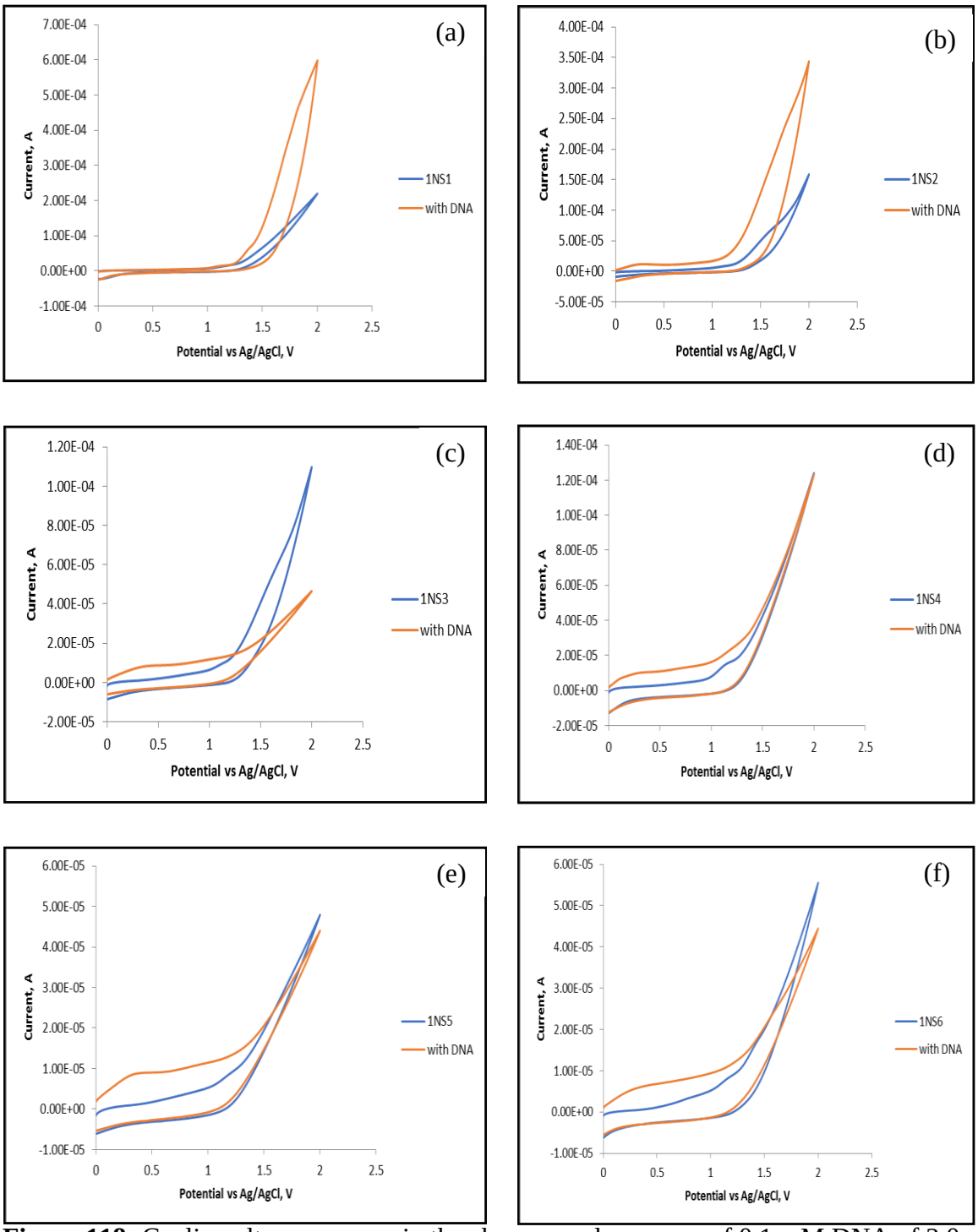

Figure 118: Cyclic voltammograms in the absence and presence of 0.1 mM DNA of 2.0 mM of (a) 1NS1; (b) 1NS2; (c) 1NS3; (d) 1NS4; (e) 1NS5; and (f) 1NS6. Scan rate 0.1 V/s

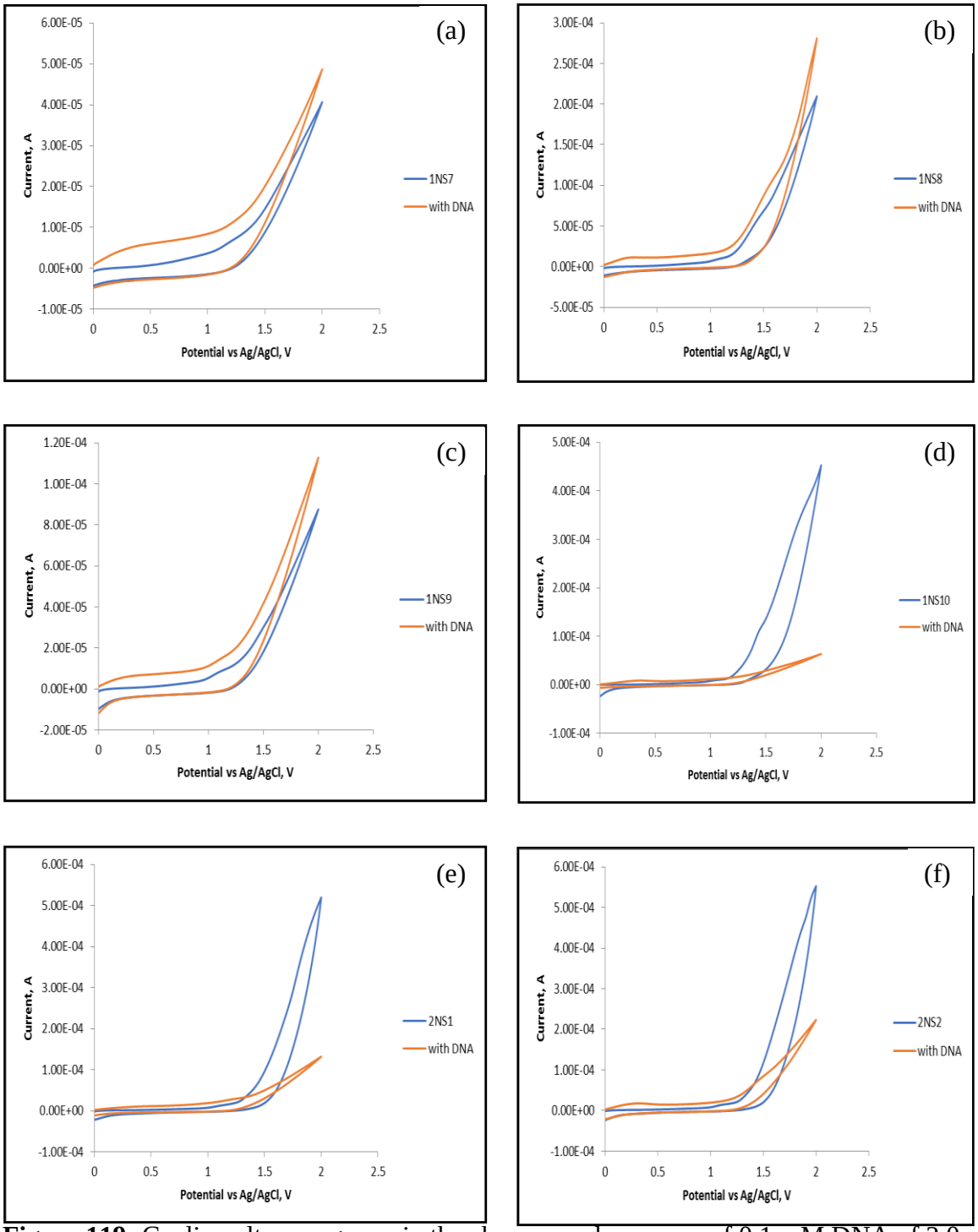

Figure 119: Cyclic voltammograms in the absence and presence of 0.1 mM DNA of 2.0 mM of (a) 1NS7; (b) 1NS8; (c) 1NS9; (d) 1NS10; (e) 2NS1; and (f) 2NS2. Scan rate 0.1 V/s

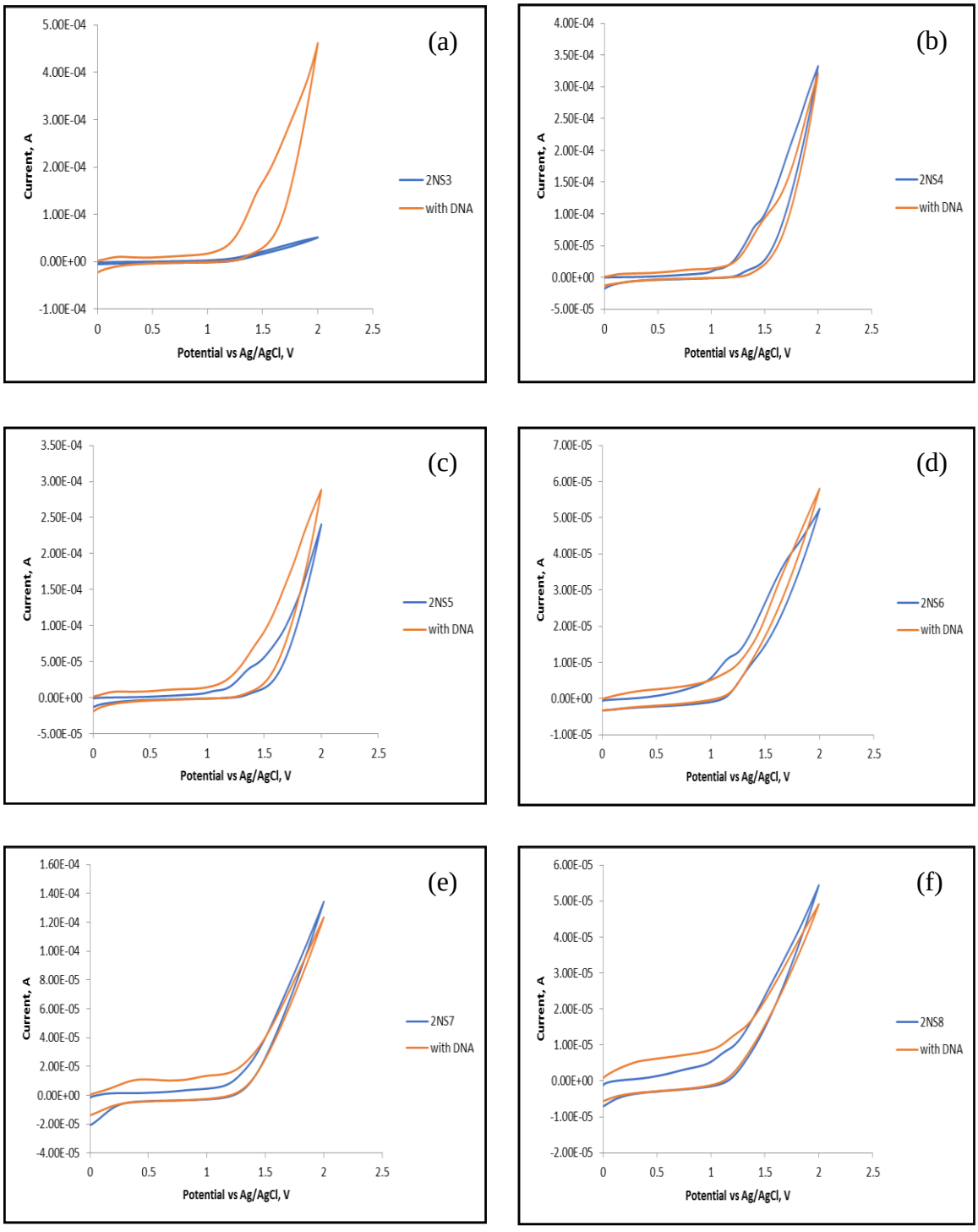

Figure 120: Cyclic voltammograms in the absence and presence of 0.1 mM DNA of 2.0 mM of (a) 2NS3; (b) 2NS4; (c) 2NS5; (d) 2NS6; (e) 2NS7; and (f) 2NS8. Scan rate 0.1 V/s

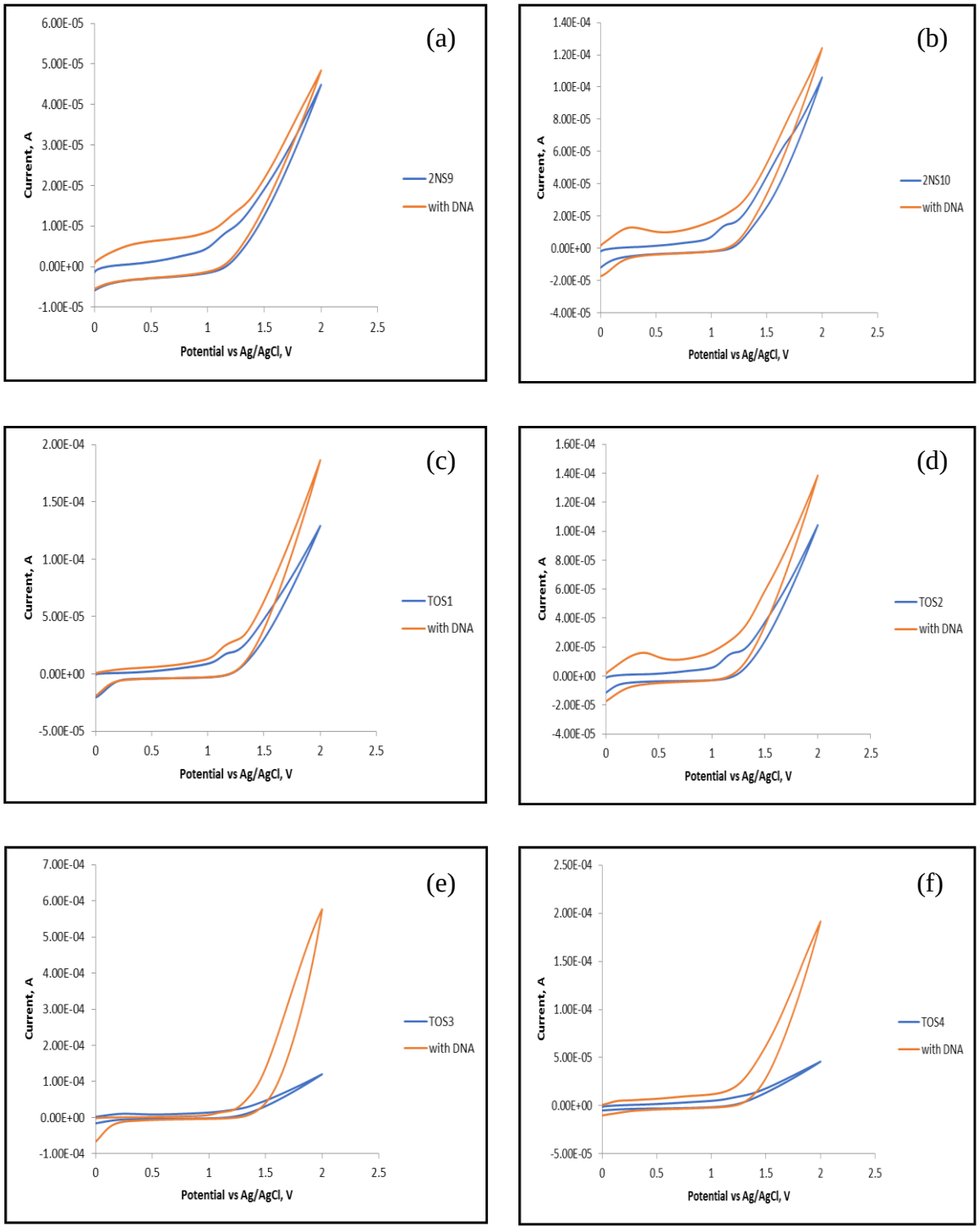

Figure 121: Cyclic voltammograms in the absence and presence of 0.1 mM DNA of 2.0 mM of (a) 2NS9; (b) 2NS10; (c) TOS1; (d) TOS2; (e) TOS3; and (f) TOS4. Scan rate 0.1 V/s

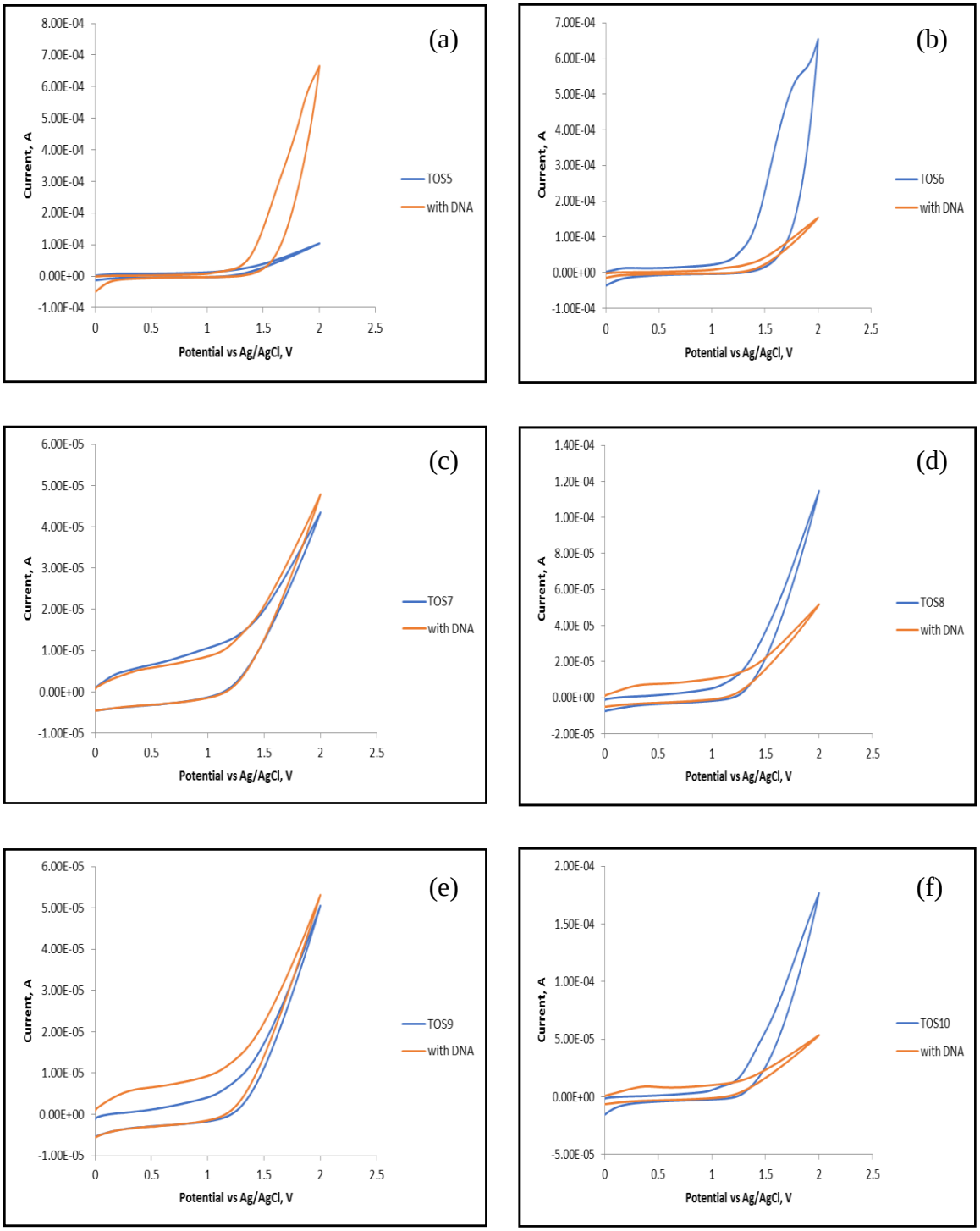

Figure 122: Cyclic voltammograms in the absence and presence of 0.1 mM DNA of 2.0 mM of (a) TOS5; (b) TOS6; (c) TOS7; (d) TOS8; (e) TOS9; and (f) TOS10. Scan rate 0.1 V/s

It is also important to note that addition of DNA to 1NS4, 1NS8, 1NS9, 2NS5, 2NS8, 2NS9, 2NS10, TOS1 and TOS2 causes the oxidation peak to increase rather than decrease. The reason for such an increase is not very clear. As a result of these results, more studies are needed to confirm the mode of binding of the sulfonato complexes with DNA.

In order to further investigate the interaction modes between the sulfonato complexes and DNA, Ethidium bromide (EtBr) displacement experiments were carried out. The fluorescence intensity of DNA is typically very low. Also, the fluorescence intensity of EtBr in Tris buffer is not high due to quenching by the solvent molecules. When DNA is added to EtBr, the fluorescence intensity of EtBr is enhanced due to the intercalation of EtBr into DNA. The intensity of EtBr bound to DNA can be quenched by the addition of another DNA intercalator that competes for the binding sites of DNA available for EtBr.[72-73] The fluorescence experiments were run for the 1NS, 2NS and TOS compunds and their graphs are shown in Figures 123–127 below. The fluorescence intensities of EB bound to CT-DNA only show a remarkable decreasing trend with the increasing concentration of complexes when the following complexes were tested: 1NS6, 1NS7, 1NS9 2NS6, 2NS7, 2NS9, TOS6, TOS7, and TOS9. This indicates that some EtBr molecules were released into solution after they were exchanged with the complexes, resulting in the fluorescence quenching of EtBr. As stated above, these observations suggest intercalative mode of binding of the complexes to DNA.

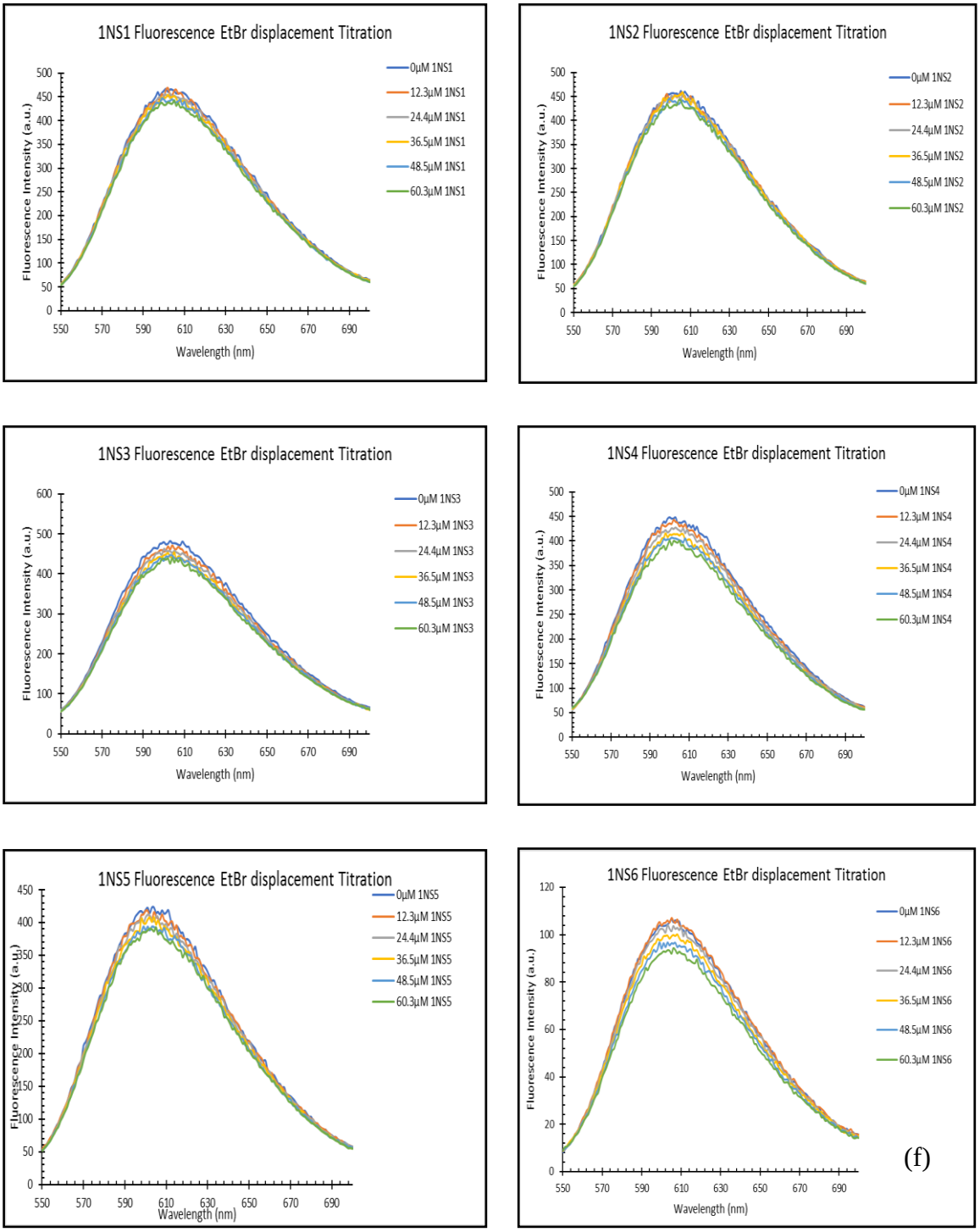

Figure 123: Ethdium Bromide displacement titration for (a) 1NS1; (b) 1NS2; (c) 1NS3; (d) 1NS4; (e) 1NS5; (f) 1NS6

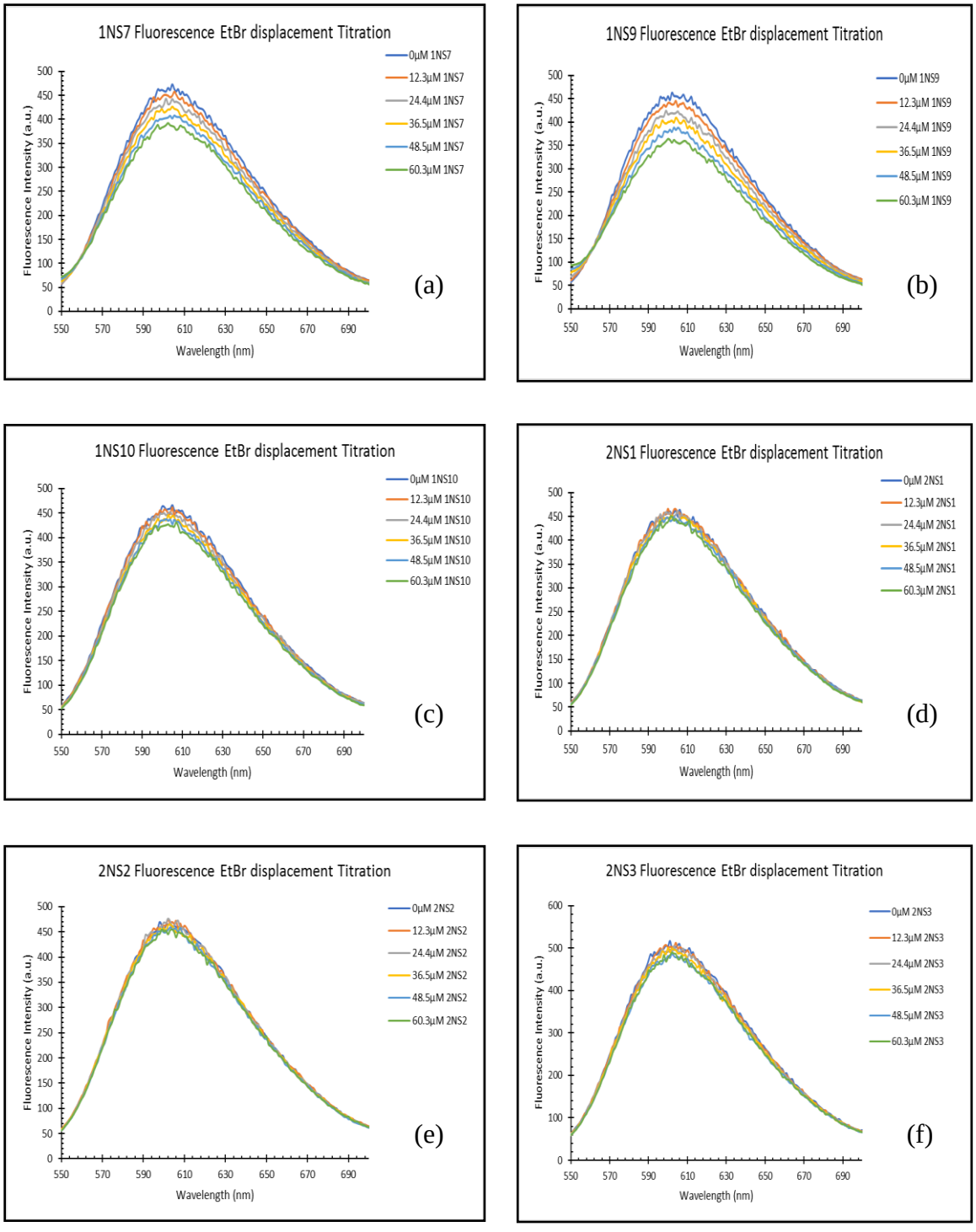

Figure 124: Ethdium Bromide displacement titration for (a) 1NS7; (b) 1NS9; (c) 1NS10; (d) 2NS1; (e) 2NS2; (f) 2NS3

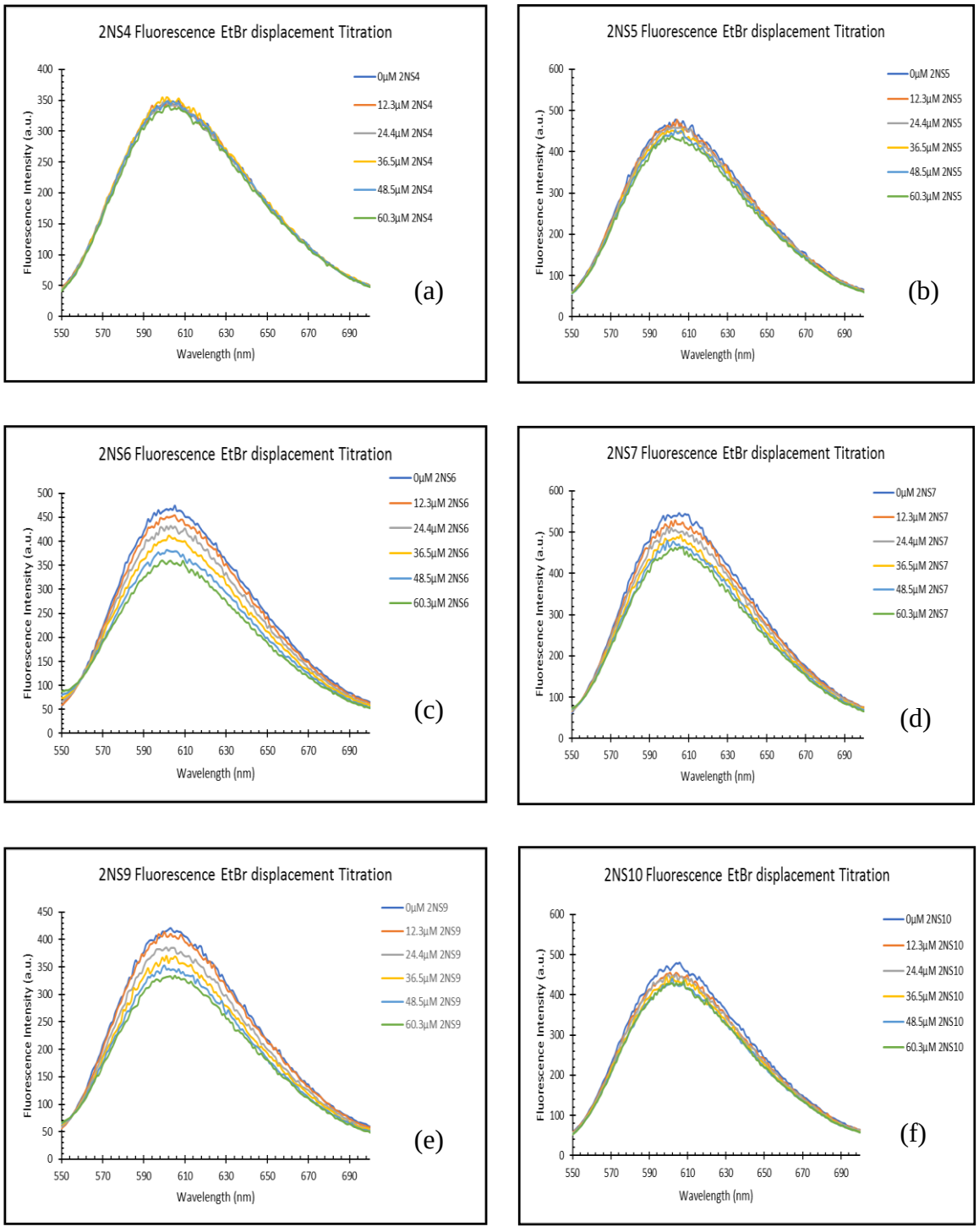

Figure 125: Ethdium Bromide displacement titration for (a) 2NS4; (b) 2NS5; (c) 2NS6; (d) 2NS7; (e) 2NS9; (f) 2NS10

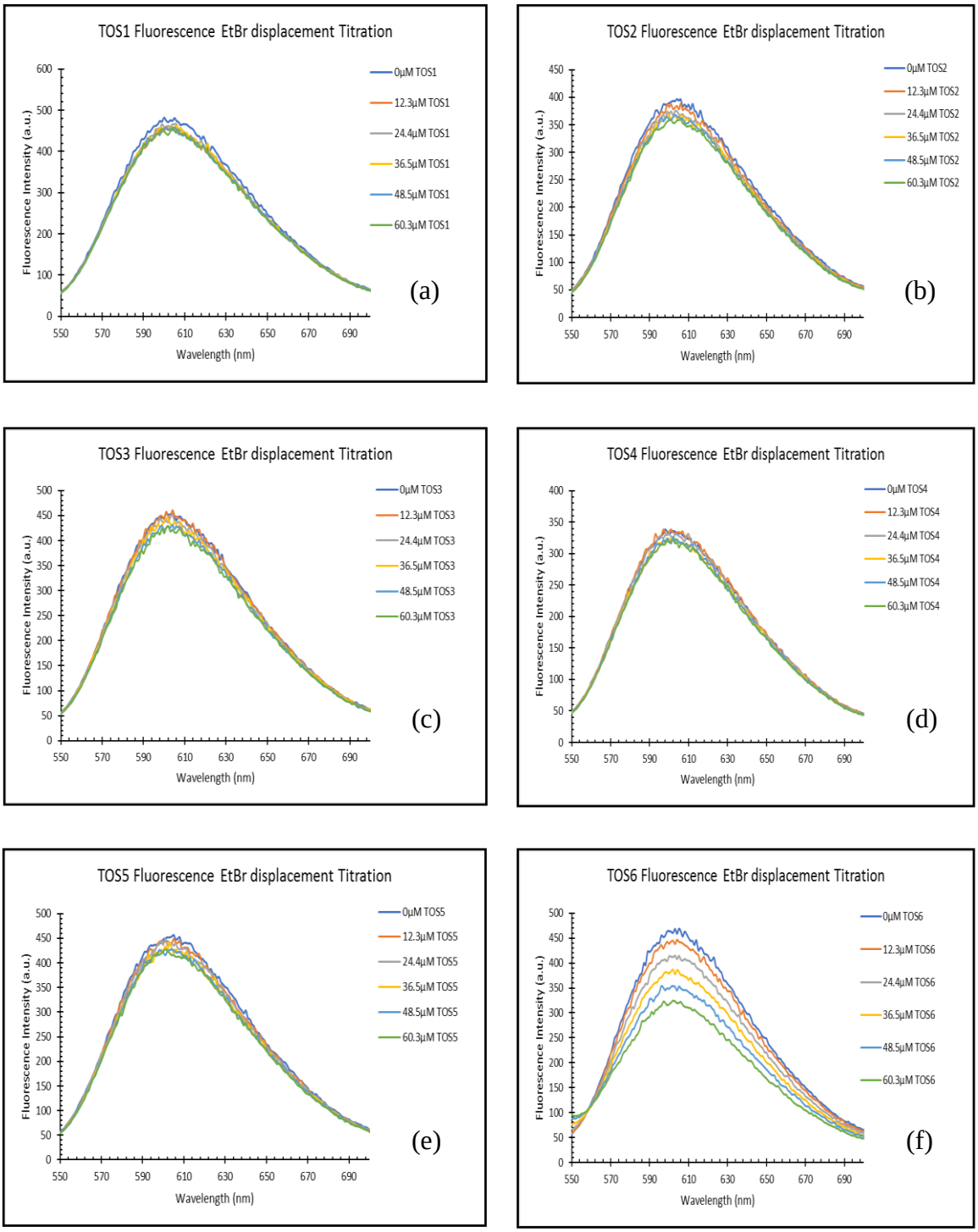

Figure 126: Ethdium Bromide displacement titration for (a) TOS1; (b) TOS2; (c) TOS3; (d) TOS4; (e) TOS5; (f) TOS6

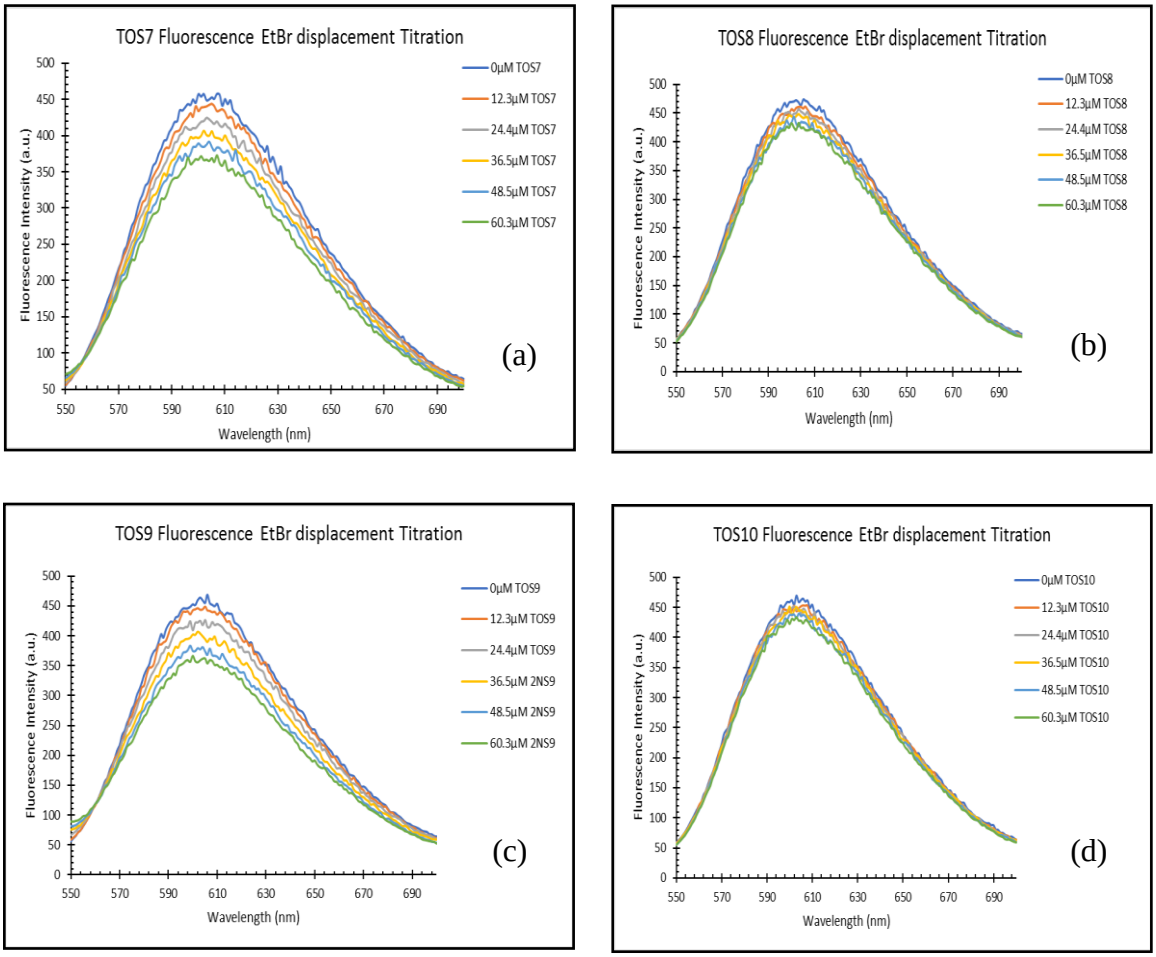

Figure 127: Ethdium Bromide displacement titration for (a) TOS7; (b) TOS8; (c) TOS9; (d) TOS10

The binding strength of the sulfonato complexes with CT-DNA can be determined using the linear Stern–Volmer equation. The equation is as follows:

$$I_o/I = 1 + K_{sv}[Q]$$

where I_o = fluorescence intensity of EtBr in the absence of the sulfonato complexes

I = fluorescence intensity of EtBr in the presence of the sulfonato complexes

Q = concentration of the sulfonato complexes

K_{sv} = linear Stern-Volmer quenching constant

By plotting the graph of I_o/I against [Q], the Stern-Volmer binding constant is given by the slope of the graph. Figures 128–136 below show the Stern-Volmer plots for the complexes (1NS6, 1NS7, 1NS9, 2NS6, 2NS7, 2NS9, TOS6, TOS7, and TOS9) that showed a decreasing trend in the EtBr displacement assay. The K_{sv} values for the complexes are given in Table 72 below:

Compound	**K_{sv} Value**	**R^2 value**
1NS6	2.72×10^3	0.9521
1NS7	3.61×10^3	0.9767
1NS9	4.79×10^3	0.9859
2NS6	5.68×10^3	0.9817
2NS7	2.96×10^3	0.9775
2NS9	4.68×10^3	0.9891
TOS6	7.62×10^3	0.9794
TOS7	3.81×10^3	0.9936
TOS9	5.55×10^3	0.9978

Table 72: Stern-Volmer binding constant for 1NS6, 1NS7, 1NS9, 2NS6, 2NS7, 2NS9, TOS6, TOS7, TOS9

The binding strength of the sulfonato complexes to CT-DNA follows the following order: TOS6 > 2NS6 > TOS9 > 1NS9 > 2NS9 > TOS7 > 1NS7 > 2NS7 > 1NS6.

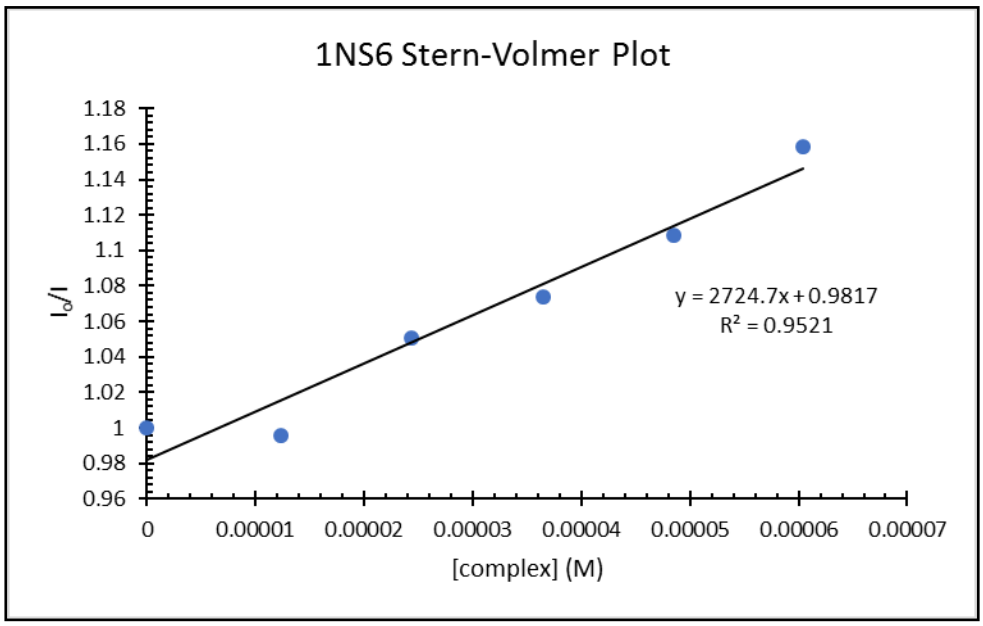

Figure 128: Stern-Volmer Plot for 1NS6

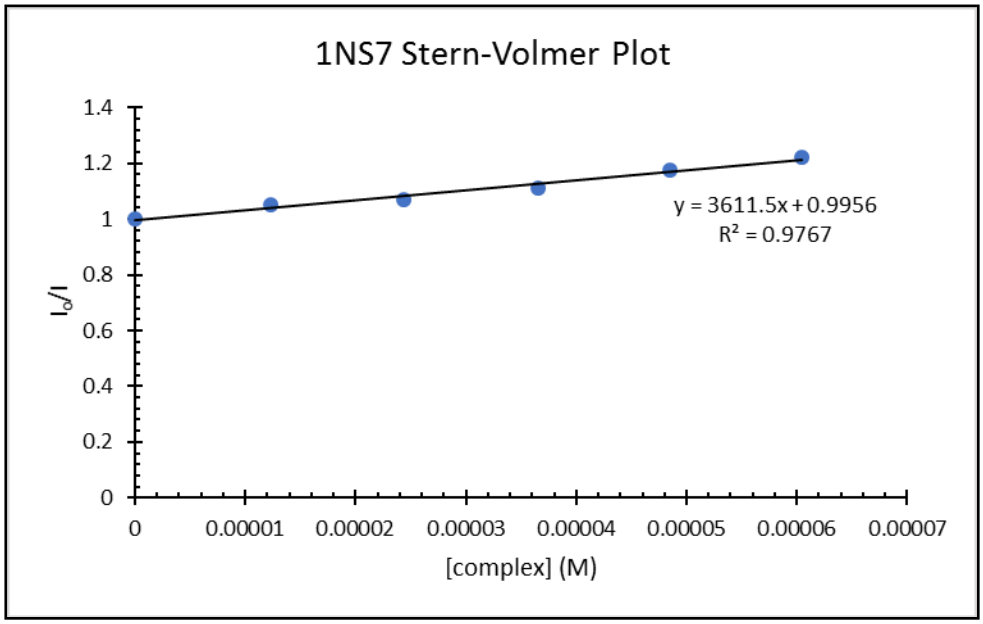

Figure 129: Stern-Volmer Plot for 1NS7

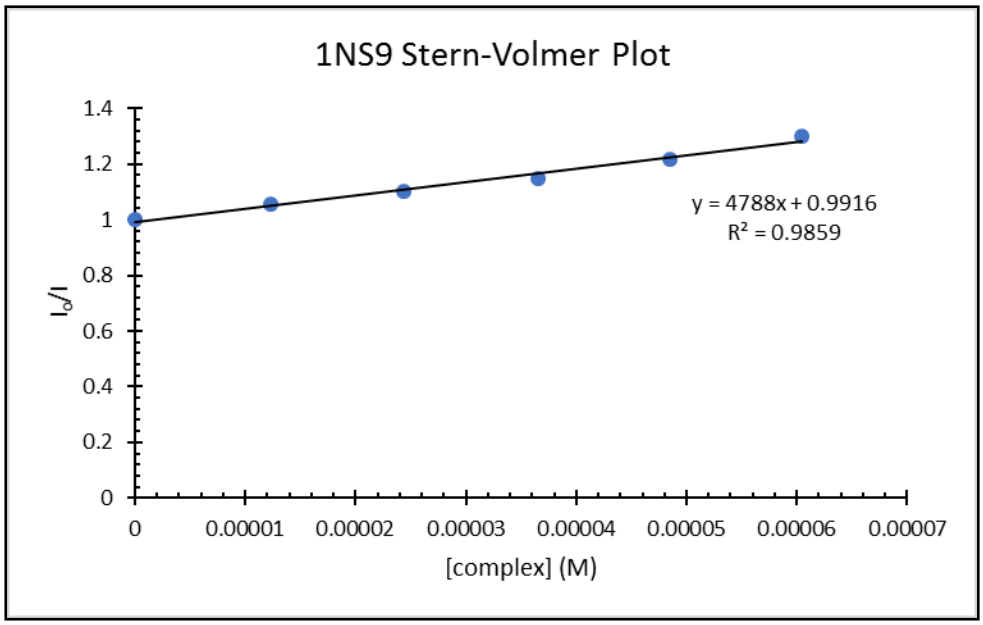

Figure 130: Stern-Volmer Plot for 1NS9

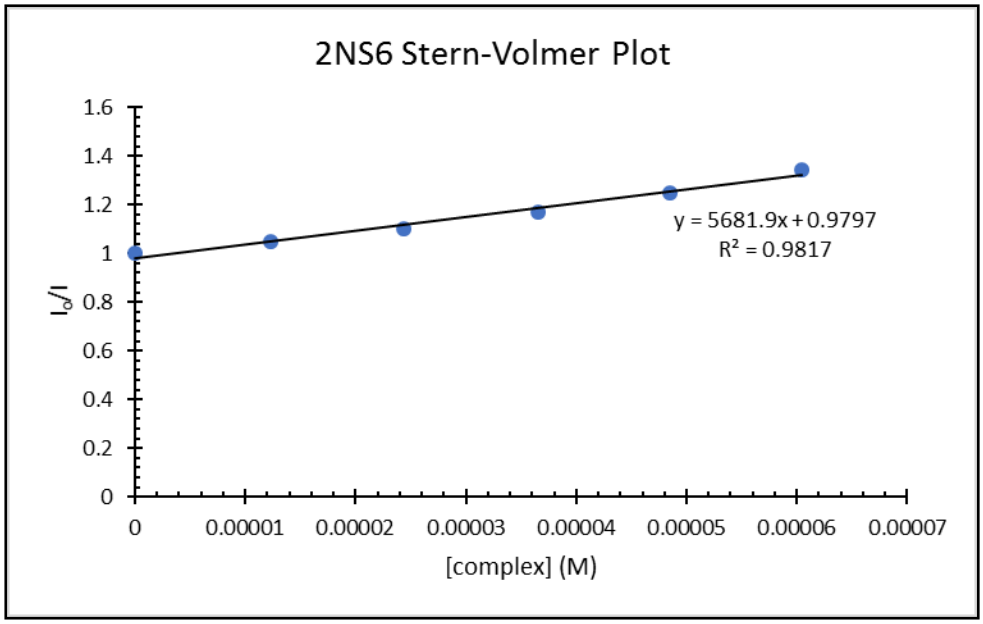

Figure 131: Stern-Volmer Plot for 2NS6

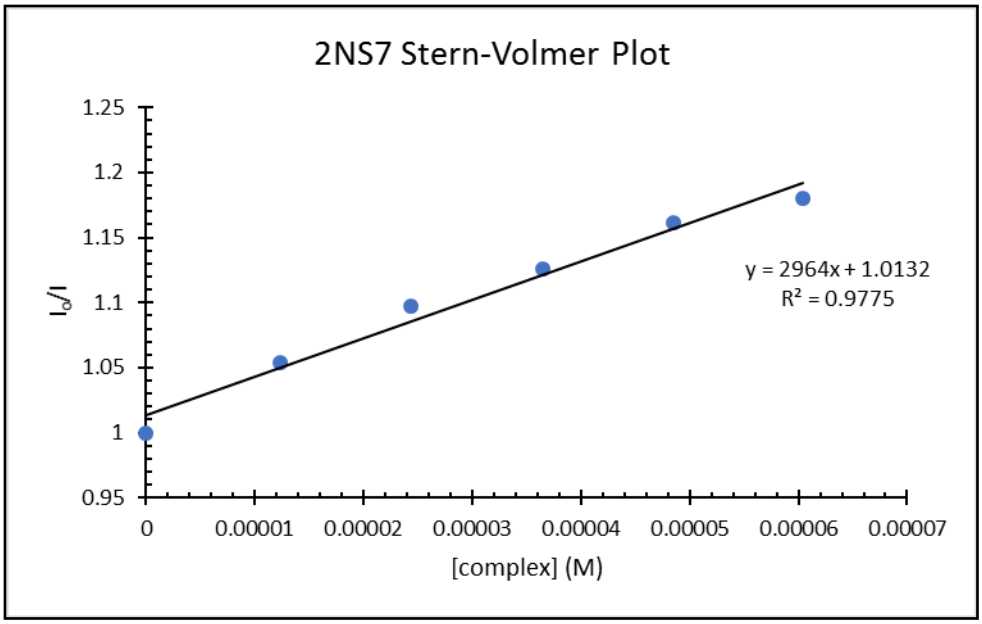

Figure 132: Stern-Volmer Plot for 2NS7

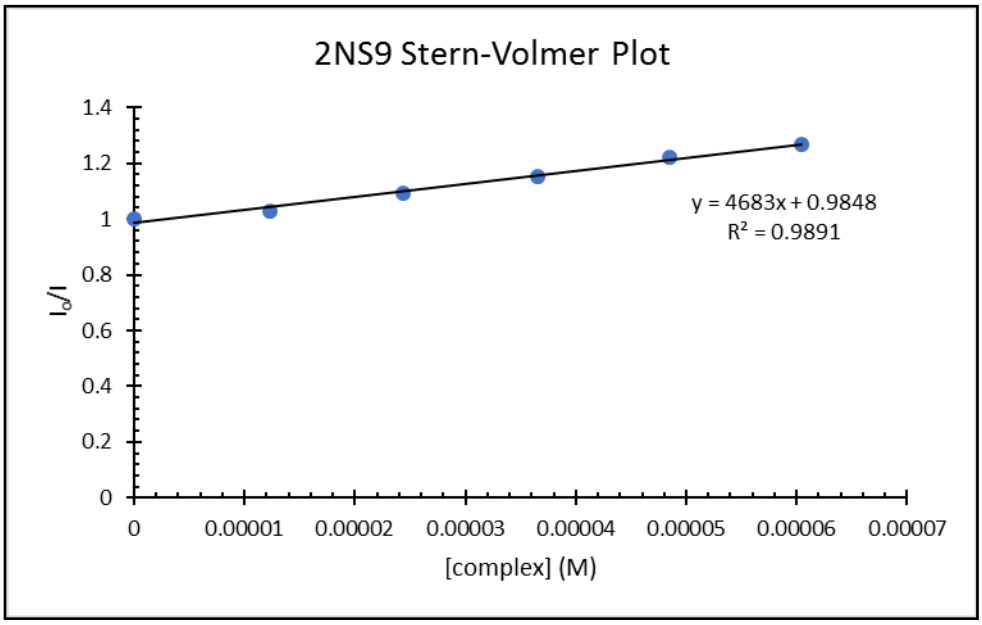

Figure 133: Stern-Volmer Plot for 2NS9

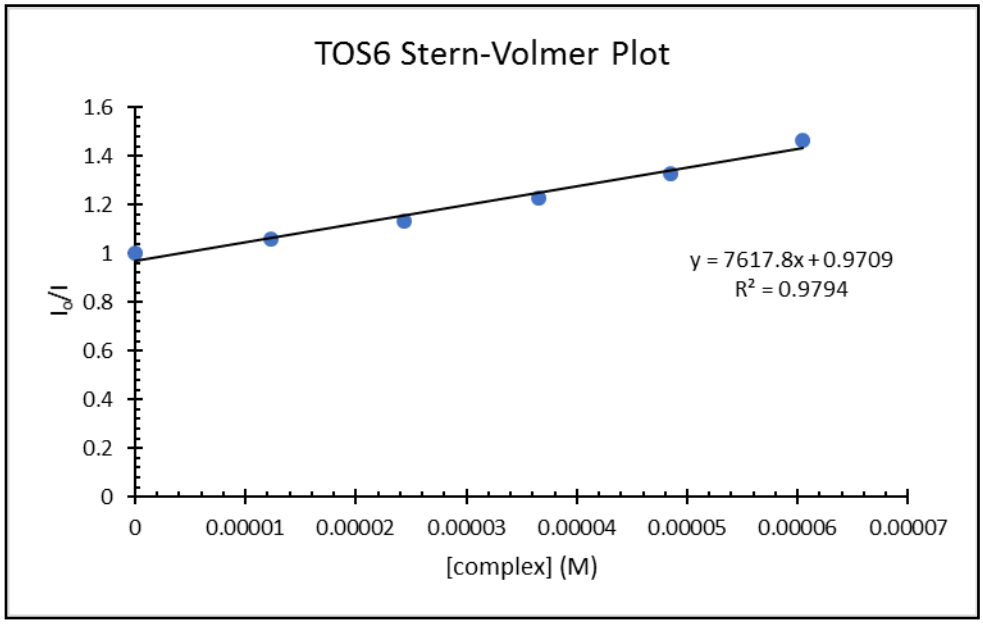

Figure 134: Stern-Volmer Plot for TOS6

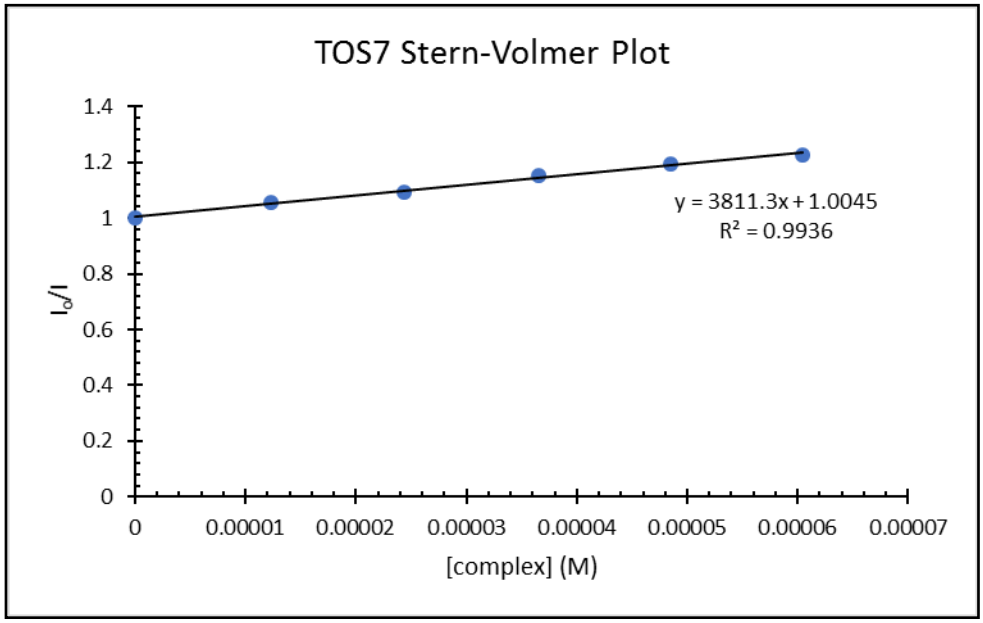

Figure 135: Stern-Volmer Plot for TOS7

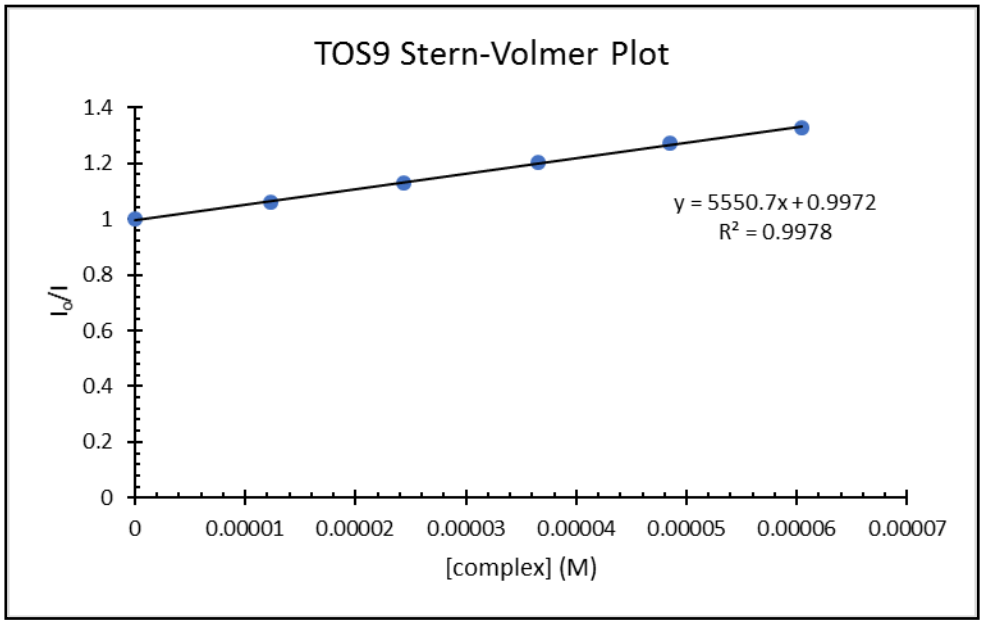

Figure 136: Stern-Volmer Plot for TOS9

The interaction of the sulfonato complexes was further investigated using gel electrophoresis. The results of gel electrophoresis DNA-binding assays are shown in Figures 137–142 below. The assay only works on compounds that are fluorescent. First, 1000 μM concentration of all the 30 sulfonato compounds (except 1NS8 and 2NS8) were prepared in DMSO. The compounds were mixed with lambda HindIII DNA markers (which give a characteristic laddering pattern in agarose electrophoresis gels), incubated for 1 hr. and loaded into the wells of the electrophoresis gel tray. The control for this experiment was DNA dissolved in water. Another control was DNA dissolved in DMSO. The codes 'W' and 'D' in Figures 137–142 represent water and DMSO. The '+' sign represents presence of DNA and the '-' represents absence of DNA. The first two wells in Figures 137–139 represent the two controls except in Figure 140 where the last two rows represent the controls. Each of the other wells in the gel tray contained the compounds in the presence (+ sign) and absence (- sign) of DNA.

After the samples are electrophoresed, they were imaged under broad band UV light to see if a laddering pattern was formed in the wells that contained compound mixed with DNA. DNA by itself is not fluorescent. However, it can be visualized in gels when mixed with fluorescent compounds. If a laddering pattern is observed, this suggests that the complexes bind (possibly intercalation) to DNA. If the laddering pattern is not observed, it suggests that the compounds do not bind to DNA. According to Figures 137–142, none of the compounds show this laddering pattern suggesting that there is no binding. However, after the samples were counterstained with EtBr, the laddering pattern was formed as expected. Since EtBr intercalates with DNA, it forms a laddering pattern when mixed with DNA.

In addition, from the above assay, we noticed that not all the compounds were fluorescent. After the samples are electrophoresed and counterstained with EtBr, it is possible to determine which of the compounds are fluorescent by observing (under broad band UV light) the wells that contain compounds alone (- sign) to see if they glow. We expect the wells that contain both compound and DNA to produce a laddering pattern after staining with EtBr (due to EtBr intercalation into DNA) and not a glow at the well itself. From this assay, it is apparent that only 1NS6, 1NS7, 2NS6, 2NS7, TOS6, and TOS7 were fluorescent. As a result, we figured that if we were going to optimize the above protocol, we would only work with the six fluorescent compounds.

In order to optimize the above gel protocol, we decided to test all the six compounds (1NS6, 1NS7, 2NS6, 2NS7, TOS6, and TOS7) at 250 μM concentrations. The results before and after counterstaining with EtBr are shown in Figures 141 and 142 below. It is apparent from Figure 141 that a laddering pattern is visible at 250 μM

concentrations. This observation then suggests that there is binding between these compounds and DNA. These results suggest that the cytotoxicity may be mediated through DNA binding although we cannot rule out other mechanisms.

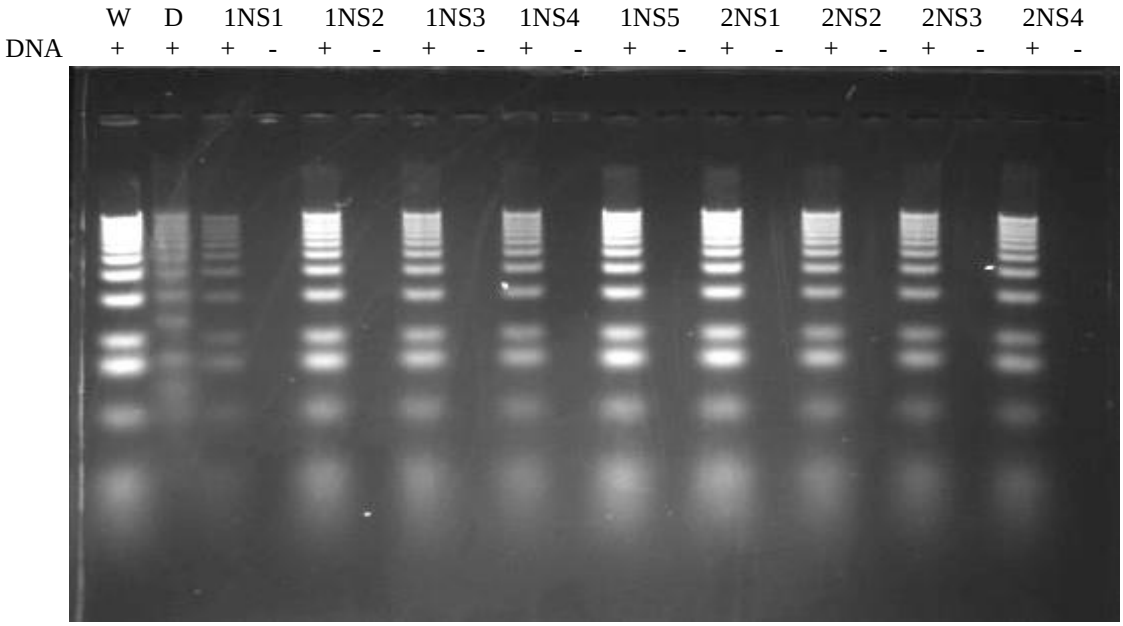

Figure 137: Gel electrophoresis DNA-binding assay of 1000 μM of 1NS1, 1NS2, 1NS3, 1NS4, 1NS5, 2NS1, 2NS2, 2NS3, and 2NS4 after counterstaining with EtBr. The complexes were dissolved in DMSO/water in the presence or absence

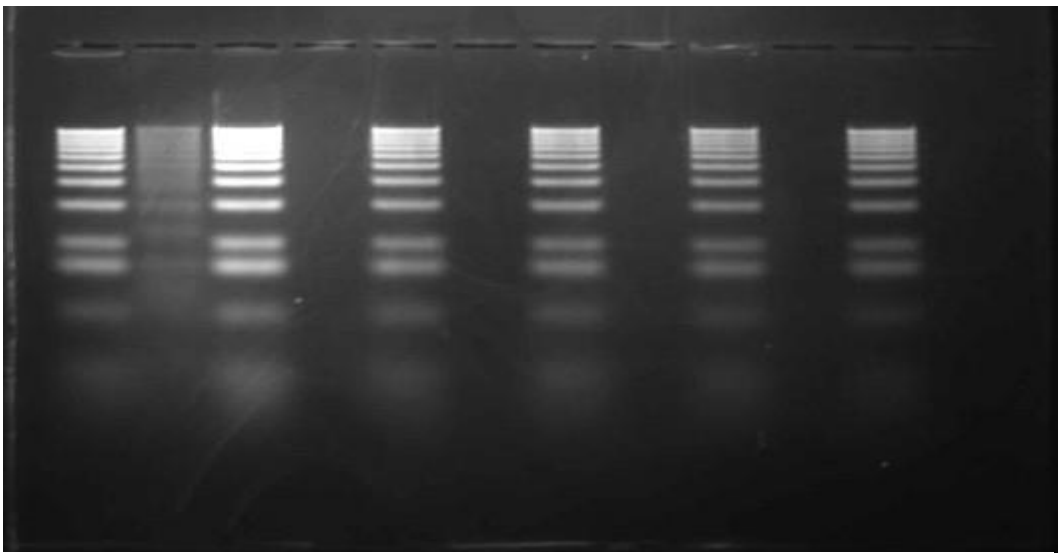

Figure 138: Gel electrophoresis DNA-binding assay of 1000 μM of TOS1, TOS2, TOS3, TOS4, TOS5 after counterstaining with EtBr. The complexes were dissolved in DMSO/water in the presence or absence of lambda HindIII DNA markers and incubated at room temperature for 1 hr.

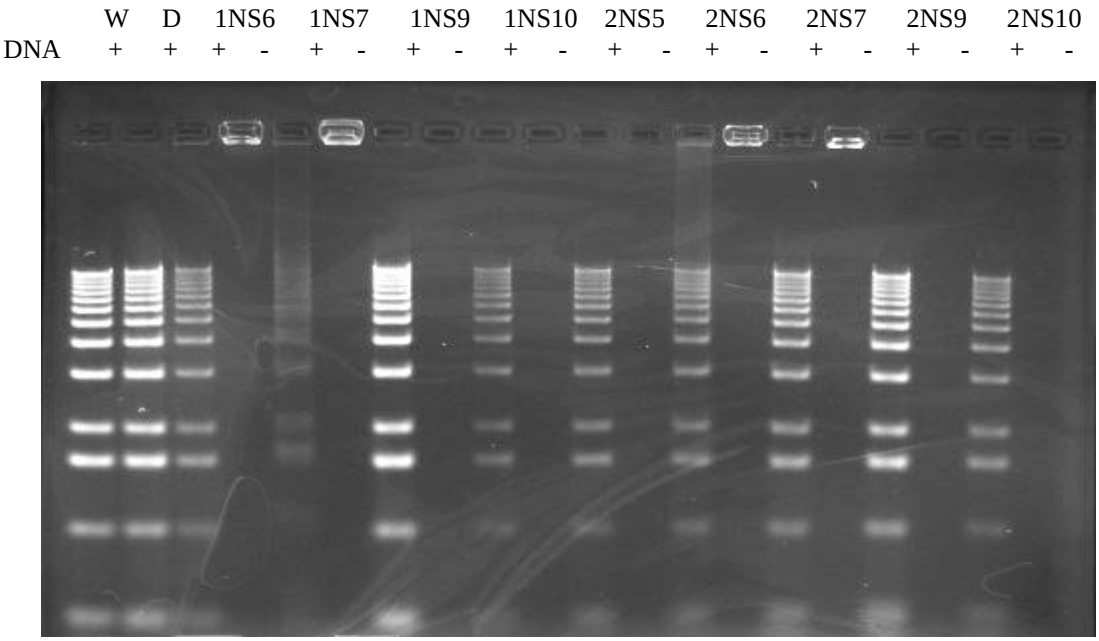

Figure 139: Gel electrophoresis DNA-binding assay of 1000 μM of 1NS6, 1NS7, 1NS9, 1NS10, 2NS5, 2NS6, 2NS7, 2NS9, and 2NS10 after counterstaining with EtBr. The complexes were dissolved in DMSO/water in the presence or absence of lambda HindIII DNA markers and incubated at room temperature for 1 hr

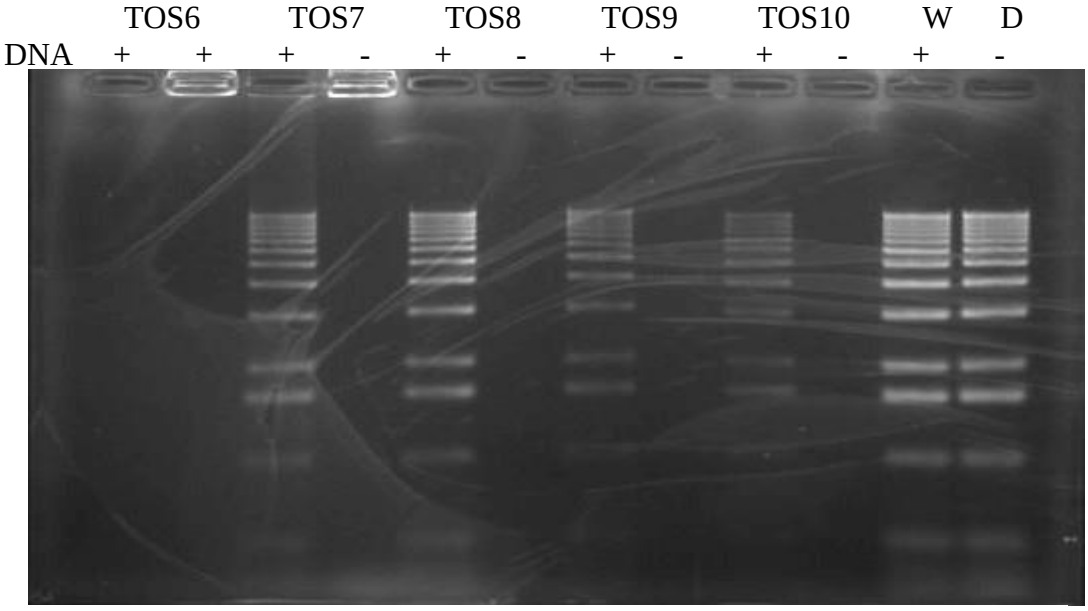

Figure 140: Gel electrophoresis DNA-binding assay of 1000 μM of TOS6, TOS7, TOS8, TOS9, and TOS10 after counterstaining with EtBr. The complexes were dissolved in DMSO/water in the presence or absence of lambda HindIII DNA markers and incubated at room temperature for 1 hr

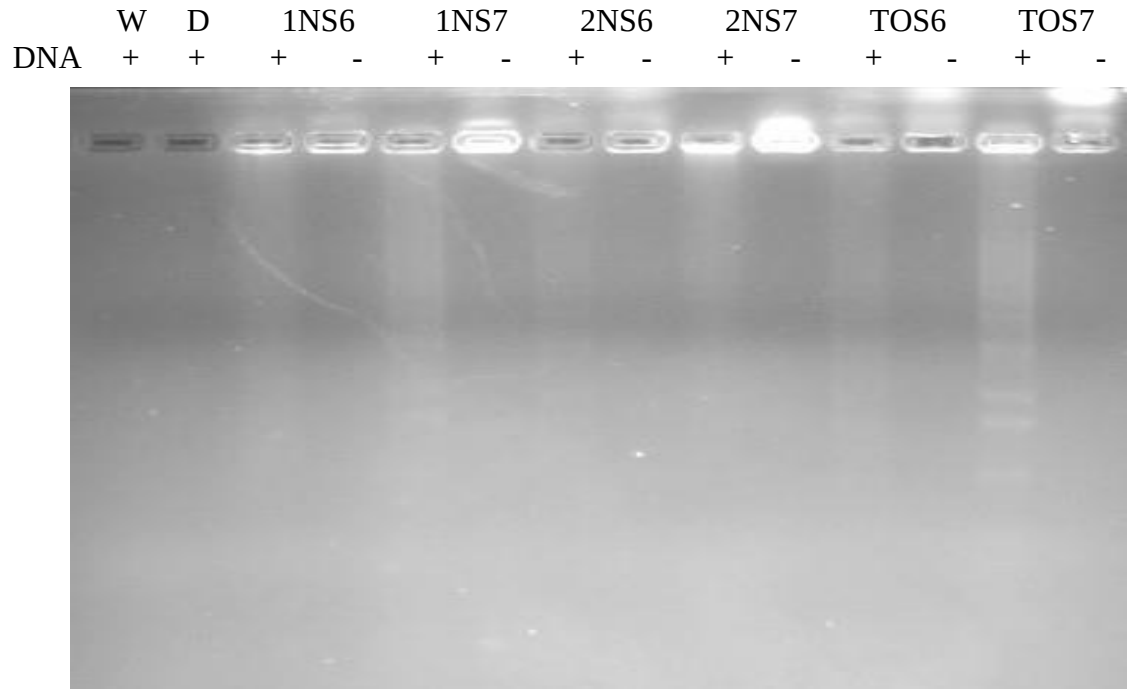

Figure 141: Gel electrophoresis DNA-binding assay of 250 μM of 1NS6, 1NS7, 2NS6, 2NS7, TOS6 and TOS7 prior to counterstaining with EtBr. The complexes were dissolved in DMSO/water in the presence or absence of lambda HindIII DNA markers and incubated at room temperature for 1 hr

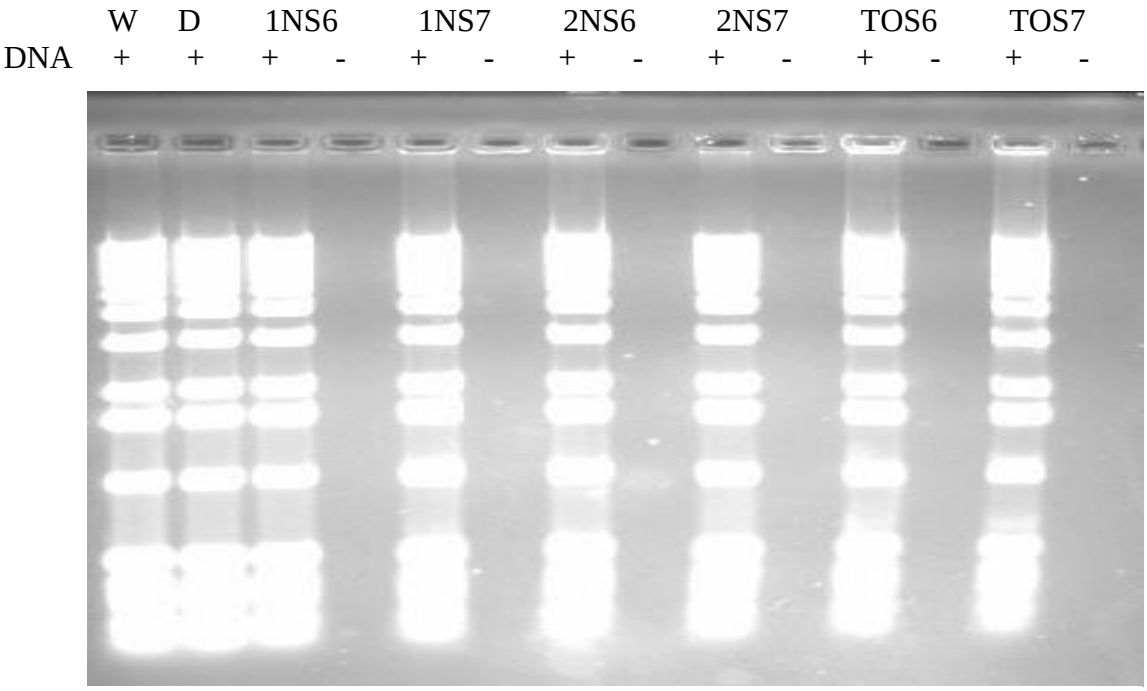

Figure 142: Gel electrophoresis DNA-binding assay of 250 μM of 1NS6, 1NS7, 2NS6, 2NS7, TOS6 and TOS7 after counterstaining with EtBr. The complexes were dissolved in DMSO/water in the presence or absence of lambda HindIII DNA markers and incubated at room temperature for 1 hr

The final test that was carried out to investigate the DNA-binding mode of the sulfonato complexes is viscosity studies. It is considered the least ambiguous means of studying the DNA-binding mode of metal complexes.[59] The interaction of the complexes with CT-DNA was studied by measuring the change in the viscosity of CT-DNA upon addition of the complexes to it. DNA viscosity is strictly dependent on the changes in length that may occur due to the interaction between a small molecule and DNA's double helix.[74] An intercalator causes a separation in DNA base pairs for it to be accomodated in the DNA structure.[74] This usually leads to a lengthening of the DNA helix and an increase in DNA viscosity. For example, classical intercalators like ethidium bromide have been shown to increase the length of DNA resulting in an increase in its relative viscosity.[75-77] A covalent binder (e.g. cisplatin) shortens the length of the DNA double helix.[78] This causes a decrease in the relative viscosity of DNA. Groove binders like Hoechst 33258 have been shown not to cause an increase in length of the DNA helix and consequently does not change the relative viscosity of DNA.[76-77].

Figure 143 below shows the effects of EtBr and complexes 1NS6, 1NS7, 1NS9, 2NS6, 2NS7, 2NS9, TOS6, TOS7, TOS9 on the viscosity of CT-DNA. These were the complexes that showed intercalative mode of binding in our Ethidium bromide displacement assay. As shown in this figure, the relative viscosity of CT-DNA increases steadily as the complex concentrations increase. According to the figure, this was also the behavior of EtBr. This increase in viscosity is due to the lengthening of the DNA helix to accommodate the sulfonato complexes. The degree of viscosity is according to the following order: TOS9 ~ EtBr > 2NS9 > TOS7 > 1NS9 > 1NS7 > 2NS6 > TOS6 >2NS7

>1NS6. These results suggest that the mode of binding of the complexes to DNA is through intercalation.

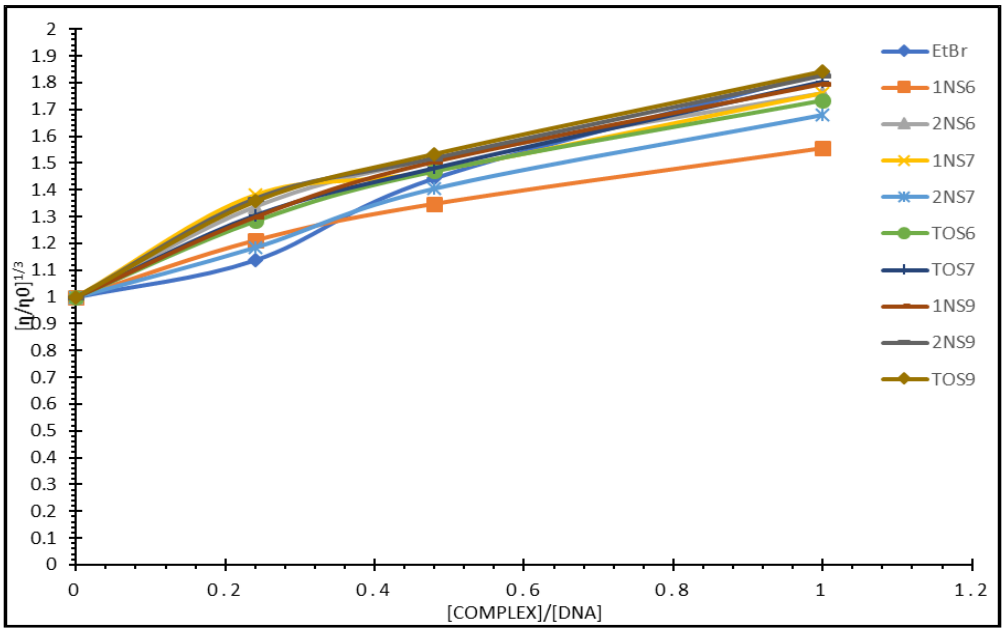

Figure 143: Relative viscosity $(\eta/\eta_o)^{1/3}$ of CT-DNA (0.2 mM) in buffer solution (10X Phosphate Buffered Saline at pH 7.2) in the presence of increasing amount of complexes and EtBr

‘

CHAPTER IV: CONCLUSION

In summary, a series of pentycarbonato (PC) complexes (PC1 – PC10) of the general formula *fac*-$(CO)_3$(α-diimine)$ReOC(O)O(CH_2)_4CH_3$ were successfully synthesized with yields ranging from 66–84%. We synthesized these compounds according to the published[49] protocol developed in the Mandal lab for PC1–PC7. The yields for PC1–PC7 were close to the published yields. PC8 – PC10 were newly synthesized with yields ranging from 74–78%. A series of novel sulfonato rhenium complexes of the type $XRe(CO)_3Z$ [X = α-diimines and Z = tosylate, 1-naphthalenesulfonate and 2-naphthalenesulfonate] were successfully synthesized from the PC compounds in a second step with yields ranging from 70–99%.

For the cytotoxicity studies, of all the compounds tested (TOS1, TOS2, TOS3, TOS4, TOS5, TOS6, TOS8 and TOS9) only TOS4 had IC_{50} value (IC_{50} = 4.83 ± 0.151 μM) lower than 5 μM and thus was the only active compound against U937 lymphoma cell line. The organorhenium compounds 1NS7 and TOS7 was highly active (IC_{50} < 1.00 μM) on MCF-7 and MDA-MB-231 breast cancer cells. Lippard and his group at MIT have synthesized a Re(V) complex bearing a bathophenanthroline ligand that is ligand 6 in this study.[50] This compound was shown to exhibit IC_{50} values of 0.285 ± 0.035 and 0.475 ± 0.161 against MCF-7 and MDA-MB-231 breast cancer cells. In this study, we have explored the structure–activity relationship (SAR) studies for all the 1NS, 2NS and TOS compounds tested against breast cancer and lymphoma cells. It is apparent that the sulfonato organorhenium compounds bearing bathophenanthroline (ligand 6) and bathocuproin (ligand 7) showed remarkable activity against breast cancer cells. This is possibly due to the increased lipophilic character of the rhenium compounds. It is very

likely that the lipophilicities of the α-diimine ligands considered in this study follow the following trend: ligands 7 > 6 > 9 > 4 ~ 5 ~ 8 > 3 ~ 10 > 2 > 1.

We can expect that the lipophilicities of the organorhenium sulfonato compounds follow a similar trend. The cytotoxicity studies against breast cancer cells were only performed on sulfonato complexes containing ligands 1–8. For all the 1NS, 2NS and TOS compounds tested, the following are the trends observed based on IC_{50} values on Tables 7 and 8 in the appendix. For the MCF-7A cancer cells, the 1NS, 2NS and TOS compounds showed the following trends: **1NS:** 1NS7 < 1NS4 < 1NS6 < 1NS2 < 1NS3 < 1NS1; **2NS**: 2NS6 < 2NS4 < 2NS5 < 2NS8 < 2NS7 < 2NS1 < 2NS2 < 2NS3; **TOS**: TOS7 < TOS6 < TOS4 < TOS5 < TOS2 < TOS8 < TOS3 < TOS1. For the MDA-MB-231 cancer cells, the 1NS, 2NS and TOS compounds showed the following trends: **1NS:** 1NS7 < 1NS6 < 1NS4 < 1NS3 < 1NS2; **2NS**: 2NS6 < 2NS4 < 2NS8 < 2NS5 < 2NS7 < 2NS2 < 2NS3 < 2NS1; **TOS**: TOS7 < TOS6 < TOS4 < TOS5 < TOS8 < TOS3 < TOS2. Even though the trends are not exactly the same as that of the ligands, we see a very close simililarity especially in that of the TOS compounds. We did not see a similar trend in the IC_{50} values for the lymphoma cells. The following is the trend that was observed: TOS4 < TOS8 < TOS5 < TOS6 < TOS2 < TOS9 < TOS1 < TOS3.

For the mechanistic studies, we have observed that the organorhenium complexes partially intercalate with DNA. In the UV-Vis titration graphs for all the 1NS, 2NS and TOS graphs, hypochromism was observed for each compound. However, bathochromism was not observed in any of the graphs. This suggests that the compounds potentially follow moderate intercalation with DNA. The absence of a bathochromic shift also suggests that the mode of interaction with DNA could possibly be groove-binding

mechanism. The cyclic voltammograms of the 1NS, 2NS and TOS compounds (except 2NS4 and 2NS6) in the absence and presence of DNA showed no decrease in the oxidation peak intensity upon addition of DNA to the complexes, indicating that there is little or no interactions between the complexes and DNA. Addition of DNA to 2NS4 and 2NS6, reduces the peak intensity suggesting interactions between the complexes and DNA. On the other hand, addition of DNA to 1NS4, 1NS8, 1NS9, 2NS5, 2NS8, 2NS9, 2NS10, TOS1 and TOS2 causes the oxidation peak to increase rather than decrease. The reason for such an increase is not very clear.

In the ethidium bromide displacement assay, the fluorescence intensities of EtBr bound to CT-DNA only show a remarkable decreasing trend with the increasing concentration of complexes when the following complexes were tested: 1NS6, 1NS7, 1NS9 2NS6, 2NS7, 2NS9, TOS6, TOS7, and TOS9. This indicates that some EtBr molecules were released into solution after they were exchanged with the complexes, resulting in the fluorescence quenching of EtBr. This suggests intercalative mode of binding of the complexes (1NS6, 1NS7, 1NS9 2NS6, 2NS7, 2NS9, TOS6, TOS7, and TOS9) to DNA. The binding strength of the sulfonato complexes to CT-DNA follows the following order based on the Stern-Volmer plots: TOS6 > 2NS6 > TOS9 > 1NS9 > 2NS9 > TOS7 > 1NS7 > 2NS7> 1NS6.

Based on the gel electrophoresis experiments, after testing all the six fluorescent compounds (1NS6, 1NS7, 2NS6, 2NS7, TOS6, and TOS7) at 250 μM concentrations, it was apparent that the cytotoxicity may be mediated through DNA binding. The final and least ambiguous DNA-binding study carried out was viscosity. This test would often confirm if the DNA binding mechanism is intercalation. The 9 sulfonato complexes that

showed intercalative mode of binding in the Ethidium bromide displacement assay were tested. The relative viscosity of CT-DNA was shown to increase steadily as the complex concentrations increase. This was also the behavior of EtBr. This increase in viscosity is due to the lengthening of the DNA helix to accommodate the sulfonato complexes. The degree of viscosity is according to the following order: TOS9 ~ EtBr > 2NS9 > TOS7 > 1NS9 > 1NS7 > 2NS6 > TOS6 >2NS7 >1NS6.

The results of all the DNA-binding studies carried out confirmed that the following complexes: 1NS6, 1NS7, 1NS9, 2NS6, 2NS7, 2NS9, TOS6, TOS7 and TOS9 bind to DNA intercalatively at least partially. We cannot confirm full intercalation due to the inconsistencies we see in the UV-Vis and cyclic voltammetry results which do not suggest intercalation. It is also apparent that the complexes that showed intercalation to DNA are also the most lipophilic of all the compounds tested. However, we did not see increase in intercalation with increase in lipophilicity. The DNA-binding results did not show much correlatation with the cytotoxicity data for compounds tested. The only correlation that was observed is that TOS7, which was shown to have increased the viscosity of CT-DNA the most (since the cytotoxicities of 1NS9, 2NS9 and TOS9 were not tested) was also the most potent against MCF-7A and MDA-MB-231 breast cancer cell lines.

References

1. Siegel, R. L.; Miller, K. D.; Jemal, A., Cancer statistics, 2018. *CA: A Cancer Journal for Clinicians* **2018,** *68* (1), 7-30.

2. Centers for Disease Control and Prevention Leading Cancer Cases and Deaths, Male and Female, 2015. www.cdc.gov/cancer/dataviz (accessed July 24).

3. National Cancer Institute Common cancer types. https://www.cancer.gov/types/common-cancers (accessed July 24).

4. Institute, N. C. Types of Cancer Treatment. https://www.cancer.gov/about-cancer/treatment/types (accessed April 20).

5. Frederick, L.; Nolan, C.; Scott, C.; Slade, E.; Oregon Public, B.; Annenberg/Cpb, Rediscovering biology. molecular to global perspectives 8, 8. Annenberg/CPB: S. Burlington, VT, 2003.

6. Moding, E. J.; Kastan, M. B.; Kirsch, D. G., Strategies for optimizing the response of cancer and normal tissues to radiation. *Nature reviews. Drug discovery* **2013,** *12* (7), 526-542.

7. Masood, S., Estrogen and progesterone receptors in cytology: a comprehensive review. *Diagnostic cytopathology* **1992,** *8* (5), 475-91.

8. Mohibi, S.; Mirza, S.; Band, H.; Band, V., Mouse models of estrogen receptor-positive breast cancer. *Journal of Carcinogenesis* **2011,** *10*, 35.

9. Wilder, P. T.; Weber, D. J.; Winstead, A.; Parnell, S.; Hinton, T. V.; Stevenson, M.; Giri, D.; Azemati, S.; Olczak, P.; Powell, B. V.; Odebode, T.; Tadesse, S.; Zhang, Y.; Pramanik, S. K.; Wachira, J. M.; Ghimire, S.; McCarthy, P.; Barfield, A.; Banerjee, H. N.; Chen, C.; Golen, J. A.; Rheingold, A. L.; Krause, J. A.; Ho, D. M.; Zavalij, P. Y.;

Shaw, R.; Mandal, S. K., Unprecedented anticancer activities of organorhenium sulfonato and carboxylato complexes against hormone-dependent MCF-7 and hormone-independent triple-negative MDA-MB-231 breast cancer cells. *Molecular and cellular biochemistry* **2017**.

10. Dean-Colomb, W.; Esteva, F. J., Her2-positive breast cancer: herceptin and beyond. *European journal of cancer (Oxford, England : 1990)* **2008,** *44* (18), 2806-12.

11. Widakowich, C.; de Castro, G.; de Azambuja, E.; Dinh, P.; Awada, A., Review: Side Effects of Approved Molecular Targeted Therapies in Solid Cancers. *The Oncologist* **2007,** *12* (12), 1443-1455.

12. Yan, L.; Rosen, N.; Arteaga, C., Targeted cancer therapies. *Chinese journal of cancer* **2011,** *30* (1), 1-4.

13. Khan, R. A.; Arjmand, F.; Tabassum, S.; Monari, M.; Marchetti, F.; Pettinari, C., Organometallic ruthenium(II) scorpionate as topo IIα inhibitor; in vitro binding studies with DNA, HPLC analysis and its anticancer activity. *Journal of Organometallic Chemistry* **2014,** *771*, 47-58.

14. Rosenberg, B.; Van Camp, L.; Krigas, T., Inhibition of Cell Division in Escherichia coli by Electrolysis Products from a Platinum Electrode. *Nature* **1965,** *205* (4972), 698-699.

15. Rosenberg, B.; Vancamp, L.; Trosko, J. E.; Mansour, V. H., Platinum Compounds: a New Class of Potent Antitumour Agents. *Nature* **1969,** *222* (5191), 385-386.

16. Galanski, M.; Jakupec, M. A.; Keppler, B. K., Update of the preclinical situation of anticancer platinum complexes: novel design strategies and innovative analytical approaches. *Current medicinal chemistry* **2005,** *12* (18), 2075-94.

17. Knopf, K. M.; Murphy, B. L.; MacMillan, S. N.; Baskin, J. M.; Barr, M. P.; Boros, E.; Wilson, J. J., In Vitro Anticancer Activity and in Vivo Biodistribution of Rhenium(I) Tricarbonyl Aqua Complexes. *Journal of the American Chemical Society* **2017,** *139* (40), 14302-14314.

18. Hartmann, J. T.; Lipp, H. P., Toxicity of platinum compounds. *Expert opinion on pharmacotherapy* **2003,** *4* (6), 889-901.

19. Rajeswaran, A.; Trojan, A.; Burnand, B.; Giannelli, M., Efficacy and side effects of cisplatin- and carboplatin-based doublet chemotherapeutic regimens versus non-platinum-based doublet chemotherapeutic regimens as first line treatment of metastatic non-small cell lung carcinoma: a systematic review of randomized controlled trials. *Lung cancer (Amsterdam, Netherlands)* **2008,** *59* (1), 1-11.

20. Jung, Y.; Lippard, S. J., Direct cellular responses to platinum-induced DNA damage. *Chem Rev* **2007,** *107* (5), 1387-407.

21. Galluzzi, L.; Senovilla, L.; Vitale, I.; Michels, J.; Martins, I.; Kepp, O.; Castedo, M.; Kroemer, G., Molecular mechanisms of cisplatin resistance. *Oncogene* **2012,** *31* (15), 1869-83.

22. Bloemink, M. J.; Reedijk, J., Cisplatin and derived anticancer drugs: mechanism and current status of DNA binding. *Metal ions in biological systems* **1996,** *32*, 641-85.

23. O'Dwyer, P. J.; Stevenson, J. P.; Johnson, S. W., Clinical pharmacokinetics and administration of established platinum drugs. *Drugs* **2000,** *59 Suppl 4*, 19-27.

24. Hartinger, C. G.; Metzler-Nolte, N.; Dyson, P. J., Challenges and Opportunities in the Development of Organometallic Anticancer Drugs. *Organometallics* **2012,** *31* (16), 5677-5685.

25. Gasser, G.; Ott, I.; Metzler-Nolte, N., Organometallic Anticancer Compounds. *Journal of Medicinal Chemistry* **2011,** *54* (1), 3-25.

26. Peacock, A. F.; Sadler, P. J., Medicinal organometallic chemistry: designing metal arene complexes as anticancer agents. *Chemistry, an Asian journal* **2008,** *3* (11), 1890-9.

27. Martins, P.; Marques, M.; Coito, L.; Pombeiro, A. J.; Baptista, P. V.; Fernandes, A. R., Organometallic compounds in cancer therapy: past lessons and future directions. *Anti-cancer agents in medicinal chemistry* **2014,** *14* (9), 1199-212.

28. Zhang, P.; Sadler, P. J., Advances in the design of organometallic anticancer complexes. *Journal of Organometallic Chemistry* **2017,** *839*, 5-14.

29. Leonidova, A.; Gasser, G., Underestimated Potential of Organometallic Rhenium Complexes as Anticancer Agents. *ACS Chemical Biology* **2014,** *9* (10), 2180-2193.

30. Yan, Y. K.; Cho, S. E.; Shaffer, K. A.; Rowell, J. E.; Barnes, B. J.; Hall, I. H., Cytotoxicity of rhenium(I) alkoxo and hydroxo carbonyl complexes in murine and human tumor cells. *Die Pharmazie* **2000,** *55* (4), 307-13.

31. Wang, W.; Yan, Y. K.; Andy Hor, T. S.; Vittal, J. J.; Wheaton, J. R.; Hall, I. H., Synthesis, X-ray structures, and cytotoxicity of rhenium(I) carbonyl 2-(dimethylamino)ethoxide complexes. *Polyhedron* **2002,** *21* (20), 1991-1999.

32. Top, S.; Vessières, A.; Pigeon, P.; Rager, M.-N.; Huché, M.; Salomon, E.; Cabestaing, C.; Vaissermann, J.; Jaouen, G., Selective Estrogen-Receptor Modulators

(SERMs) in the Cyclopentadienylrhenium Tricarbonyl Series: Synthesis and Biological Behaviour. *Chembiochem : a European journal of chemical biology* **2004,** *5* (8), 1104-1113.

33. Illan-Cabeza, N. A.; Garcia-Garcia, A. R.; Moreno-Carretero, M. N.; Martinez-Martos, J. M.; Ramirez-Exposito, M. J., Synthesis, characterization and antiproliferative behavior of tricarbonyl complexes of rhenium(I) with some 6-amino-5-nitrosouracil derivatives: crystal structure of fac-[ReCl(CO)3(DANU-N5,O4)] (DANU=6-amino-1,3-dimethyl-5-nitrosouracil). *Journal of inorganic biochemistry* **2005,** *99* (8), 1637-45.

34. Ma, D. L.; Che, C. M.; Siu, F. M.; Yang, M.; Wong, K. Y., DNA binding and cytotoxicity of ruthenium(II) and rhenium(I) complexes of 2-amino-4-phenylamino-6-(2-pyridyl)-1,3,5-triazine. *Inorganic chemistry* **2007,** *46* (3), 740-9.

35. Orsa, D. K.; Haynes, G. K.; Pramanik, S. K.; Iwunze, M. O.; Greco, G. E.; Ho, D. M.; Krause, J. A.; Hill, D. A.; Williams, R. J.; Mandal, S. K., The one-pot synthesis and the fluorescence and cytotoxicity studies of chlorotricarbonyl(α-diimine)rhenium(I), fac-(CO)3(α-diimine)ReCl, complexes. *Inorganic Chemistry Communications* **2008,** *11* (9), 1054-1056.

36. Kermagoret, A.; Morgant, G.; d'Angelo, J.; Tomas, A.; Roussel, P.; Bastian, G.; Collery, P.; Desmaële, D., Synthesis, structural characterization and biological activity against several human tumor cell lines of four rhenium(I) diseleno-ethers complexes: Re(CO)3Cl(PhSe(CH2)2SePh), Re(CO)3Cl(PhSe(CH2)3SePh), Re(CO)3Cl(HO2C–CH2Se(CH2)2SeCH2–CO2H) and Re(CO)3Cl(HO2C–CH2Se(CH2)3SeCH2–CO2H). *Polyhedron* **2011,** *30* (2), 347-353.

37. Collery, P.; Mohsen, A.; Kermagoret, A.; D'Angelo, J.; Morgant, G.; Desmaele, D.; Tomas, A.; Collery, T.; Wei, M.; Badawi, A., Combination of three metals for the treatment of cancer: gallium, rhenium and platinum. 1. Determination of the optimal schedule of treatment. *Anticancer research* **2012,** *32* (7), 2769-81.

38. Leonidova, A.; Pierroz, V.; Rubbiani, R.; Lan, Y.; Schmitz, A. G.; Kaech, A.; Sigel, R. K. O.; Ferrari, S.; Gasser, G., Photo-induced uncaging of a specific Re(i) organometallic complex in living cells. *Chemical Science* **2014,** *5* (10), 4044-4056.

39. Oriskovich, T. A.; White, P. S.; Thorp, H. H., Luminescent Labels for Purine Nucleobases: Electronic Properties of Guanine Bound to Rhenium(I). *Inorganic chemistry* **1995,** *34* (7), 1629-1631.

40. Zobi, F.; Spingler, B.; Fox, T.; Alberto, R., Toward novel DNA binding metal complexes: structure and basic kinetic data of [M(9MeG)2(CH3OH)(CO)3]+(M = 99Tc, Re). *Inorganic chemistry* **2003,** *42* (9), 2818-20.

41. Zobi, F.; Blacque, O.; Sigel, R. K. O.; Alberto, R., Binding Interaction of [Re(H2O)3(CO)3]+ with the DNA Fragment d(CpGpG). *Inorganic chemistry* **2007,** *46* (25), 10458-10460.

42. Jamieson, E. R.; Lippard, S. J., Structure, Recognition, and Processing of Cisplatin−DNA Adducts. *Chemical Reviews* **1999,** *99* (9), 2467-2498.

43. Reedijk, J., *Metal-Ligand Exchange Kinetics in Platinum and Ruthenium Complexes*. 2008; Vol. 52, p 2-11.

44. Simpson, P. V.; Casari, I.; Paternoster, S.; Skelton, B. W.; Falasca, M.; Massi, M., Defining the Anti-Cancer Activity of Tricarbonyl Rhenium Complexes: Induction of

G2/M Cell Cycle Arrest and Blockade of Aurora-A Kinase Phosphorylation. *Chemistry – A European Journal* **2017,** *23* (27), 6518-6521.

45. Collery, P.; Santoni, F.; Ciccolini, J.; Tran, T. N.; Mohsen, A.; Desmaele, D., Dose Effect of Rhenium (I)-diselenoether as Anticancer Drug in Resistant Breast Tumor-bearing Mice After Repeated Administrations. *Anticancer research* **2016,** *36* (11), 6051-6057.

46. Collery, P.; Bastian, G.; Santoni, F.; Mohsen, A.; Wei, M.; Collery, T.; Tomas, A.; Desmaele, D.; D'Angelo, J., Uptake and efflux of rhenium in cells exposed to rhenium diseleno-ether and tissue distribution of rhenium and selenium after rhenium diseleno-ether treatment in mice. *Anticancer research* **2014,** *34* (4), 1679-89.

47. Collery, P.; Mohsen, A.; Kermagoret, A.; Corre, S.; Bastian, G.; Tomas, A.; Wei, M.; Santoni, F.; Guerra, N.; Desmaele, D.; d'Angelo, J., Antitumor activity of a rhenium (I)-diselenoether complex in experimental models of human breast cancer. *Investigational new drugs* **2015,** *33* (4), 848-60.

48. Parson, C.; Smith, V.; Krauss, C.; Banerjee, H. N.; Reilly, C.; Krause, J. A.; Wachira, J. M.; Giri, D.; Winstead, A.; Mandal, S. K., Anticancer Properties of Novel Rhenium Pentylcarbanato Compounds against MDA-MB-468(HTB-132) Triple Node Negative Human Breast Cancer Cell Lines. *British journal of pharmaceutical research* **2015,** *4* (3), 362-367.

49. Mbagu, M. K.; Kebulu, D. N.; Winstead, A.; Pramanik, S. K.; Banerjee, H. N.; Iwunze, M. O.; Wachira, J. M.; Greco, G. E.; Haynes, G. K.; Sehmer, A.; Sarkar, F. H.; Ho, D. M.; Pike, R. D.; Mandal, S. K., Fac-tricarbonyl(pentylcarbonato)(α-diimine)rhenium complexes: One-pot synthesis, characterization, fluorescence studies,

and cytotoxic activity against human MDA-MB-231 breast, CCl-227 colon and BxPC-3 pancreatic carcinoma cell lines. *Inorganic Chemistry Communications* **2012,** *21*, 35-38.

50. Suntharalingam, K.; Awuah, S. G.; Bruno, P. M.; Johnstone, T. C.; Wang, F.; Lin, W.; Zheng, Y. R.; Page, J. E.; Hemann, M. T.; Lippard, S. J., Necroptosis-inducing rhenium(V) oxo complexes. *Journal of the American Chemical Society* **2015,** *137* (8), 2967-74.

51. Cheung-Ong, K.; Giaever, G.; Nislow, C., DNA-damaging agents in cancer chemotherapy: serendipity and chemical biology. *Chemistry & biology* **2013,** *20* (5), 648-59.

52. Sirajuddin, M.; Ali, S.; Badshah, A., Drug–DNA interactions and their study by UV–Visible, fluorescence spectroscopies and cyclic voltametry. *Journal of Photochemistry and Photobiology B: Biology* **2013,** *124*, 1-19.

53. Palchaudhuri, R.; Hergenrother, P. J., DNA as a target for anticancer compounds: methods to determine the mode of binding and the mechanism of action. *Current Opinion in Biotechnology* **2007,** *18* (6), 497-503.

54. Zuber, G.; Quada, J. C.; Hecht, S. M., Sequence Selective Cleavage of a DNA Octanucleotide by Chlorinated Bithiazoles and Bleomycins. *Journal of the American Chemical Society* **1998,** *120* (36), 9368-9369.

55. Silvestri, C.; Brodbelt, J. S., Tandem mass spectrometry for characterization of covalent adducts of DNA with anticancer therapeutics. *Mass Spectrom Rev.* **2012,** *2*, 1-20.

56. Lerman, L. S., Structural considerations in the interaction of DNA and acridines. *Journal of Molecular Biology* **1961,** *3* (1), 18-IN14.

57. LePecq, J. B.; Paoletti, C., A fluorescent complex between ethidium bromide and nucleic acids. Physical-chemical characterization. *J Mol Biol* **1967,** *27* (1), 87-106.

58. K.R, S. G.; Mathew, B. B.; Sudhamani, C. N.; Naik, H. S. B., Mechanism of DNA Binding and Cleavage. *Biomedicine and Biotechnology* **2014,** *2* (1), 1-9.

59. Wilder, P. T.; Weber, D. J.; Winstead, A.; Parnell, S.; Hinton, T. V.; Stevenson, M.; Giri, D.; Azemati, S.; Olczak, P.; Powell, B. V.; Odebode, T.; Tadesse, S.; Zhang, Y.; Pramanik, S. K.; Wachira, J. M.; Ghimire, S.; McCarthy, P.; Barfield, A.; Banerjee, H. N.; Chen, C.; Golen, J. A.; Rheingold, A. L.; Krause, J. A.; Ho, D. M.; Zavalij, P. Y.; Shaw, R.; Mandal, S. K., Unprecedented anticancer activities of organorhenium sulfonato and carboxylato complexes against hormone-dependent MCF-7 and hormone-independent triple-negative MDA-MB-231 breast cancer cells. *Molecular and cellular biochemistry* **2018,** *441* (1-2), 151-163.

60. Sohrabi, N., *Binding and UV/Vis spectral investigation of interaction of Ni(II) piroxicam complex with calf thymus deoxyribonucleic acid (Ct-DNA): A thermodynamic approach*. 2015; Vol. 7, p 533-537.

61. Anbu, S.; Kandaswamy, M.; Suthakaran, P.; Murugan, V.; Varghese, B., Structural, magnetic, electrochemical, catalytic, DNA binding and cleavage studies of new macrocyclic binuclear copper(II) complexes. *Journal of inorganic biochemistry* **2009,** *103* (3), 401-410.

62. Skyrianou, K. C.; Perdih, F.; Turel, I.; Kessissoglou, D. P.; Psomas, G., Nickel–quinolones interaction: Part 3 — Nickel(II) complexes of the antibacterial drug flumequine. *Journal of inorganic biochemistry* **2010,** *104* (7), 740-749.

63. Arslantas, A.; Devrim, A. K.; Necefoglu, H., The Interaction of Sheep Genomic DNA with a Cobalt(II) Complex Containing p-Nitrobenzoate and N,N′-Diethylnicotinamide Ligands. *International Journal of Molecular Sciences* **2007,** *8* (12), 1225-1233.

64. Biver, T., Use of UV-Vis Spectrometry to Gain Information on the Mode of Binding of Small Molecules to DNAs and RNAs. *Applied Spectroscopy Reviews* **2012,** *47* (4), 272-325.

65. Jiang, C.-W.; Chao, H.; Li, H.; Ji, L.-N., Syntheses, characterization and DNA-binding studies of ruthenium(II) terpyridine complexes: [Ru(tpy)(PHBI)]2+ and [Ru(tpy)(PHNI)]2+. *Journal of inorganic biochemistry* **2003,** *93* (3), 247-255.

66. Yang, G.; Jian Zhong, W.; Wang, L.; Liang Nian, J.; Tian, X., Study of the interaction between novel ruthenium(II)-polypyridyl complexes and calf thymus DNA. *Journal of inorganic biochemistry* **1997,** *66* (2), 141-144.

67. Biver, T.; Lombardi, D.; Secco, F.; Tine, M. R.; Venturini, M.; Bencini, A.; Bianchi, A.; Valtancoli, B., Kinetic and equilibrium studies on the polyazamacrocycle neotetren: metal-complex formation and DNA interaction. *Dalton transactions (Cambridge, England : 2003)* **2006,** (12), 1524-33.

68. Biver, T.; Pulzonetti, M.; Secco, F.; Venturini, M.; Yarmoluk, S., A kinetic analysis of cyanine selectivity: CCyan2 and Cyan40 intercalation into poly(dA-dT) x poly(dA-dT) and poly(dG-dC) x poly(dG-dC). *Archives of biochemistry and biophysics* **2006,** *451* (2), 103-11.

69. Biver, T.; Cavazza, C.; Secco, F.; Venturini, M., The two modes of binding of Ru(phen)(2)dppz(2+) to DNA: thermodynamic evidence and kinetic studies. *Journal of inorganic biochemistry* **2007,** *101* (3), 461-9.

70. Coppel, Y.; Coulombeau, C.; Coulombeau, C.; Lhomme, J.; Dheu-Andries, M. L.; Vatton, P., Molecular modelling study of DNA-Troeger's bases interactions. *Journal of biomolecular structure & dynamics* **1994,** *12* (3), 637-53.

71. Erkkila, K. E.; Odom, D. T.; Barton, J. K., Recognition and Reaction of Metallointercalators with DNA. *Chemical Reviews* **1999,** *99* (9), 2777-2796.

72. Li, X.-W.; Yu, Y.; Li, Y.-T.; Wu, Z.-Y.; Yan, C.-W., Synthesis, structure, cytotoxic activities and DNA-binding properties of tetracopper(II) complexes with dissymmetrical N,N′-bis(substituted)oxamides as ligands. *Inorganica Chimica Acta* **2011,** *367* (1), 64-72.

73. Dhara, K.; Roy, P.; Ratha, J.; Manassero, M.; Banerjee, P., Synthesis, crystal structure, magnetic property and DNA cleavage activity of a new terephthalate-bridged tetranuclear copper(II) complex. *Polyhedron* **2007,** *26* (15), 4509-4517.

74. Topala, T.; Bodoki, A.; Oprean, L.; Oprean, R., *Experimental techniques employed in the study of metal complexes-DNA -interactions*. 2014; Vol. 62, p 1049-1061.

75. Shahabadi, N.; Mohammadi, S.; Alizadeh, R., DNA Interaction Studies of a New Platinum(II) Complex Containing Different Aromatic Dinitrogen Ligands. *Bioinorganic chemistry and applications* **2011,** *2011*, 429241.

76. Long, E. C.; Barton, J. K., On demonstrating DNA intercalation. *Accounts of Chemical Research* **1990,** *23* (9), 271-273.

77. Suh, D.; Chaires, J. B., Criteria for the mode of binding of DNA binding agents. *Bioorganic & medicinal chemistry* **1995,** *3* (6), 723-8.

78. Kapicak, L.; Gabbay, E. J., Topography of nucleic acid helixes in solutions. XXXIII. Effect of aromatic cations on the tertiary structures of deoxyribonucleic acid. *Journal of the American Chemical Society* **1975,** *97* (2), 403-408.